NRL Report 6641

Scintillation Range Noise and Related Phenomena in Water Wave Profiling with Microwave Radar

A. M. King, C. M. Morrow, C. G. Myers, and C. L. Moody

Radar Division
Tracking Branch

September 3, 1968

NAVAL RESEARCH LABORATORY
Washington, D.C.

This document has been approved for public release and sale; its distribution is unlimited.

CONTENTS

Abstract iii
Problem Status iii
Authorization iii

INTRODUCTION 1

BACKGROUND AND THEORETICAL CONSIDERATIONS 6

ANALYSIS OF SCINTILLATION RANGE NOISE THROUGH THE REPRESENTATION OF THE SIGNAL BY ITS SPECTRAL COMPONENTS 8

RADAR SYSTEM CONSIDERATIONS IN OCEAN-WAVE PROFILING 14

- General System Requirements 14
- Some Possible Wave-Profiling Techniques 15
- The NRL Broadband FM-CW Radar 17

THEORETICAL ANALYSIS OF SCINTILLATION RANGE NOISE IN AN FM-CW RADAR 18

- Balanced Interferometer Discriminator 18
- Linear Discriminator 40

SIMULATOR STUDIES OF MULTIPATH PROPAGATION 42

- Waveguide Simulation of Multiple Reflections from an Ocean Surface 42
- Analysis of Waveguide Simulation of Free-Space Multipath Interference 42
- Equipment Operation 48
- Simulation Details 48
- Extent of Targets Simulated 63
- Simulator Comparison to a Functional Radar 69
- Simulator Comparison to Computer Analysis 71
- Comparison of Frequency Discriminators 76
- Comparison of Phasor Plot to Computer Program 78
- Conclusions from Simulator Studies 81

EXPERIMENTS AT THE CHESAPEAKE BAY BRIDGE FACILITY 85

- Installation of Antennas 85
- Wave-Staff Installation 87
- The Data-Recording System 89
- Stray Propagation Paths and Other Sources of Experimental Error 93
- Propagation Experiments 94
- General Comments on the Bay Bridge Data 107
- Discussion of Excerpts from the Bay Bridge Chart Records 109

Applicability of the Interferometer Discriminator Multipath Theory to the Bay Bridge FM-CW Radar 112
Explanation of the Observed Range Noise in Terms of the Two-Path FM-CW Theory 150
Possible Improvements in the Wave-Profiling Techniques Used at the Bay Bridge Facility 160
Significance of the Bay Bridge Results in Ocean-Wave Profiling 167

CONCLUSIONS 168

General Findings 168
Suggested Specifications for an FM-CW Wave-Profiling Radar System 169
Techniques for the Evaluation of an Airborne Wave-Profiling System 170

ACKNOWLEDGMENTS 171

REFERENCES 172

GLOSSARY OF TERMS 174

ABSTRACT

Wave-profile recording by radar from a low-flying conventional aircraft offers a means of rapidly collecting large amounts of oceanographic data over wide areas of the ocean in a relatively short time. A series of radar experiments has been conducted from a laboratory suspended beneath the Chesapeake Bay Bridge. The purpose of the series of experiments was to study the problems of wave-profile recording and to make comparisons with standard radar altimetry.

Theoretical and experimental analyses based on the work conducted at the bridge laboratory indicate that target-scintillation noise limits the accuracy of a microwave radar used for wave profiling. However, it has been concluded that a properly designed airborne FM-CW radar can produce ocean-wave recordings of sufficient accuracy for all ordinary oceanographic purposes. The specifications for such a system have been developed. One of the basic requirements has been found to be a broad transmitted spectrum, probably in excess of 100 Mc/sec; this requirement appears to be independent of the exact form which the radar system takes.

PROBLEM STATUS

This is an interim report; work on the problem is continuing.

AUTHORIZATION

NRL Problem R02-13
Project No. RF 001-02-41-4004

Manuscript submitted September 1, 1967.

SCINTILLATION RANGE NOISE AND RELATED PHENOMENA IN WATER WAVE PROFILING WITH MICROWAVE RADAR

INTRODUCTION

Wave-profile recording by radar from a low-flying conventional aircraft offers a means of rapidly collecting large amounts of oceanographic data over wide areas of the ocean in a relatively short time. The data acquisition can be carried out in the locations where conditions of the greatest significance exist, and transient phenomena such as the buildup of the sea state associated with a moving storm front can be observed over the entire area of interest rather than at a limited number of fixed stations.

In addition to the advantages resulting directly from the mobility of the airborne installation, the profile recorder can readily produce data which can be synthesized only with difficulty from wave-staff time records. The fact that the aircraft velocity is high with respect to the velocity of propagation of ordinary storm waves means that the wave record is very nearly a true space function taken along the track of the aircraft. Thus, directional wave spectra which can be determined only by an elaborate spaced array of fixed wave sensors can readily be obtained in the air by flying over the same area on different aircraft headings.

The capabilities offered by the high-speed airborne platform have led to a considerable and continuing effort, in which many organizations have participated, to develop wave-measuring instrumentation and other airborne equipment. Of the many approaches to wave recording that have been proposed, only one has been considered in the investigation reported here. This is the use of a narrow-beam microwave radar (Fig. 1), to obtain a true profile recording along the line of flight by continuously and precisely measuring the range from the aircraft to the water surface. As indicated in the figure, the system concept involves the use of narrow-beam antennas for both transmission and reception so as to restrict the water surface contributing to the received signal to as small an area as possible. The energy returning from the illuminated surface will, however, always be deflected or scattered throughout a solid angle much larger than that subtended by the receiving aperture, and the entire aircraft may at times be more or less uniformly illuminated. This scattered return makes it possible for secondary paths involving aircraft structure to exist and requires that a practical installation be planned with some care. The geometry shown in the illustration, where the antennas are recessed in the bomb bay and surrounded by reflecting structures, should in general be avoided.

When surface features of the scale of the wind-generated waves common in the open ocean are to be resolved, the considerations involved in forming and stabilizing very narrow radar beams lead to a requirement that the operational altitude be relatively low, probably less than 1000 ft for a system useful in general oceanographic work.

There are, of course, numerous practical problems that must be solved in developing an operational system based on this concept, and a few of these are touched on in the paragraphs which follow. The present investigation has, however, been concerned with the determination of the basic characteristics which a successful wave-profiling radar should or must have, and with the determination of the performance which can then be expected, rather than with the development of operational components. An experimental microwave radar based on the low-altitude wave-profiling concept was developed by the Radar Tracking Branch prior to 1960, and in that year a series of flight tests was performed with an airborne version of this system. This work has been reported by Morrow (1)

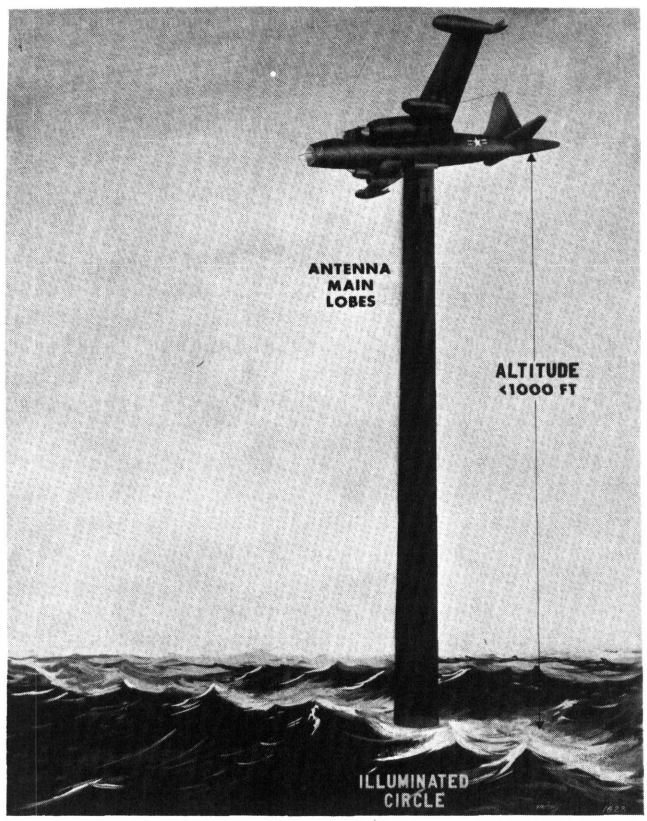

Fig. 1 - Wave profile recording with a pencil-beam microwave radar

and led to the conclusion that this application of microwave radar was a promising means for the collection of oceanographic data.

In order to explore the technique at greater length than was feasible during the airborne exercise, and in particular to determine the ultimate accuracy attainable under reproducible conditions, a new series of theoretical and experimental studies was undertaken, and the results of this work form the basis for the present report. Although no further airborne evaluation has been attempted, these findings are believed to place the design of an improved airborne system on a firm theoretical and experimental basis. In pursuing these investigations three main approaches have been employed. In the first place the physical system consisting of the radar and a multi-element target taken together has been analyzed theoretically. This analysis has been restricted to relatively simple targets by the complexity of the calculations involved, but it is felt that the radar has been characterized in a satisfactorily realistic manner and that the results have led to a useful insight into the more complex real target cases.

A second approach has been the use of a carefully constructed target simulator using the delays of closed waveguide paths to represent the spacing in range of multiple target elements. This technique has permitted the simulation of modes of operation that were awkward to handle theoretically, and has permitted the actual experimental radar to be used as a signal source so that experimental variables that were eliminated or idealized in the theoretical approach could be introduced under conditions of controlled target configuration.

Finally, a field exercise was performed in which a complete wave-profile radar system, especially instrumented to permit adjustment of all significant parameters, was operated using a real water target. This field work was performed at the Chesapeake Bay Bridge Facility, where a gondola laboratory is hung beneath the East Channel span of the bridge. This facility offers an unobstructed downward view of the water waves from a height of about 60 ft and houses the experimental equipment. While the range provided is smaller by at least a factor of 4 or 5 than any operating altitude that has been seriously considered for airborne work, a satisfactory antenna geometry could still be provided. It was possible to place a high-resolution wave staff in the water at the center of the water area being illuminated by the radar and so obtain a reference wave record for direct point-by-point comparison with the radar height record. The range of wind and wave conditions was obviously narrower than that found in open ocean, but over a period of a few months a variety of conditions was encountered with waves as high as three feet and winds of over 40 miles per hour. Description and interpretation of the wave records obtained at the Bay Bridge Facility form the section titled "Experiments at the Chesapeake Bay Bridge Facility."

In both the experimental and theoretical work, the principal and in some cases the only concern has been with the way in which range noise, in particular target-scintillation noise, limits the accuracy of a radar wave-profile recording. Since in this respect the wave-profiling problem has much in common with any precision ranging application, it is believed that many of the results are of general interest. However, the analysis is most directly applicable to the problem of continuous, accurate radar height measurement at relatively short ranges with a water surface as the target.

Range noise for the purpose of this discussion is considered to be any random or unpredictable fluctuation which is superimposed on the true range coordinate of a radar target. This form of noise exists to some degree in all radar systems, but ordinarily it becomes a critical problem only in precision ranging applications where the accuracy sought is of the same order of magnitude as the physical dimensions of the target. This is almost always the case in wave-profile measurement, where the target is the section of water surface illuminated by the radar. The size of the illuminated patch can be reduced only by either narrowing the radar beam, which means increasing the antenna size, or by reducing the operational altitude. A larger antenna makes the aircraft installation more difficult and involves a weight and cost penalty as well, while a reduction of the altitude below a certain minimum will increase the hazard of the operation.

As a consequence of these practical considerations, the designer is constrained to make the illuminated area no smaller than is necessary to resolve the wave features that are of interest with the required precision. Water waves other than the small capillaries tend to have lengths that are large relative to their heights. The ratio of length to height is commonly around 20:1 and may be much larger, while theory indicates that 7:1 is the minimum possible, and a ratio much less than 10:1 is rarely observed in practice. Thus the patch size that satisfies the resolution requirement will have a radial or "horizontal" dimension that will often be greater than the wave height being measured by the system. The illuminated section of water surface will also have an axial depth, because the large wave slopes will cause the range to vary across the area involved, and the short wavelets entirely within the illuminated patch will create range differences equal to their heights. The axial depth of the water target will generally be many times smaller than the radial dimension, but it may be an appreciable fraction of the wave height and will at times represent many wavelengths of the microwave radiation. The water surface will thus be a complex scintillating target characterized by a constantly changing pattern of cancellations and reenforcements between the radar echoes originating at different points in the illuminated area.

The effect of this unavoidable scintillation on ranging accuracy turns out to be potentially more serious in the case of radar wave-profiling than in the case of radar

altimetry in general. This is true because the situation facing the designer of a surface profiling system differs from that of the altimeter designer in several ways. In the first place, since the ocean waves are small compared to the features of concern in most altimetry, the profile radar must use a relatively narrow beam to secure the necessary resolution. The small illuminated area that results will contain a relatively small number of reflecting facets or scatterers to contribute to the radar return, and spatial averaging will be less effective in maintaining uniform signal properties at the receiver. As a consequence scintillation rates tend to be lower, and the probability of a deep fade, persisting for an appreciable period, becomes higher. At the same time, the amount of filtering or time averaging which can be used is restricted by the need to pass all of the significant components of the wave-contour signal. Finally, the differential range accuracy required in wave profiling may exceed that needed in any ordinary application of altimetry.

It has been found as a matter of practical experience that when system parameters are chosen to permit accurate recording of wind-driven storm waves, as differentiated from very long swells, the scintillation spectrum will invariably overlap the signal spectrum to such a degree that none of the consequences of scintillation can be entirely eliminated by filtering the height record. This is the basic difficulty which distinguishes the profiling problem from that of accurate altimetry in general, and as a consequence of this fundamental distinction, altimetry techniques must be adapted to wave profiling with special care. Even in the case of such a critical application of altimetry as automatic flare-out and landing, a relatively large target area is illuminated by a relatively broad radar beam, and the amount of spatial averaging of scintillation effects that takes place is far greater than in the case of the narrow-beam wave-profiling radar. In addition, the needed response time is not as short in the altimeter case as it is in wave-profiling, and filtering may be used more effectively to reduce the level of whatever range noise exists. In other less critical altimeter applications range noise can in general be averaged out even more effectively, and it is evident that a principle which has been used successfully in a certain altimeter application may be less successful when applied to a wave-profiling radar, where spatial and time averaging cannot be used to the same extent to reduce target-scintillation effects.

If amplitude fading were the only consequence of the scintillation of a complex target, the provision of an adequate dynamic range would insure good results, and the range noise level would be determined only by the effective signal-to-noise ratio that could be maintained in the receiver. The system parameters that theoretically limit ranging accuracy in the presence of system noise, and the conflicting requirements introduced when target motion must also be accurately sensed, have been widely discussed in the literature (2,3).

As a practical matter, a system having acceptably small range errors contributed by internal noise proves to be readily realized for the wave-profiling application. However, external factors are not as easily controlled, and the behavior of the complex target leads to the generation of an additional range-noise component which is superimposed directly on the desired profile signal and which exists no matter how great the dynamic range of the system may be or how far above the receiver noise threshold the signal may remain. The mechanism by which these range errors are generated is somewhat analogous to that for the radar-angle-noise case, which has been discussed by Dunn, King, and Howard (4) and others, in that it involves the varying interference between the waves backscattered by different parts of the illuminated target. This phenomenon can obviously occur only when the target is at least comparable in dimensions to the radar wavelength. In the case of a practical wave-profiling radar, the antenna beamwidth requirements insure that the wavelength will be a small fraction of the target dimensions, and thus scintillation effects will inevitably be a problem.

Aside from amplitude fading, one of the possible effects of target scintillation is evidently a range variation within the physical depth of the illuminated surface as the apparent mean point of reflection is changed by signal cancellations. This effect has been referred to as "bright-spot-wander." If the changes in apparent range were indeed confined to the axial depth of the target, the problem would not appear to be too serious, since the target depth is generally a small fraction of the height of the larger, longer waves which the radar can resolve. In addition, a good deal of averaging would be expected to take place, with range shifts to the physical extremes of the illuminated water very rare. Unfortunately, the true situation is much more complicated and less favorable, and under adverse conditions when system bandwidth is inadequate it is found that the apparent point of reflection can be shifted in range by many times the physical depth of the target, so that the desired profile is literally buried in the noise. The work on which this report is based has been concerned principally with this type of range noise and has involved computation of range errors for assumed target conditions, use of a waveguide multipath simulator to produce experimentally the effects of controlled target scintillation, and field measurements over water at the Chesapeake Bay Bridge Facility to evaluate noise levels actually generated when tracing different surface profiles.

The essential components of the experimental radar system are illustrated in Fig. 2. The original version of this radar was described by Morrow (1) in reporting the earlier series of wave-profile experiments, including the airborne tests. The present system used for the experiments reported herein is essentially a ground-based refinement of the former system, with improved dynamic characteristics for a more accurate evaluation of target effects.

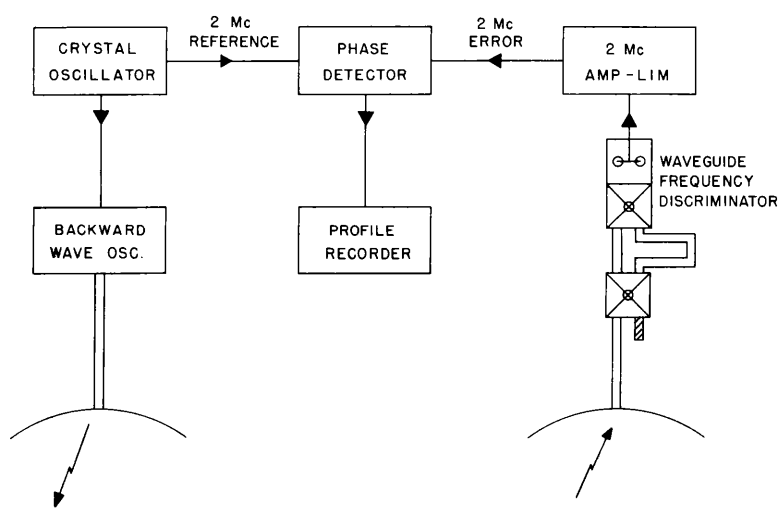

Fig. 2 - Basic components of the FM-CW wave-profile radar system; F_0 = 9510 Mc/sec, ΔF = ±200 Mc/sec, f_m = 2.215 Mc/sec

Range information is obtained by phase comparison at 2.215 Mc/sec of the detected, single-frequency, sinusoidal modulation that deviates or frequency modulates a microwave continuous wave carrier (FM-CW) of 9510 Mc/sec over an optional bandwidth that may be varied up to a maximum of ±200 Mc/sec. Modulation phase delay varies directly with the transit time of the microwave energy to and from the target, with the undelayed signal from the modulator providing the basis for comparison.

To summarize, the purpose of the study related in this report is the evaluation of certain effects of the unavoidable target scintillation that occurs when a radar target

creates a complex pattern of reflections and interferences. The water surface as viewed near vertical incidence by a narrow-beam radar is found to represent such a complex target, and particular emphasis is given to scintillation range noise and the minimization of the resulting range errors in an FM-CW precision ranging system of the type described.

BACKGROUND AND THEORETICAL CONSIDERATIONS

It has been suggested that the essential characteristic of the target-scintillation mechanism is that of a changing pattern of interference between radio-frequency waves originating at different points of an array of reflectors or scatterers. In order for this interference pattern to distort the modulation envelope of the probing radiation, a second requirement must be met, that of varying time delays between the waves that interfere. These delays must be appreciable in terms of the periods of the modulation frequencies and thus in terms of the range delays which the system is attempting to sense. It should be noted at this point that a system which does not employ modulation of a carrier but senses, for example, the phase of a single low-frequency wave is not vulnerable to target scintillation to the same degree as a modulated transmission. The reason for this distinction lies in the circumstance that the envelope phases of a modulated carrier are encoded in the relative phase relationships between the carrier and the individual sidebands. These relative phases can be disrupted to a degree which would not be possible for the modulating wave itself.

The disruptive effects of interference between modulated carriers which have experienced different propagation delays have been known to communications engineers since the earliest use of long-range short-wave transmissions. The principal result in the case of amplitude-modulated waves is to create the effect of drastic overmodulation, which causes nonlinear distortion products to appear in the received envelope. Other effects such as alteration of the modulation-frequency spectrum may also occur. The effects on the intelligibility of speech and the fidelity of musical reproduction are familiar to all short-wave listeners.

When frequency-modulation techniques were first investigated in the 1930's it was naturally hoped that an FM system could be designed which would be less vulnerable to multipath interference than existing AM communication links. A number of investigations were made, but it was apparent from the beginning that FM was not a panacea in this situation. The earliest discussion in the technical literature appears to be that of Crosby (5) in 1936. Crosby described the results of a coast-to-coast experimental link operating on 9 and 18 Mc/sec and also presented an analytical result for the two-path case with single-tone modulation. He concluded that intelligibility was poorer and distortion more severe with FM than with AM. Crosby (6) published additional material in 1941, and the FM multipath problem in communication was discussed by a number of authors in the following years. Among them were Corrington (7) in 1945, Meyers (8) in 1946, Stumpers (9) in 1947, and Gerks (10) in 1949. This list of references is by no means exhaustive, and many other writers have touched on the problem. Wheeler (11) in 1942 presented a general analysis of common-channel interference which is readily adapted to the multipath case, and other discussions of FM interference may also be pertinent. With the exception of Wheeler, all of the authors cited base their theoretical analyses on the "instantaneous frequency" concept, in which the instantaneous frequency is defined to be the time derivative of the phase function specifying the angular position of the phasor which represents the received signal. This resultant phasor is derived by addition of the phasors for the individual signals arriving over paths having different time delays. The receiver output is then taken to be proportional to the frequency function only, which of course implies the use of a perfect limiter followed by a perfect linear frequency discriminator.

The question immediately arises as to how performance might differ were the receiver less than ideal in one or both of these respects. The work of Wheeler (11), which includes the cases of filter discriminators driving square-law and envelope detectors, indicates that interference rejection may indeed be degraded if amplitude limiting does not occur. Receiver characteristics are also considered by Gerks (10), who discusses the adverse effects of inadequate discriminator bandwidth in an otherwise ideal system and points out that multipath distortion may be minimized by proper design in this respect.

The theoretical and experimental work of Arguimbau (12,13) and his associates also dealt with the influence of the receiver design on the distortion levels that could be achieved, and they showed that a sophisticated receiver having sufficiently good limiting action should provide acceptably low distortion for a very high percentage of the time in certain types of multipath environment. A receiver based on this philosophy was designed and constructed and was demonstrated to provide performance superior to AM over a multipath circuit simulated by delay lines. This work caused renewed interest in the use of FM on a transoceanic communications link. Unfortunately the nature of multipath propagation over the ocean proved to be more complex than the laboratory simulation, and the technique failed to provide the needed improvement. Apparently, a multiplicity of propagation paths existed such that the level received over the strongest single path was generally exceeded by the sum of the remaining paths, even though they were individually weaker. Under these conditions the enhanced capture effect provided by the improved receiver could not operate to select the undistorted single path, and the detected modulation remained garbled. This finding is of interest in the wave-profiling case because of the possibility that the multiple reflections from the illuminated surface patch also represent this type of complexity and that the performance of an ideal receiver may be equally disappointing in this application.

In the 1950's references to radar ranging made their appearance in the unclassified literature, and the FM multipath problem was discussed by Sollenberger in 1955 (14), Vinti in 1957 (15), and Becker in 1958 (16). Sollenberger discussed the errors caused by ground reflections in a multistatic missile-tracking radar operating on the phase of single-tone modulation and demonstrated theoretically and by means of a delay-line simulator that use of sufficiently broadband FM could provide a large reduction in range errors. Sollenberger (14) again used the instantaneous-frequency approach in his theoretical work, and his experimental receiver evidently approached the assumed ideal closely in a practical sense, since his experimental data agreed quite closely with the calculated curves. Vinti (15) gave a general analysis of ranging errors caused by multipath propagation in FM systems which included the effect of antenna parameters, and also presented a discussion of the case of multitone modulation.

During this latter period the wave-profiling problem was under discussion at NRL following the evaluation of an unsuccessful radar sea and swell recorder at the request of the Naval Oceanographic Office. The system under investigation employed a transmitted bandwidth of only about 4 Mc/sec, and although it performed satisfactorily during bench tests with a delay-line closed path it failed to record recognizable wave profiles. Antenna-range experiments with complex targets strongly suggested that some form of multipath interference was responsible for the high range-noise levels experienced, and Howard (17) in 1956 extended Gerks' (10) analysis to the specific case of target scintillation in precision ranging. No previous discussion of errors due to multipath delays at the target itself has been found in the technical literature.

Howard's analysis showed that the apparent point of reflection as determined by an FM-CW system could theoretically fall outside the physical array of reflecting elements and could in fact be displaced in range from the physical location by many times the physical depth. The multiplying factor which could exist for small transmitted bandwidths was found to depend on the depth of the multipath cancellation, tending towards infinity

for an infinitely deep null. As the frequency deviation, and hence the transmitted bandwidth, was increased the theoretical range errors became smaller, and at a sufficiently large frequency deviation the apparent range was never found to shift beyond the physical extent of the target array. Being derived from Gerks' two-path, single-frequency example, this analysis was admittedly based on an over-simplification of the actual wave-profiling situation, and it was rigorously accurate only for the ideal receiver implied by the instantaneous frequency assumption. Nevertheless, it seemed reasonable to assume that range noise would be minimized to some extent by broadband FM, and a wave-profiling radar was designed in accordance with this assumption and eventually evaluated in an aircraft over a number of different ocean-surface conditions. This work has been discussed by Morrow (1) and showed that useful wave-profile recordings could be obtained under many conditions. Under certain conditions, however, the range-noise level remained objectionably high; it seemed in general to be considerably greater than that predicted by theory, and failed to show the expected sustained downward trend as the frequency deviation was increased. In the hope of resolving the questions left unanswered by the aircraft experiments, it was decided to undertake further theoretical and experimental work on the precision ranging problem. The theoretical work has been directed toward computer analysis based on assumptions more nearly representing the physical system than the perfect limiter-discriminator chain. The experimental work has involved measurements with an improved waveguide multipath simulator and field work at the Chesapeake Bay Bridge Facility, where simultaneous radar and wavestaff data could be recorded.

ANALYSIS OF SCINTILLATION RANGE NOISE THROUGH THE REPRESENTATION OF THE SIGNAL BY ITS SPECTRAL COMPONENTS

The effects of scintillation interference in specific circumstances may be demonstrated in several ways. The purely analytical approach can be rigorous in simple cases and leads to the most useful quantitative results. However, the equations are complex and are not readily related to the physical mechanism, so a qualitative physical analysis may be useful as a starting point. The case of AM or narrowband FM may be treated by phasor representation of the carrier and sidebands, and this treatment has been presented by Morrow (1) for an FM transmission and a three-point target. An alternative is the spectrum point of view, in which the target is considered to operate on the individual spectral lines of the probing transmission. The effect of physical spacing between transmitter and target on a radar transmission is normally viewed as the introduction of a time delay which is determined by the distance involved and the velocity of propagation. However, an equally valid point of view is that the target spacing is characterized by a phase-versus-frequency function, $\phi(\omega)$, where ϕ is the phase of the radio-frequency wave received through the distance in question relative to the phase at zero distance. For a single target element at range R giving a propagation-path distance of $2R = D_p$, the phase function is a straight line of constant slope (Fig. 3). If a modulated transmission represented by a carrier and a system of sidebands is received over this propagation path, the phase function will operate to produce a relative shift of $\pm\Delta\phi_1$ radians between adjacent spectral lines, and

$$\Delta\phi_1 = \frac{d\phi}{d\omega} \times \Delta\omega$$

where

$$\frac{d\phi}{d\omega} = \frac{D_p}{c} = \Delta t \text{ and } \Delta\omega = \omega_p,$$

the fundamental modulation frequency. Thus, $\Delta\phi_1 = \omega_p \cdot \Delta t$, and each spectral line is displaced relative to its neighbors by the phase angle represented by the range delay at the modulation frequency.

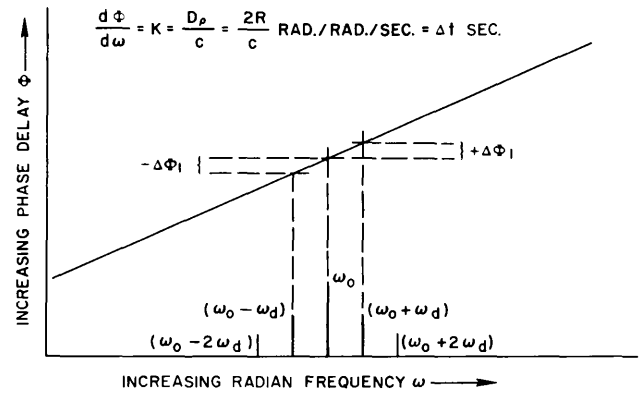

Fig. 3 - Phase-frequency function for a single-element target at range R

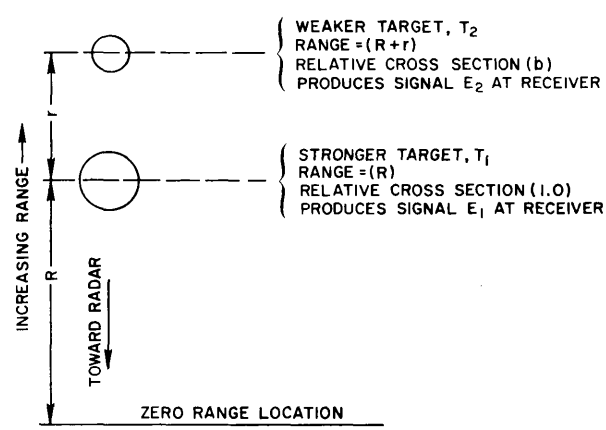

Fig. 4 - A two-element target array

Modulation theory shows that when this relative shift occurs throughout the region covered by the signal spectrum, the effect will be to shift the envelope of the time function through the phase angle $\Delta\phi_1$ as measured at the fundamental modulation frequency, and this is also equivalent to translating the whole function in time by the interval Δt.

In this instance we have evidently used a devious line of reasoning to obtain an obvious result. However, in the case of multiple or complex targets the same reasoning is valid, and the results here will be less obvious. The case of a two-element target is diagrammed in Fig. 4. The significant parameters will be the spacing of the elements in range r and the relative cross section that each one presents to the radar, the ratio b. As a simplifying assumption we will take the illumination to be a plane wave so that the lateral separation is not significant, and we will rule out the possibility of multiple reflections between elements. In this case the received signal will be the sum of two waves which are identical except for a difference in amplitude and a time displacement due to the propagation distance, $2r = d$. In analyzing the effects of the element spacing we may take the range of T_1 to be zero without any loss of generality, and when this is done the relative phase progression as a function of frequency may be diagrammed as in Fig. 5a and 5b. In this figure the phasor representing the signal E_1 reflected by target element T_1 does not shift with frequency, while the phasor for E_2 rotates as indicated relative to E_1. The progression of the phase angle ϕ_s will evidently be symmetrical

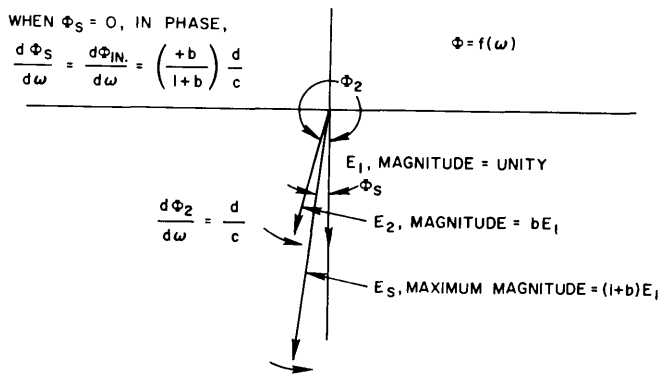

(a) Near the in-phase condition

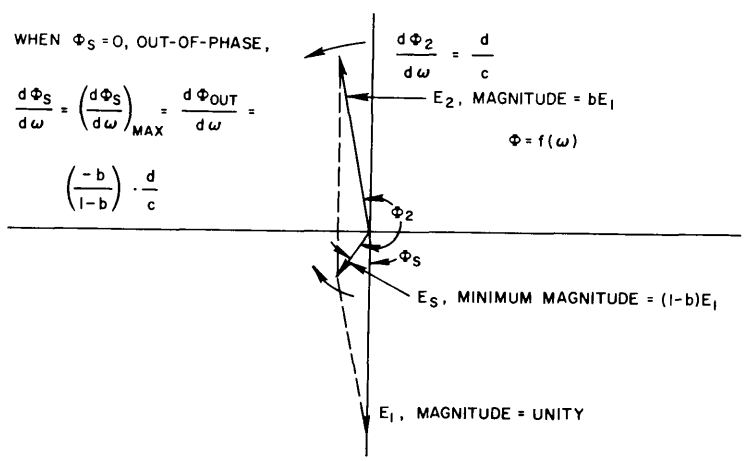

(b) Near the out-of-phase condition

Fig. 5 - Phasor relationships for a two-element target

about the positions for $\phi_s = 0$, but the rate of rotation will be nonuniform, and the rates at $\phi_s = 0$ will be different for the in-phase and out-of-phase conditions. Referring to Fig. 5a, where the phasors E_1 and E_2 are near the in-phase relationship, we may deduce that at $\phi_s = 0$,

$$\frac{d\phi_s}{d\omega} = \left(\frac{+b}{1+b}\right)\left(\frac{d\phi_2}{d\omega}\right)$$

This follows from the phasor geometry, since we have at $\phi_s = 0$:

$$\frac{dy_s}{d\omega} = \frac{dy_2}{d\omega} = 0$$

$$\frac{dx_s}{d\omega} = \frac{dx_2}{\phi\omega} \quad \text{and}$$

$$\frac{d\phi_s}{d\omega} = \left(\frac{dx_s}{d\omega}\right)\left(\frac{1}{E_s}\right), \frac{d\phi_2}{d\omega} = \left(\frac{dx_2}{d\omega}\right)\left(\frac{1}{E_2}\right)$$

so that

$$\frac{d\phi_s}{d\omega} = \left(\frac{d\phi_2}{d\omega}\right)\left(\frac{E_2}{E_s}\right), \text{ but}$$

$$E_2 = b \cdot E_1$$

$$E_s = (E_1 + E_2) = (1 + b)\ E_1 \text{ , and}$$

$$\left(\frac{d\phi_s}{d\omega}\right)_{\text{in-phase}} = \left(\frac{+b}{1+b}\right)\left(\frac{d\phi_2}{d\omega}\right) = \left(\frac{+b}{1+b}\right)\left(\frac{d}{c}\right) \ .$$

By applying a similar line of reasoning to the out-of-phase geometry of Fig. 5b, we may show that

$$\left(\frac{d\phi_s}{d\omega}\right)_{\text{out-of-phase}} = \left(\frac{-b}{1-b}\right)\left(\frac{d}{c}\right).$$

In the out-of-phase case the negative sign indicates that for $b < 1.0$, E_s will have a sense of rotation opposite to that of E_2. An idealized phase-frequency function is displayed in Fig. 6a and 6b. In both parts of the figure a carrier and sideband system is located on the frequency axis, with the carrier at a ϕ_s zero crossing, but in Fig. 6a the chosen crossing corresponds to E_1 and E_2 in-phase while in Fig. 6b the out-of-phase condition is chosen. It may be deduced from the phasor geometry that the shape of this phase function will be dependent only on the amplitude ratio b, while a change in target spacing will merely stretch or shrink the plot along the frequency axis, as indicated by the expression for peak separation shown in Fig. 6a:

$$\Delta\omega_{(\text{Peak})} = \frac{2\pi c}{d} = \frac{\pi c}{r} \ .$$

When T_1 is at a range other than zero, the periodic function shown will of course be superimposed on the uniform phase slope due to this original range displacement.

Recalling now that the relative phase rotation experienced by the adjacent lines in the spectrum of a periodic function is equal to the phase shift of the modulation envelope, we may deduce the effect of a two-element target on a narrow-band transmission of the sort shown in the figures. In Fig. 6a, where the signals reflected from the target elements are in phase at the carrier frequency, we have:

$$\Delta\phi_{\text{in}} = \left(\frac{+b}{1+b}\right)\left(\frac{d}{c}\right)\ \omega_p \ ,$$

assuming that we can take the phase slope to be uniform over the interval $(\omega_{\text{in}} \pm \omega_p)$. This means that apparent point of reflection will be shifted toward the more distant, weaker target by a fraction of the target spacing given by $[+b/(1 + b)]$. (The quantity b is taken to be positive and less than unity.) In the out-of-phase case of Fig. 6b, on the other hand, we have

$$\Delta\phi_{\text{out}} = \left(\frac{-b}{1-b}\right)\left(\frac{d}{c}\right)\omega_p \ ,$$

and again assuming that ω is small enough so that the phase slope may be taken as uniform, we may conclude that the relative sideband phase rotations will be always greater than those due to a propagation path d units long. Moreover, the multiplying factor, $[-b/(1 - b)]$ has a negative sign, so that the apparent envelope phase will correspond to a point of reflection closer to the radar than that of the stronger target

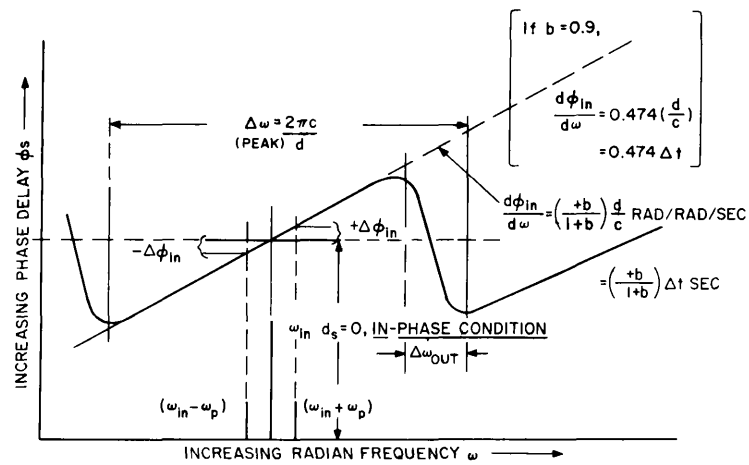

(a) With a carrier located at the in-phase zero crossing

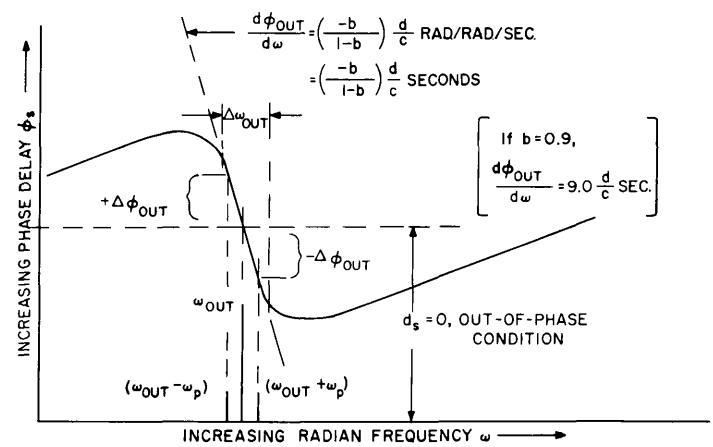

(b) With a carrier located at the out-of-phase zero crossing

Fig. 6 - Idealized phase-frequency function for a two-element target

element, T_1. It is these exaggerated phase shifts that can be produced by an out-of-phase signal relationship that may cause high levels of range noise to be generated by target scintillation.

At microwave frequencies many wavelengths may be contained in the length d, and a small motion of the target may shift the signal from a region of high phase slope to a region of low or nearly zero slope, with a corresponding shift in the apparent position of the target array. Figure 7 illustrates the apparent target positions produced when $b = 0.9$, with the transmitted spectrum assumed to be so narrow that all of the spectral lines are operated upon by the maximum slope factor at the out-of-phase point, $[-b/(1-b)]$. In the example shown, this factor is 9.0, and the apparent shift in position will be 9.0 times the element spacing; because of the negative sign this will represent a decrease in apparent range. At the in-phase point, the maximum positive shift occurs and is found to be 0.474 times the depth. (A value of $b = 0.9$ is not unrealistic experimentally, since a fading range of over 30 db is often experienced when viewing a water

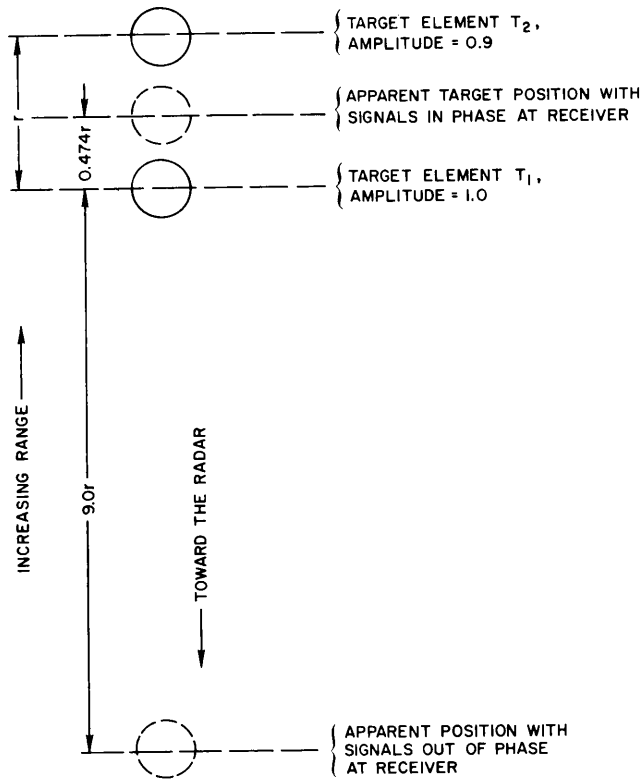

Fig. 7 - Apparent position in range of a two-element target array using narrow-band illumination

target at X band.) The range shifts diagrammed may be verified analytically for the narrow-band limit, and while the graphical result applies rigorously only in the limit, it may be expected to have useful application to practical systems using transmission bandwidths that are small compared to the high-slope frequency interval ($\Delta\omega_{out}$ in Fig. 6b). For those bandwidths for which this line of reasoning is valid, neither the exact nature of the modulating function nor the method of processing the received signal has any bearing on the amplitude of the scintillation noise. This will be true because, so far as the receiver is concerned, the alteration of the signal is exactly the same as that due to an actual change in range position, and there is no physical basis for rejecting the result as spurious. Thus pulse, AM-CW, FM-CW, and all other types of transmission will be subject to the same degree of scintillation range noise in the narrow-band case, and no type of receiver processing can lead in this case to the elimination of scintillation noise which occupies the same spectral region as the desired range function. It should be emphasized that the term narrow band is here used in the relative sense defined earlier, and that for targets only a few inches in depth the narrow-band theory may still apply for transmission bandwidths of the order of 100 Mc/sec.

When the transmission bandwidth is broadened so that the system of spectral lines extends beyond the region of high phase slope or extends over several phase periods ($\Delta\omega_{(Peak)} = 2\pi c/d$) the effects of target scintillation become much more complex, and the graphical spectrum point of view does not appear to be very useful in obtaining quantitative results. Consideration of the phase function does, however, strongly suggest that use of a sufficiently broad transmitted spectrum would prevent the maximum range displacements calculated for the narrow-band case from occurring. This would be expected,

since only a fraction of the spectral lines of the broad transmission would be affected by the maximum phase slopes at the out-of-phase points.

One might also suspect that the noise level for broadband transmissions would no longer be entirely unaffected by signal processing, since the amplitudes as well as the phases of the various spectral components will be differently affected. This turns out to be true in the FM-CW case, which has been examined in greatest detail.

RADAR SYSTEM CONSIDERATIONS IN OCEAN-WAVE PROFILING

General System Requirements

The selection of an optimum system for an airborne wave-profiling application is beyond the scope of the work reported here. However, a brief review of the basic factors seems indicated in order to place the analytical work on range noise in the proper perspective.

Any technique which can be applied to altimetry in general is a potential candidate for consideration in wave profiling, but, as discussed previously, there are special requirements to be met in the wave-profiling application that will decrease the desirability of some schemes and render others totally unsuitable. Some of the negative factors in wave profiling follow.

1. A relatively small illuminated patch is required, and consequently a narrow antenna beam. To obtain all of the ocean-wave data of interest to oceanographers, beamwidths of less than 3 degrees are needed at altitudes considered practical for the operation of fixed-wing aircraft.

2. As a further consequence of the small patch size, spatial averaging will be relatively poor, and the properties of the received signal will vary more drastically. The spectral distribution of these variations will extend to lower frequencies and will overlap the desired signal spectrum to a greater extent.

3. The required signal-information bandwidth will be relatively high, and it may not be possible to filter out the effects of microphonics and other sources of receiver noise. It is known from experimental results that it will never be possible to remove all the effects of scintillation range noise by filtering.

4. Because of the need to minimize scintillation noise at the source, the transmitted spectrum must be quite broad. A minimum of about 100 Mc/sec appears to be necessary to control target-noise levels in practical situations.

5. The precision of the range measurement must be relatively high by altimetry standards, and the percentage stability must be extremely high; at least on a short-term basis it must be of the order of a few parts in 1000, as compared to the 5-percent accuracy specification common in radio altimetry.

There are a few positive factors which favor the system designer in the wave-profiling application. Among these are the following.

1. The system will not be required to operate over a large range of altitude variation. A change of a few percent about the normal operational height may be all that must be accommodated. The modulating function may thus be optimized for this height, and critical distance phenomena and range ambiguities at other altitudes are not a factor.

2. The flight altitude chosen will be relatively low because of patch-size requirements and the increasing sensitivity to aircraft attitude at higher altitudes. Operation at 500 ft appears to provide a reasonable compromise, and this altitude will lead to relatively high average signal levels at the receiver. Receiver sensitivity can be relatively low, and control of local leakage effects is less critical. However, the advantage of a high average signal is partially offset by the larger dynamic fading range experienced with the small illuminated patch.

3. The system need not possess any range resolution (as opposed to ranging accuracy) capability, although some degree of discrimination will reduce the effects of local leakage and long-path undesired echoes.

To summarize, the following considerations apply to the design of a wave-profiling radar:

- The illuminated patch must be small enough to resolve the ocean waves of interest. This limitation means a diameter of no more than a few feet.

- Less spatial and time averaging will be possible than in altimetry.

- The signal-information spectrum will overlap the scintillation spectrum, so that all of the scintillation noise cannot be effectively filtered out.

- To control scintillation range noise at the source a broad transmitted spectrum must be used. This spectrum will probably need to have a width of 100 Mc/sec or greater.

- The range measurement must be precise, both in terms of absolute accuracy and percentage stability. (Incremental ranges of a few inches in several hundred feet must be sensed.)

- The system need not be operable over a wide range of altitudes.

- The altitude will always be low, a few hundred feet, and received power will always be relatively high.

- Possession of a range-resolution capability is not a fundamental requirement.

Some Possible Wave-Profiling Techniques

There are, of course, many alternative techniques that could be used as the basis for a wave-profiling radar, but it has not appeared obvious that any system proposed in the unclassified literature offers a clear-cut overall advantage over the wideband FM-CW concept that was employed in the current investigation. It seems clear that an ultra-short-pulse radar having a pulse length in space of the order of the physical depth of the target array would give results that could not be bettered by any other system. However, the realization of such a radar presents serious difficulties, including those connected with the preservation of a bandwidth of several thousand megacycles in all portions of the receiver ahead of the video range-tracking circuits. The high range-resolution capability of such a system is unimportant in the profiling situation; thus the technique appears to be wasteful from the viewpoint of design economics, even if technically at all feasible.

A pulse system having only the bandwidth needed to minimize scintillation noise offers the advantage of sufficient range resolution to gate out local leakage and other undesired echoes having long path differences, but whatever transmission bandwidth is dictated by range noise considerations must be preserved in the receiver through the i-f and video amplifiers. The provision of even moderate receiver sensitivity under these

conditions is costly, even though it is now technically quite straightforward. The system bandwidth required to effect a substantial reduction in scintillation noise would appear from the spectral-analysis point of view to be substantially the same as that for a CW system. The trend of the range noise for bandwidths covering many of the target phase intervals discussed in this analysis may differ from the FM-CW case in the same way that different types of FM-CW processing differ from each other, but it seems doubtful that any order-of-magnitude advantage would result from the use of a pulsed transmission. Only a rigorous theoretical analysis or an experimental comparison would definitely settle this point. Unless a decisive advantage does indeed exist in this respect, the additional complication and cost of the pulse system appears unjustified.

If pulse techniques are ruled out, there remain a number of ways of using a CW transmission. It appears that an AM-CW transmission employing a single modulating frequency will always be inferior to a properly chosen FM-CW signal covering the same spectrum. Again considering the effect of scintillation from the spectral-analysis point of view, it seems clear that the single pair of sidebands that exist in the AM case may be subjected to exaggerated phase rotations in spite of having a large spacing from the carrier. This rotation would also be true of an FM signal employing a high modulating frequency (50 to 100 Mc/sec) and a low modulation index, but there is no apparent reason for using such an FM transmission. An accompanying disadvantage of using a modulating frequency of this order is the large number of range ambiguities that would occur. At 50 Mc/sec these would be spaced less than 10 ft of altitude apart, much too closely for even the wave-profiling application. It thus appears that a CW wave-profile radar should use an only moderately high modulating frequency and a large enough frequency deviation to cover the desired spectral interval with closely spaced lines.

A paper by Saunders (18) reviews FM-CW techniques proposed prior to 1961 and includes an extensive bibliography. Most of the altimeter systems that have been discussed in the unclassified literature since that time appear to be derived more or less directly from one of the principles discussed in this paper, and while some of the newer systems offer important improvements in altimeter characteristics, their advantages in the wave-profiling application are currently unproven.

A frequently used FM-CW technique in altimetry has been that of mixing the echo signal with a fraction of the transmitted signal and measuring the average difference frequency produced. If linear frequency modulation is used, the beat frequency will be constant except during flyback or crossover intervals, and in any case the average value is proportional to the range delay. This principle is employed in the widely used AN/APN-22 aircraft altimeter (19) and could be adapted to wave profiling if the necessary accuracy and stability of the range measurement could be achieved, and if the quantization error could be made small enough.

The so-called "fixed error" or quantization interval is the range increment represented by a single beat cycle added to each modulation period and is thus the smallest range change which can be unambiguously sensed. It is given by

$$\Delta R = \frac{c}{4\Delta f}$$

where Δf is the peak-to-peak frequency deviation.

If

$$\Delta f = 1000 \text{ Mc/sec}$$

$$\Delta R = \frac{984 \times 10^6}{4000 \times 10^6} = 0.246 \text{ ft}$$

which is probably still too large if one-foot ocean waves are to be measured. A transmitted bandwidth of this order would certainly be more than adequate to minimize target-scintillation noise, but in view of the stringent range-accuracy requirement the system might be somewhat difficult to realize. Boesch and Hardinger (20) have proposed a technique in which an aperiodic linear slope modulation is used, which permits the system to interpolate within the quantization interval if an average is taken over a representative sample of the aperiodic function. Other techniques for avoiding the quantization of the height indication have been discussed by Kalmus (21) and Horton (22). In the case of these FM-CW systems the transmitted bandwidth of a wave-profile radar could be limited to that needed to control target noise, but the ranging precision would have to be improved over that which has been claimed for the altimeter prototypes.

Many other types of signal processing have been used in FM-CW ranging systems, and in most cases only a detailed design analysis can lead to a useful conclusion. Systems which need amplification for processing of the entire received signal spectrum, or even of the entire beat spectrum in the homodyne case, may require inconveniently large amplifier bandwidths in the wave-profile situation. On the other hand, when only a portion, for example a single line, of a beat spectrum is selected and made the basis for range measurement, it is not obvious that all of the information contained in the received wave has been utilized. The result may not be equivalent to that given by a system which senses the modulation envelope with a broadband discriminator accepting the entire received spectrum, or processes the entire spectrum in some other way as in a short-pulse system.

The NRL Broadband FM-CW Radar

The experimental wave-profile radar will now be discussed briefly with regard to the system considerations that have been outlined. The basic elements of the radar have been diagrammed in Fig. 2. The carrier frequency of 9.51 Gc/sec permits the patch-size requirement to be met with antennas of reasonable size. Parabolic reflectors 30 in. in diameter were used during both the earlier aircraft experiments and at the Bay Bridge site and produced a main lobe having a half-power beamwidth of a little over 3 degrees and side lobes with peaks from 22 to 30 db below the main lobe. At the Bay Bridge height of 62 ft the diameter of the half-power circle on the water was a little under 4 ft.

The use of a backward-wave oscillator which is frequency modulated by swinging the electrode voltages gives the system a bandwidth capability of several hundred megacycles per second, and the frequency deviation and hence the spectrum width used can be readily and continuously varied. The choice of sinusoidal single-frequency modulation and a phase-sensing receiver leads to a simple receiver lineup, with the amplifiers following the frequency discriminator required to handle only the information bandwidth of the system. The modulating frequency of 2.215 Mc/sec is high enough to make the phase-measurement problem uncritical and in an airborne installation still permits some wander of the aircraft from the operational height without appreciable degradation of the incremental height accuracy. This technique also permits a continuous measurement of the incremental range without any quantization errors or other discontinuities in the height function. The system as illustrated does not possess any range-resolution capability and is thus vulnerable to undesired signals arriving at the receiver over all possible paths. In practice it has been found possible to keep the effects of local leakage and long spurious paths relatively small, so that the residual range noise is largely due to target multipath phenomena occurring within the illuminated patch.

During the Chesapeake Bay Bridge Facility experiments it was found desirable to add a traveling-wave tube and leveler chain to the basic wave-profile radar system.

The action of the leveler as used here is that of a fast-acting agc loop, and the bandwidth of the leveler control circuits could be extended to 50 kc/sec, which was sufficient to accommodate any fading rate encountered under fixed-installation conditions. The effect of using the levelers was to extend the dynamic range of the receiving system and reduce the direct effect of amplitude variation to a very small value, so that the height noise recorded was almost entirely due to the multipath modulation phase shifts which were to be studied. Under other circumstances, where the noise itself is not under quantitative investigation and filtering is used to smooth the profile record, a lesser dynamic range might be acceptable. Under this condition direct amplitude effects would be greatly reduced by the filter, and improvement of the amplitude characteristic beyond that provided by the postdetection limiters might not be justified. It should be emphasized that the amplitude effects discussed here are those that occur at the fading or scintillation rate and are the result of the unavoidable small residual phase shifts which occur in the receiver as a function of input-signal amplitude. The leveler chain reduces these phase shifts by providing a nearly constant rf input to the discriminator crystals and hence to the following amplifier-limiters. The leveler does not act rapidly enough to remove modulation-frequency amplitude modulation on the received wave and is not a limiter or instantaneous clipper in the sense in which these terms are normally used. True limiting with TWT's is possible over a restricted dynamic range. However, the TWT's available for the Bay Bridge work could not be set up to give effective limiting action over the range of fading experienced, and this mode of system operation was not investigated. The augmented FM-CW radar in use at the Bay Bridge Facility is diagrammed in Fig. 8.

THEORETICAL ANALYSIS OF SCINTILLATION RANGE NOISE IN AN FM-CW RADAR

Balanced Interferometer Discriminator

With an FM-CW radar, the returns from two targets at range delays M and $M + N$ seconds are given by:

$$A = \sin[\omega(t - M) + m \sin p(t - M)]$$

and

$$B = b \sin[\omega(t - M - N) + m \sin p(t - M - N)]$$

where ω is the carrier frequency in radians per second, p is the modulation frequency in radians per second, m is the index of modulation, and b is the relative target strength. When the radar receiver consists of a balanced interferometer discriminator, its output is:

$$E_0 = (A + B - C - D)^2 - (A + B + C + D)^2,$$

where

$$C = \sin[\omega(t - M - \sigma) + m \sin p(t - M - \sigma)]$$

$$D = b \sin[\omega(t - M - N - \sigma) + m \sin p(t - M - N - \sigma)]$$

and σ is the added delay, in seconds, of the longer arm of the discriminator. Performing the indicated operations, assuming an ideal square-law detector, replacing ωT by $2n\pi + \theta$, and keeping only those terms that contain the fundamental of the modulation frequency, the receiver output becomes:

$$E_0 = \sin \omega\sigma \left\{ J_1(X) \cos p[t - (2M + \sigma)/2] + b^2 \cos p[t - (2M + 2N + \sigma)/2] + b \cos\theta\, [J_1(Y) - J_1(Z)] \cos p[t - (2M + N + \sigma)/2] \right\} \tag{1}$$

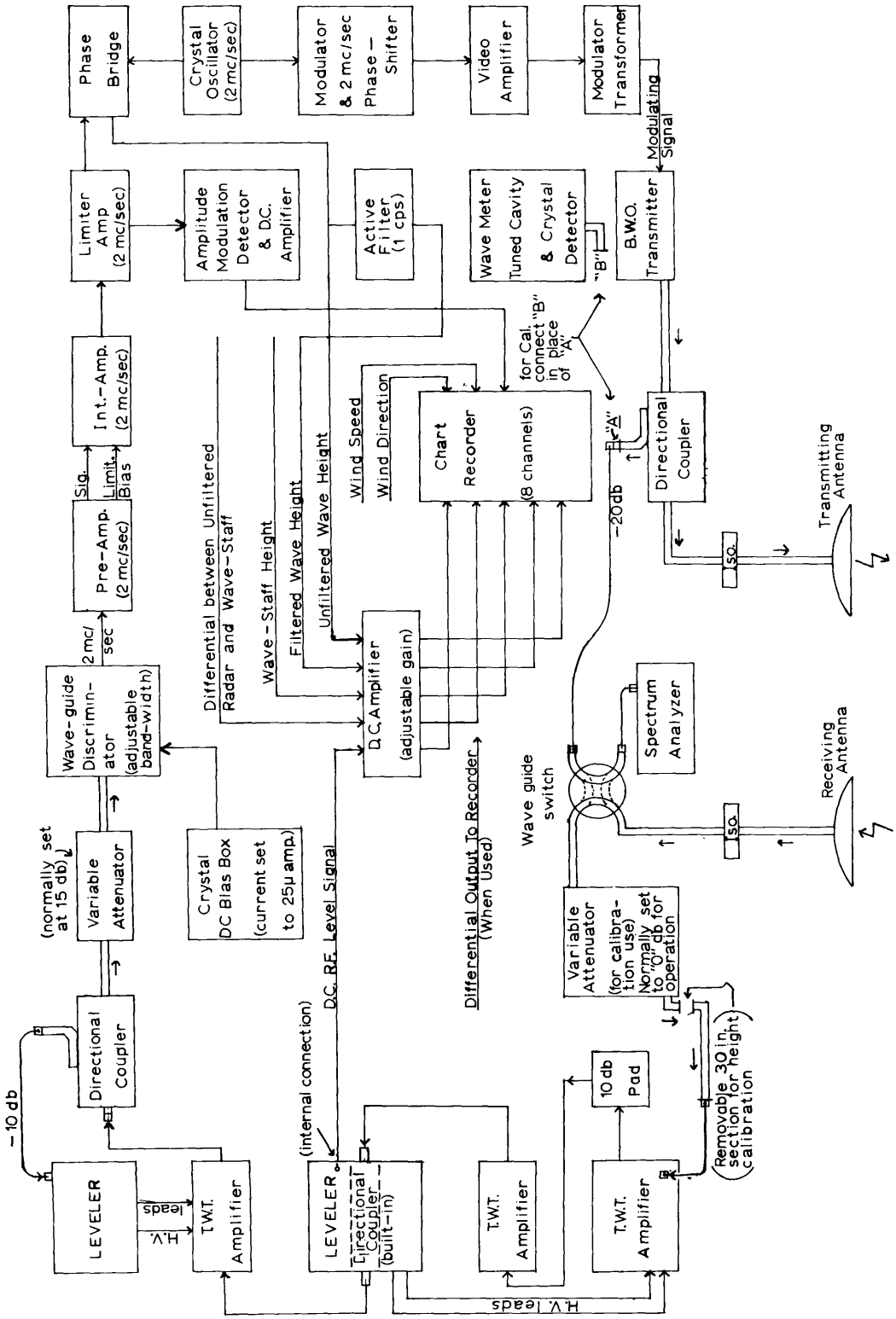

Fig. 8 - Experimental FM-CW wave-profiling radar

where J_1 indicates the first-order Bessel function of the first kind, $X = 2m \sin p(\sigma/2)$, $Y = 2m \sin p[(N+\sigma)/2]$, $Z = 2m \sin p[(N-\sigma)/2]$, and θ is the rf phase difference between the two returns. For the receiver output to be a maximum, both $\sin \omega\sigma$ and $J_1(X)$ have to be near their maximum values. If ω is large compared to $pm = 2\pi\Delta F$, there is no conflict between the conditions. The quantity $J_1(X)$ has a very broad maximum around $X = 1.841$. For $m > 0.921$, the optimum value of σ is given by:

$$\sigma = (2/p) \sin^{-1} (0.921/m).$$

If $m > 10$, σ is accurately given by:

$$\sigma = 1.841/pm = 0.293/\Delta F.$$

The calculated value of σ is adjusted so that $|\sin \omega\sigma| = 1$. The maximum adjustment is approximately equal to $(5/6)(\Delta F/F_0)$, where F_0 is the rf carrier frequency. With ΔF as large as 30 percent of F_0, the value of $J_1(X)$ will be within 10 percent of its maximum value. At smaller values of ΔF, the adjustment of σ has little effect on the value of $J_1(X)$. When $m < 0.921$, $J_1(X)$ cannot attain its maximum value. The value of $\sin p(\sigma/2)$ is set equal to one by making

$$\sigma = \pi/p = 1/2f_m,$$

where f_m is the frequency of the modulating signal. This result gives $J_1(X)$ the largest value possible for the index of modulation that has been used.

Range delay, in this paper, is defined as the difference in seconds between the single-target delay and the composite-target delay. The single-target delay is $1/p$ times the phase angle of E_0, when $b = 0$, and is found to be $M + \sigma/2$. The range delay is given by

$$\alpha = (1/p) \tan^{-1} \left[\frac{b J_1(X) \sin pN + b \cos\theta \, [J_1(Y) - J_1(Z)] \sin pN/2}{J_1(X) \, [1 + b^2 \cos pN] + b \cos\theta \, [J_1(Y) - J_1(Z)] \cos pN/2} \right]. \tag{2}$$

From the sign convention that has been used, a negative range delay indicates an apparent shift of the composite target towards the radar. Figure 9 shows plots of range delay, in units of the discriminator delay, for several values of b. The abscissa is calibrated in units of N/σ and $mpN/2\pi = \Delta F \cdot N$. The curves show the extremes of possible range delay, i.e., $\theta = 0$ or $\theta = \pi$. Upon examination of the range delay, Eq. (2), several properties of the curves can be determined. For N/σ near zero, the rf in-phase $(\theta = 0)$ curve has a slope $b/(1+b)$, and the out-of-phase $(\theta = \pi)$ curve has a slope of $-b/(1-b)$. The range delay for quadrature rf phase $(\theta = \pm\pi/2)$ has a slope of $b^2/(1+b^2)$, which is also the locus of the $\theta = 0$ and $\theta = \pi$ curve crossings. The behavior of the function $[J_1(Y) - J_1(Z)]$ gives more information about the curves. When N/σ is near zero, the function is almost equal to $2J_1(X)$. This result gives the in-range peak to the $\theta = \pi$ curve. When $N/\sigma = 2$, the function is approximately equal to $-1.6\, J_1(X)$. This result gives the in-range peak to the $\theta = 0$ curve; the peak reaches a maximum for b near 0.5. The first two zeros of the function occur at N/σ slightly greater than one and slightly less than three, and are indicated on the plots as the points where the two curves cross. When using the $\Delta F \cdot N$ scale factor, two things should be remembered. One is that the scale factor is good only for those values of p and N such that $\sin p(N/2) \approx pN/2$, and, two, that σ is proportional to $(\Delta F)^{-1}$. The curves indicate that as ΔF is increased, the spread of the range delays about the $b^2N/(1+b^2)$ line decrease. As a matter of interest, Fig. 10 shows plots of receiver output for various values of b. The zero-db reference corresponds to the receiver output in the single target case. The plots show the output for $\theta = 0$ and $\theta = \pi$.

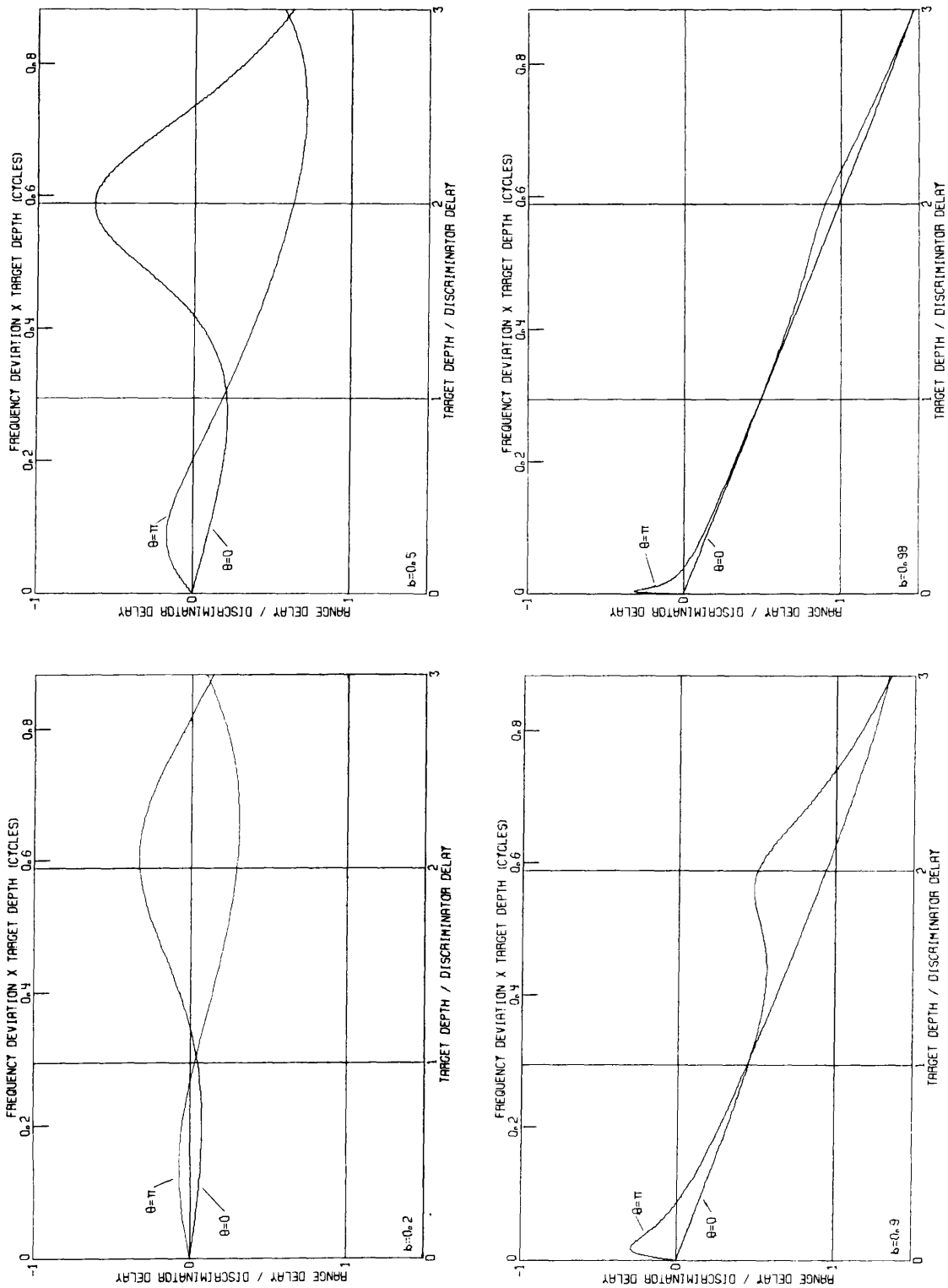

Fig. 9 - Range-delay curves for an interferometer discriminator

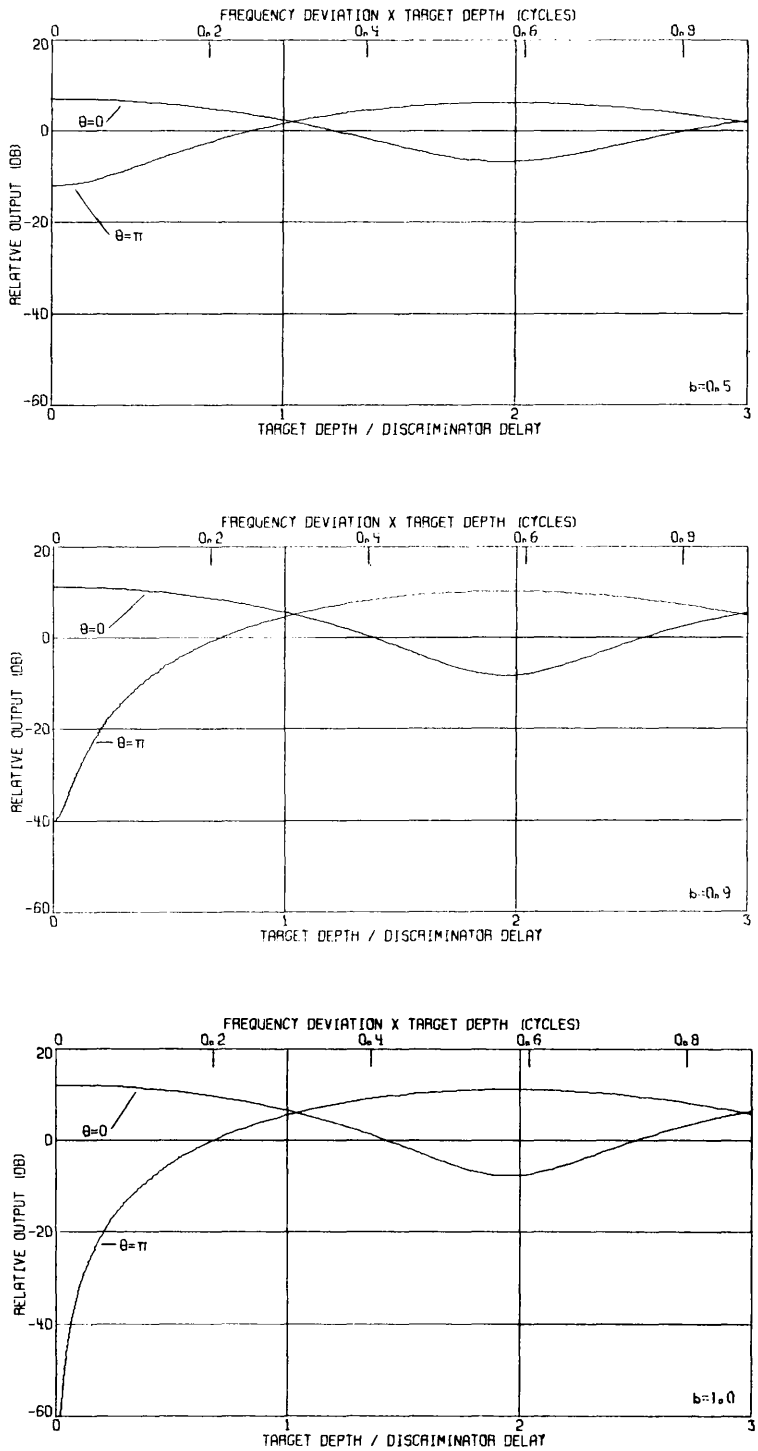

Fig. 10 - Modulation frequency output of an interferometer discriminator

Table 1
Radar Parameters for a Modulation Frequency of 2.215 Mc/sec

m	σ (nanosec)	ΔF (Mc/sec)	$1/\Delta F$ (nanosec)
8.5	15.525	18.83	53.114
16.5	8.025	36.55	27.362
30.0	4.025	66.45	15.049
50.0	2.625	110.75	9.029
87.0	1.525	192.71	5.189

Figure 11 is a plot of the extremes of range delay possible if b is allowed to assume any value between zero and one. Table 1 lists M, σ, ΔF, and $1/\Delta F$ for the modulation frequency used in the experimental work. The last column in the table is used to convert the upper scale on the figures to T in nanoseconds. Figures 12, 13 and 14 are plots of range delay in units of target depths versus target depth or index of modulation for several values of m and b. In these plots, $p = 4.430\pi \times 10^6$ rad/sec. Figure 15 shows plots of typical relative error in range delay versus rf phase curves. The plots show that the in-range delay peak is much narrower than the out-range delay peak, independent of the rf phase generating the peak. In all of the above figures, and in most of the figures to follow, if the delayed target becomes the stronger one, the curves rotate 180 degrees about the zero range-delay axis. This axis then becomes the apparent location of the delayed target.

In practice perfectly matched diodes are generally not to be found. Where β and γ are the diode efficiencies in the two arms of the discriminator, the receiver output is:

$$\begin{aligned} E_0 &= \beta(A + B - C - D)^2 - \gamma(A + B + C + D)^2 \\ &= \sin \omega\sigma \Big[(\beta+\gamma)\big\{J_1(X)\cos p(t - M - \sigma/2) + b^2 \cos p(t - M - N - \sigma/2) \\ &\quad + b\,[J_1(Y) - J_1(Z)]\cos\theta \cos p\,[t - M - (N+\sigma)/2]\big\} \\ &\quad + b\,(\beta - \gamma)\,\sin\theta\, J_1(G)[\cos p\,(t - M - N/2) + \cos p\,(t - M - \sigma - N/2)]\Big] \end{aligned}$$

where $G = 2m \overline{\sin}\, p(N/2)$. The range delay is given by:

$$a = (1/p)\tan^{-1} \frac{\left[\begin{array}{l}(\beta+\gamma)\, b^2 J_1(X)\sin pN + b\cos\theta[J_1(Y) - J_1(Z)]\sin pN/2 \\ + b(\beta-\gamma)\, J_1(G)\sin\theta[\sin pN/2 + \sin p(\sigma + N/2)]\end{array}\right]}{\left[\begin{array}{l}(\beta+\gamma)\, J_1(X)[1 + b^2\cos pN] + b\cos\theta\,[J_1(Y) - J_1(Z)]\cos pN/2 \\ + b(\beta-\gamma)\, J_1(G)\sin\theta\,[\cos pN/2 + \cos p\,(\sigma + N/2)]\end{array}\right]}$$

It is seen that the rf in-phase and out-of-phase ($\theta = 0$ and $\theta = \pi$) range-delay curves are not changed, and that a quadrature rf phase term has been added. The first two maxima of the quadrature term occur at $N \approx \sigma$ and 3σ. If $|\beta - \gamma| \leq 0.2$, the range delay due to the quadrature term will be less than $\pm 0.05\sigma$.

One problem present in wideband FM transmitters is the presence of amplitude modulation on the output. The two-target return for an FM signal with fundamental AM is:

$$A = [1 + \delta \cos p\,(t - M)]\sin[\omega(t - M) + m \sin p(t - M)]$$

and

$$B = b[1 + \delta \cos p(t - M - N)]\sin[\omega(t - M - N) + m \sin p(t - M - N)]$$

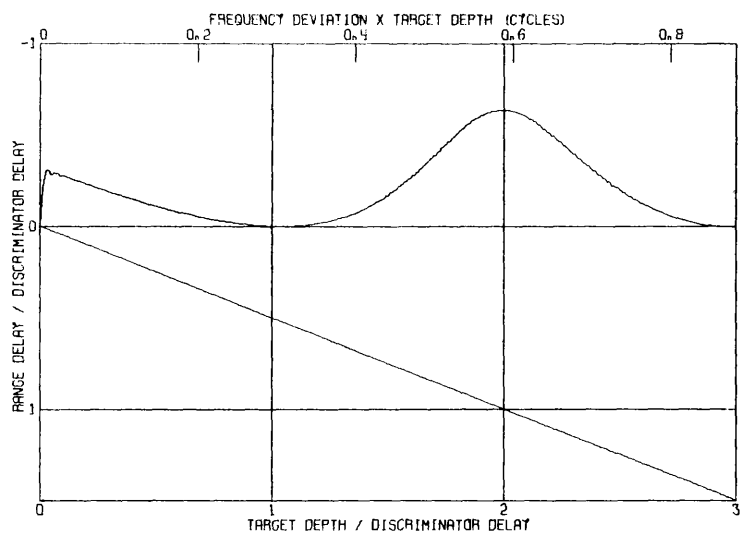

Fig. 11 - Extremes of range delay for an interferometer discriminator

where δ is the percent AM. The receiver output becomes:

$$
\begin{aligned}
E_0 = \sin \omega\sigma \Big[& [(2 + \delta^2 \cos p\sigma) J_1(X) - (\delta^2/2) J_3(X)] \\
& [\cos p(t - M - \sigma/2) + b^2 \cos p(t - M - N - \sigma/2)] \\
& + b \cos \theta \, [2 + \delta^2 \cos p(N + \sigma)] J_1(Y) - [2 + \delta^2 \cos p(N - \sigma)] J_1(Z) \\
& - (\delta^2/2)[J_3(Y) - J_3(Z)] \cos p[t - M - (N + \sigma)/2] \\
& + b\delta \sin \theta \cos p[(N + \sigma)/2] [J_0(Y) - J_2(Y)] \\
& - \cos p[(N - \sigma)/2][J_0(Z) - J_2(Z)] \cos p[t - M - (N + \sigma)/2] \\
= \sin \omega\sigma \Big[& (AA)[\cos p(t - M - \sigma/2) + b^2 \cos p(t - M - N - \sigma/2)] \\
& + b[(BB) \cos \theta + \delta(CC) \sin \theta] \cos p[t - M - (N + \sigma)/2] \Big].
\end{aligned}
$$

Mirror symmetry has been assumed in choosing the phase of the AM, because the AM is generated by physical devices that have no hysteresis.

The range delay is given by:

$$
a = (1/p) \tan^{-1} \left[\frac{b^2(AA) \sin pN + b[(BB) \cos \theta + \delta(CC) \sin \theta] \sin pN/2}{(AA)(1 + b^2 \cos pN) + b[(BB) \cos \theta + \delta(CC) \sin \theta] \cos pN/2} \right].
$$

If the AM is second harmonic, the target returns are:

$$
A = [1 + \delta \cos 2p(t - M)] \sin[\omega(t - M) + m \sin p(t - M)]
$$

and

$$
B = b[1 + \delta \cos 2p(t - M - N)] \sin[\omega(t - M - N) + m \sin p(t - M - N)].
$$

The receiver output becomes:

$$
\begin{aligned}
E_0 = \sin \omega\sigma \Big[& (2 + \delta \cos p\sigma + \delta^2 \cos 2p\sigma) J_1(X) - [\delta \cos p\sigma + (\delta^2/2)] J_3(X) \\
& + (\delta^2/2) J_5(X) [\cos p(t - M - \sigma/2) + b^2 \cos p(t - M - N - \sigma/2)] \\
& + b \cos\theta [2 + \delta \cos p(N + \sigma) + \delta^2 \cos 2p(N + \sigma)] J_1(Y) \\
& - [2 + \delta \cos p(N - \sigma) + \delta^2 \cos 2p(N - \sigma)] J_1(Z) \\
& - [\delta \cos p(N + \sigma) + (\delta^2/2)] J_3(Y) \\
& + [\delta \cos p(N - \sigma) + (\delta^2/2)] J_3(Z) \\
& + (\delta^2/2)[J_5(Y) - J_5(Z)] \cos p[t - M - (N + \sigma)/2] \Big] \\
= \sin \omega\sigma \Big[& (DD)[\cos p(t - M - \sigma/2) + b^2 \cos p(t - M - N - \sigma/2)] \\
& + b(EE) \cos \theta \cos p[t - M - (N + \sigma)/2] \Big].
\end{aligned}
$$

The range delay is given by:

$$
a = (1/p) \tan^{-1} \left[\frac{b^2(DD) \sin pN + b(EE) \cos \theta \sin pN/2}{(DD)(1 + b^2 \cos pN) + b(EE) \cos \theta \cos pN/2} \right].
$$

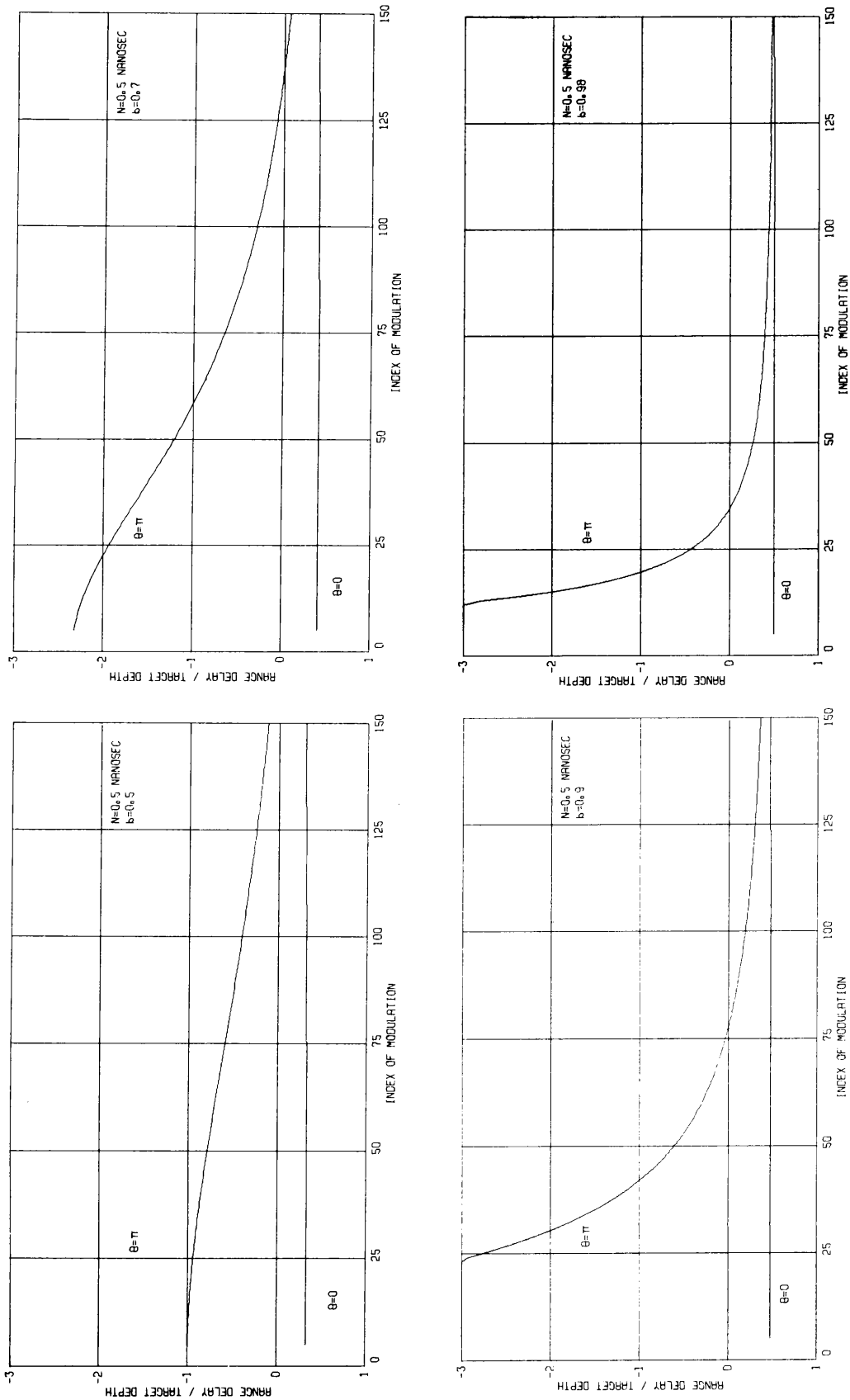

a. N = 0.5 nsec

Fig. 12 - Range delay versus index of modulation

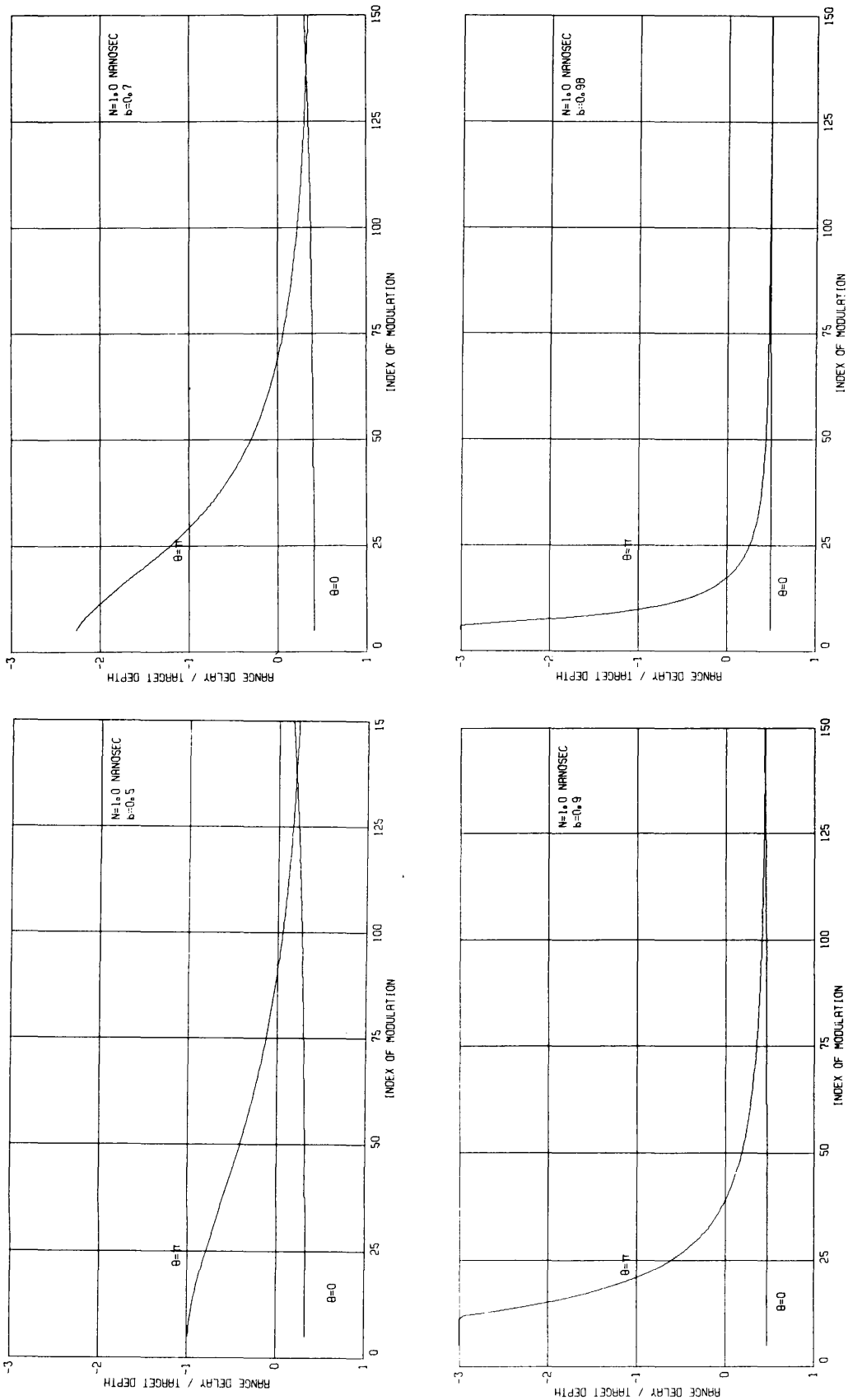

b. N = 1.0 nsec

Fig. 12 (Cont'd) - Range delay versus index of modulation

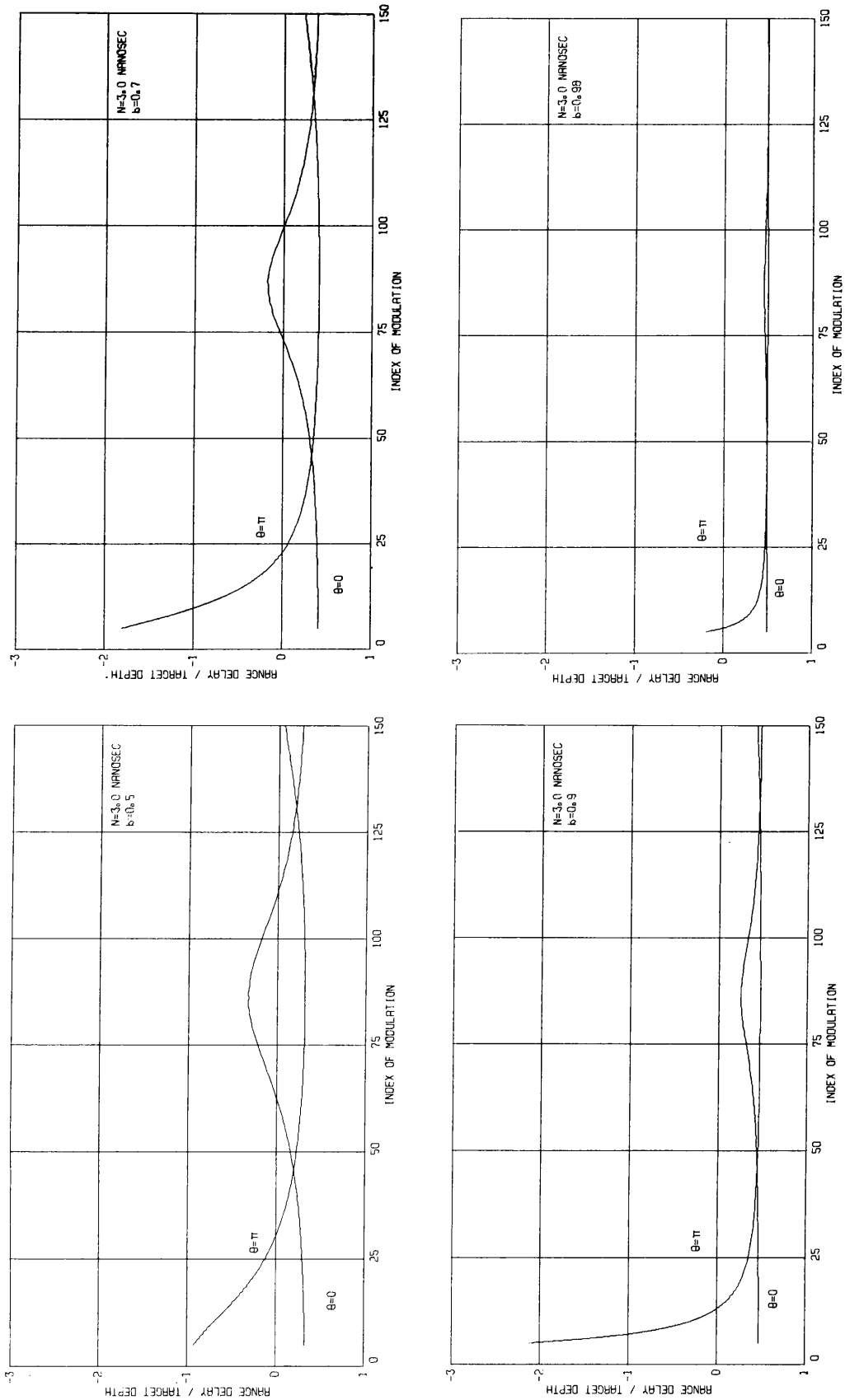

a. N = 3.0 nsec

Fig. 13 - Range delay versus index of modulation

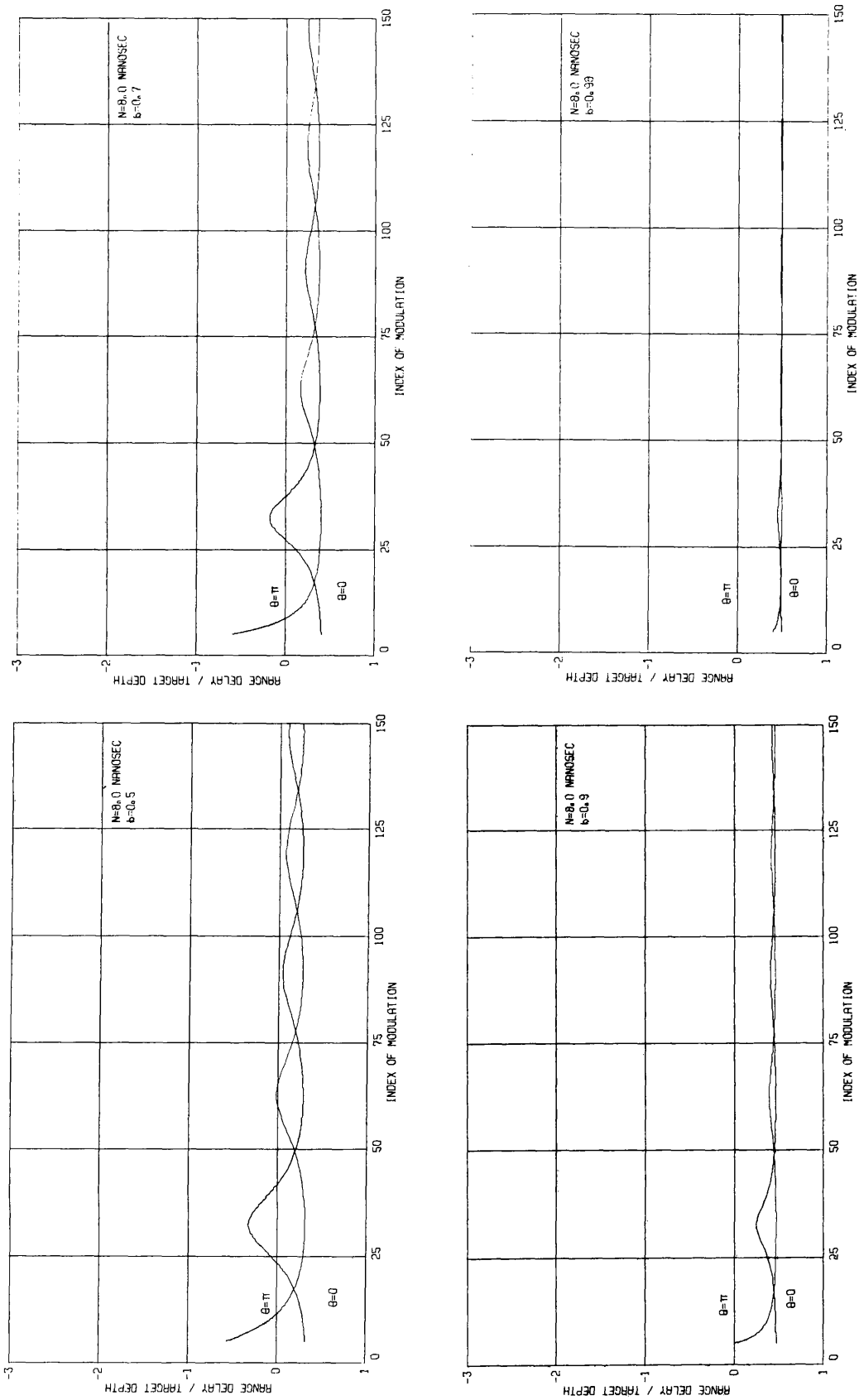

b. N = 8.0 nsec

Fig. 13 (Cont'd) - Range delay versus index of modulation

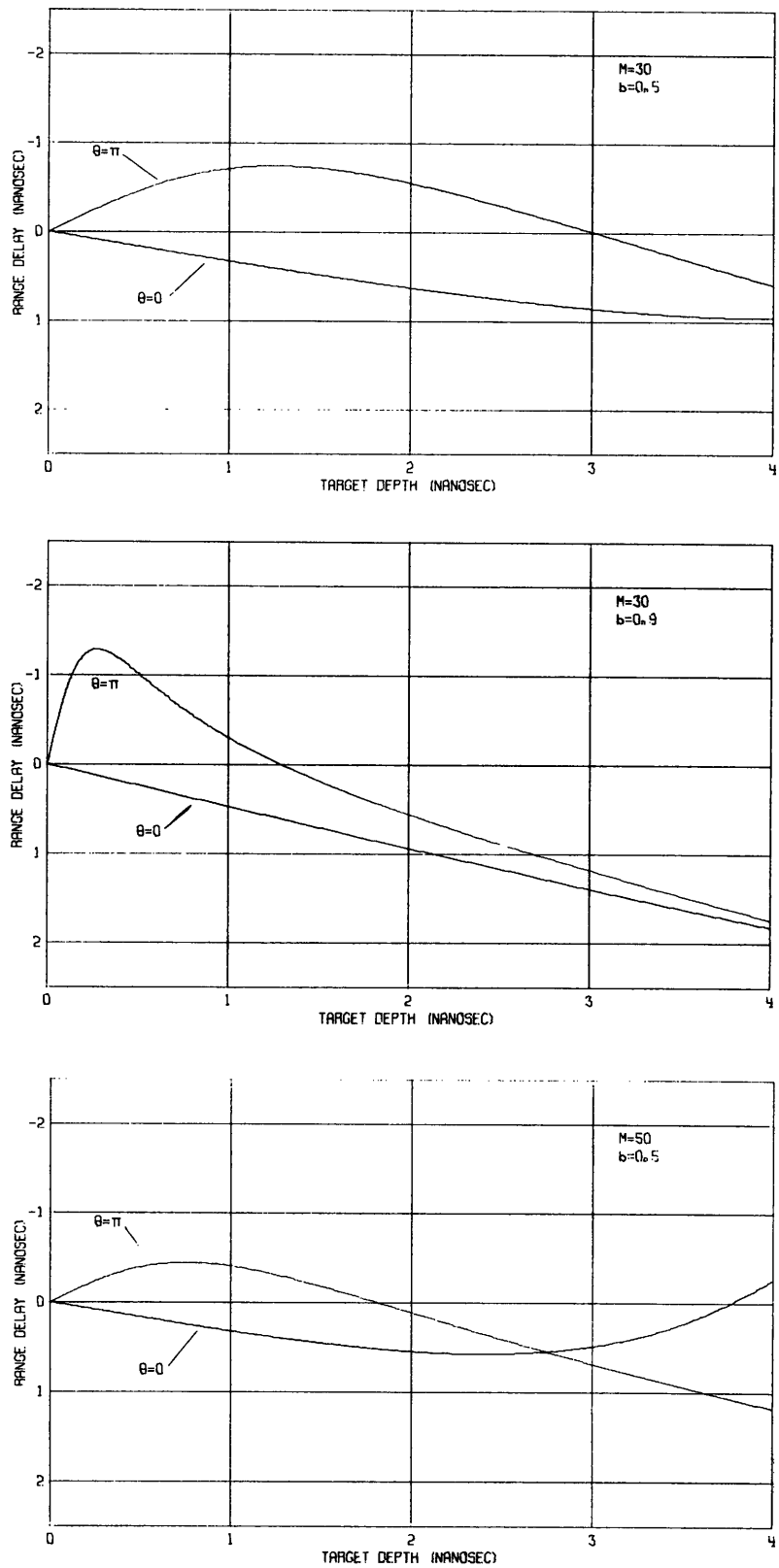

Fig. 14 - Range delay versus target depth

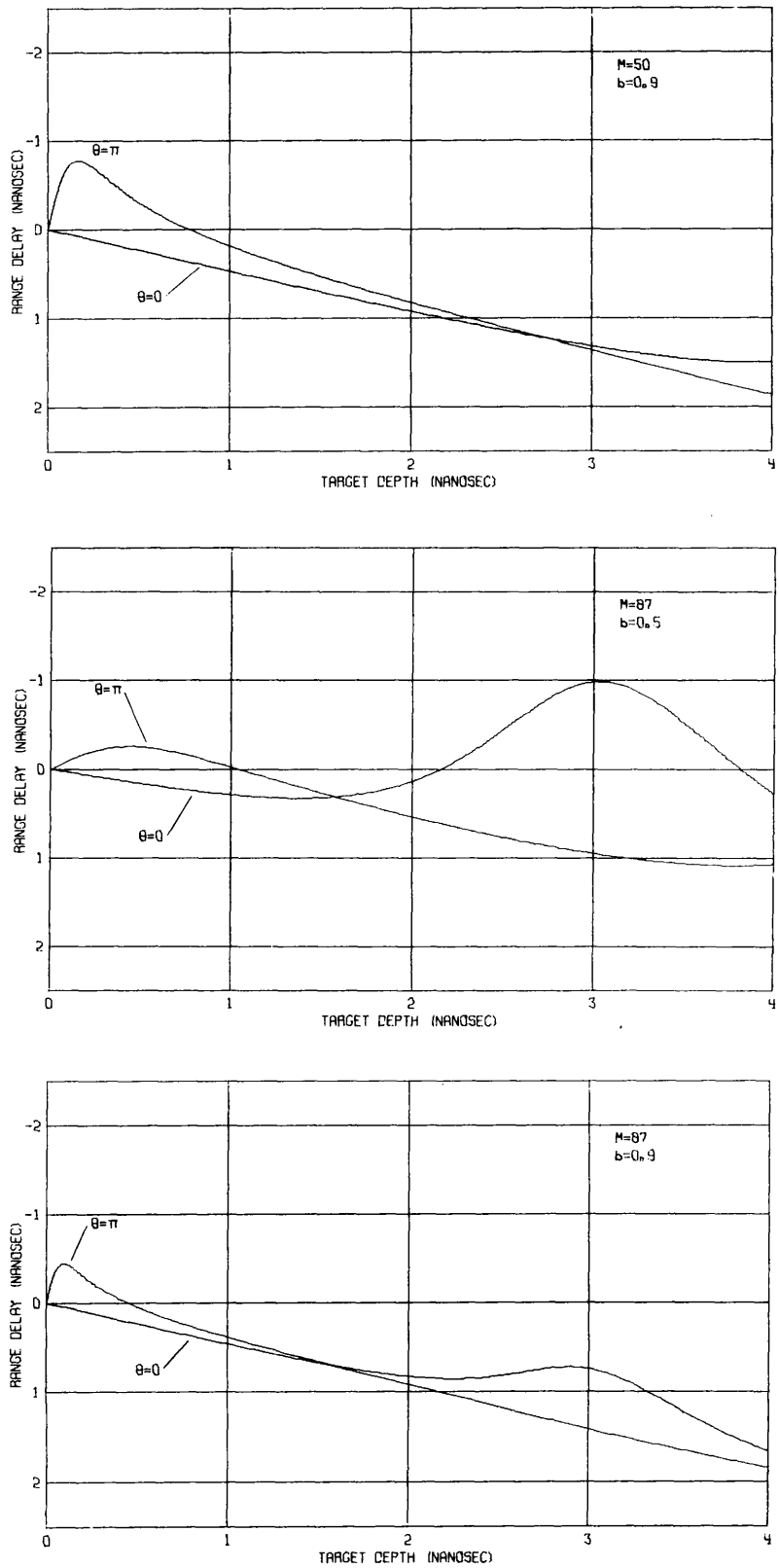

Fig. 14 (Cont'd) - Range delay versus target depth

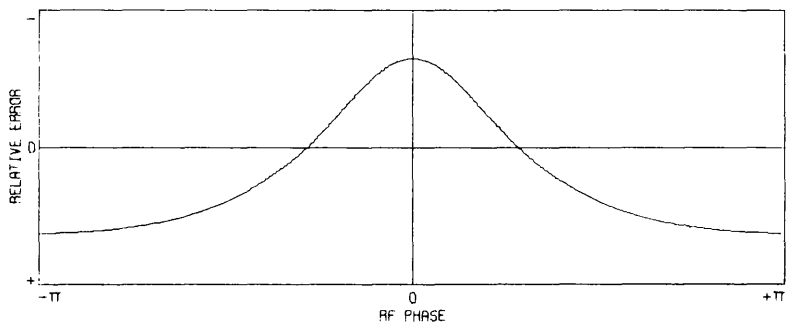

a. $\theta = 0$ gives in range delay

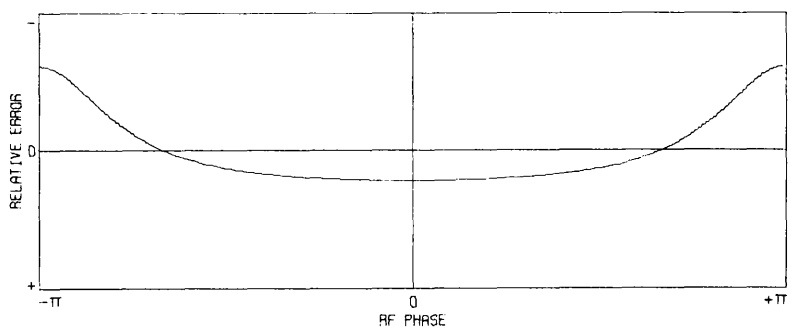

b. $\theta = \pi$ gives in range delay

Fig. 15 - Relative error in range delay versus rf phase angle θ

Figures 16, 17, and 18 show that the amplitude modulation has only a small effect on the range-delay curves. Figure 16 shows the range delay for 50-percent fundamental AM, $\theta = 0$ and $\theta = \pi$, and for several values of b. Figure 17 is also for 50-percent AM, but $\theta = \pm \pi/2$. Figure 18 shows the range delay for 50-percent second-harmonic AM with $\theta = 0$ and $\theta = \pi$. The 50-percent AM used for these plots is considerably more than would be expected in most physical systems. Figures 16 and 18 can be compared to Fig. 9. With no AM, Fig. 17 becomes a straight line with a slope of $b^2/(1 + b^2)$.

An investigation of the three-target case was made to see if it would give some additional information about the FM-CW radar behavior. The mathematical manipulation is essentially the same as for the two-target case, with the addition of the terms:

$$E = z \sin [\omega(t - M - \mu) + m \sin p(t - M - \mu)]$$

and

$$F = z \sin [\omega(t - M - \mu - \sigma) + m \sin p(t - M - \mu - \sigma)]$$

where z is the relative strength and μ is the delay, in seconds, of the third target (T_3). The other terms have been defined previously. Using the same conditions that were used in the two-target case, plus letting $\omega\mu = 2n\pi + \phi$, the receiver output is:

$$\begin{aligned} E_0 &= (A + B + E - C - D - F)^2 - (A + B + E + C + D + F)^2 \\ &= \sin \omega\sigma \Big[J_1(X)[\cos p(t - M - \sigma/2) + b^2 \cos p(t - M - N - \sigma/2) \\ &\qquad + z^2 \cos p(t - M - \mu - \sigma/2)] \\ &\quad + b\,[J_1(Y) - J_1(Z)] \cos\theta \cos p[t - M - (N + \sigma)/2] \\ &\quad + z\,[J_1(U) - J_1(V)] \cos\phi \cos p[t - M - (\mu + \sigma)/2] \\ &\quad + bz\,[J_1(P) - J_1(Q)] \cos(\theta - \phi) \cos p\,[t - M - (N + \mu + \sigma)/2] \Big]. \end{aligned}$$

where

$$U = 2m \sin p\,[(\mu + \sigma)/2]$$

$$V = 2m \sin p[(\mu - \sigma)/2]$$

$$P = 2m \sin p[(N - \mu + \sigma)/2]$$

$$Q = 2m \sin p[(N - \mu - \sigma)/2].$$

The rf phase difference between the reference and the third target is given by ϕ. The range delay is given by:

$$a = (1/p) \tan^{-1} \frac{\left[\begin{array}{l} (b^2 \sin pN + z^2 \sin p\mu)\, J_1(X) + b[J_1(Y) - J_1(Z)] \cos\theta \sin pN/2 \\ + z\,[J_1(U) - J_1(V)] \cos\phi \sin p\mu/2 \\ + bz[J_1(P) - J_1(Q)] \cos(\theta - \phi) \sin p\,(N + \mu)/2 \end{array}\right]}{\left[\begin{array}{l} (1 + b^2 \cos pN)\, J_1(X) + b\,[J_1(Y) - J_1(Z)] \cos\theta \cos pN/2 \\ + z^2\, J_1(X) \cos p\mu + z[J_1(U) - J_1(V)] \cos\phi \cos p\mu/2 \\ \pm bz[J_1(P) - J_1(Q)] \cos(\theta - \phi) \cos p(N + \mu)/2 \end{array}\right]}.$$

Since the range delay is a complicated function of several variables, it is difficult to predict the behavior of any particular combination. Figures 19, 20, and 21 show

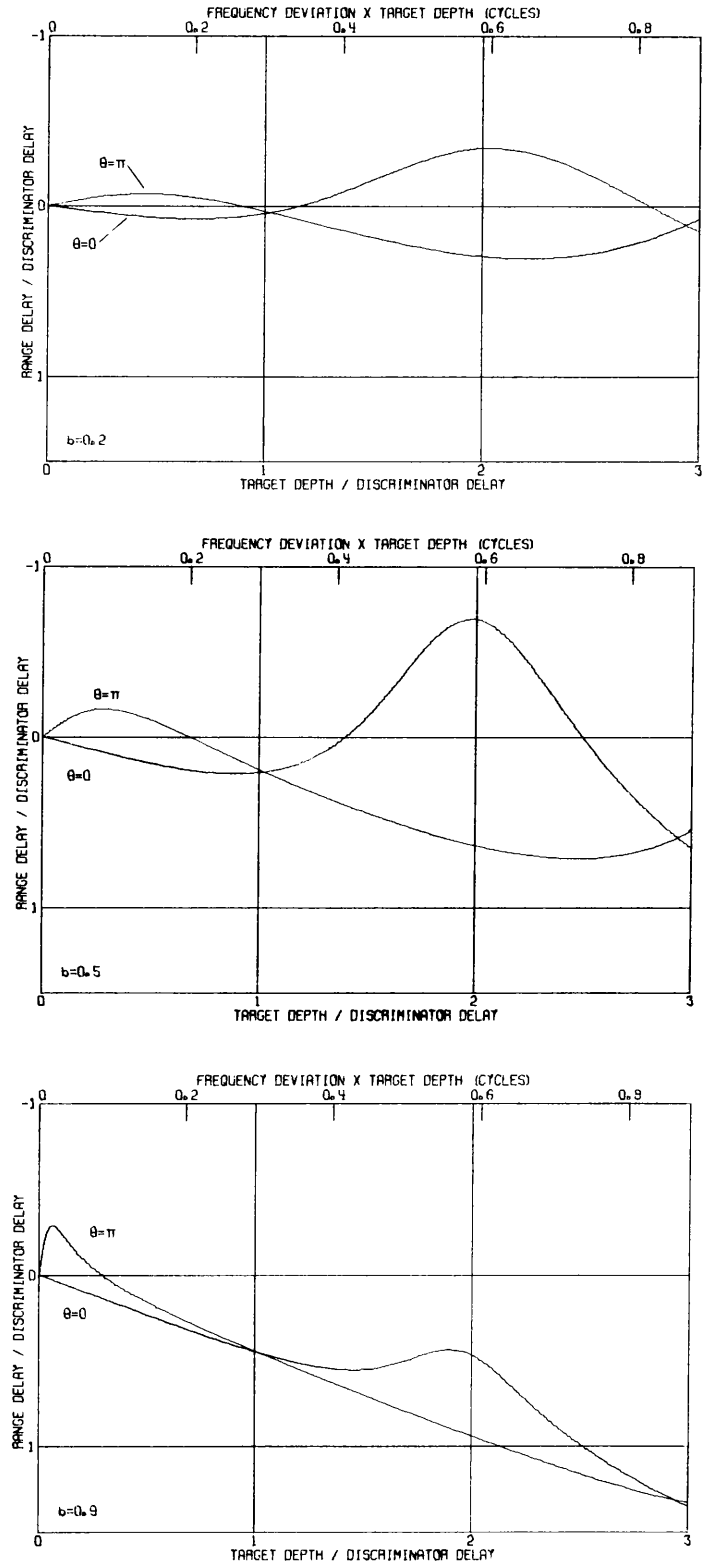

Fig. 16 - Range-delay curves for an interferometer discriminator. The modulation signal contains 50 percent fundamental-frequency amplitude modulation. $\theta = \pi$, $\theta = 0$.

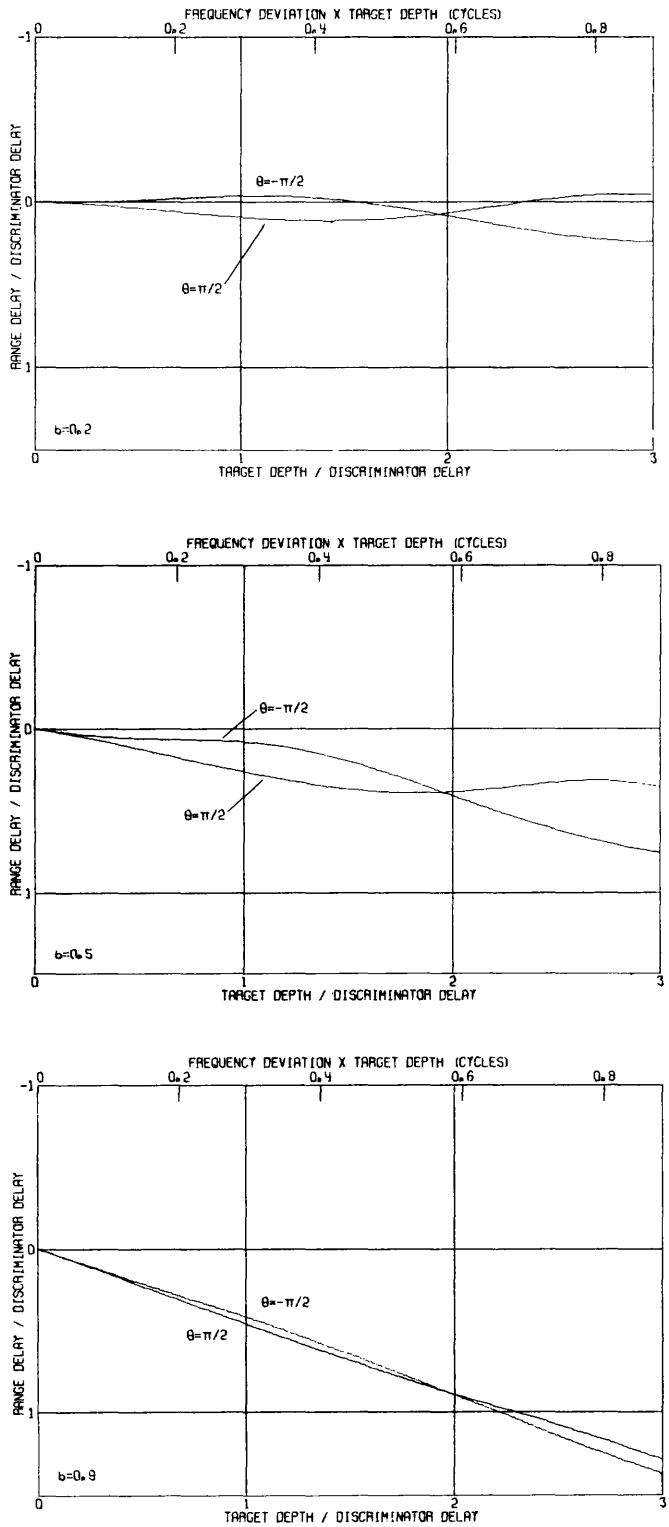

Fig. 17 - Range-delay curves for an interferometer discriminator. The modulation signal contains 50 percent fundamental-frequency amplitude modulation. $\theta = \pi/2$, $\theta = -\pi/2$.

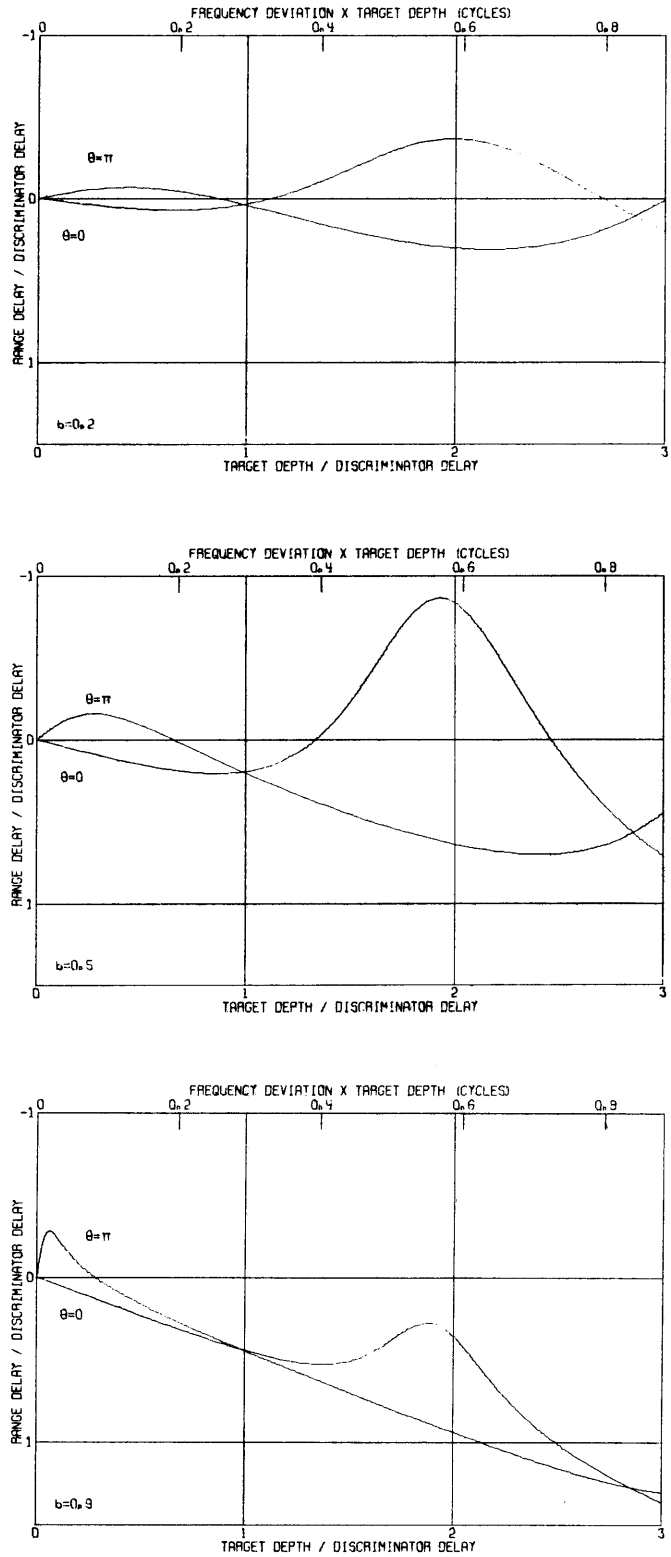

Fig. 18 - Range-delay curves for an interferometer discriminator. The modulation signal contains 50 percent second-harmonic amplitude modulation.

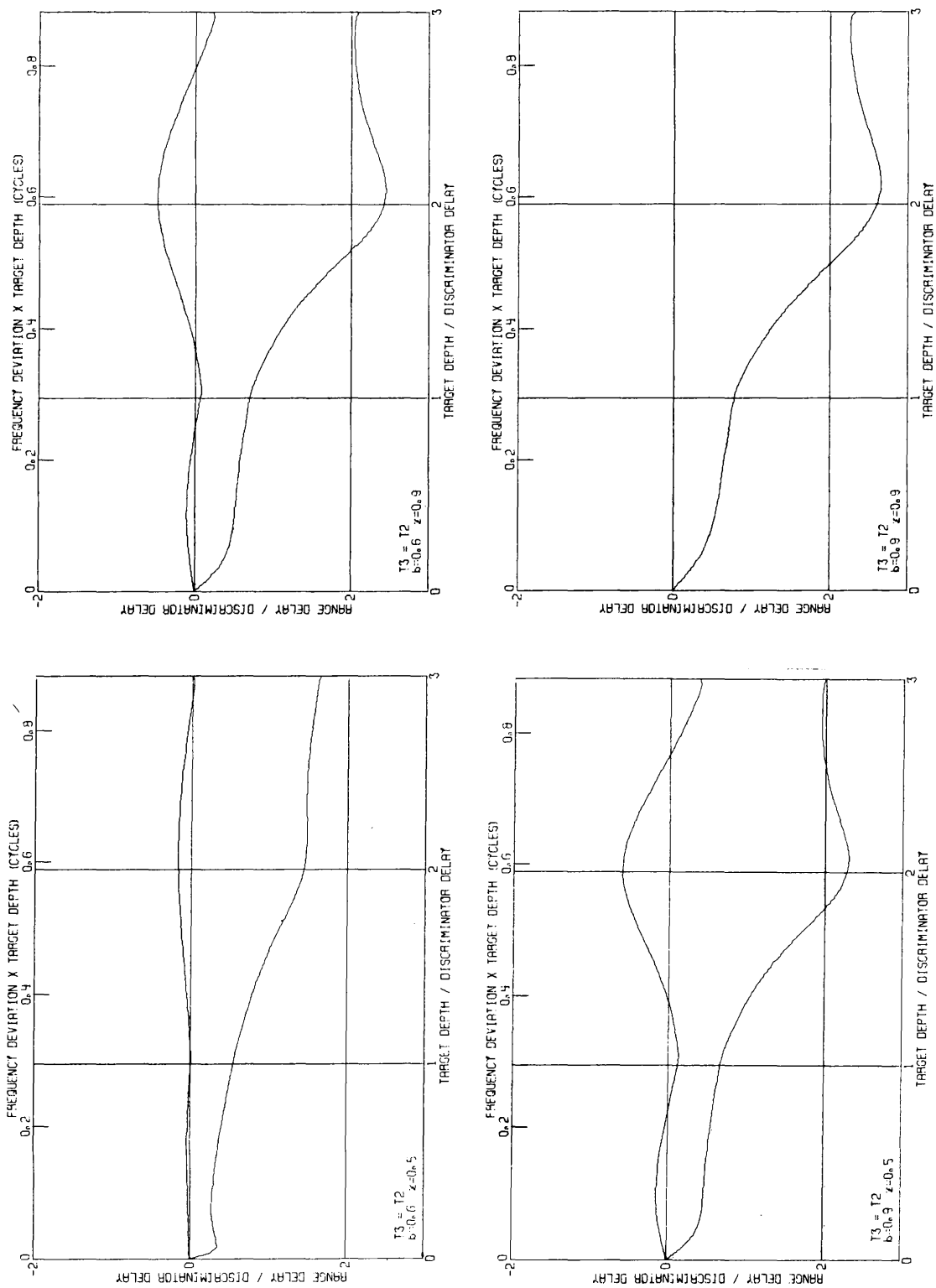

Fig. 19 - Extremes of range delay for three targets. Target 3 has the same radar range as target 2.

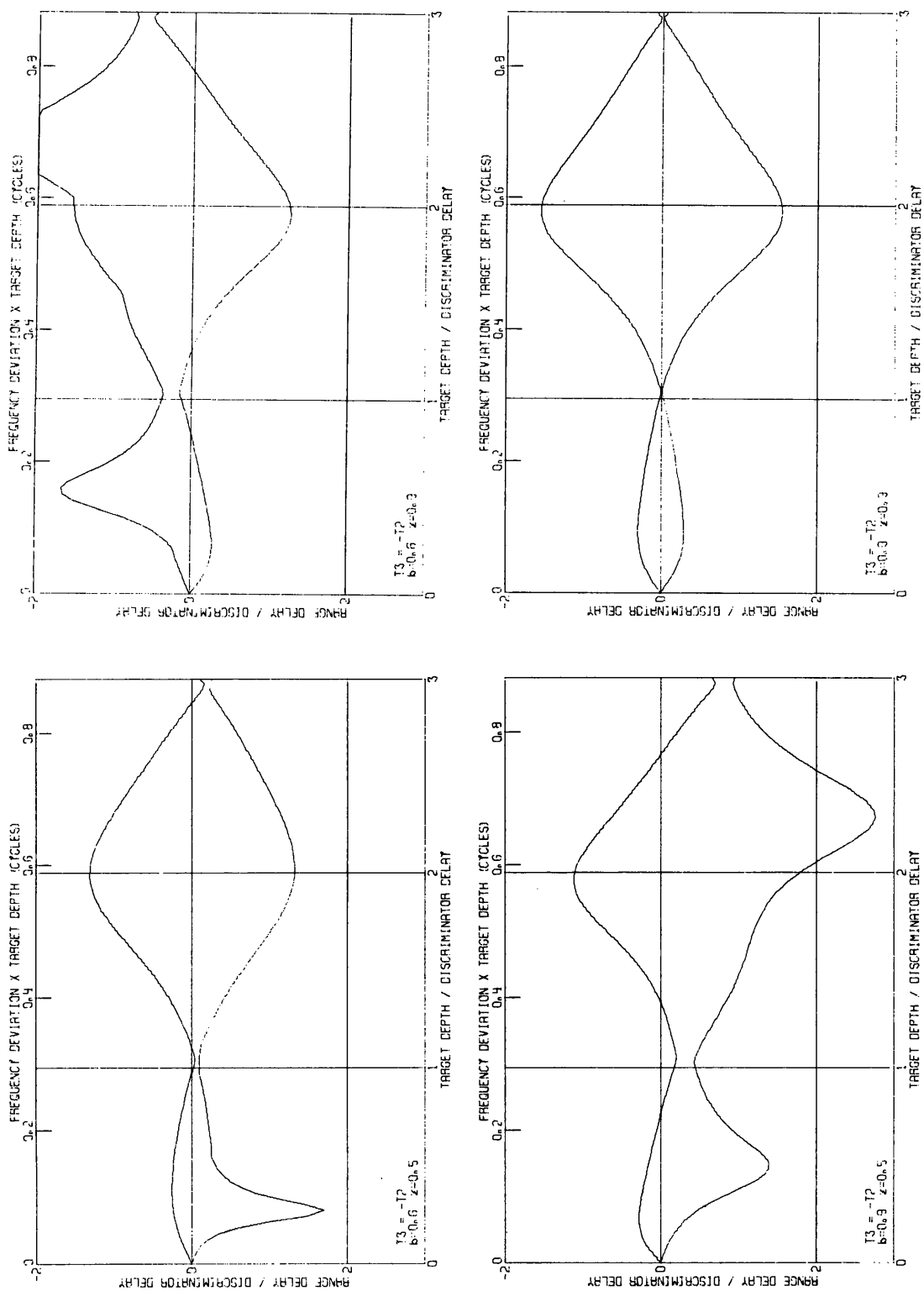

Fig. 20 - Extremes of range delay for three targets. Target 3 and target 2 are the same distance from the reference, but target 3 is closer to the radar.

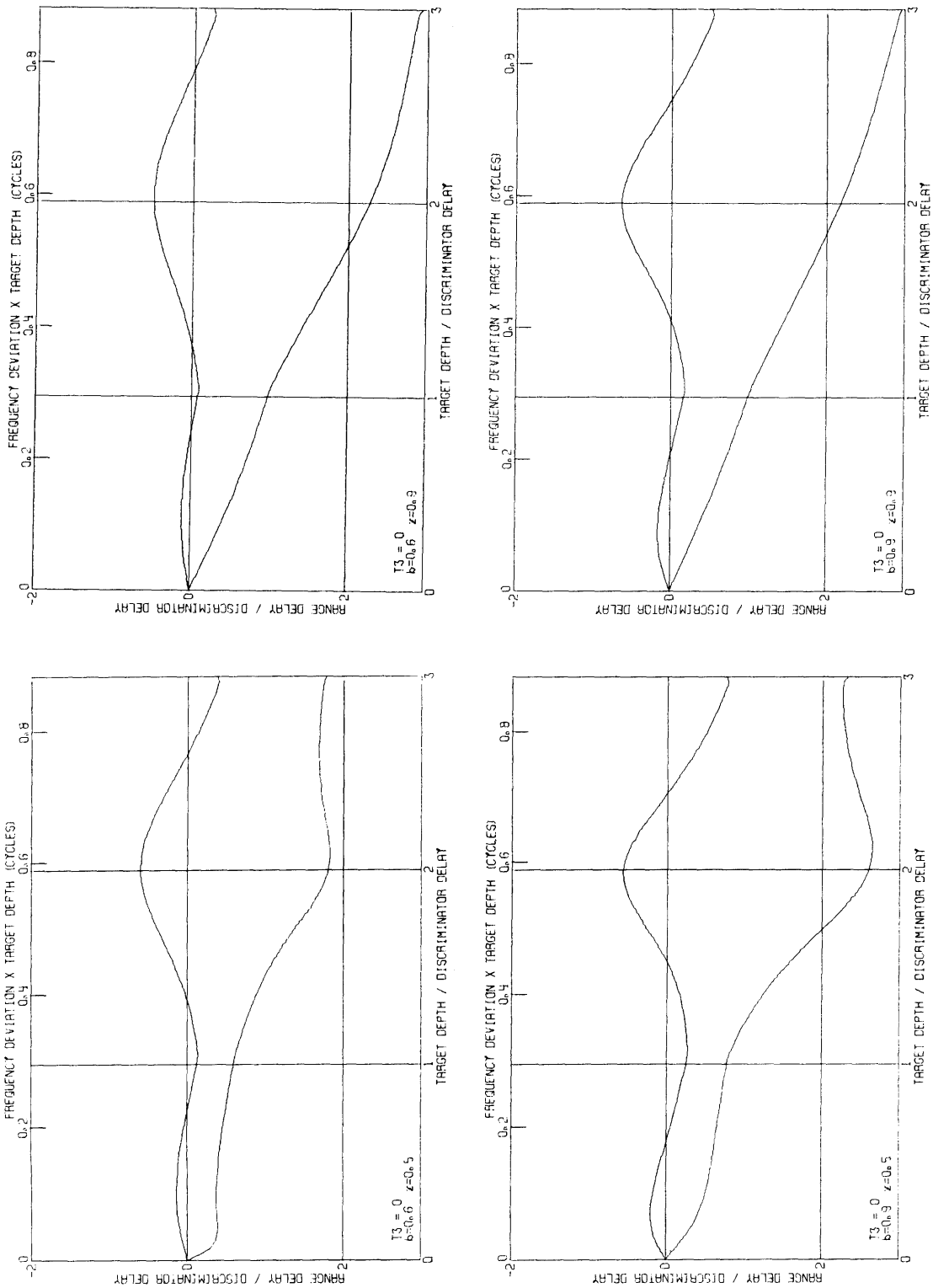

Fig. 21 - Extremes of range delay for three targets. Target 3 has the same radar range as the reference.

range-delay plots for three special relationships between N, μ, and the reference. In Fig. 19, $\mu = N$; in Fig. 20, $\mu = -N$; and in Fig. 21, $\mu = 0$. The plots in these figures show the extremes of range delay possible for the various rf phases of the three targets. In Fig. 20, $b = 0.6$, $z = 0.9$, and the off-scale peak goes almost to three times the discriminator delay.

Linear Discriminator

From Gerks (10) the output of an ideal limiter-discriminator for the two target case is:

$$E_0 = pm \cos pt + \omega_d, \text{ where}$$

ω_d is the error term, and is given by:

$$\omega_d = pG \Bigg[\sum_{n=1}^{\infty} (-1)^{n+1} b^n J_0(nG) \cos(n\theta) \sin p(t - N/2)$$
$$+ \sum_{n=1}^{\infty} \sum_{i=1}^{\infty} (-1)^{n+i+1} b^n J_{2i}(nG) \cos(n\theta) \sin p((2i+1)(t - N/2)) - \sin p((2i-1)(t - N/2))$$
$$+ \sum_{n=1}^{\infty} \sum_{i=0}^{\infty} (-1)^{n+i+1} b^n J_{2i+1}(nG) \sin(n\theta) \sin 2p((i+1)(t - N/2)) - \sin 2ip(t - N/2) \Bigg].$$

where $G = 2m \sin p(N/2)$; the other parameters have been defined previously. By filtering out all but the fundamental modulation-frequency terms, the error term reduces to

$$\omega_d = -2p \sum_{1}^{\infty} (-b)^n n^{-1} \cos n\theta J_1(nG) \sin p(t - N/2)$$
$$= -2pH(b, \theta, G) \sin p(t - N/2).$$

The receiver output becomes:

$$E_0 = p[m + 2H(b, \theta, G) \sin pN/2] \cos pt - 2H(b, \theta, G) \cos pN/2 \sin pt].$$

The range delay is obtained directly from the phase of the receiver output, and is given by:

$$a = (1/p) \tan^{-1} \left[\frac{-2H(b, \theta, G) \cos pN/2}{m + 2H(b, \theta, G) \sin pH/2} \right].$$

Computation of $H(b, \theta, G)$ was interesting, in that the series might converge after a few terms, or it might not converge until several hundred terms have been summed. As b approaches unity and/or as G approaches zero, a larger number of terms of the series was required to obtain a given degree of accuracy. The number of terms that were actually used in the plot computations was determined by:

$$n = \text{Integer value} \left[8[1 + (\ln 100 - \ln G)/\ln 100]/(1 - b) + 0.5 \right]$$

for $b \leq 0.9$ and by

$$n = \text{Integer value} \left[200 + 125(\ln 100 - \ln G)/\ln 100 + 0.5 \right]$$

for $0.9 < b$ _ 0.98. These equations were obtained by printing out the term-by-term summation of the series for several values of b and G.

Figure 22 shows plots of range delay, in units of N, versus $pmN = \Delta F \cdot N$. This scale factor is good only for those values of p and N that $\sin p(N/2) \approx pN/2$. One interesting item about the plots is that the in-phase and out-of-phase curve crossings appear to be

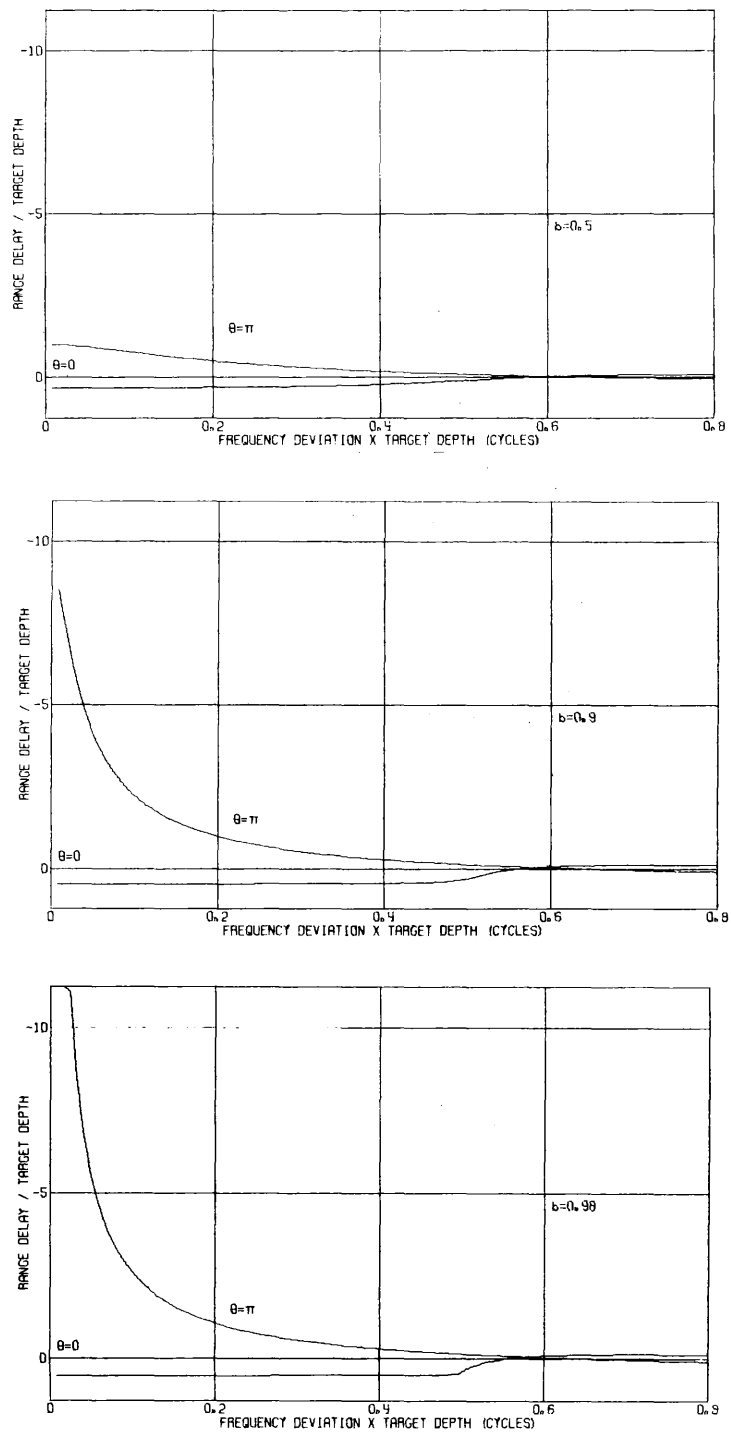

Fig. 22 - Range-delay curves for an ideal limiter and linear discriminator combination

independent of the relative target strength, and occur at a target depth that corresponds to 2σ in an equal-bandwidth interferometer receiver. The curves indicate that very large frequency deviations are required to keep the range delay small for closely spaced targets. For example, if the range delay is to be kept within one target depth for $N \leq 0.5$ nanosecond, then ΔF will have to be on the order of one gigacycle.

SIMULATOR STUDIES OF MULTIPATH PROPAGATION

Waveguide Simulation of Multiple Reflections from an Ocean Surface

A multipath simulator has the unique characteristics of duplicating the conditions that are expected to exist in the reflectivity properties of the sea without complicating it with a multiplicity of additional problems usually associated with a field installation. A radar beam illuminates the sea with a divergent beam that covers a circular area of the surface which includes many reflecting facets displaced in range from the point of reception. In the case of the Chesapeake Bay Bridge installation, where the 30-in. parabolic reflectors were mounted only 62 ft above the water surface, the half-power circle of illumination covers a diameter of approximately four feet. Reflecting facets that are displaced in range within this circle will cause a degree of uncertainty as to the locus of the exact point of reflectivity as well as the range of that point from the radar. As the antenna beam is divergent, the problems are further emphasized in the aircraft installation, since the operating range to the sea may be an order of magnitude greater (620 ft altitude), and thus a larger area will be illuminated to contribute to the depth of the reflecting target.

Figure 1 illustrates the basic design goal for the system; i.e., precise plotting of the surface profile from an aircraft in low-level flight. Simulation of a simplified multiple reflecting surface through controlled waveguide paths in the laboratory aids in the study of multipath interference and its effect on faithful reproduction of the surface contour by the equipment. The primary aim in the use of the simulator is to set up a controlled multiple delay or multipath duplication of a reflecting surface under optimum operating conditions of the electronics, and thus ascertain how closely the field installation is approaching precision ranging to the actual wave profile.

Analysis of Waveguide Simulation of Free-Space Multipath Interference

In considering the simulation of free-space propagation phenomena by closed waveguide paths we should consider the so-called dispersive effects in waveguide as evidenced by the differing group and phase velocities and the variation of these quantities with frequency. Electromagnetic propagation in a lossless free space is considered to be at the speed of light and constant regardless of frequency. However, when a broad frequency spectrum is confined to a closed waveguide, not all of the side frequencies are propagated at the same velocity. If this spectrum is split into two waveguide paths having unequal lengths and then recombined, the higher frequency pair of sidebands will not be delayed as much as the lower frequency pair. The velocity of propagation within bounded parallel planes such as a waveguide, termed the group velocity and conveying the energy in the wave, is reduced from the velocity of light by the ratio of the free-space wavelength to the guide wavelength, or λ/λ_g. The guide wavelength is a function of the physical dimensions of the guide and the frequency propagated in the guide. In order to convey intelligence, it is necessary to modulate the carrier frequency being transmitted. When this is done, there is a group of frequencies, usually centered about the carrier, that must be propagated along the guide. Since the phase velocity is a function of frequency, the waves of different frequencies in the group will be transmitted with slightly different velocities.

The component waves combine to form a "modulation envelope," which is propagated at the group velocity. A multipath simulation is shown in Fig. 23 in which the microwave signal is split into two paths of differential lengths, L_1, and L_2, each having a common phase ϕ(in) at P_1. The output rf phase, ϕ(out), will be dependent on the differential distance, ΔD_{fs} or ΔD_g in terms of wavelengths of the medium in which it has traveled. The upper portion of the figure represents two-path, free-space propagation over a distance between parallel planes P_1 to P_2. A portion of the radiated signal travels over a shorter distance, L_1 (such as the reflection from the crest of an ocean wave) and the remainder of the energy travels a longer distance, L_2 (reflecting from a lower portion of the wave front).

The lower portion of Fig. 23 represents a waveguide simulation of the above conditions. Since the group velocity in the waveguide is less than free space, it is understood that the physical lengths of the waveguide will be considerably less (72.4 percent at 9.51 Gc/sec) than the equivalent lengths of free space being simulated. Signal additions within a waveguide system are governed by the field configurations in the guide, and therefore the phase of the summed rf signals is a function of the guide wavelength.

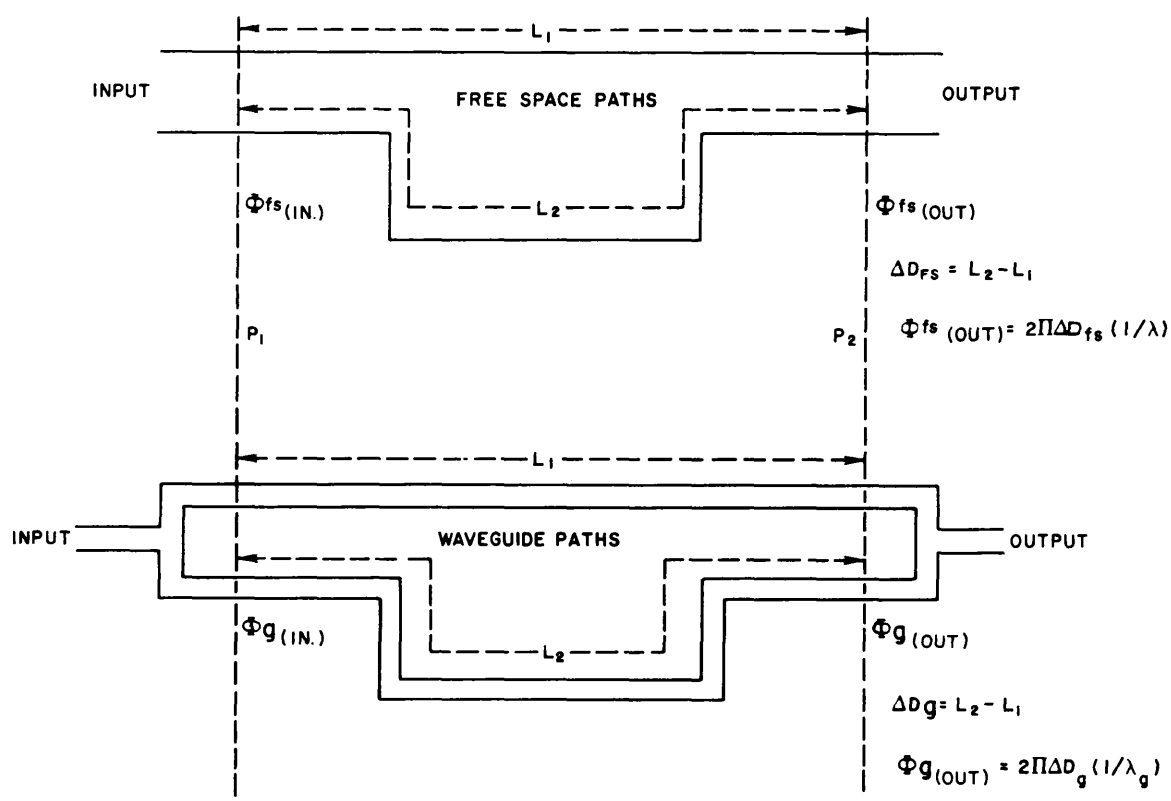

Fig. 23 - Phase and distance relationships in a waveguide multipath simulation

Thus in the figure, from purely geometric relationships, we have in the waveguide system:

$$\phi_g = 2\pi \Delta D_g \left(\frac{1}{\lambda_g}\right) \text{ radians,}$$

and in the case of the free-space paths:

$$\phi_{fs} = 2\pi \, \Delta D_{fs} \left(\frac{1}{\lambda}\right) \text{ radians.}$$

In the waveguide simulator under discussion, we are at liberty to adjust the initial phase relationship at any frequency by means of a phase shifter, but require that the phase changes versus frequency be matched as well as possible. The phase differentials for two frequencies f_1 and f_2 of which f_2 is the higher are given by:

$$\Delta\phi_g = \phi_{g_2} - \phi_{g_1}$$

$$\Delta\phi_g = 2\pi \, \Delta D_g \left(\frac{1}{\lambda_{g_2}} - \frac{1}{\lambda_{g_1}}\right),$$

and in free space

$$\Delta\phi_{fs} = \phi_{fs_2} - \phi_{fs_1}$$

$$\Delta\phi_{fs} = 2\pi \, \Delta D_{fs} \left(\frac{1}{\lambda_2} - \frac{1}{\lambda_1}\right) .$$

For exact simulation

$$\Delta\phi_g = \Delta\phi_{fs} \text{ and it follows that}$$

$$\frac{\Delta D_{fs}}{\Delta D_g} = \frac{\left[\frac{1}{\lambda_{g_2}} - \frac{1}{\lambda_{g_1}}\right]}{\left[\frac{1}{\lambda_2} - \frac{1}{\lambda_1}\right]} .$$

We have in free space

$$\lambda = \frac{c}{f}$$

and in waveguide the well-known relationship

$$\lambda_g = \lambda \Big/ \sqrt{1 - \left(\frac{f_c}{f}\right)^2}$$

or

$$\lambda_g = \frac{c}{f\sqrt{1 - \left(\frac{f_c}{f}\right)^2}}$$

where c is the free-space velocity of propagation and f_c is the cutoff frequency of the waveguide in use. Making these substitutions we obtain

$$\frac{\Delta D_{fs}}{\Delta D_g} = \frac{\frac{f_2}{c}\sqrt{1 - \left(\frac{f_c}{f_2}\right)^2} - \frac{f_1}{c}\sqrt{1 - \left(\frac{f_c}{f_1}\right)^2}}{\frac{f_2}{c} - \frac{f_1}{c}}$$

and if we further let $f_2 = f_1 (1 + K)$ we have

$$\frac{\Delta D_{fs}}{\Delta D_g} = \frac{\frac{f_1(1+K)}{c}\sqrt{1 - \frac{1}{(1+K)^2}\left(\frac{f_c}{f_1}\right)^2} - \frac{f_1}{c}\sqrt{1 - \left(\frac{f_c}{f_1}\right)^2}}{\frac{f_1}{c}(1+K) - \frac{f_1}{c}}$$

and cancelling the common factor f_1/c gives

$$\frac{\Delta D_{fs}}{\Delta D_g} = \frac{(1+K)\sqrt{1 - \frac{1}{(1+K)^2}\left(\frac{f_c}{f_1}\right)^2} - \sqrt{1 - \left(\frac{f_c}{f_1}\right)^2}}{K}$$

This may also be written in the form

$$\frac{\Delta D_{fs}}{\Delta D_g} = \frac{\sqrt{(1+K)^2 - \left(\frac{f_c}{f_1}\right)^2} - \sqrt{1 - \left(\frac{f_c}{f_1}\right)^2}}{K}$$

and further rearrangement gives

$$\frac{\Delta D_{fs}}{\Delta D_g} = \frac{\sqrt{\left[1 - \left(\frac{f_c}{f_1}\right)^2\right] + 2K + K^2} - \sqrt{1 - \left(\frac{f_c}{f_1}\right)^2}}{K} .$$

Inspection of this equation shows that the required length ratio is a function of K, the fractional frequency change, as well as of the initial frequency f_1 and the simulation of free space cannot therefore be precise over large fractional bandwidths. In many cases of practical interest, however, K will be small compared to unity, and in this case we may further simplify the expression for $(\Delta D_{fs}/\Delta D_g)$ by noting that the numerator of the fraction will then be of the form

$$\frac{\sqrt{[x] + \Delta x} - \sqrt{x}}{K}$$

where x is equal to the radical $1 - \left(\frac{f_c}{f_0}\right)^2$,

and Δx is equal to $2K + K^2$; therefore

$$\sqrt{x + \Delta x} - \sqrt{x} = \sqrt{x\left(1 + \frac{\Delta x}{x}\right)} - \sqrt{x} ,$$

and since

$$\lim_{\Delta x \to 0} \sqrt{x\left(1 + \frac{\Delta x}{x}\right)} = \sqrt{x}\left(1 + \frac{1}{2} \cdot \frac{\Delta x}{x}\right)$$

we have

$$\sqrt{x + \Delta x} - \sqrt{x} = \frac{\sqrt{x} \cdot \Delta x}{2x} = \frac{\Delta x}{2\sqrt{x}}$$

as an approximation good for small values of Δx. We may write as an approximation good for small K that

$$\frac{\Delta D_{fs}}{\Delta D_g} = \left(\frac{1}{K}\right) \cdot \frac{K + K^2/2}{\sqrt{1 - \left(\frac{f_c}{f_1}\right)^2}}$$

and dropping the second-order term in K^2 we have simply

$$\frac{\Delta D_{fs}}{\Delta D_g} = \frac{1}{\sqrt{1 - \left(\frac{f_c}{f_1}\right)^2}} .$$

We conclude from this result that to obtain equal phase increments about a given design frequency, f_0, the differential length ΔD_g in the waveguide simulator must be made shorter by the factor

$$\sqrt{1 - \left(\frac{f_c}{f_0}\right)^2}$$

so that

$$\Delta D_g = \Delta D_{fs} \sqrt{1 - \left(\frac{f_c}{f_0}\right)^2}$$

and this may also be written in the form

$$\Delta D_g = \Delta D_{fs} \sqrt{1 - \left(\frac{\lambda_0}{\lambda_c}\right)^2} = \Delta D_{fs} \left(\frac{\lambda_0}{\lambda_g}\right) .$$

This result may also be obtained by equating the derivatives of the phase-frequency functions (23). The number of guide wavelengths contained in a simulated differential length of guide, ΔD_g, will evidently be smaller than the number of free-space wavelengths contained in the equivalent differential length of free space, ΔD_{fs}. As an example, it is desired to simulate an equivalent differential free-space length of one foot in WR-90 (RG-52/U) standard X-band waveguide at 9.51 Gc/sec. The differential length of the waveguide is calculated

$$\Delta D_g = \Delta D_{fs} \sqrt{1 - \left(\frac{\lambda_0}{\lambda_c}\right)^2} = 0.724 \text{ ft},$$

where the cutoff wavelength for this guide is λ_c = 4.572 cm. In one foot of free space there are found 9.67 free-space wavelengths; while in the 0.724 ft of waveguide, there are only 5.07 guide wavelengths. The number of guide wavelengths in the simulated path is therefore reduced by $[1-(f_c/f_0)^2]$ or 0.525 from the number of free-space wavelengths. This might at first glance appear contradictory in view of the normal assumption that frequency-dependent effects in interference phenomena are governed by the number of wavelengths in the various paths, and that similar behavior in two systems requires equal numbers of wavelengths in corresponding paths. The reason that this does not hold true in the present instance lies in the fact that the waveguide behaves as a dispersive medium, and the change of phase velocity with frequency changes the guide

wavelength in the example cited by an amount nearly as large as that produced directly by the reciprocal wavelength-frequency relationship. Since the two effects are additive, the number of guide wavelengths in the equivalent waveguide path must be made smaller by the appropriate factor to produce the same phase-frequency relationships that exist in free space.

As indicated above, the equivalence between a waveguide system and free-space paths can be exact only at one frequency, since the length adjustment factor is itself frequency dependent. However, in the case of the bandwidths involved in the present study the phase differences that accumulate are relatively small.

The percentage error of the rf phase progression is illustrated in Fig. 24 as a function of deviation from a design center frequency of 9.51 Gc/sec. Typical maximum modulation bandwidth used in the simulation study was ±200 Mc/sec, therefore limiting this error in the simulation of free space to a ±2 percent. It may be shown that error in a waveguide simulation may become excessive when the frequency region transmitted through the guide approaches the cutoff frequency, f_c, in the dominant TE_{10} mode. A comparison example of how the percentage error increases at a lower center frequency illustrates this point. When a modulated spectrum of 8.4 Gc/sec ±200 Mc/sec is used in the same waveguide, the resulting phase progression error is +4.1 percent at 8.2 Gc/sec and -3.4 percent at 8.6 Gc/sec. Normally the WR-90 waveguide would not be used beyond its recommended operating range of 8.2 to 12.4 Gc/sec, and therefore the simulation error would not exceed the example cited for the given 200-Mc/sec frequency deviation. It is therefore evident in the case of the system constants applying to the wave-profile radar that phase relationships in the waveguide simulator depart to only a rather small extent from the free-space relationships under investigation. It may be noted that the simulator phase delays cannot be derived by applying a common incremental time delay to both the modulation envelope and the rf carrier wave train. If, for example, one were to take the time delay that would produce the incremental envelope phase shift in free space and derive an rf phase shift from it, one would obtain a very large phase-angle correction that would be comparable to the maximum free-space phase differential itself. This procedure is evidently not valid, since it confuses group and phase-velocity phenomena.

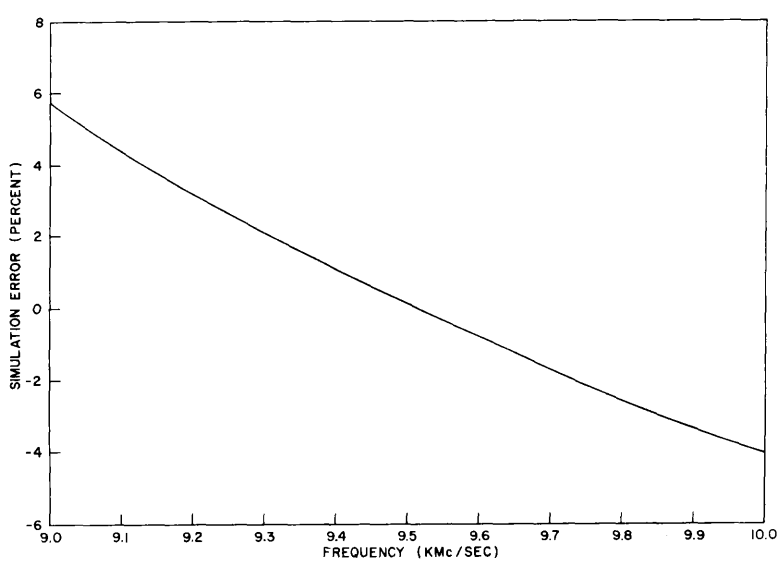

Fig. 24 - Percentage error of the rf phase progression in a waveguide simulation of free space plotted versus frequency based on a center frequency of 9.51 Gc/sec in RG-52U waveguide

Equipment Operation

The basic radar system is shown in simplified block diagram form in Fig. 2. The equipment shown in Fig. 25 is an expansion of the basic system to closed waveguide paths plus instrumentation relating to the simulator studies; and Fig. 8 is an expansion of the basic system for critical measurement of water waves and other synoptic variables at the Chesapeake Bay Bridge installation. Both installations utilize essentially the same basic equipment, with the exception that the field equipment radiates through space to a complex reflecting target and has an additional TWT-leveling amplifier in its receiver. The simulator in effect simplifies the complex water-wave target into two or three points of reflectivity to study the effect of the multipath interference in a closed-waveguide system.

Frequency modulation of a microwave backward-wave oscillator (BWO) is used to obtain a measure of transmission delay by phase comparison of the demodulated return with the modulating reference signal. The reference is a 2.215 Mc/sec sinusoid obtained from a crystal oscillator. It is simultaneously used for detection in the quadrature phase bridge of the receiver, and to deviate the helix control voltage of the BWO transmitter via appropriate modulation circuits. The extent of this voltage swing determines the spectral bandwidth of the significant side frequencies radiated in the microwave envelope. The single-frequency modulating sinusoid deviates the X-band carrier frequency of 9.51 Gc/sec over a controllable bandwidth of from approximately ±5 to ±200 Mc/sec at the rate of the 2.215 Mc/sec reference. Microwaves are used primarily to obtain a narrow beam from a convenient size antenna in order to spot-illuminate at short range and resolve the fine structure in each ocean wave.

The receiver recovers the reflected radiation from the moving surface, minimizes the effect of amplitude variations, detects the modulation, and compares the phase of the recovered 2.215 Mc/sec modulation with the reference to obtain a dc voltage output dependent on the instantaneous target range. A surface profile is recorded as the water waves approach and recede from the radar, since the phase of the recovered modulation is dependent on the travel time to and from the target.

Deviations in the instantaneous range to the water surface are frequently found to occur at a rate considerable faster than the actual movement of the surface. Target scintillation and interference between multiple points of reflection within the illuminated area covered by the beam are postulated as the source of these rapid deviations. The effect of this multipath interference is probed both in the laboratory and field experiments in order to develop a technique for minimization of error in precise surface-profile reproduction by radar.

The simulator permits controlled rf phase variations between two or more closed waveguide paths while the other system parameters are held constant. The effect on the modulation phase at the receiver due to multiple-path reinforcements and cancellations serves to verify the theoretical studies as well as determining systematic shortcomings in the practical equipment.

Simulation Details

Both a two-path reflecting surface and a three-path surface are duplicated by the simulator, in which both the rf phase and amplitude of these simulated paths may be accurately controlled. The differential path lengths may also be altered to suit the range of radial displacements from the radar that might be expected within a practical target. This displacement is accomplished by splitting the signal from the transmitter into two or more closed waveguide loops of differential path lengths, operating individually on the amplitude and rf phase of each path, and then recombining them at the receiver. This is illustrated by the block diagram of the simulator in Fig. 25. Typical differential path

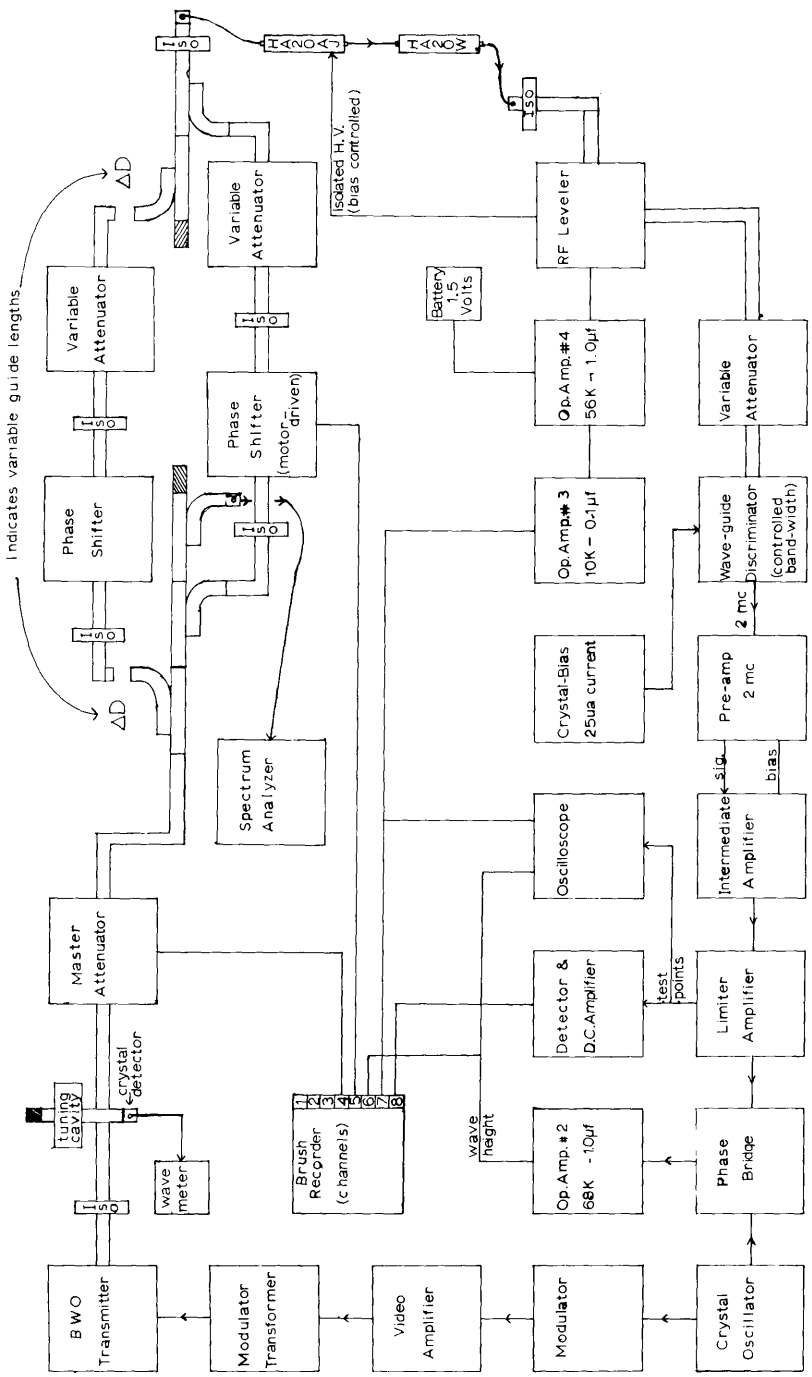

Fig. 25 - Block diagram of waveguide simulator for controlled studies of multipath interference in an FM-CW wave-profiling radar system

lengths, ΔD of 0.5 to 10 nanoseconds of equivalent range delay within the target are continuously swept with the motor-driven phase shifter through rf phase cancellations and additions (360 degrees) while the relative amplitudes were probed over a 20 db range with the variable attenuators. Various indices of frequency modulation (by varying the frequency deviation) are likewise probed by varying the modulator amplitude while observing the effect on the spectrum analyzer.

When an unmodulated, continuous wave carrier is split into two equal length paths, $\Delta D = 0$, both attenuated zero db (unity ratio of relative amplitudes), and their rf phase is in phase (zero degrees), the combined amplitude of the two paths will be twice the individual path level; and when they are out of phase (180 degrees), the combined amplitude will be zero. This condition serves as a check on the insertion losses of the microwave components used in the individual paths as well as their relative accuracies of calibration. These conditions should likewise be satisfied when the rf attenuators are set at any other point of equal value, assuming accurate calibrations, equal insertion loss, and rf phase stability versus attenuation. If one attenuator is left at zero db and the other at 6.02 db, then the combination will cause the summed or combined amplitude to vary in a ratio from 1.5 to 0.5 as the rf phase progresses through the 360 degrees. The characteristics of the waveguide components should remain constant over the modulation bandwidth of interest. The essential portions of the closed waveguide paths are shown in the upper right area of Fig. 25. Two traveling-wave tubes (HA-20AJ and HA-20W) follow the waveguide paths and are controlled by the rf leveler to increase the dynamic range of the equipment. Monitoring of the changes in rf level during cancellations and additions is accomplished by sampling the leveler control voltage and recording it on channel 7 of the multichannel recorder. This leveling operation further aids in minimizing any nonlinear effects in the waveguide discriminator or receiver amplifiers that follow. The wave height or indicated range is sensed by the phase bridge and recorded on channel 6.

When frequency modulation is applied to the carrier, FM-CW, a simplification of the processes of sideband cancellations and additions as it affects the modulation phase of the combined two-path signals is not so easily evident. A vector addition of first-order sidebands, when the frequency deviation is small, will show that the range error resulting from two paths differing in delay by 3 nanoseconds and combining at an amplitude ratio of 0.5 to 1 will be 1.32 times the target depth. The following two cases illustrate by vectorial combination of the modulation sidebands how it is possible to have the indicated range move above and below the point of primary reflection. An assumption is made that the loci of primary unit reflection of the radar's beam is from a point on the wave's crest, as illustrated by point 1 on the sketch shown on Fig. 26. In addition, a secondary path of reflection within the radar beam and located 1-1/2 ft below the crest of the wave at point 2 causes simultaneous interference with the primary reflection from point 1. The amplitude of the reflection from point 2 is arbitrarily chosen to be one-half as strong as that from point 1, or at an amplitude ratio of 0.5 to 1. The differential delay of 3 nanoseconds is approximately the transit time of the secondary signal in propagating over the additional distance of 3 ft round trip; i.e., the reflection time from point 2 relative to point 1.

The in-phase and out-of-phase cases define the extremes of modulation phase shift or range error resulting from two-path interference.

Case 1: Fig. 26 shows in solid line form the vectorial combination when the rf carrier that travels over both paths remains in phase; i.e., the 1-1/2 ft range differential is an even number of rf quarter wavelengths and therefore the two reflected signals constructively combine. The vector S_1 represents the return from point 1 at an arbitrary modulation phase of 45 degrees with an amplitude of 6.7 units. The combining vector S_2 is shown at a relative phase angle of $47°24'$ with an amplitude of 3.35 units, or one-half the magnitude of S_2. Since S_2 represents the reflection from point 2, its phase angle is delayed an additional $2°24'$ relative to S_1. This is the computed equivalent phase shift obtained from the proportion 3 ft/$2°24'$ = 444.2 ft/360° where 444.2 ft is one wavelength

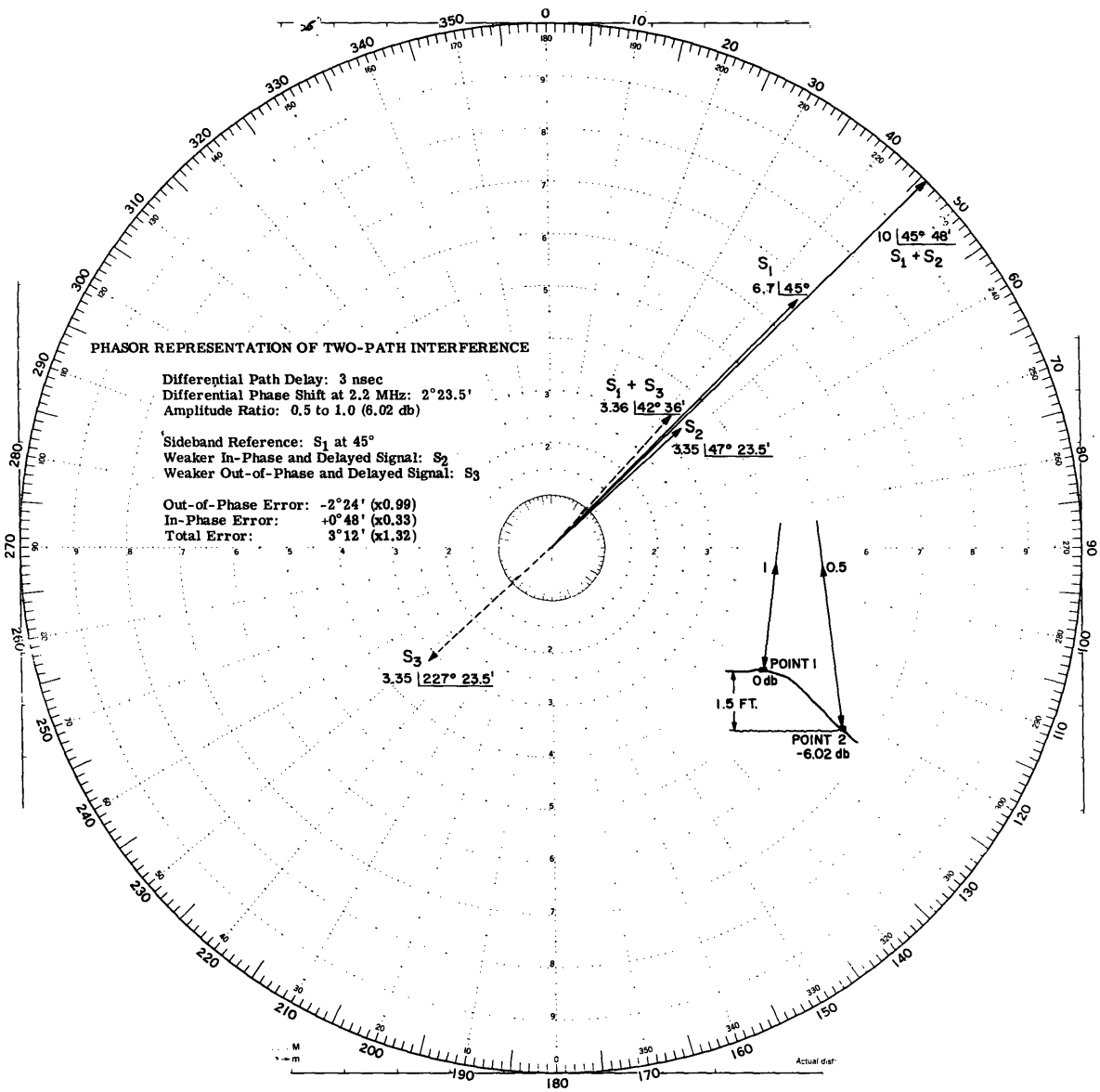

Fig. 26 - Phasor representation of two-path interference; differential path delay 3 nsec, amplitude ratio 0.5 to 1.0 (6.02 db)

or 360° of the modulation frequency. This is computed from $\lambda = c/f$, where c is the free-space electromagnetic velocity of 984 ft per microsecond and f is 2.215 Mc/sec. The vector sum of S_1 with S_2 yields a third vector, S_1 plus S_2, which has a phase angle of 45°48′ and an amplitude of 10 units. Therefore the in-phase error to the primary path is a +0°48′ as the result of interference from the secondary path.

Case 2: Fig. 26 also illustrates in dotted line form when the rf carriers destructively combine or are out of phase, i.e., the 1-1/2 ft range differential is an odd number of rf quarter wavelengths. The vector S_1, representing the primary path reflection from point 1, is now summed with vector S_3, which is the out-of-phase equivalent to S_2 in case 1 above. The resultant vector sum yields the vector, $S_1 + S_3$, which has a phase angle of 42°36′ and an amplitude of 3.36 units. In this case the out-of-phase error to the primary path is a -2°24′ from the arbitrary phase reference of 45 degrees of vector S_1. The sum of these two phase errors of +0°48′ and -2°24′ yields a peak total error of 3°12′ as the rf paths scintillate from the in-phase to out-of-phase case; i.e., the 1-1/2 ft range differential of the two paths shifts by one-quarter rf wavelength. This shift or change is approximately 0.3 in., or less than 2 percent of the range differential. Thus for the parameters chosen, the phase that affects the indicated radar range may oscillate between 45°48′ and 42°36′ as the rf phase moves from an in-phase to out-of-phase condition. The total phase error between these extremes of 3°12′ is 1.32 times the 2°24′ phase shift that would take place when one path or the other were completely absent.

A similar in-phase and out-of-phase polar presentation of two-path interference is given in Fig. 27 to illustrate the large range error that may occur when the amplitudes of the two combining vectors are more nearly equal to each other even though the axial displacement or range delay between the two interfering points is not greatly different from the previous example. An amplitude ratio of 0.9 to 1 is chosen with the magnitudes of the combining vectors SB_2 and SB_1 scaled to 4.5 to 5.0 units respectively. As the rf carrier phase changes from constructive to destructive interference (0° to 180°), the combination of these two vectors is shown for the in-phase case as SB_{12} having a magnitude of 9.5 units, and for the out-of-phase case as SB_{12} with a magnitude of 0.5 units. The net change in magnitude is a ratio of 19 to 1, with the total modulation phase shift error of 18°18′ which represents an error multiplier of 9.18 times over the 2-degree phase shift that would take place if the reflection were either totally from point 1 or from point 2. The 1.25 ft of target depth or axial displacement between these points is equivalent to differential round-trip path delay of 2.5 nanoseconds, or proportional to the 2-degree differential phase of the modulation components. The two cases shown in Fig. 27 graphically illustrate the extremes of the phase and magnitude errors, while Fig. 28 presents a continuous plot of the indicated delay time from the phasor combinations as the rf carrier phase changes through 360°. The plot indicates the relative time displacement between the two target points, with the primary reflection point shown as target 1 at the zero delay time reference. The dotted points are the computed position of the indicated range throughout the carrier cycle.

It is obvious from this study that if both axially displaced points of reflection give the same magnitude of reflectivity, or the two paths have an amplitude ratio of unity, then the in-phase indicated target position will be half-way between the two points, or at a net phase angle that bisects the two summing vectors. The out-of-phase vector summation will also bisect the included angle between the two combining vectors, with a total phase error of 90 degrees between the in-phase and out-of-phase cases. Given the same 2.5-nanosecond delay described previously and shown on Fig. 27, with the exception that the vectors SB_1, SB_2, and SB_2' are all of equal length at 5 units, then SB_{12} will have a magnitude of approximately ten units at an angle of 46° and SB_{12}' will have a magnitude of 0.175 at an angle of 316°. This represents a net change in magnitude of 57 to 1 between the pair with a total phase-shift error of 90°. A plot similar to Fig. 28 for these parameters would show a curve that varied from +1.25 nanoseconds to a peak of -111 nanoseconds

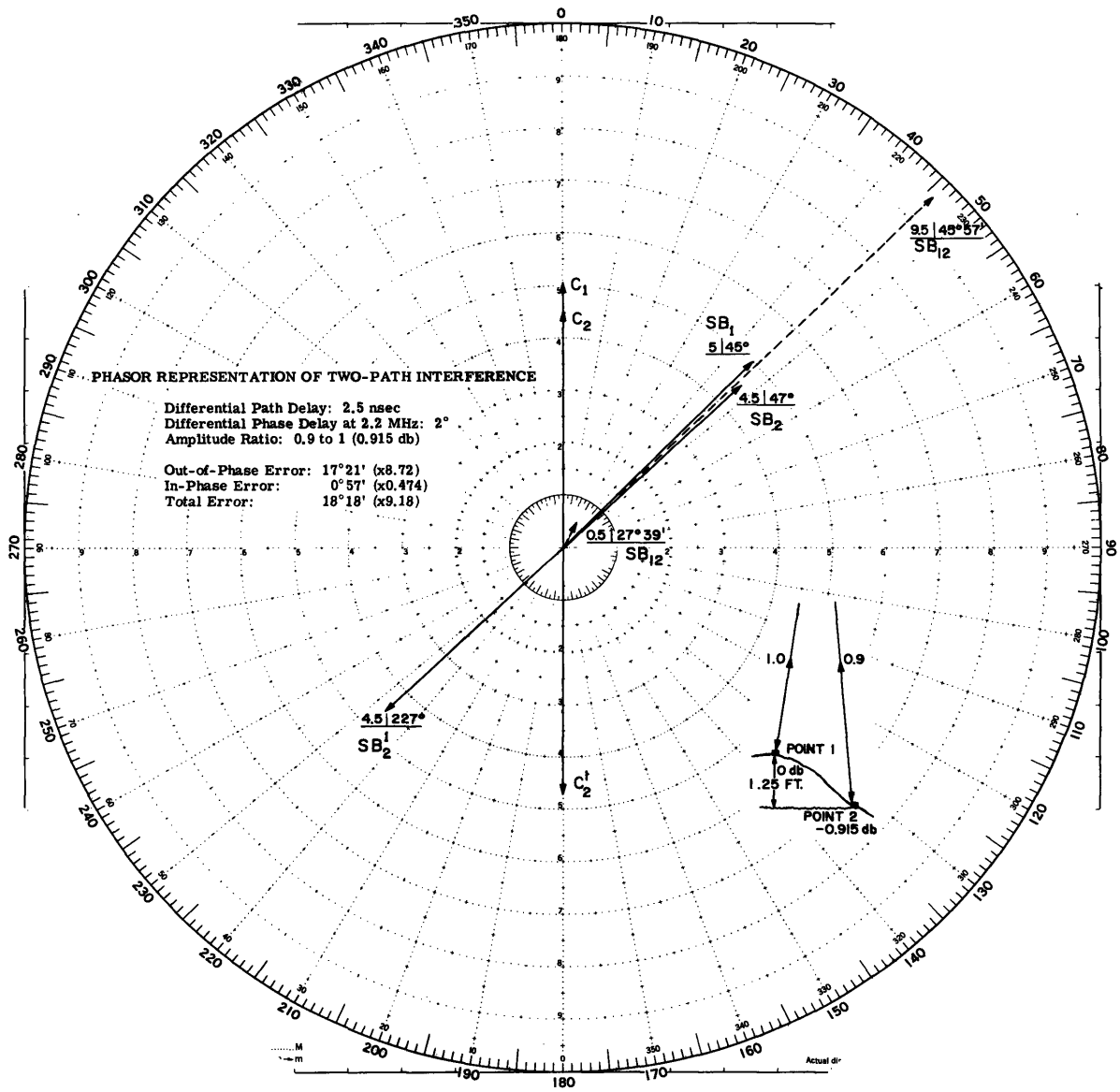

Fig. 27 - Phasor representation of two-path interference; differential path delay 2.5 nsec, amplitude ratio 0.9 to 1.0 (0.915 db)

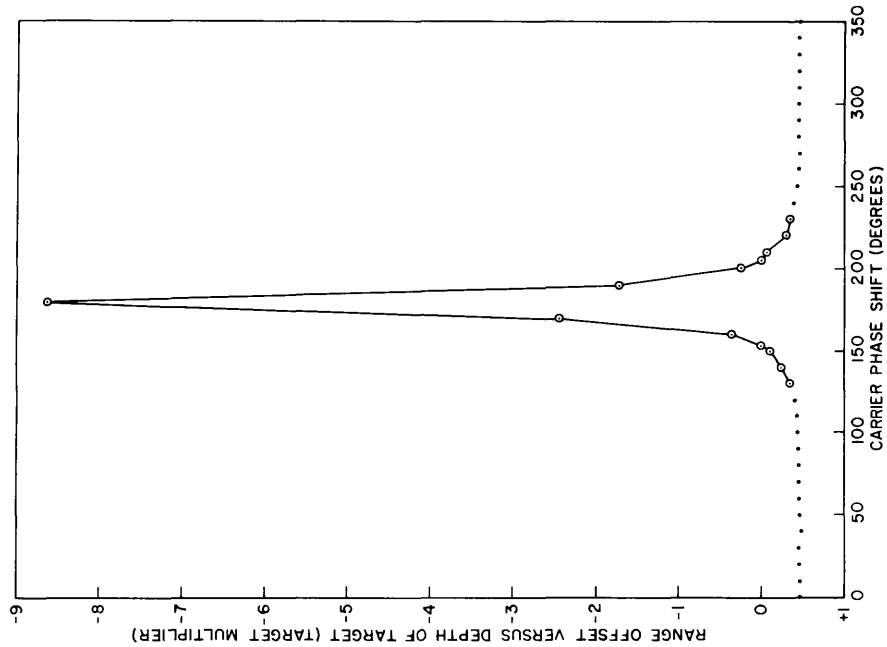

Fig. 29 - Narrow-band target error for two-path interference, amplitude ratio 0.9 to 1, 2.5 nsec delay to weaker path

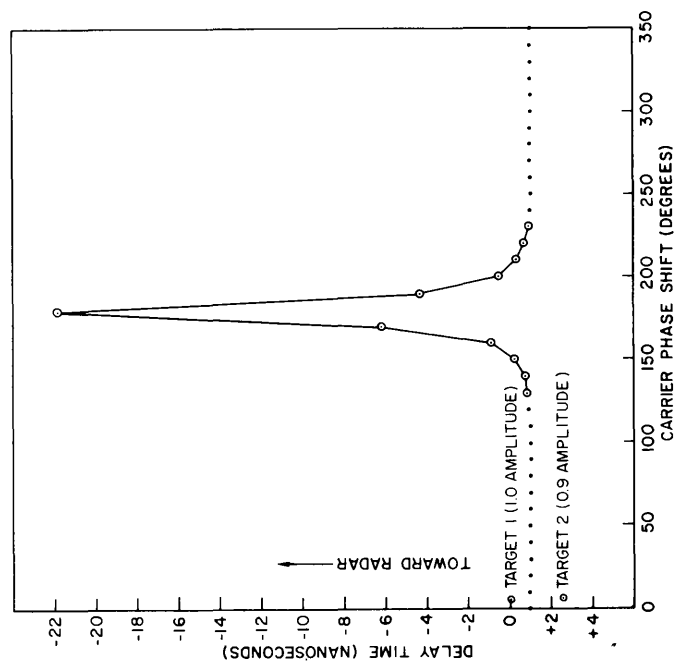

Fig. 28 - Narrow-band two-path interference characteristics, amplitude ratio 1 to 0.9, target delay time 2.5 nsec

as the carrier shifts through 360°. Also a plot similar to Fig. 29 would show a curve that varied from a +0.5 multiplier to a -44.5. It may be pointed out that when a narrow frequency deviation is used in two-path interference of equal amplitude paths, the total phase-shift error will always be 90° regardless of the differential delay time between the two interfering paths or the frequency used for modulating the transmitter. Such changes would of course modify the magnitude of the delay times and target multipliers indicated in Figs. 28 and 29 respectively. Simulation of these conditions is not practical due to extreme changes in signal level that would appear at the output of the two recombining waveguide paths, especially when a narrow bandwidth is used. The probability of only two paths of exactly equal amplitude return existing in the practical field installation is remote; however, the examples given should serve to illustrate the reason for large "positive spiking" when a narrow bandwidth of modulation is used in the electronic equipment.

A phasor representation of three-path narrow-band FM interference has been presented by Morrow (24), showing similar positive or decreasing range "spikes" as the microwave returns pass through carrier cancellations or are 180° out of phase. The effect is most pronounced when the number of paths is small and the amplitude of the supplementary path or paths approach that of the primary path.

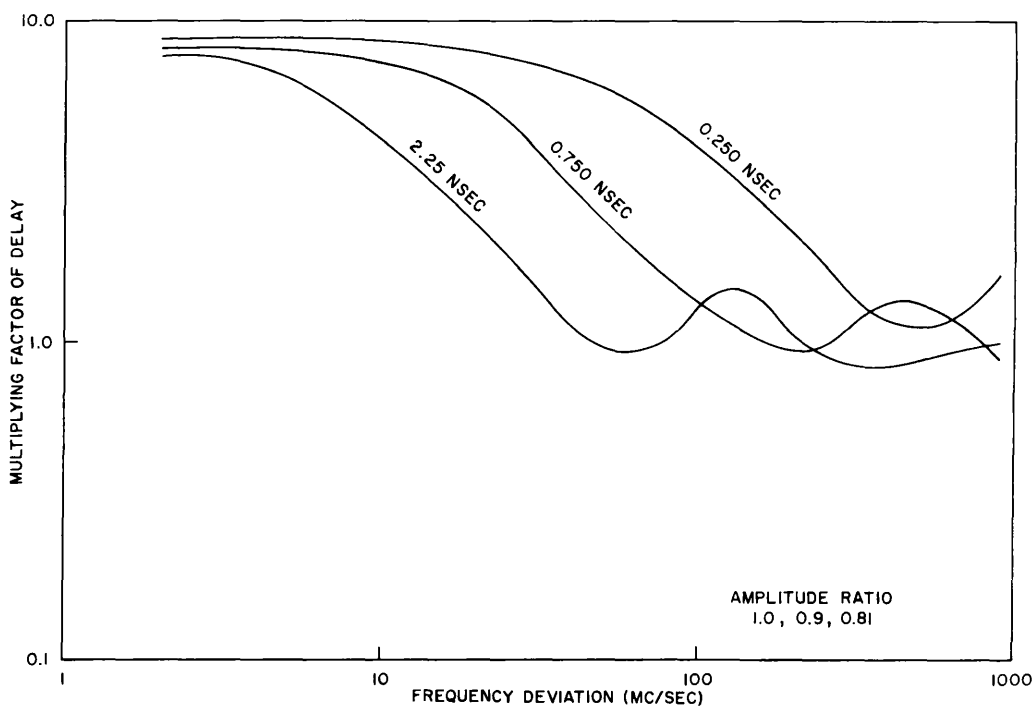

Fig. 30 - Composite plot of three-path interference between each of three different targets showing delay error multiplication versus frequency deviation

Figure 30 is a composite plot of a three-path simulator study of each of three differentially delayed supplementary paths to illustrate the nature of error reduction as a function of transmitted bandwidth. For this study a third path was added to the simulator, although it is not illustrated in the block diagram of Fig. 25. The two paths that are illustrated shall be referred to as the primary path, containing the motor-driven phase shifter and set to unity amplitude; and the supplementary path, containing a variable

length of waveguide, ΔD. For this three-path study the amplitude of the supplementary path was set to 0.81 that of the primary path, and the length ΔD was adjusted for a differential delay of 0.25 nanosecond. The third path was added with its amplitude set to 0.9 and its length equal to that of the primary path. The frequency deviation was then varied over a wide bandwidth while range data were recorded. From this data a "multiplying factor of delay" was computed using the peak-to-peak range error recorded relative to ΔD for each known step of frequency deviation to plot the topmost curve of Fig. 30. The supplementary path length ΔD was then changed to each of the remaining delay times and the procedure repeated to yield the composite plot of three curves.

The study illustrates the need for broad bandwidth to bring the response to a multipath target within its own physical dimensions. This means that if axially displaced points on an illuminated wave surface are separated by 1.1 ft, then the differential round-trip propagation delay will be 2.25 nanoseconds. To reduce the positive spiking in the indicated radar range to within this 1.1 ft, assuming the given amplitude relationships are as stated, then a frequency deviation of 45 Mc/sec is required. Furthermore if this same error-reduction ratio is desired for a lesser axial displacement of the interfering elements, say a delay time of 0.75 nanosecond between the two round-trip returns, then a frequency deviation of 160 Mc/sec is required to reduce the multiplier to unity or the positive spikes within the physical depth of the target. Choice of operating bandwidth is therefore a statistical problem dependent on the resolution desired from the equipment. When a narrow beam of radiation (3° or less) is used at low altitude (500 ft or less), then the probability of large differential delays in an open ocean wave is remote.

The eight-channel chart recorder illustrated in block form in Fig. 25 is used to monitor the parameters of the simulator, of which Fig. 31 is a typical recording. A rather close comparison of the narrow-band phasor combinations of Figs. 27 through 29 previously described may be made with the simulator recording of Fig. 31 at the first Bessel order of carrier crossing as observed on the spectrum analyzer or at a frequency deviation of 5.33 Mc/sec. The "target depth" of the simulator is recorded on channel 6 by separately observing the indicated range in the presence of the primary path alone to establish a "boresight" reference, and then the secondary path is observed alone to give a differential range offset. In this case the secondary path has an increased path delay of 2.5 nanoseconds (ΔD_g = 21-3/8 in.) and the recorder gain was set at a level so the "target depth" or differential range offset between the two waveguide paths deflects the channel 6 chart by five units. This "target depth" deflection of five units is used over the narrow-band portion (5.33 to 33 Mc/sec) of changes in frequency deviation. The recorder gain on channel 6 is doubled over the wide-band portion of Fig. 31; i.e., the target depth shows a deflection of ten units. It may be observed that "positive spiking" (to the left of the primary target's boresight) occurs. At the lowest recorded deviation of 5.33 Mc/sec, the peak-to-peak range deflection is 47.5 units. This is shown as 45 units to the left of the primary target boresight and 2.5 units to the right. This total deflection is an error of 9.5 times the "target depth" of five units. Except for the large spike when the two paths are at rf phase opposition, the indicated range remains during the bulk of the phase cycle at approximately 2.5 units below or to the right of the primary target's boresight. This situation is analogous to the vector presentation of Fig. 27, previously discussed for the in-phase condition, where the indicated range (derived from SB_{12}) is half-way between the primary and the secondary targets (derived from SB_1 and SB_2). The 2.5 units of Fig. 31 is a 0.5 multiplier of the target depth of 5 units. This value corresponds to the computed 0.474 multiplier shown in Fig. 29 for the bulk of the phase cycle.

The simulator record of Fig. 31 not only substantiates the previous narrow-band analysis, but also shows a decrease in the indicated range error as the bandwidth or frequency deviation is increased. The recording shows a peak-to-peak deflection of the indicated range on channel 6 of ten units when operated at a frequency deviation of

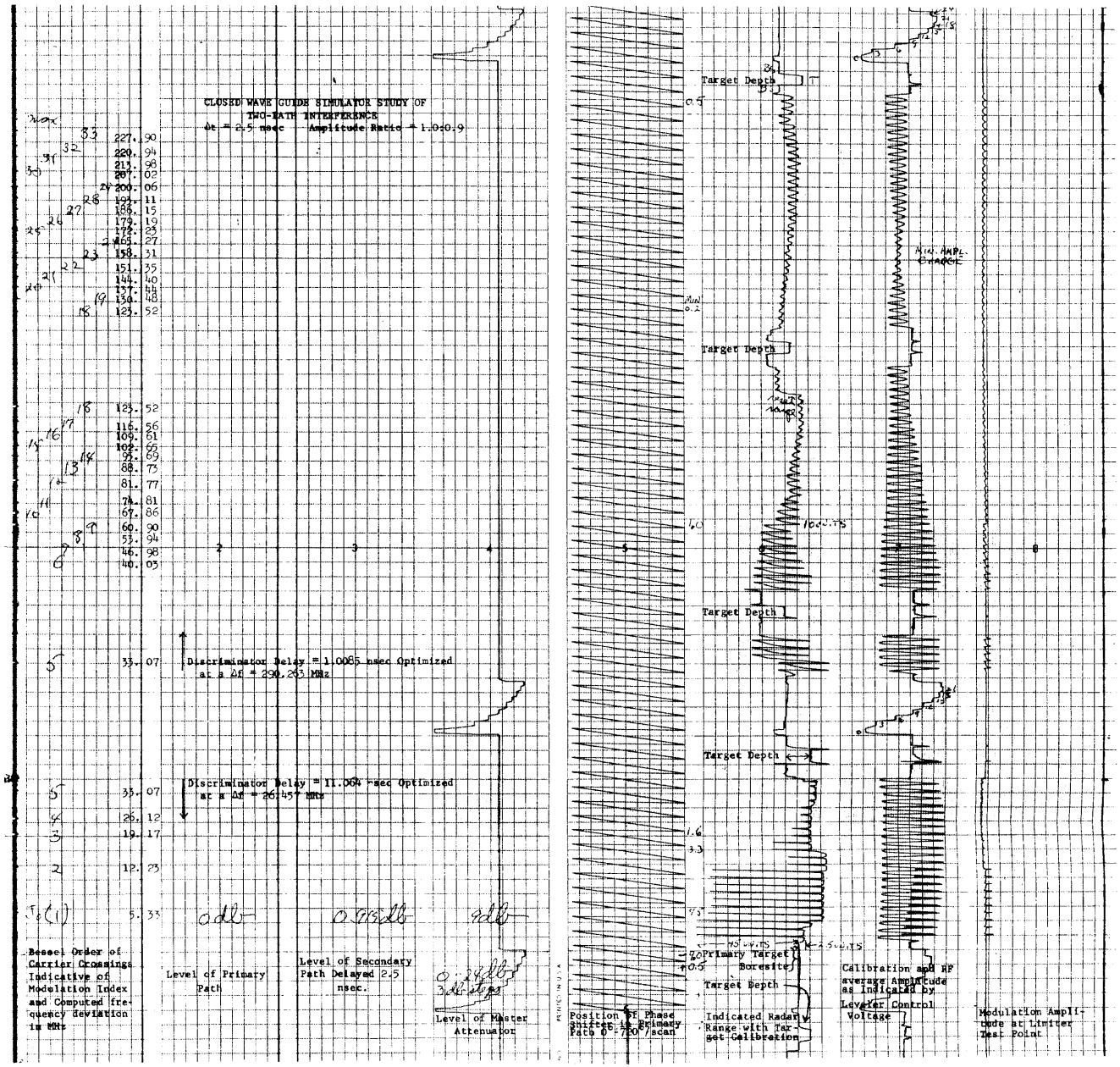

Discrete Intervals of Carrier Crossings as Observed on Spectrum Analyzer to Indicate Frequency Deviation.

Notations of Path Delay and Amplitude Ratio between Primary and Secondary Paths

Primary:		Secondary:
0 db	(1.0 to 0.9)	-0.915 db
0 nsec		2.5 nsec

Level of Master Attenuator

Position of Phase Shifter in Primary Path (0° to 720°)

Range Readout of Radar from Phase Detector with Target Calibration.

RF Amplitude of Combining Paths as Indicated from RF Leveler Ampl. with Amplitude Calibration.

DC Amplitude of Detected Modulation from Limiting Ampl.

Fig. 31 - Simulation recording of multiple functions (see Fig. 25) for a fixed target delay of 2.5 nsec and an amplitude ratio of 1 to 0.9

(PAGE 58 BLANK)

This page intentionally left blank.

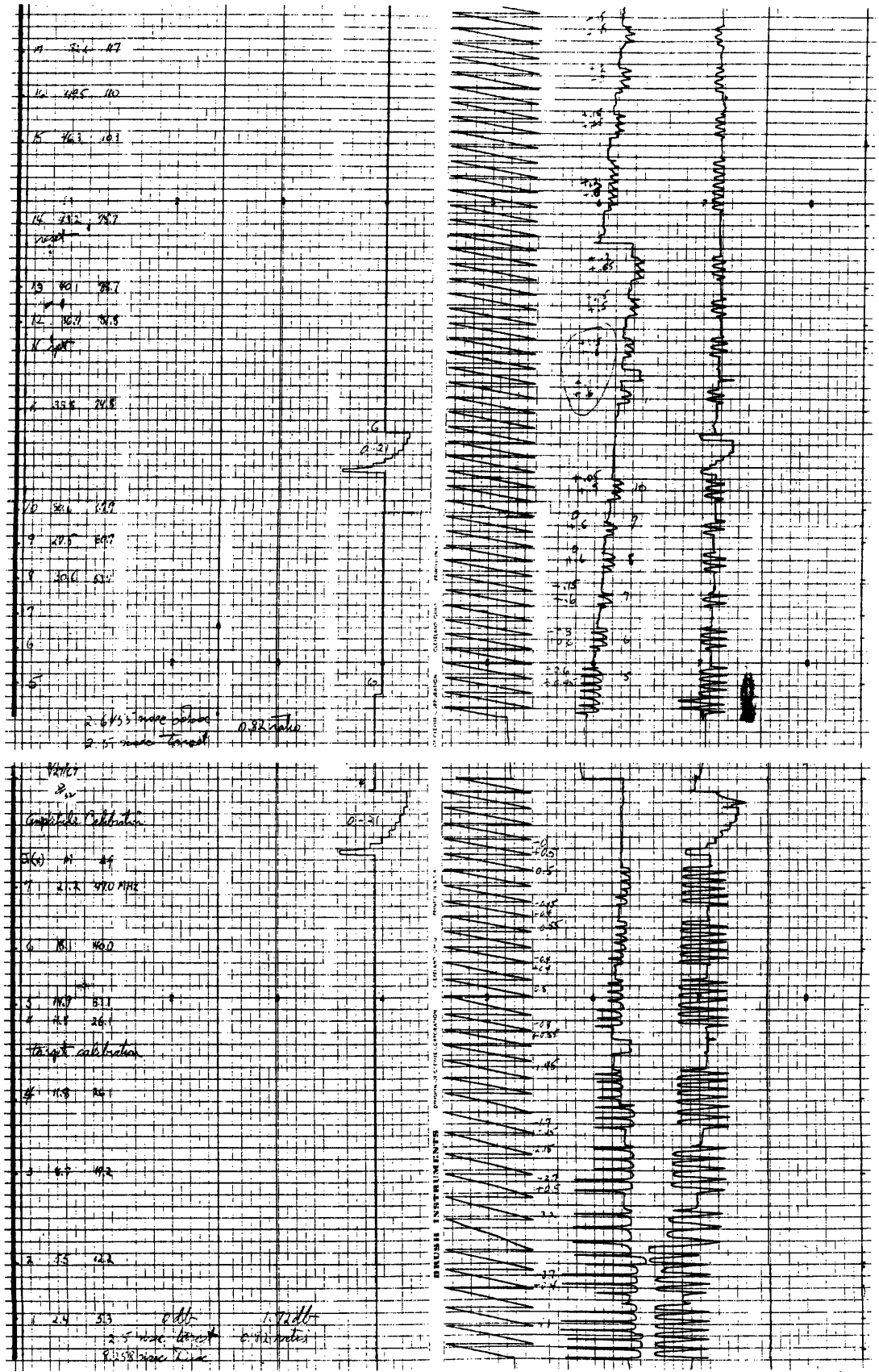

Discrete Intervals of Carrier Crossings as Observed on Spectrum Analyzer to Indicate Frequency Deviation. 0 to 117 Mc/sec

Notations of Path Delay and Amplitude Ratio between Primary and Secondary Paths

Primary: 0 db (1.0 to 0.82) 0 nsec

Secondary: -1.72 db 2.5 nsec

Level of Master Attenuator

Position of Phase Shifter in Primary Path. (0° to 720°)

Range Readout of Radar from Phase Detector with Target Calibration.

RF Amplitude of Combining Paths as Indicated from RF Leveler Ampl. with Amplitude Calibration.

DC Amplitude of Detected Modulation from Limiting Ampl.

Fig. 32 - Two-path simulation of a fixed target delay of 2.5 nsec and an amplitude ratio of 1 to 0.82 showing two segments of data for a change in the waveguide discriminator bandwidth

This page intentionally left blank.

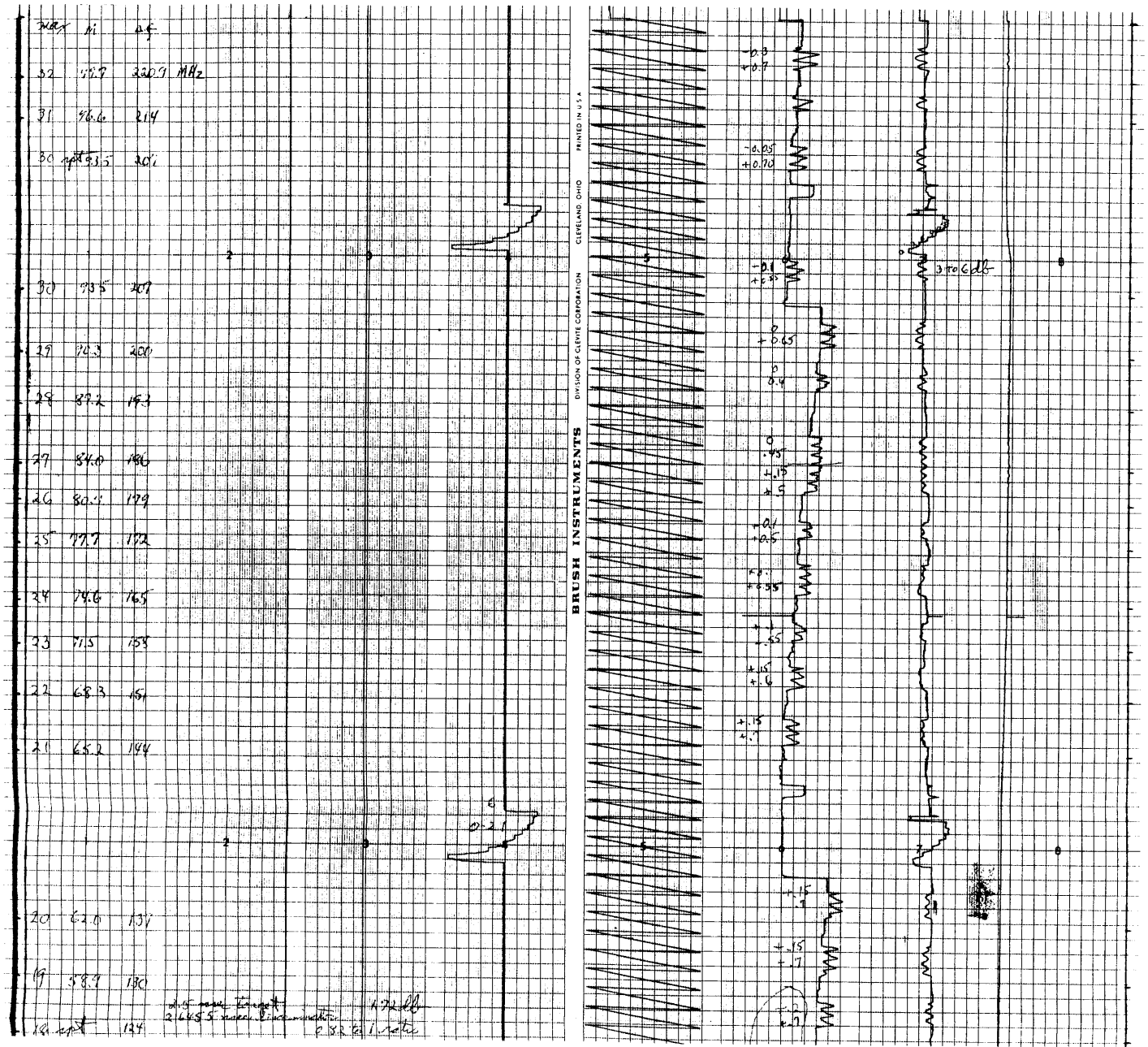

Discrete Intervals of Carrier Crossings as Observed on Spectrum Analyzer to Indicate Frequency Deviation. 124 to 221 Mc/sec

Notations of Path Delay and Amplitude Ratio between Primary and Secondary Paths

Primary: 0 db (1.0 to 0.82), 0 nsec

Secondary: -1.72 db, 2.5 nsec

Level of Master Attenuator

Position of Phase Shifter in Primary Path (0° to 720°)

Range Readout of Radar from Phase Detector with Target Calibration.

RF Amplitude of Combining Paths as Indicated from RF Leveler Ampl. with Amplitude Calibration.

DC Amplitude of Detected Modulation from Limiting Ampl.

Fig. 33 - Continuation of the recording shown in Fig. 32 for wide-band frequency deviations from 124 to 220 Mc/sec

This page intentionally left blank.

60.9 Mc/sec, as indicated on channel 1. This represents a target error multiplier of unity as scaled relative to the target depth of ten units. At a frequency deviation of 123.52 Mc/sec it may be noted that "positive spiking" has virtually vanished, and the indicated range remains near the midpoint between the primary and secondary targets throughout the phase cycle. The position of the motor-driven phase shifter in the primary path is indicated on channel 5 with the "sawtooth" read-out covering a 0° to 720° change in relative rf phase between the two paths, or two full rf phase cycles. Other dynamic characteristics of the simulation equipment are monitored on channels 7 and 8. Channel 7 shows the changes in rf level during calibration and throughout the phase cycle, while channel 8 shows the change in detected modulation amplitude. Calibration level of the master attenuator at the input of the simulator is monitored on channel 4. Amplitude ratios and differential path lengths are noted on channels 2 and 3, as well as any pertinent parameters of the simulator operation. It is noted that the discriminator delay was increased over the narrow-band portion of the test. This was done to increase the discriminator sensitivity when a small deviation is used and thereby avoid marginal operation of the equipment. Increasing the discriminator delay narrows the acceptance bandwidth of the interferometer discriminator and makes the receiver more sensitive to the narrow transmitted bandwidth in order to avoid system error. It is evident from the leveler control voltage, recorded on channel 7 and calibrated in 3-db steps which are based on the calibration of the master attenuator, that the net rf level may fade under these conditions from essentially zero to in excess of 20 db without affecting the indicated range. At 0 db of the master attenuator, the leveler appears to be overloaded and causes some range offset, and at -24 db the leveler begins to lose control. Within these extremes the equipment should faithfully reproduce the effects of the multipath interference.

The simulator studies shown in Figs. 32 and 33 are also for a two-path differential delay of 2.5 nanoseconds, but at a relative amplitude ratio of 0.82 to 1. The target error multiplication factor is indicated on the left side of the channel 6 record for each deviation step based on a "target depth" of ten units both for the in-phase and out-of-phase cases. The plus or minus is used with this factor to indicate position relative to primary target boresight. These recordings indicate that any frequency deviation in excess of ±47 Mc/sec for the two-path parameters chosen yields very little improvement in the target-error multiplication factor. The two figures show a greater definition of the fine structure at each progressive deviation step than that shown in Fig. 31, although the experimental procedure was similar.

A theoretical computer analysis of two-path interference discussed in this report provides a more rigorous basis for simulator study than the simple phasor representation described previously. Functionally the computer determines the phase shift of the modulation by accounting for the effect of all the significant upper and lower side frequencies. The single vectorial combination is essentially correct for a low modulation index and serves to represent pictorially the effect of multipath error. However, it is evident from the simulator records of Figs. 31 through 33 that as the frequency deviation is increased, the modulation phase shift rapidly diminishes from the error computed by the simple phasor study.

Extent of Targets Simulated

A complete series of simulator measurements was made using progressive steps of secondary path delay between 0.3 and 10 nsec at each of five amplitude ratios while the frequency deviation was progressively increased from 5.3 to 235 Mc/sec. Path delay was obtained by inserting additional lengths of waveguide in the secondary path. Since the waveguide propagation time is dependent on both the guide's length and the rf wavelength, it is necessary to determine the ratio of transmission delay within the guide relative to free space at the center frequency used; i.e., 9.51 Gc/sec. The deviation of

this computed constant of 1.38070 is approximately ±2 percent as the frequency is changed by ±200 Mc/sec from the center frequency, and therefore the change in propagation time within the guide as the frequency is modulated may be neglected. The waveguide delay time in nanoseconds used in the simulator was computed from

$$\Delta t = \Delta D_g \times 1.38070/11.808$$

where ΔD_g is the guide length in the secondary path in inches, 1.38070 is the guide's propagation ratio at the center frequency of all observed spectra, and 11.808 is the free-space propagation velocity (c) in inches per nanosecond (note: 11.808 in. per nanosecond is equal to 300×10^6 meters per second). The differential length, or distance ΔD_g, of the two waveguide paths was changed from 2.5 to 86 in. in progressive steps to cover the respective changes of Δt from 0.3 to 10 nsec of differential path delay. These delay times selected are equivalent to having two points of reflection on the water wave's surface displaced in radial distance from the radar (assuming single direct reflection) differing by 1.77 in. to 59.04 in. In order to have direct reflection from two points displaced by 59 in., a gravity wave with a slope of 17 degrees and an illumination of a 16-ft spot would be necessary. Such a condition would exceed the undesirable features that could limit the radar resolution of a stormy sea with the airborne system. A calm sea with wind-blown ripples of two inches or less in height would normally not be expected to be resolved, since more than half of the wave's length (or even several ripple wave lengths) would be included within the divergent antenna beam of illumination. This limitation results in spatial averaging of the fine surface structure, with the average range changes being smoothed out to a flat surface when the multipath effects are minimized. However, a gravity wave of two-inch height and a length of at least twice the beam diameter on an otherwise glassy sea may be resolved, assuming the use of a sufficient frequency deviation to minimize the radar-range "noise." Such a small target delay of 0.3 nsec, simulating a wave height of 1.77 in., does serve to verify the theoretical requirement for increasing transmitted bandwidth in the simulator in order to maintain the multipath error to within the "target depth." The repeatability of the equipment in resolving these small range changes is also a measure of the system's stability.

It may be observed on channel 6 (sixth trace from left) of the simulator record of Fig. 34 where two equal path lengths are used ($\Delta D_g = 0$) that although no offset between the boresight of the primary path (BS) and the position of the secondary path or target (T) is shown, some small range change takes place as the rf phase is shifted. Channel 6 gain for this study was the same as shown on Fig. 33, and therefore the range error indicated for the equal paths is essentially constant at 0.5 nsec regardless of the frequency deviation.

When a small differential path delay of 0.702 nsec is used as in Fig. 35, then positive spiking occurs over most of the operating bandwidth. This indicates that an extremely large bandwidth or frequency deviation is required to reduce the target error multiplier toward unity. It may be noticed that the rf level shown on channel 7 of both Figs. 34 and 35 changes by approximately 20 db regardless of the frequency deviation being used. The simulator recordings of Figs. 31 through 33, where a longer differential path delay was used (2.5 nsec), show progressively less change in the rf level on channel 7 as the frequency deviation is increased. A more constant rf level results because the energy in a portion of the wideband transmitted spectrum will be reinforced on combination due to constructive rf phasing at the frequency and delay used, while at the same time another portion will be in phase opposition and hence reflected and absorbed in the isolators or directional couplers of the simulator. The propagated energy may therefore be "balanced" as the rf phase of one path is swept through 360 degrees with a variable phase shifter.

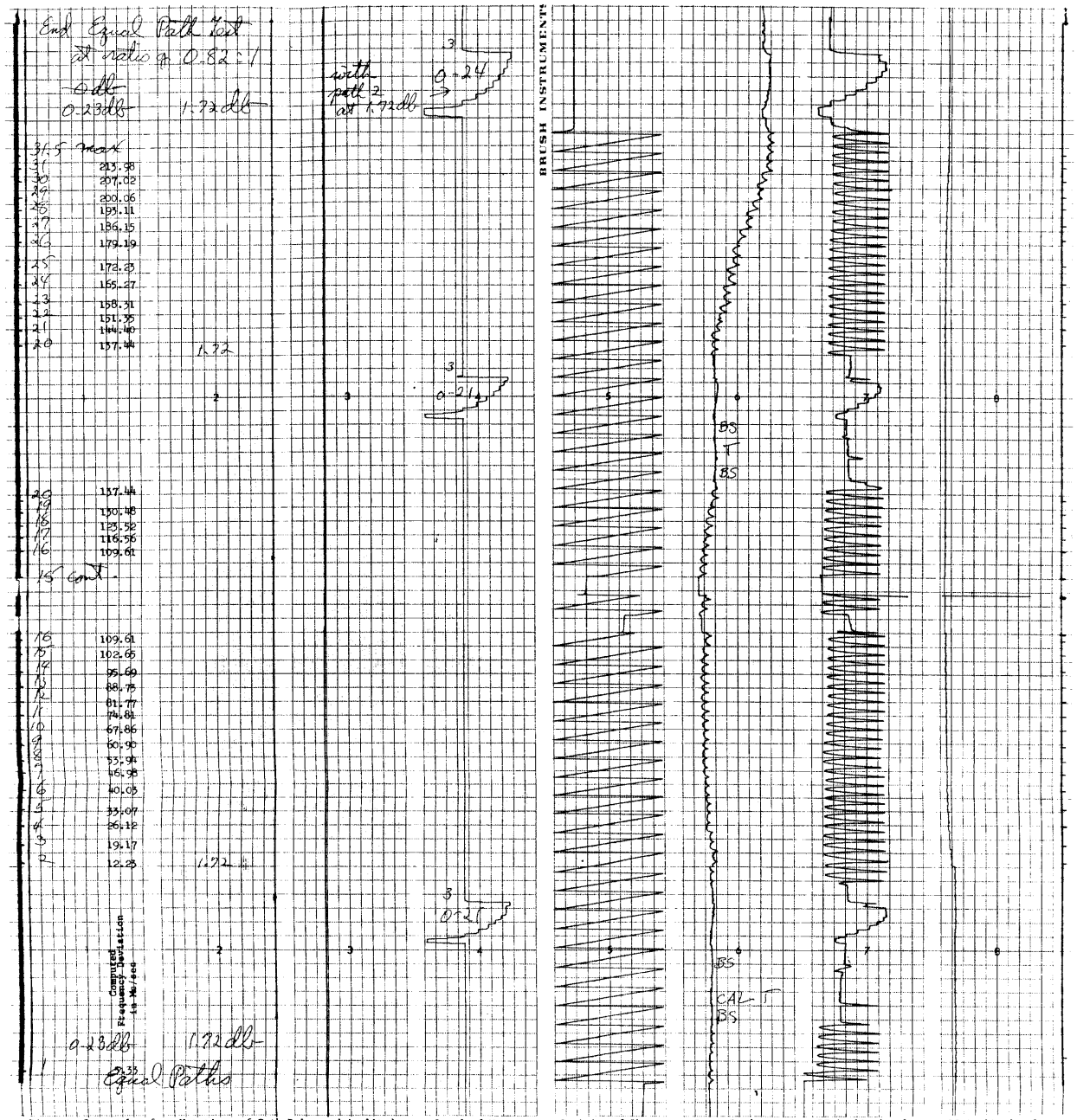

Discrete Intervals of Carrier Crossings as Observed on Spectrum Analyzer to Indicate Frequency Deviation.

Notations of Path Delay and Amplitude Ratio between Primary and Secondary Paths

Primary: 0 db (1.0 to 0.82) 0 nsec (equal paths)

Secondary: -1.72 db 0 nsec

Level of Master Attenuator

Position of Phase Shifter in Primary Path (0° to 720°)

Range Readout of Radar from Phase Detector with Target Calibration.

RF Amplitude of Combining Paths as Indicated from RF Leveler Ampl. with Amplitude Calibration.

DC Amplitude of Detected Modulation from Limiting Ampl.

Fig. 34 - Two-path simulation of interference when paths are of equal delay length. One path is rf phase shifted through 360 degrees and has an amplitude ratio of 1 to 0.82 relative to the other path. This plot indicates the stability of the simulator over a dynamic amplitude range of 0 to 28 db and a frequency deviation from 12.2 to 214 Mc/sec (second to 31st Bessel zero crossing).

(PAGE 66 BLANK)

This page intentionally left blank.

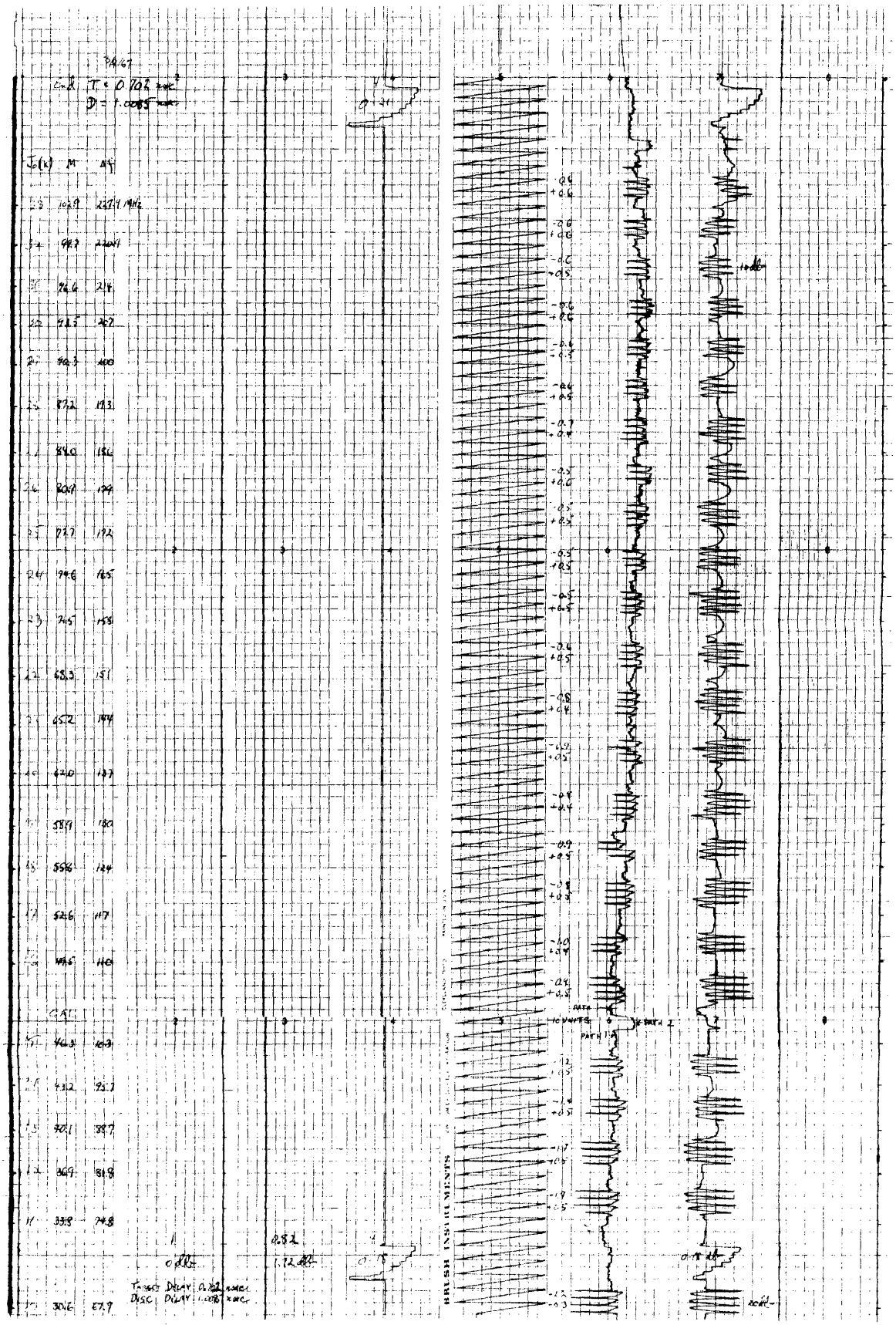

Fig. 58 - Two-path waveguide simulation where one path is delayed 0.702 nsec and has an amplitude ratio of 1 to 0.82 relative to the other path

This page intentionally left blank.

The distribution of the sidebands in a wideband FM waveform is not uniform; i.e., they follow a Bessel order of amplitude progressions in which the energy rises toward the bandwidth extremes when sinusoidal modulation is employed. The computed frequency deviation of 158 Mc/sec used on the simulator records of Figs. 31 or 33 appears to cause the minimum change in power output from the multipath combination and is indicated on channel 7. Figure 36 is a steady-state plot of phase interference in the simulator when the same 2.5-nsec delay path is used. Both paths were set to equal amplitude and brought to a phase null with a calibrated phase shifter at the center frequency (no modulation) of 9.51 Gc/sec. The calibration phase scale was set to 180 degrees at this null point. Then the CW carrier from the BWO was offset ±20 Mc/sec, ±50 Mc/sec, etc., and the combination was again nulled at each frequency increment in order to obtain the rf phase plot versus frequency deviation. It is evident that these single carrier measurements substantiate the cause of the balancing effect to the net rf level due to a phase progression of the side frequencies in a wideband frequency deviation. Since a differential path length exists, when the wavelength or frequency is changed the interfering wavelengths may be in phase at one frequency and out of phase at another.

The above explanation of differential rf phasing properties in the waveguide is needed to better visualize why the net rf level ceases to change during rf cancellations and reinforcements of a two-path simulation shown in Figs. 31 through 33 when the frequency deviation is approximately 158 Mc/sec and the differential path delay is 2.5 nsec. This effect would likewise be evident in the free-space case in a similar manner within the accuracy noted for K in the preceding introduction. The simulator record of Fig. 34, where the delay of the secondary path is made equal to the primary path, and at an amplitude ratio of 0.82 to 1.0 similar to Figs. 32 and 33, shows a consistent fading range of 20 db in the net rf level regardless of the deviation used. Although the guides do give a differential delay to the frequencies within each group in each path, the combination phases of any "instantaneous frequency" within the groups are now both equally delayed, and so the entire spectrum simultaneously goes through cancellations and additions as the motor-driven phase shifter in the primary path is rotated.

Thus it is evident that when longer differential delays are used in the simulator, i.e., insertion of longer guide lengths in the secondary path, a smaller deviation is necessary to reach a balance of the average rf level of the recombined groups as the phase is swept. This average rf level shown on channel 7 on Fig. 33 will again change from this balance as the deviation is increased beyond 158 Mc/sec to approximately 300 Mc/sec, where the rf wavelengths of the side frequencies would be again equally balanced.

Simulator Comparison to a Functional Radar

If we assume that an airborne radar records the profile of a storm at sea where the wave slope reaches a theoretical maximum of 17 degrees, and if the illuminating spot on the surface consists of a half-power circle of 16 ft (3 degree beam from an altitude of 300 ft), it is possible for two points of reflection at opposite edges of the beam to be displaced in range by five feet. A five-foot radial target displacement causes a differential delay between the two echoes of approximately 10 nsec. It is clear that any multipath delay in excess of 10 nsec for the conditions stated must be derived from other sources previously discussed. Therefore the two-path simulator studies are limited to the region of delay from 0 to 10 nsec or from 0 to 9.84 ft of equivalent free-space length in the secondary path. A computed 7-1/8 ft of waveguide produces this differential delay of 10 nsec at the center frequency of 9.51 Gc/sec.

A closed waveguide simulator neglects the problem of local antenna leakage or cross-coupling that is always present in some degree in a practical profiling system. For such a system as the one described in this report, it is therefore of value to minimize this additional signal path to a level in excess of the minimal reflected signal. Since the

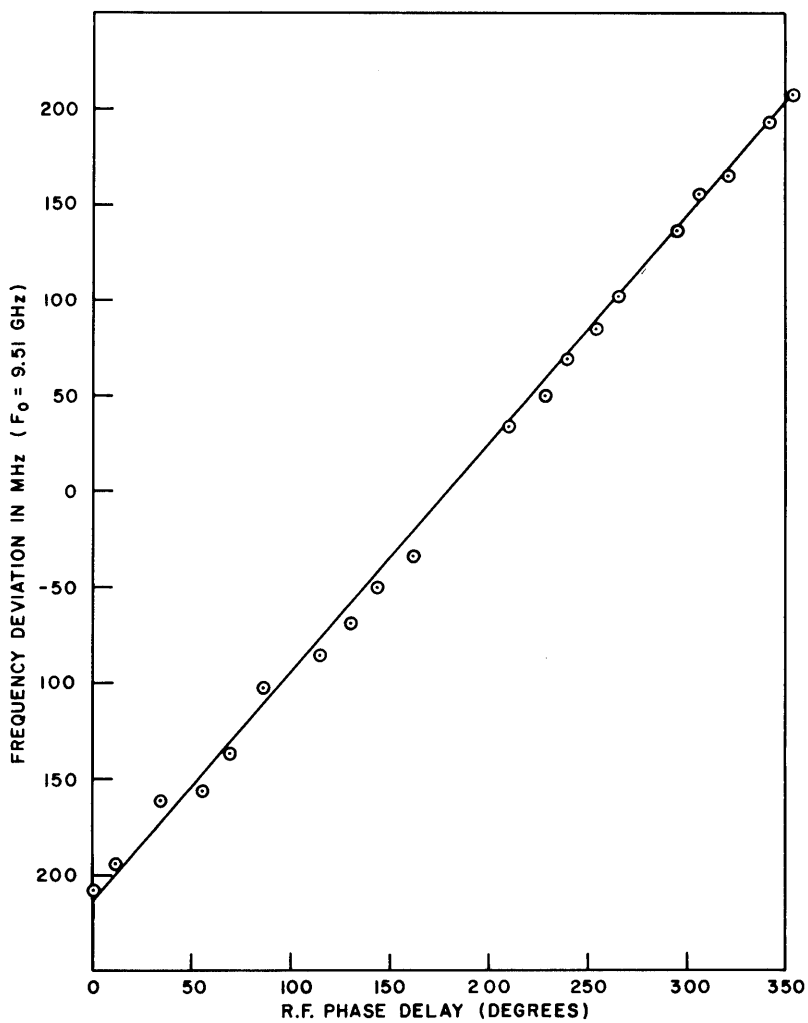

Fig. 36 - Two-path cancellation of side frequencies in waveguide for 2.5-nsec delay

modulation phase carried by the leakage signal may be mixed with the reflected signal, it may also be desirable to adjust the phase of the reflected signal's modulation (by choice of operational altitude) for minimal phase offset. This means that the modulation phase of the desired signal reflected from the water will be 180 degrees out of phase to that of the undesired leakage signal when the radar is located at odd multiples of 111 ft above the water. One wavelength of the 2.215 Mc/sec modulation frequency is 444 ft, and operation at an altitude comparable to any odd 90-degree interval of this wavelength will be helpful in minimizing large range excursions during the deep fades in the return. Antenna isolation and cross-coupling rejection previously discussed is of course an added necessity and must be maintained at a level lower than the deepest signal fades in the echo from the water surface. A tracking microwave filter at the input of the receiver described by Morrow (25) that could be servo controlled with the modulation frequency would be useful in minimizing these problems.

Simulator Comparison to Computer Analysis

Both the simulator studies and the computer analysis show close correspondence within an equivalent wave height of four inches or less when amplitude ratios of 0.82 to 1.0 or less are used. However, when the amplitudes of the two paths are more nearly equal, such as the case of the 0.9 to 1.0 ratio of relative amplitudes (Fig. 30), a considerable difference may develop due to equipment instability. The in-phase carrier amplitude for this ratio of the combined paths becomes 1.9, and the out-of-phase amplitude is 0.1. This 19-to-1 fading range calls for a system stability over a 25.6-db range and is therefore beyond the capability of the single rf leveling system as used in the simulator. This problem is particularly noticeable at this ratio when the frequency deviation is less than 70 Mc/sec or for delays less than 3 nsec. The control voltage of the rf leveler indicates the average rf level that enters the TWT amplifier that is being controlled. This voltage is calibrated on channel 7 of the simulator records by means of the master attenuator via a single path system. It appears that the leveler and limiter combination will maintain phase stability over a 21-db range, so if all sidebands of the FM spectrum do not exceed these amplitude extremes, the results of the simulator tests should correspond to the computer analysis. The phase-critical portions of the receiver are all operated at an optimum amplitude level, so that the dynamic input changes have a minimum effect on the system's internal phase shift.

This effect was verified through a series of simulator tests when a two-path ratio of 0.82 to 1 was used. Each spectral line adds vectorially with its composite mate, with the combined amplitude varying from 1.82 to 0.18 as its phase is respectively shifted from in phase to out of phase. This 10-to-1 amplitude range (20 db) must be accepted by the receiver without causing any perceptible modulation phase distortion during the demodulation, amplification, and limiting process. Since the range readout is unchanged as the master attenuator is shifted through 21 db, this condition appears to be satisfied.

A computer printout of the ratio of range delay above and below the primary target relative to the differential delay between the two targets is shown in Figs. 37a through 37c. Figure 37a compares the simulator data of Figs. 32 and 33 (shown in composite form as circled dots), with the computer information shown in discrete intervals. The bar-graph steps are selected at indices of modulation corresponding to the order number of carrier crossings $[J_{(0)}X]$.

The horizontal steps from 1 through 34, labeled at each fifth carrier crossing, cover selected m values from 2.4 through 106 which represent selected frequency deviations (Δf) of 5.3 through 235 Mc/sec. These values of m, or indices of modulation, are easily duplicated on the simulator by observing the spectral line of the carrier on a spectrum analyzer as the level of modulation is varied. As the amplitude of the modulating voltage applied to the BWO transmitter is increased from zero, side frequencies will appear

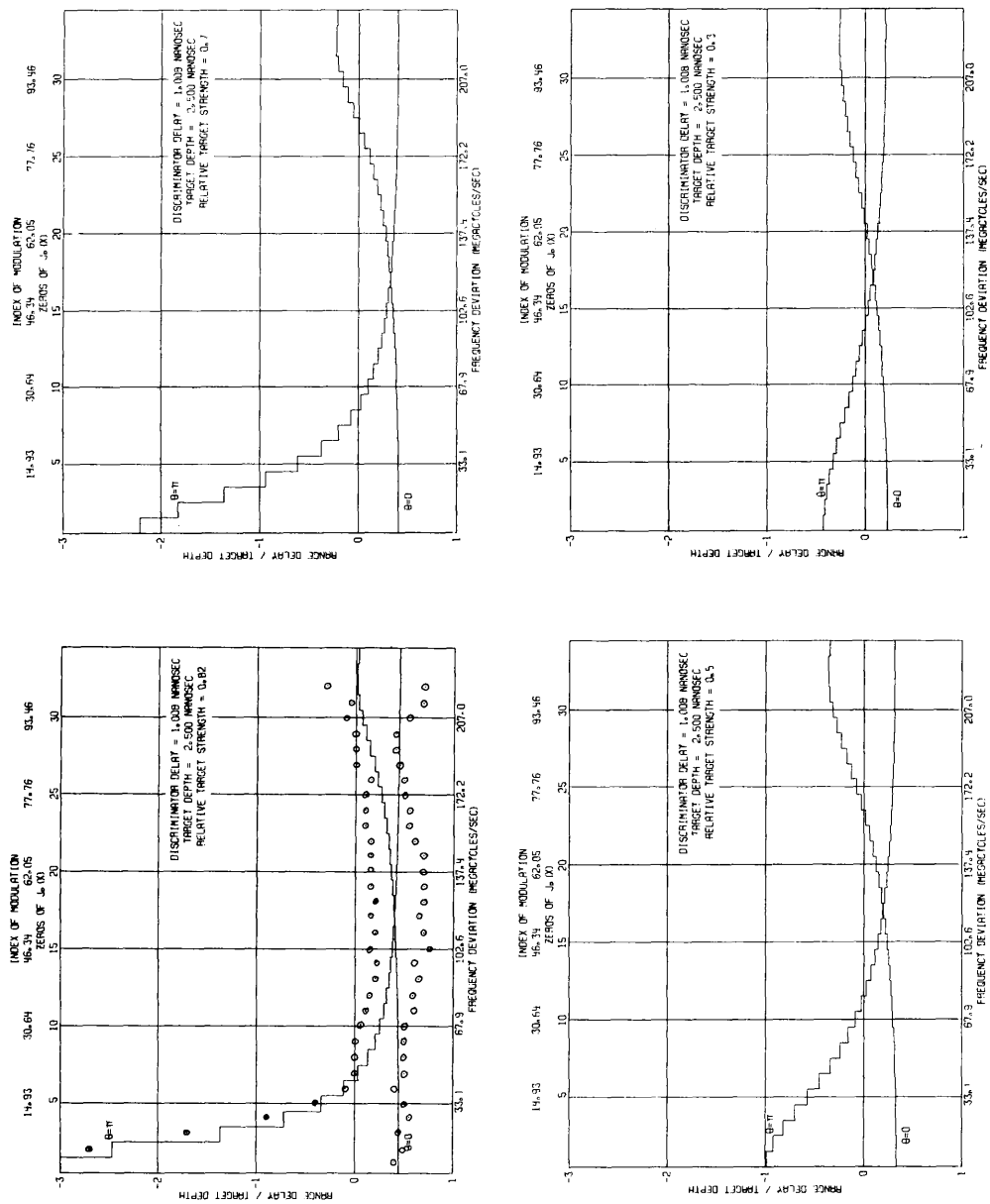

(a) Computer plot of two-path interference where one path is delayed 2.5 nsec and has each of four different amplitude ratios relative to the other path. Plots show in-phase and out-of-phase range-delay error in terms of differential path delay or target depth versus discrete frequency deviation intervals. Simulator data obtained are from Figs. 31 through 33 and are overlayed on plot of relative target strength of 0.82 to show comparison.

Fig. 37 - Range delay relative to target depth versus frequency deviation for two-path interference of a frequency-modulated system as computed from a theoretical simulation

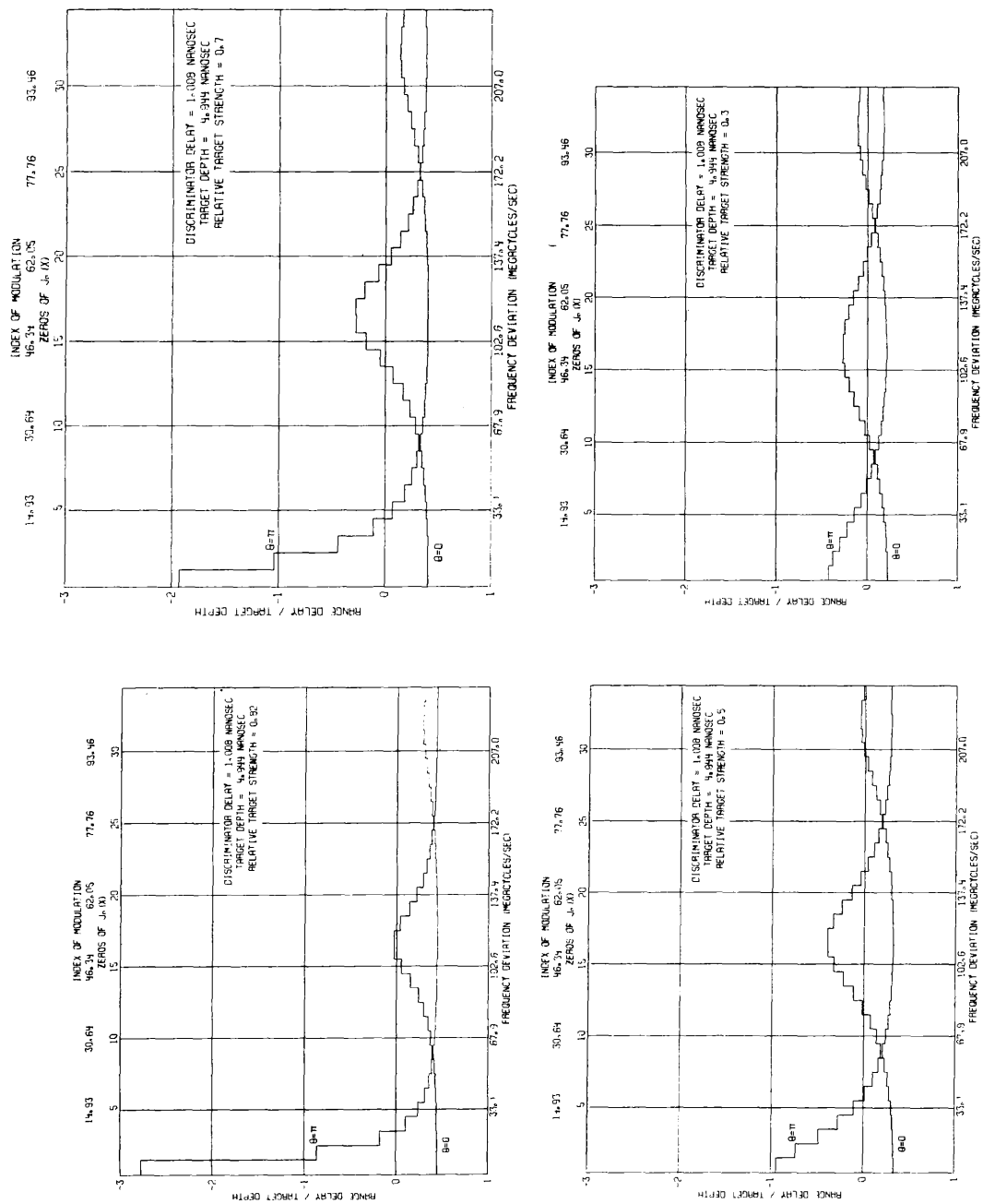

(b) Computer plots similar to Fig. 37(a), except relative target depth or path delay is 4.944 nsec for the same relative amplitude ratios or target strength to show comparison

Fig. 37 (Cont'd) - Range delay relative to target depth versus frequency deviation for two-path interference of a frequency-modulated system as computed from a theoretical simulation

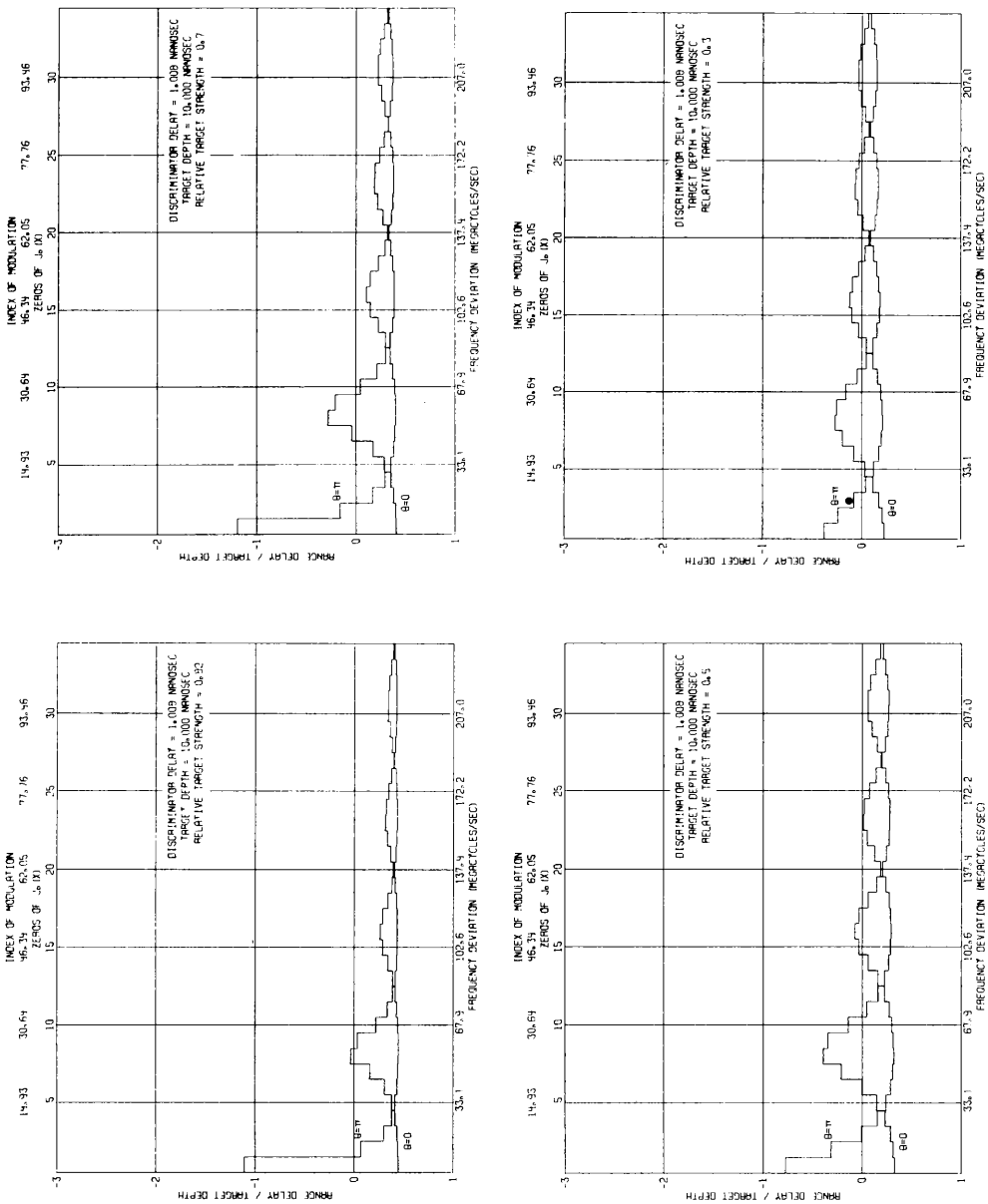

(c) Computer plots similar to Fig. 37(a) and 37(b), except relative path delay is 10 nsec

Fig. 37 (Cont'd) - Range delay relative to target depth versus frequency deviation for two-path interference of a frequency-modulated system as computed from a theoretical simulation

with the carrier on the analyzer. A continuing increase will cause the carrier to collapse to zero at an m of 2.4 for the first time, 5.52 for the second, 14.9 for the fifth, etc. The side frequencies are separated by the frequency of the modulation, and their relative amplitudes follow the laws of Bessel functions for their side-frequency order. The frequency deviation ($\Delta f = m \times f_m$) is a computed value which is consistent to the frequency spread of significant side frequencies on either side of the carrier. Thus the spectral bandwidth used is essentially twice the frequency deviation.

The computer bar graph printout for each target delay and amplitude ratio shows two values of "target depths" in the vertical plane for each step of modulation index selected, i.e., at each integer Bessel order crossing $[J_0(X)]$ of the carrier's zero value. The value above the zero ordinate line starts at the peak out-of-phase range error (for the first carrier $J_0(1)$ crossing) in target depth, while that below the zero line indicates the in-phase range errors.

The computer plot of two-path interference shown in Fig. 38 in discrete intervals illustrates the in-phase and out-of-phase errors in terms of "target depths" or multiplication factor with respect to integer steps of carrier zeroes or as a function of modulation index or frequency deviation. The simulator plot shown in Fig. 35 is intended to duplicate the computer plot of Fig. 38 (which also shows in composite the simulator data points obtained from Fig. 35) and is presented to indicate system limitations in a closed waveguide simulator. The amplitude ratio of 1.72 db between the two paths causes a carrier-amplitude change of 20 db as the differential rf phase is shifted through reinforcements and cancellations (0 to 180 degrees). Since the differential delay of 0.702 nsec is equivalent to 0.56 degree at the modulation frequency, it is necessary to operate the readout portion of the radar near the stability limits of the receiver. Range "noise" in the receiver results from lack of both phase and amplitude stability, and in this instance the calibrated delay or target depth of ten units on channel 6 of Fig. 35 is equivalent to 4.15 in. of wave height. It appears that the base line of "boresight" of channel 6 wanders or deviates by approximately one inch of range, or nearly 25 percent of the target depth. This instability inherently limits the range resolution to a wave height of one inch and makes it difficult to show good correlation on the composite plot of Fig. 38.

In addition, it may be noted on the equal-path simulation shown in Fig. 34, where the range amplitude is calibrated on a delay basis of 2.5 nsec for ten units of deflection, that the indicated delay error is 0.5 nsec peak to peak. The differential delay of the mechanical waveguide sections is essentially zero, since the plumbing is in an "equal-path" or symmetrical configuration. The cause of this experimental error may be related to internal reflections within the waveguide sections, motor-driven rf phase shifter delay changes, system amplitude effects, or coaxial mismatches in the TWT section that influences modulation phase. In any event an experimental error is present that limits the accuracy of simulation. This peak-to-peak delay error of 0.5 nsec is equivalent to a target depth of three inches of wave height that is almost constant regardless of the frequency deviation being used.

The composite computer plot shown in Fig. 37a with simulator data obtained from Figs. 31 through 33 is also calculated on the same amplitude ratio as Fig. 35, but a longer differential target delay of 2.5 nsec is used. Here it is possible to improve the correlation of computer and simulator data, since the experimental error in the simulator represents a smaller percentage of the target delay. The recorded range noise is not as evident on channel 6 of Figs. 31 through 33 as it is on Fig. 35, because range sensitivity has been reduced by approximately 11 db to cause a 2.5-nsec target depth to deflect the chart by ten units. On Fig. 35 an equal deflection was obtained for the 0.702-nsec target depth at the increased gain setting. The 2.5-nsec target delay is equivalent to a modulation phase shift of two degrees or to a shift in wave height of 14-3/4 in.

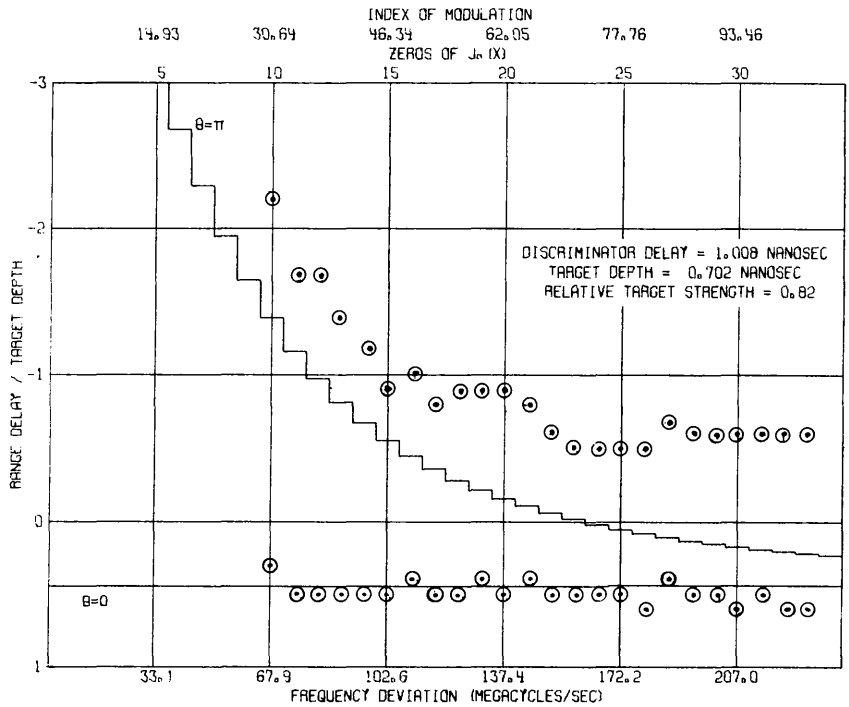

Fig. 38 - Computer plot of two-path interference with composite data from simulator derived from Fig. 35

Computer plots of two-path interference for various amplitude ratios and path delays are illustrated in Fig. 37. It is evident from these plots that a smaller frequency deviation might be chosen for the reduction of multipath error when the two-path delay or displacement is large. However, since it is desirable to maintain a small error for a heterogeneous mixture of target delays that might be expected in a complex ocean wave, it is necessary to choose a frequency deviation sufficiently wide to minimize the errors for the short as well as the long delays. A deviation of ±100 Mc/sec appears desirable for maintaining target resolution to something less than six inches.

Comparison of Frequency Discriminators

The relative merit of an interferometer type of waveguide discriminator and a waveguide filter type was investigated with the simulator. The interferometer discriminator's bandwidth is controlled by the differential length of two equal-amplitude paths, as indicated by the schematic in Fig. 39. A longer differential length (or delay) in the two paths reduces the optimum bandwidth of the interferometer, as indicated by the plot. Maximum sensitivity is obtained when the deviation and delay are optimized; i.e., when a frequency deviation of 83 Mc/sec is used, the differential length of the waveguide arms should be 30 in. of guide, or one path delayed 3.51 nsec relative to the other path. The optimum frequency deviation should not be exceeded for a given interferometer delay due to nonlinearity in its phase response to the side-frequency components. Less than optimum deviation may be used at reduced sensitivity.

Phasing of the two rf paths is adjusted for maximum output of the transmitted modulation by means of the dielectric phase shifter shown in the photographic insert on Fig. 39. The signals in the two paths are combined in a dual balanced crystal mixer in which the series-connected diodes effectively reject the common-mode changes in the amplitude of

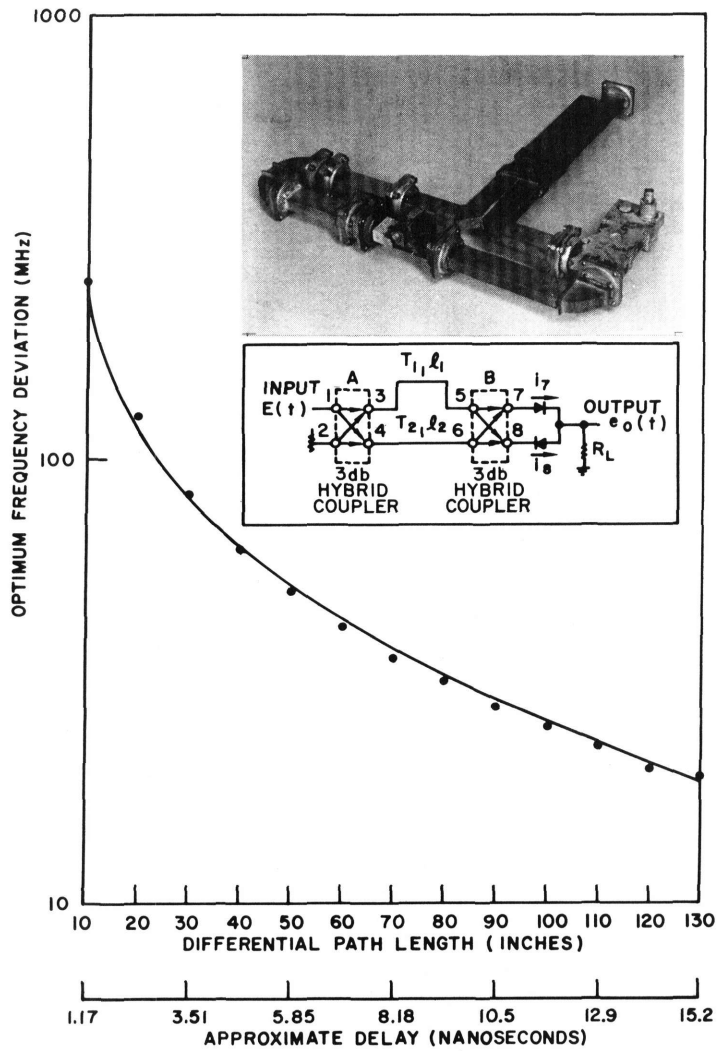

Fig. 39 - Optimum bandwidth of interferometer discriminator

the modulation. The phase interference of the signals over the differential paths produce a balanced or unbalanced drive to the crystals dependent on the incoming frequency. This results in detection of the modulation frequency by the alternate cancellations and reinforcements of current flow in the individual crystals. A dc bias current of 20 to 25 microamps improves the low-level sensitivity of the detectors by approximately 9 db, but it is important that the average rf power level does not cause an increase in the bias current. Such a change causes a shift in driving impedance to the preamplifier and hence a phase shift in the detected modulation.

The interferometer or phase discriminator is functionally similar to the two-path waveguide simulator, and therefore caused a possible doubt in the validity of simulation when two multipath systems are connected in series. It was also observed that a nonlinear boresight shift takes place when a wideband interferometer was used in conjunction with a narrow frequency deviation as the center frequency was shifted by ±20 Mc/sec.

A twin-filter type of waveguide discriminator was therefore constructed in order to limit the differential delay of the detector to less than one rf wavelength. A pair of two-cavity bandpass waveguide filters with their center frequencies offset from the radar carrier by 175 Mc/sec were connected in each arm of a power splitter driving the pair of matched crystal diodes. A twin-filter discriminator is shown in schematic form on the insert in Fig. 40 along with the individual filter response and the calculated voltage output from the crystal diodes. The linear bandwidth of this filter discriminator is 9.5 ± 0.1 Gc/sec as indicated in the calculated plot. The algebraic voltage output of a pair of reverse-driven matched diodes will produce a zero voltage output at the center frequency of 9.5 Gc/sec and change through ±60 mv as the frequency is deviated ±100 Mc/sec. Comparison tests show that marginal change in the multipath error from the simulator was observed regardless of the discriminator type being used, although the twin filter was less sensitive to center frequency changes. The twin-filter discriminator's insertion loss is approximately 8 db at the center frequency. This loss is because the off-frequency reactance of the cavity filters reflect half of the energy into the load of the 3-db hybrid coupler, in addition to the insertion loss of the filters at their band centers. The interferometer discriminator vectorially recombines the split paths in the dual balanced mixer and therefore has less loss and increased sensitivity to the modulation components of the FM wave. A band-limiting filter may be a desirable adjunct to the interferometer discriminator when the signal-to-noise ratio is low. When the noise factor of the TWT-leveler combination is relatively low and the system is operating at close range, wideband system noise or interference from other radars does not normally cause a problem. No difficulty was observed with the simulator in this respect due to the closed guide configuration. Adequate control range of the leveler, however, is most important to minimize system error when the amplitude ratio of the two paths approaches unity.

Comparison of Phasor Plot to Computer Program

At a modulation index of 0.9 the carrier amplitude is 1.0 and the first-order side frequencies are 0.5, which is essentially the ratio of a 100-percent AM spectrum. The FM waveform, however, does have a second-order side-frequency amplitude of 0.117 and a third-order amplitude of 0.01787. These side frequencies are not considered to cause a significant difference over pure AM when the higher order of pairs are 10 percent or less.

Therefore a vector representation of either an AM or an FM waveform of these values is considered comparable, and Fig. 41 shows a two-path interference case in polar form in which only first-order side frequencies are considered. The differential delay is 10 nsec, and the relative amplitudes are 0.3 to 1.0, or 10.46 db. The resultant vector SB_{12} of the in-phase combination of SB_1 and SB_2 shows an angular shift of

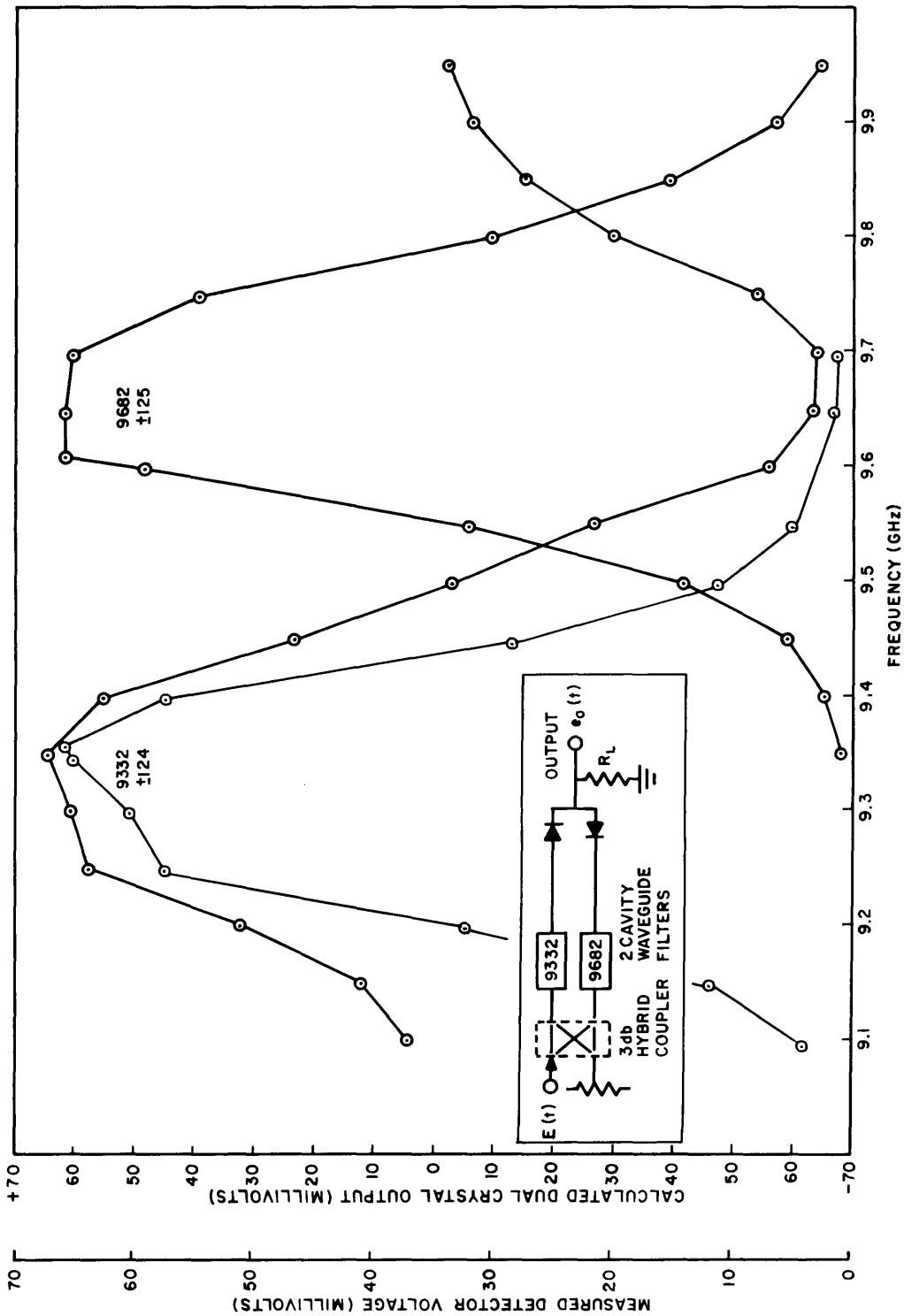

Fig. 40 - Waveguide frequency discriminator characteristics: Twin-Filter type (each filter measured at 1/2 output level for 1.1 milliwatt input to filter

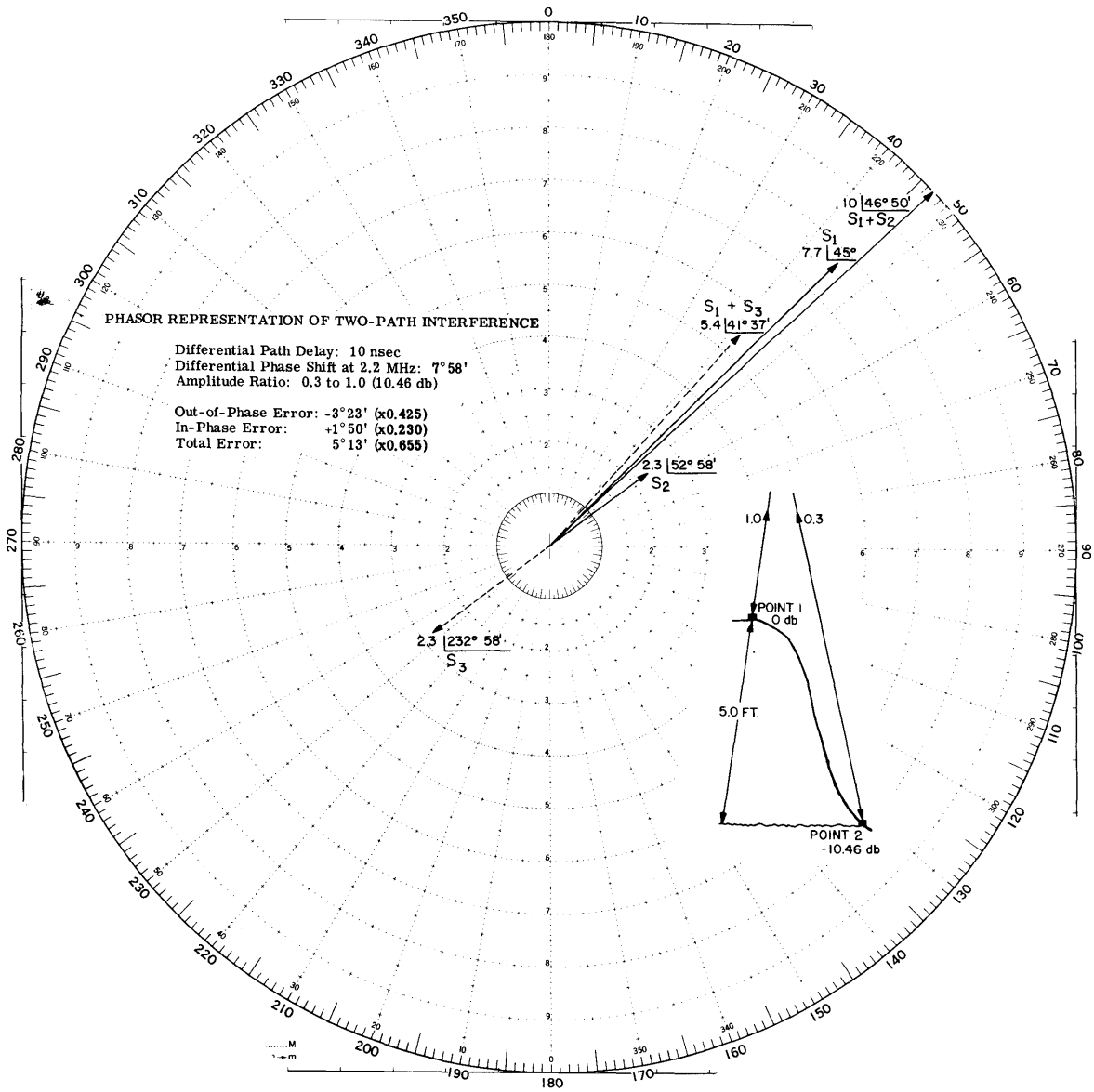

Fig. 41 - Phasor representation of two-path interference; differential path delay 10 nsec, amplitude ratio 0.3 to 1.0 (10.46 db)

+1°50′; and when the two vectors are combined out of phase, the resultant shifts to -3°23′. This peak-to-peak uncertainty of 5°13′ means that a 6.55-nsec error may exist in ranging to the primary target even though the secondary target's return is over 10 db less than that of the primary target when a small frequency deviation is used. When the two rf paths are in phase, the indicated round-trip range is 2.3 nsec more than the primary (closer and strong) target; and when the rf paths are out of phase, the indicated range will be 4.25 nsec less than that of the true round-trip range. This error will decrease as the frequency deviation is increased, as indicated by the composite set of curves shown in Fig. 42 as obtained from recorded simulator data. The form of the plot relates three amplitude ratios over a range of frequency deviation from 1 to 140 Mc/sec. The curves all represent a two-path simulator differential delay of 10 nsec. The error illustrated by the vector plot of Fig. 41 and described previously is found on Fig. 42 at the 2-Mc/sec deviation (2.215 × 0.9) and the -0.655 multiplier (6.55 nsec peak error out of 10 nsec) on the 10-db curve (0.3 to 1.0 ratio). The family of curves illustrates the total range error, or algebraic sum of the in-phase and out-of-phase errors, in terms of target depths or target error multiplier at various amplitude ratios and frequency deviations. The simulator error values plotted consider the effect of the higher order side frequencies at deviations greater than 2 Mc/sec (M = 0.9) up to a deviation where the discriminator's output should depart from a linear function. Amplitude ratios of approximately 3 db, 10 db, and 20 db are plotted and show that for this 10-nsec target, a frequency deviation of 30 Mc/sec is the first optimum or minimum peak-to-peak error over a wide range of relative target amplitudes. This effect may likewise be noted on the computer plots of Fig. 37c. The second optimum deviation occurs at 80 Mc/sec. However, when the differential range or "target depth" between primary and secondary paths is smaller, such as 2.5 nsec, the first optimum does not occur until greater than 100 Mc/sec, as indicated on Figs. 43 and 44. Figure 44 is an expansion of the computer plot of Fig. 37a, with simulator data points added in composite form to show the comparison. The algebraic sum of the in-phase and out-of-phase multipath errors is shown as a peak-to-peak target multiplier to illustrate the fact that when the amplitude ratios approach unity in the simulator (0.82), it is difficult to reduce the range noise below some minimum threshold, in this case 0.053 of the target depth or a peak-to-peak error delay of 0.1325 nsec. This 0.82 amplitude ratio causes the carrier amplitude to change by 20 db.

Figure 45 is a composite showing the comparison between the simulator's measured peak-to-peak error for a 4.944-nsec delay between the two waveguide paths with the peak-to-peak error in terms of target depth derived from the computer program, as shown on Fig. 37b. This plot is an expansion near the first minimum in the "target depth" multiplication factor. In this case the carrier amplitude changes by 14.1 db between the in-phase and out-of-phase condition, and all errors are also in terms of the algebraic sum of the in-phase and out-of-phase offset scaled to target depths.

Conclusions from Simulator Studies

It is important that the operating equipment function normally over the full dynamic range of target scintillation, i.e., amplitude fades due to both multipath interference and target aspect angle normal to the narrow radiated antenna beam. When this dynamic range is exceeded, impedance changes in the circuit result in a modulation phase shift causing false range readout. This shift was illustrated by the large error observed when the discriminator detectors were overdriven by large signals, or conversely when the TWT leveler and receiver limiters had insufficient input to function within their linear mode of operation.

The use of the simulator permits a controlled introduction of multiple interfering paths in order to verify experimentally the dictates of the theory. The ability of the

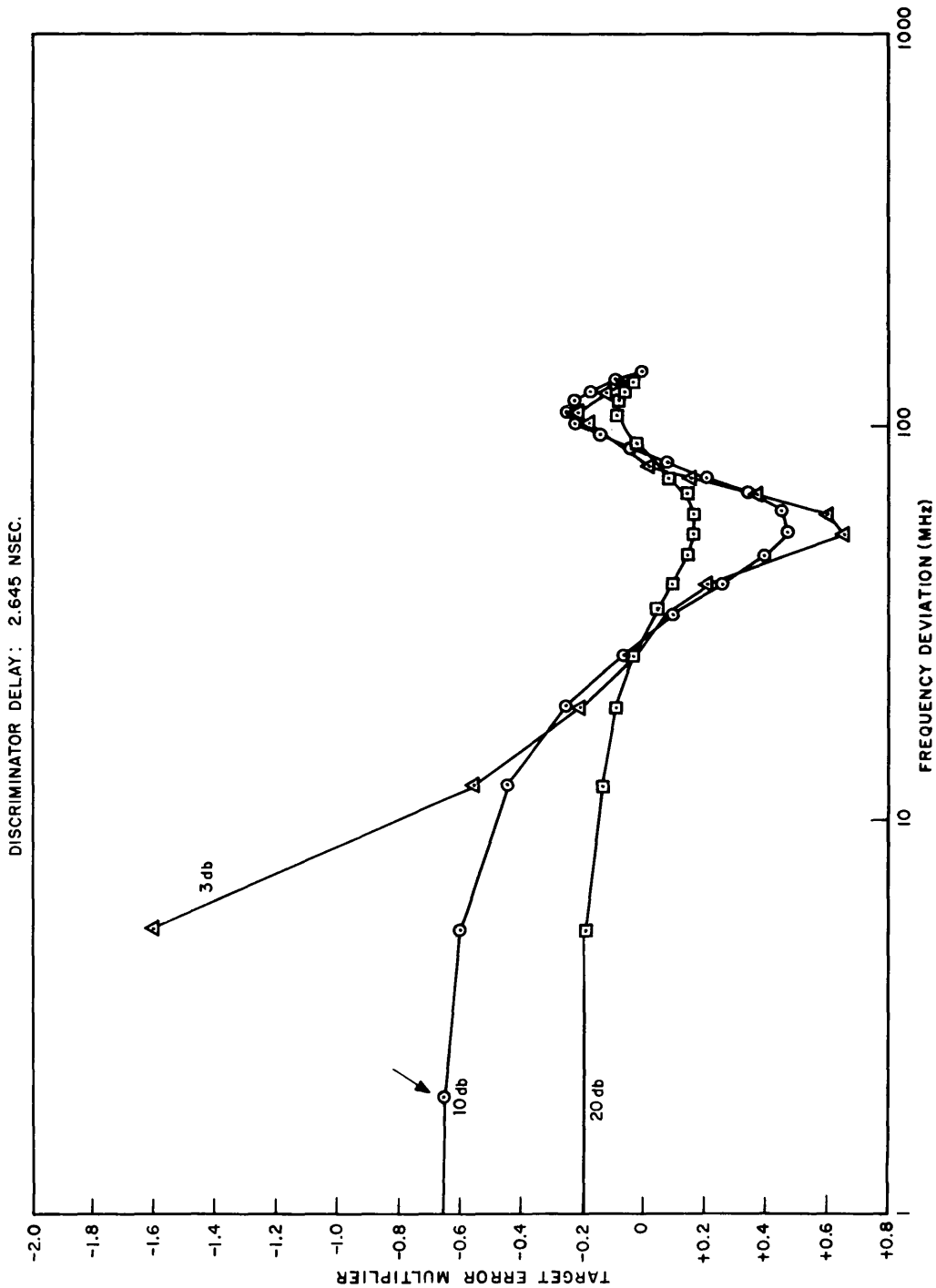

Fig. 42 - Two-path interference distortion versus frequency deviation for 10 nanosecond target depth, discriminator delay 2.645 nsec

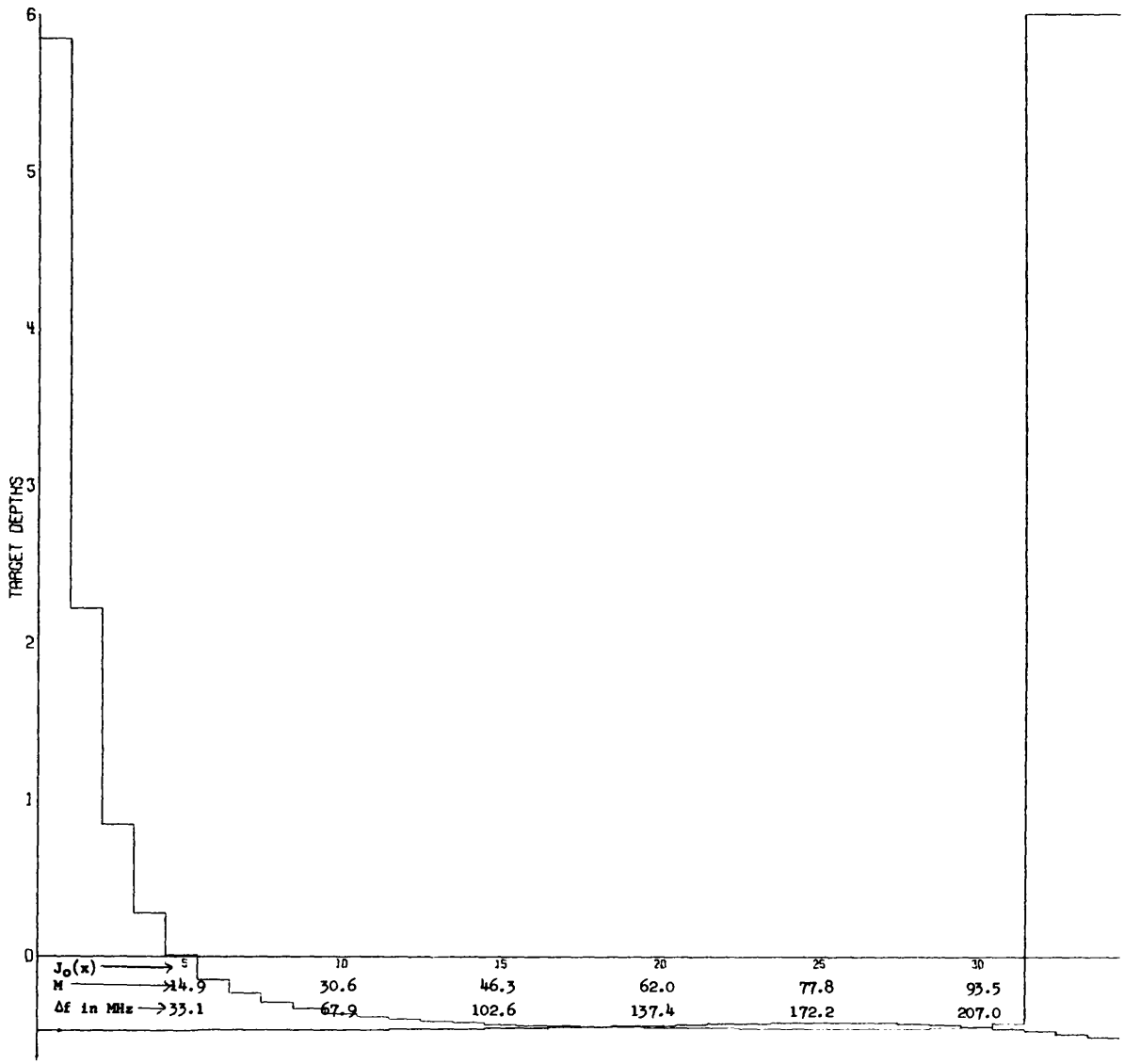

Fig. 43 - Computer plot of two-path interference; differential path delay 2.5 nsec, fixed discriminator delay 2.646 nsec, amplitude ratio 0.9 to 1 (0.915 db)

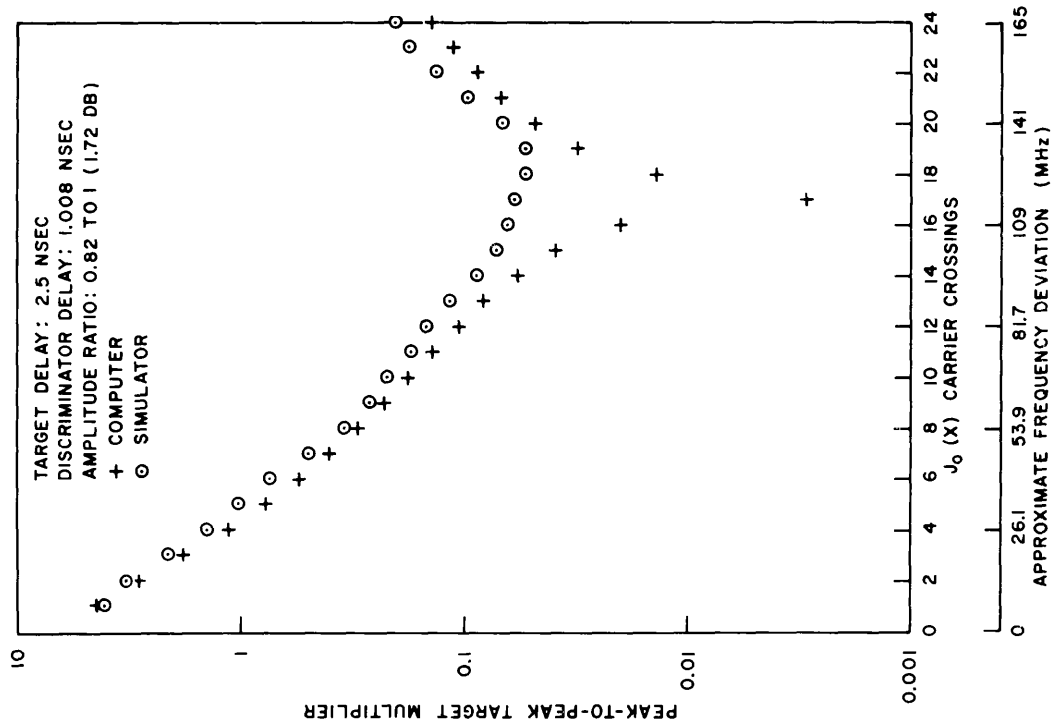

Fig. 44 - Two-path interference comparison: simulator versus computer

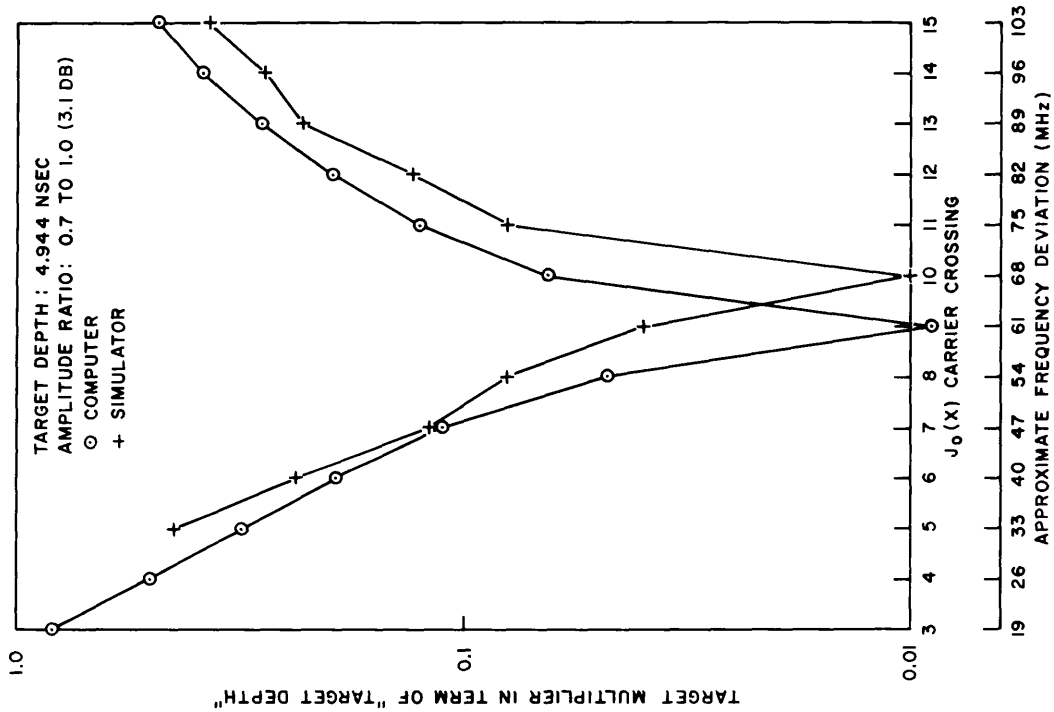

Fig. 45 - Comparison of two-path error in simulator with computer

equipment to reproduce a profile adequately is found lacking only when an insufficient bandwidth is transmitted or the dynamic amplitude limit of receiver is exceeded.

High ocean waves should be adequately resolved using the equipment described with a frequency deviation of 30 to 40 Mc/sec. However, in order to maintain system accuracy for the wide range of sea conditions expected while profiling the open ocean, it appears desirable to use a frequency deviation somewhat greater than 100 Mc/sec. The simulator measurements show good correlation with the theoretical error predicted, provided the amplitude limits of linear receiver operation is not exceeded.

EXPERIMENTS AT THE CHESAPEAKE BAY BRIDGE FACILITY

Installation of Antennas

The field work at the Chesapeake Bay Bridge Facility was undertaken in order to explore scintillation range noise in greater detail than had been possible during the earlier aircraft experiments. The range of wave conditions occurring on Chesapeake Bay was of course very restricted compared to that observed from an aircraft, but the possibility of a point-by-point quantitative comparison between radar and wavestaff records made the site attractive in spite of this limitation.

The final antenna placement is shown in Figs. 46 and 47. Figure 46 also shows the wavestaff in position. When the installation was first made the antennas were placed side by side at the north end of the gondola, with the edges of the 30-in. reflectors spaced about 10 in. apart. The range-noise level was found to be very high under this condition, and oscilloscope observations of the detected modulation showed that the phase frequently shifted by as much as 90 degrees in the direction of increasing range. Experiments with movable pads of microwave absorber indicated that no significant amount of energy was reaching the receiver except through the main lobe of the receiving antenna, so that the large phase excursions observed were apparently being caused by signals doubly reflected between the antennas or gondola structure and the water surface. In order to minimize this type of undesired echo the antennas were separated, as shown in the figure, to give an included angle between the axes of the main lobes of about 34 degrees. This change in antenna positioning caused a large reduction in the range noise level, and 90-degree phase shifts were no longer observed. From purely geometrical considerations it would appear that the probability of strong double reflections must be greatly reduced with the new location, but residual effects inevitably existed, and these cannot be readily calculated or directly measured. These effects must be considered along with target scintillation as possible contributors to the observed noise level. In an aircraft wave-profiling installation it would be difficult to obtain as large an angular offset as that used at the Bay Bridge, but the decrease of the doubly reflected signal with increasing altitude will almost certainly be governed by a higher exponent of the range than the desired signal, and the relative level may well be insignificant at normal operational heights of several hundred feet. It is also possible that a lesser angle would have given substantially the same result, but owing to the extreme difficulty of mounting the antennas at intermediate positions under the gondola no other angular separation was tried, and it can only be said that precisely vertical incidence should be avoided at very short ranges.

With the antennas at the final locations, the distance from each reflector to the illuminated patch on the water was found to be about 62 ft. This is within the "near zone" of the antennas as the term is used in radiation-pattern measurements, and to make certain that no peculiarities existed some short-range patterns were run. A convenient distance happened to be 56 ft, and this was considered to be sufficiently close to the desired distance. The half-power beamwidth was found to be close to

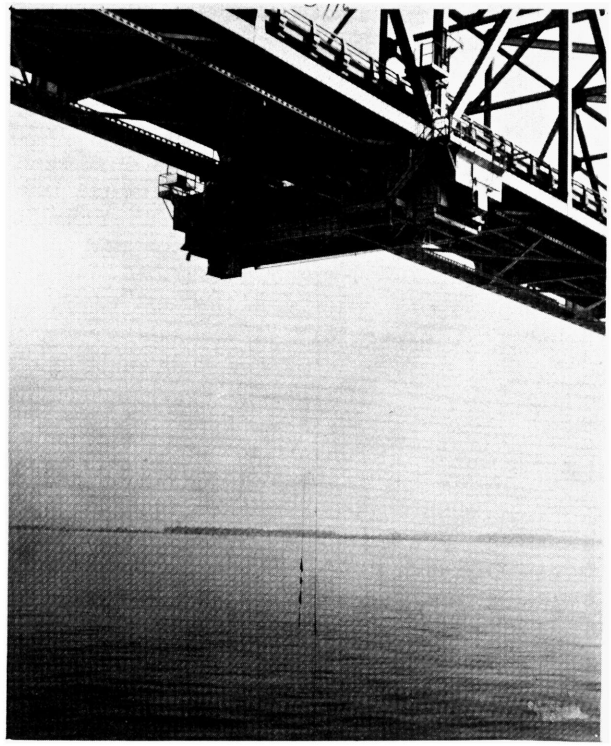

Fig. 46 - The Chesapeake Bay Bridge Facility, looking northeast

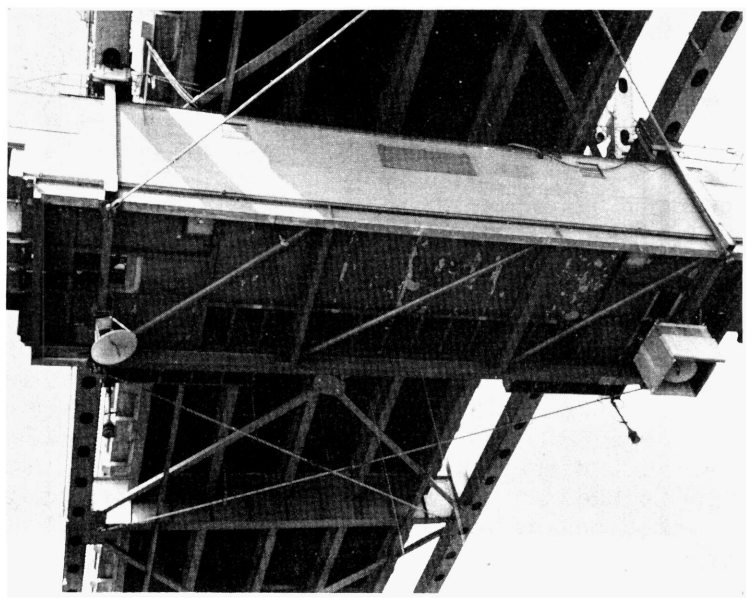

Fig. 47 - The Chesapeake Bay Bridge Facility, viewing the east wall and underside of the gondola

3.5 degrees in both the E and H planes, and at the Bay Bridge this beamwidth resulted in a nearly circular patch having a diameter of 3.9 ft, at the circle of half-power illumination. The side lobes were at least 22 db down in the E plane and over 26 db down in the H plane, and the first side-lobe peaks were 8 to 9 degrees off axis. The antennas were mounted so that the E plane was vertical and was defined by the centers of the two antennas and the center of the illuminated patch.

Using the best available figures on antenna efficiency and effective aperture, the loss between transmitter output and receiver input was calculated on the basis of a perfect specular reflection at the water surface. This loss was found to be 17 db, with an uncertainty of about ±1 db. During the radar exercises the total loss was measured by comparing the received signal levels with those produced by a closed calibration loop connected between the transmitter and the receiver. Since antenna efficiencies can be assumed relatively constant, the variation of the total loss can be assumed due to variations occurring over the propagation path. All loss figures quoted are the total loss as just defined. For the sake of brevity this will be called simply the "path" loss. The minimum path loss measured during the exercises was about 5 db greater than the calculated loss for the specular condition and was observed only when the wind was very low.

Wave-Staff Installation

The wave staff was a high-resolution resistance wire type with a helical sensing wire partially embedded in a 5/16-in.-diameter plastic core. The pitch of the helix was about 1/8 in., and the active section of the staff was 10 ft long. The staff was hung vertically in the water, as shown in Fig. 46, and was positioned by means of auxiliary guide lines as nearly as possible in the center of the illuminated patch on the water. An optical sight was used to set the position at the beginning of an operation and to check the position at intervals during data recording. The portion of the wave staff having the largest potential radar cross section was the electronics package located at the top of the active portion of the staff. This unit consisted of a short section of 3-in. pipe capped at both ends with fittings for attaching the staff and support line welded to the caps at opposite ends. With the staff positioned to place the mean water level at the midpoint of the sensing wire, the electronics case was about 6 ft above the water and was thus a potential source of an undesired radar echo which could not be separated from the surface return and which might modify the radar results. To determine whether or not such an effect did exist, a radar wave record was made while the staff was pulled repeatedly into the illuminated region and out again. This test showed that the presence of the staff in the radar beam caused no change in the wave record that could be detected by visual inspection of the chart. This negative result indicated that the staff was unlikely to be a source of trouble but did not entirely rule out the possibility of an appreciable contribution to the echo from this source under all circumstances. To provide an additional margin of safety the electronics case was covered with microwave absorber. Repeated tests with the treated staff under several different wave conditions verified the earlier finding that there were no effects visible in the radar record.

The wave records obtained with the wave staff were generally used in two ways: first, as a direct check on the accuracy of the radar wave record under different conditions, and second as a means of reconstructing the surface features as they existed in space and were viewed by the radar. This reconstruction of the water surface from the time history of the water level at a point is at best only approximate. Two basic difficulties are involved here. In the first place, the wave staff as used has no ability to sense direction, and in cases where waves having significant amplitudes arrive from more than one direction it will obviously be impossible to separate the various wave systems once their effect has been summed into a single time function. Fortunately, visual observations at the Bay Bridge Facility showed that there was generally a predominant wave system moving with the local wind, and in this case the problem is simpler; only the second

difficulty, which lies in the variable velocity of propagation of water waves, must be faced. Unlike electromagnetic and acoustic waves, which have a constant velocity characteristic of the medium, water waves have a velocity which depends primarily on their length. A mathematical relationship can be derived from classical gravity-wave theory which leads to the following relationship between the period T, which is observed by the wave staff, and the crest-to-crest length L, of the moving wave on the surface of the water:

$$L = 5.12T^2 \text{ ft}$$

where T is in seconds. This formula is strictly applicable only to infinite trains of simple harmonic waves. On the surface of the ocean this condition is fairly well represented by the systems of long low swells which sometimes occur. In the much more typical condition, when wind-driven waves of highly variable period exist, the application of the relationship is very far from rigorous, but it does offer a means for comparing wave conditions in an approximate way. In deriving this classical formula quoted for the length of a gravity wave, it is further assumed that the idealized wave is being propagated in "deep" water, that is, without being influenced by interaction of the wave circulation with the bottom. For practical purposes waves in water having a depth greater than half their length are negligibly affected by the bottom (26), and this condition was satisfied at the Bay Bridge in virtually all cases. The water in the vicinity of the gondola was over 80 ft deep, and only very occasionally did low swells a few inches in height have lengths approaching twice this depth, or 160 ft.

The way in which the classical formula was used to characterize the wave records is shown in Fig. 48. The scaled half-periods were used to calculate an L_1, L_2, L_3, etc., and these were paired with the corresponding H values to obtain an average crest to trough slope for each "half" wave scaled. It is not claimed that this process is in any sense a mathematically rigorous application of the classical formula, and it is recognized that the accuracy with which the reconstructed slopes represent the true slopes on the surface of the water will be highly variable. Nevertheless it is believed that this process offers a means of describing the surface which permits useful comparisons to be made, and that the statistics derived are at least related to the actual surface features more closely than the wave-staff time function. However, in order to avoid the implication of a closer correspondence than could reasonably be hoped for, the slope values in question will always be called the "calculated" or "reconstructed" slopes when mentioned in the text.

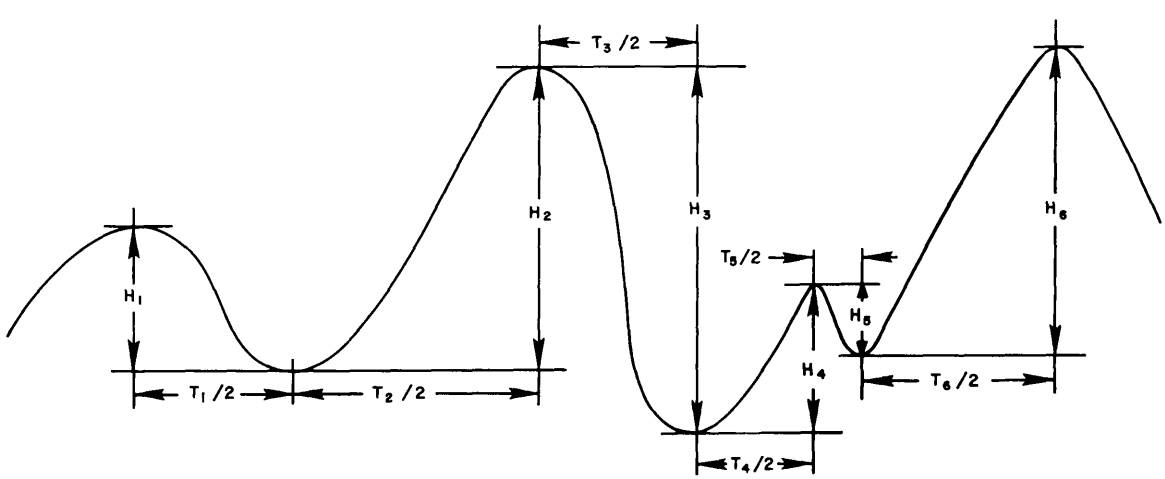

Fig. 48 - Scaling procedure for wave-staff records

The Data-Recording System

A sample of the type of chart-data record made during most of the Bay Bridge exercises is shown in Fig. 49a. The wind speed and direction information recorded on the two upper traces was obtained with an instrument located on the bridge structure about 165 ft above the water. The filtered radar height record was band limited by a five-section active filter having a nominal cutoff frequency of 1 cps. The phase and amplitude characteristics of this filter and also its transient response characteristics are shown in Fig. 50. Within its pass band the filter introduces an essentially constant time delay of about 0.4 sec. The wave-staff record was not filtered in any way external to the unit, and the internal circuitry was known to have sufficient bandwidth to reproduce any frequency components that could be created by the water surface. The "fast" radar channel was slightly filtered during this exercise and most others by a single-section RC filter having a time constant of 0.002 sec. The purpose of this filter was to attenuate higher frequency interference which otherwise tended to obscure the low-level features of the record and which might at times have overloaded the amplifiers that preceded the recorder. Since the 10 to 90 percent pen response time of the recorder was close to 0.004 sec, this filter did not alter the effective bandwidth of the recording very appreciably. The speed of response of the rf amplitude recordings on the bottom traces was limited only by the recorder; all the electronic circuits were many times faster. As indicated in the system block diagram, Fig. 8, the rf level input is derived from the control circuits of the first microwave leveler in the TWT amplifier chain. The amplitude scale obtained in this way is roughly logarithmic and was verified during each exercise by a closed-path calibration procedure. A chart record made during such a calibration is shown in Fig. 49b. The second amplitude channel, labeled "limiter bus," is derived by rectifying the modulation frequency signal after detection and amplification and indicates the point at which the signal falls below the clamping level at a particular limiter.

The slight broadening of the wave-height trace that is evident during closed-path calibration and also at times during wave recording is primarily 60-cps ripple. Almost all of this ripple was introduced via the BWO transmitter apparently because of residual 60-cps frequency modulation of about ±1 Mc/sec on the BWO output. It is believed that this residual modulation was translated into a phase offset of the 2.215 Mc/sec desired modulation by a slight frequency dependence of the phase delays in the microwave components of the receiver. The effect was somewhat greater when the narrower band discriminators were in use and is responsible for part of the thickening of the height trace when operating at the lower frequency deviations. There is also a small amount of transient noise and jitter seen on the height trace. This was a somewhat variable quantity apparently partly due to internal causes and partly to the low-frequency radio interference that has been discussed elsewhere. Since the scale of the height record is here 20 lines to one foot of height, the transient excursions represent less than 0.1 ft of height.

The closed-path signal was obtained via a 20-db directional coupler and included a section of coaxial cable having a loss of 2.6 db. Thus 22.6 db must be added to the tabulated attenuator settings to obtain the total path loss. At a reading of slightly over 40 db the leveler loop became unstable under steady-state conditions and fluctuated over the range shown. There was not, however, a corresponding level fluctuation, as shown by the limiter record in Fig. 49b at 45 db. At this level a small amount of system random noise is evident, and at the 50-db setting, or 72.6 db total path loss, the peak-to-peak phase noise represents about 0.5 ft of wave height.

Since transient phenomena caused by target rf wave interference can theoretically be very brief compared to the periods of the target motion, there can be no assurance that a given speed of response will be adequate. It was therefore considered advisable

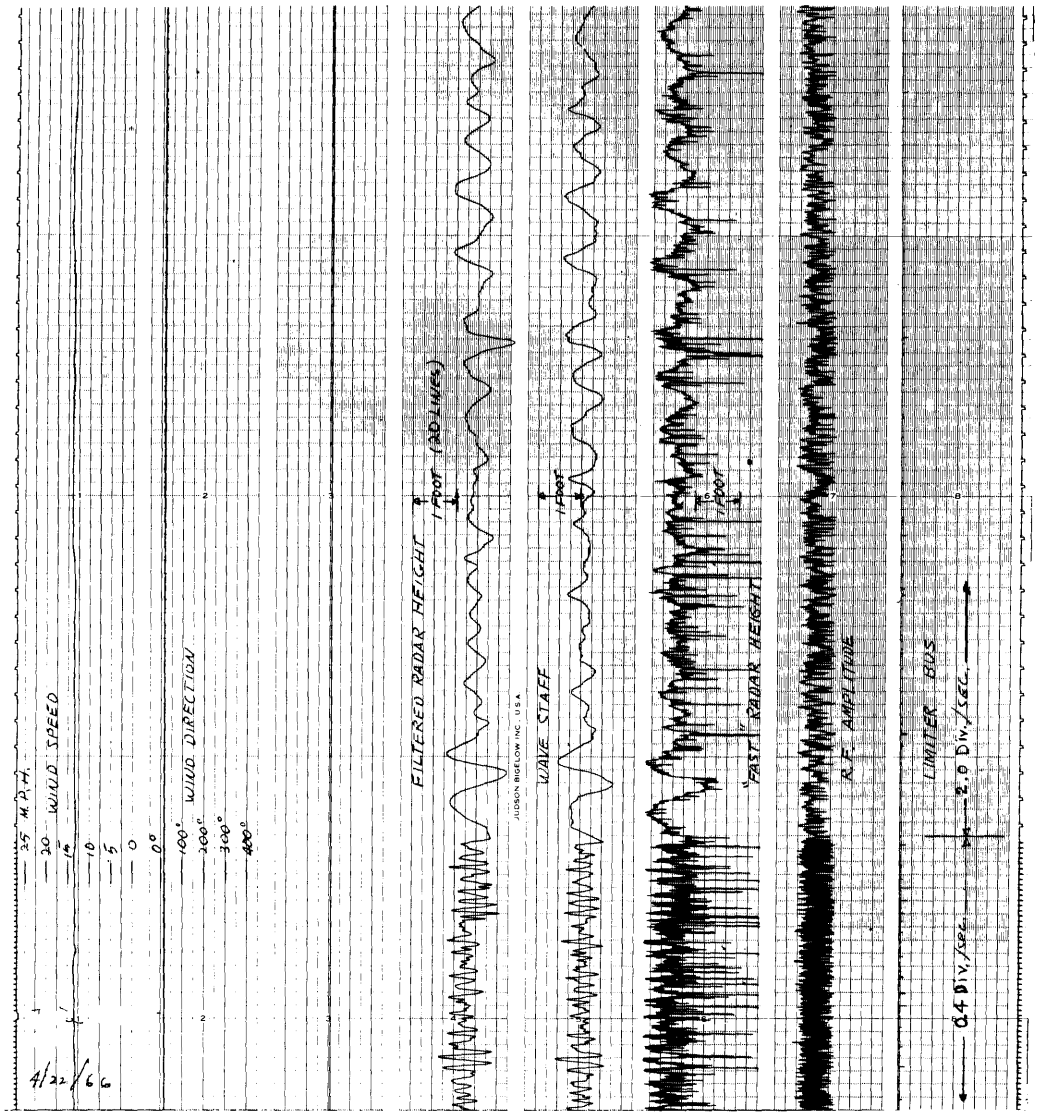

(a) Typical format for data recording

Fig. 49 - Chart recordings at the Chesapeake Bay Bridge Facility

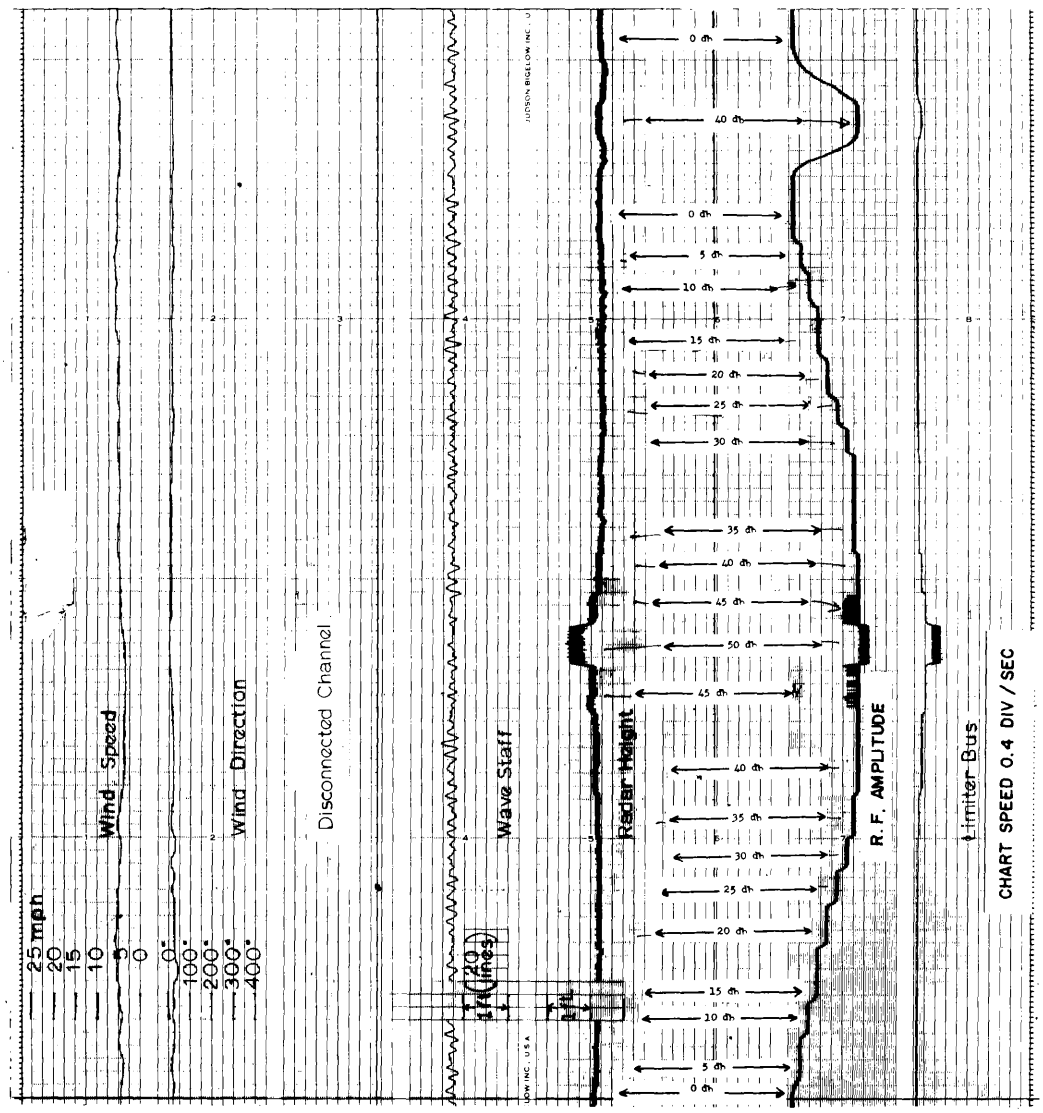

(b) Example of closed-path system calibration

Fig. 49 (Cont'd) - Chart recordings at the Chesapeake Bay Bridge Facility

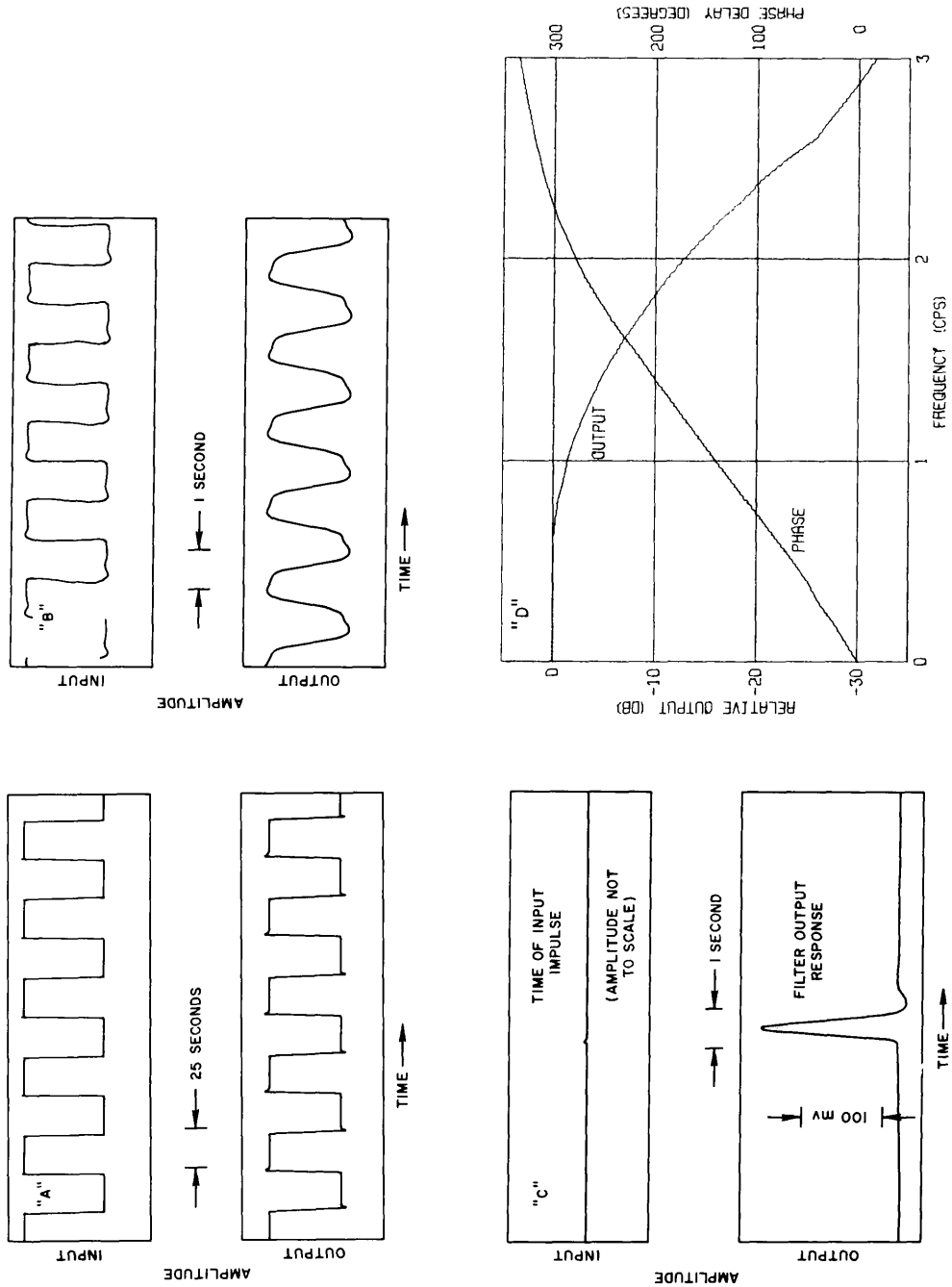

Fig. 50 - Characteristics of the active RC filter used to smooth the filtered radar record

to investigate the accuracy with which the short spikes in the radar wave height and signal level records were being reproduced. This was done by making a series of simultaneous recordings with the chart recorder normally used connected in parallel with a mirror-galvanometer oscillograph. The galvanometer system had a speed of response between four and five times as high, the 10 to 90 percent rise time of the trace being 0.9 milliseconds compared to 4.0 milliseconds for the chart recorder; and the maximum paper speed of 25 in./sec allowed features of the order of one millisecond long to be resolved.

The lengths and heights of over 50 of the shortest noise spikes were scaled from the simultaneous recordings for comparison. These spikes were found to be very nearly triangular in shape near their peaks, and the shortest ranged between five and ten milliseconds wide at the base of the triangle. The largest amplitude discrepancy found was about 12 percent in the case of a spike six milliseconds wide and representing 2.8 ft of wave height. Only three spikes in the sample of 50 were in error on the chart record by more than 5 percent, and in most cases the error was comparable to the accuracy of the scaling process. In all cases where there was a significant difference the amplitude was smaller on the normal chart record, as would be expected from the rise-time limitation.

It was concluded that the four-millisecond rise time of the chart recorder was adequate to reproduce all of the essential features of the radar signals and that the use of a higher speed recording system was not justified.

Stray Propagation Paths and Other Sources of Experimental Error

One of the basic sources of experimental uncertainty is found to be the possible existence of stray propagation paths which would allow a signal to reach the receiver by a route other than that involving the desired single reflection at the water surface. Such undesired stray paths might involve both reflections from gondola structure and coupling via energy radiated in the antenna side lobes, and could also involve a variable reflection from the water. Since the wave-profiling radar being studied did not possess a range-gating capability, all of these possible paths were potential sources of error if the amplitude of a stray signal was ever an appreciable fraction of the desired signal, so an investigation of stray signals was clearly necessary.

Aside from the undesired signal propagation paths which have been mentioned, other sources of error or extraneous noise are radio interference and the direct effect of signal amplitude on the wave-height indication. No significant microwave interference was ever observed at the Bay Bridge site, but intense fields at the lower radio frequencies were often present. A high-powered transmitting station which is located nearby on the Western shore of Chesapeake Bay was apparently the source of these signals. No precise field-strength measurements were made, but a wire hanging a few feet below the gondola was found at times to develop a signal of over 20 volts peak to peak at the high-impedance input of an oscilloscope. In addition to causing the interference pickup mentioned above in connection with the radar "fast" channel recording, these intense fields sometimes caused a high noise level to be produced in the wave-staff record. This noise was apparently a cross-modulation effect caused by high-level rf energy feeding into the wave-staff sensing circuit. At times this interference made the staff unusable until it was found that dropping one or more wires from the West side of the gondola to the water produced enough shielding to virtually eliminate the problem.

The direct effect of signal amplitude was measured during each closed-path amplitude calibration such as that of Fig. 49b, and although it was not entirely negligible and was, like the transient noise, slightly variable from day to day, it was always small, never

more than about 0.25 ft of height over the full range of amplitude calibration. In most cases it could have accounted for only a small fraction of the total range noise observed.

Propagation Experiments

In order to attack the most serious problem, that of stray signals, a succession of experiments was conducted to prove or disprove the existence of all of the specific paths of undesired propagation which could be visualized. The experimental technique involved the use of panels of microwave absorber which were manipulated with poles and lines into various positions near one or the other of the two antennas. The pads of microwave absorber were of the carbonized hair type in sections 24 by 24 in. square with a rated absorption ratio of 30 db at X band when measured at vertical incidence. For transmission directly through the pad, the signal was thus reduced by 15 db for a single layer or 30 db for a double layer. The individual sections of absorber were fixed to a plywood backing to construct the larger panels used. These tests were performed on a day when the wind was relatively low and changing gradually through a range of speeds, during which the nature of the radar return was markedly affected. Because this series of observations appears to offer some insight into the reflection mechanism as well as into the possible geometry of the undesired propagation paths, it seems worthwhile to describe the procedure in detail.

When the exercise under discussion was started, the wind was fairly steady at 5 to 8.5 mph and was blowing almost directly out of the north. The waves were 0.25 to 0.70 ft high, with 0.08 ft and smaller ripples evident during calmer portions of the record. The amplitude record showed a typical scintillation pattern, with the path loss ranging frequently from 25 db to 60 db and fades to over 60 db fairly rare (Fig. 51). The predominant period in the fading spectrum has been found to be somewhat variable, but it is invariably shorter than the predominant wave period, and the wave-period features of the amplitude and wave-height records are correlated only weakly if at all. At times persistent, deep fading seems to be more probable during passage of a wave crest than a trough, and at other times fading seems slightly more frequent on the side slopes than on either the crests or the troughs. At other times all of these forms of correlation are absent, and even when they are present it is never possible to predict the wave record with any confidence from the amplitude record. From these considerations, and from the general behavior of the signal as well, it appears that the fading mechanism is one of interference and cancellation, with steering of the beam by the wave slope occasionally having a slight influence but never producing a deep dropout by itself. The failure of beam steering to cause large signal losses in turn implies that a significant amount of broadening or scattering of the beam must generally take place, since wave slopes large enough to deflect the transmitted beam entirely outside the receiving aperture certainly occur on many occasions.

The radar records at the start of the exercise are also more or less typical of the records obtained for moderate wind and wave conditions. Since the amplitude record shows the characteristic scintillation pattern of sharp minima and broad maxima, the critical cancellations capable of producing large range errors would be expected to be relatively brief, and it is hardly surprising that much of the range noise appearing in the wave-height record takes the form of short, sharp spikes. However, the correlation between amplitude minima and height spikes is by no means perfect or consistent throughout the mass of data which has been accumulated. A few general observations can be made and will be stated now as an aid to the interpretation of the results to be discussed.

1. Large increasing-range spikes representing more than about 5 nsec of range delay almost invariably occur during a pronounced fade. In fact, such high-amplitude peaks seem to be virtually prohibited unless the path loss exceeds 50 db, and are not very likely unless 55 or 60 db is reached.

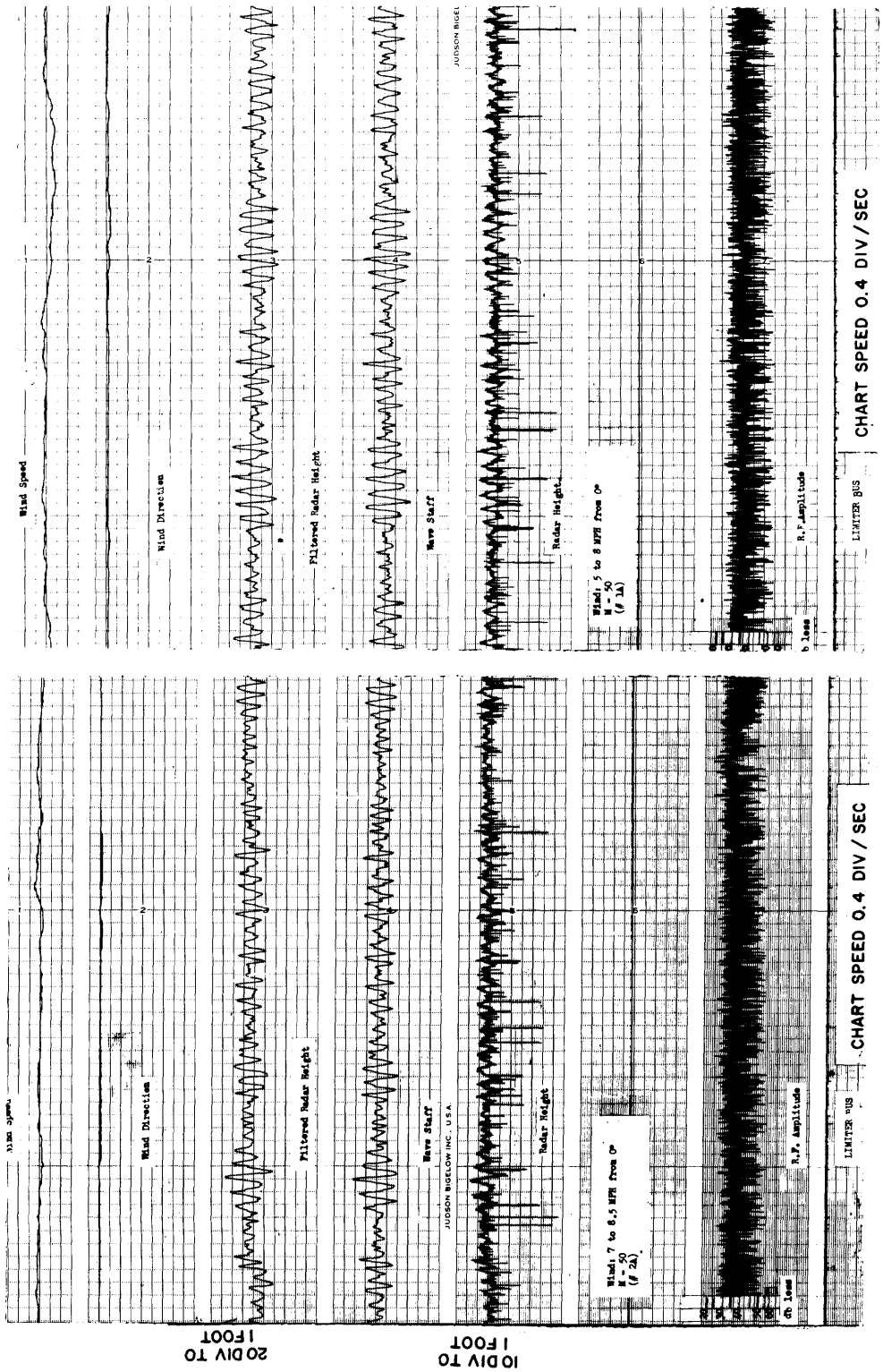

Fig. 51 - Recording under light wind conditions when deep fading and noise spiking occur; note that the radar can follow the longer waves accurately

2. A deep fade, even one exceeding 60-db loss, does not always produce a range spike, although there is a high, somewhat variable probability that it will do so.

3. Lower amplitude height spikes, both increasing range and decreasing range, are not as strikingly correlated with deep fades, and while they are more likely to occur at a signal minima than elsewhere, and rarely coincide with maxima, they may occur at almost any level below the absolute maximum for the wave condition that exists.

4. Occasionally, there is a rapid alternation between a decreasing-range error and an increasing-range error, as though only a minor change in the pattern of rf cancellation were needed to switch the sign of the error. Much more commonly, however, both decreasing-range and increasing-range spikes stand alone, so it is not probable that the target will pass through the configuration for one polarity in order to reach that for the other, and it clearly is not necessary that it do so.

5. Large decreasing-range spikes, over about 3 nsec range delay, are apparently prohibited at the wider frequency deviations used, and at some deviations are restricted to about 1.5 nsec, with spikes of even this amplitude rare. This limitation suggests that direct leakage over the relatively short path between antennas is never significant, and has other implications as well if the constraints imposed by the two-path theory can be applied more broadly. The theory indicates that unless very large differences in delay can exist, as for example in a direct leakage path, decreasing-range errors above a certain magnitude cannot be generated by any two-path combination. This limiting magnitude is related to the frequency deviation in a different way, depending upon the range of path delays involved, so that the nature of the error spikes may offer a clue to the mechanism of reflection at the target. Further reference to this point will be made as experimental results are discussed in greater detail.

The first stray-path test was made by hanging a vertical panel of absorbing material just to the north of the transmitting antenna, that is, on the side towards the receiving antenna. The panel was 4 by 4 ft in size and was hinged in the middle. When folded it formed a double layer of absorber extending about one foot below the rim of the dish and spaced about three inches from it. When unfolded the panel was extended three feet below the antenna, and in this position blocked the line of sight from the adjacent part of the transmitting aperture to the illuminated patch on the water. The main purpose of this procedure was to block any direct leakage paths involving high-angle side lobes. With the pad folded, no changes in the amplitude or wave-height records were evident. This was considered to be strong evidence that direct leakage was not a significant problem. A second panel was then installed to probe the possibility of signal scattered or reflected to the water entering the receiving antenna via the side lobes that were directed downward. This panel was a double layer of absorber 2 by 4 ft in area that was pulled up against the bottom of the shell of absorbing panels that permanently surrounded the receiving antenna. It was positioned horizontally to cover the north half of the opening facing the water. In this position it blocked the line of sight from a portion of the antenna to the illuminated patch. This panel caused a loss in the average signal amplitude of about 5 db, but the pattern of fading and the range between the minimum and maximum path loss was not obviously changed, and the height noise was not noticeably reduced or increased. This result was considered to rule out any significant contribution from stray paths having this geometry.

The vertical pad at the transmitting antenna was then unfolded to hang three feet below the rim of the reflector. The maximum signal amplitude was reduced by about another 5 db by this change, while the minimum amplitude was changed little if any. However, fades to the minimum level were much more frequent, and the frequency and size of downward height spikes were markedly increased. Refolding the pad restored the height and amplitude records to their previous appearance. The significance of this result was not clear at the time, and further tests were made with the panel in the folded position.

Unmounted pads of absorbing material were next placed above the receiving antenna, overlapping the rim of the dish so as to block any signal entering a back lobe after reflection from a part of the gondola structure. No change in the records was apparent while the pads were being put in place, which seemed to rule out any important contribution from signal arriving over such a stray path.

During the period when the last pad tests were being performed, the wind was gradually dying down, and a change in the records that was correlated with the wind speed was observed. This change was gradual enough at first so that there was no difficulty in evaluating the tests, but the character of the height and amplitude records eventually changed very significantly. Over an interval of 45 minutes the wind speed fell from a relatively steady 7 mph to less than 2 mph with the anemometer occasionally stopping entirely. As the wind fell the signal amplitude peaks increased, reaching a level 3 db higher (minimum path loss now about 22 db) during the calmest period. The level during the deepest fades did not increase appreciably (perhaps 1 db). At the same time the frequency of large downward or increasing-range spikes was greatly reduced, while the reduction of upward or decreasing-range spiking was not obvious. Aside from a slight (perhaps 20 percent) reduction in the maximum wave heights there was no observable change in the nature of the wave-staff record.

The vertical pad at the transmitting antenna was unfolded to hang three feet below the rim again. This time there was no visible change in the amplitude record and no apparent increase in height spiking. Evidently the surface reflection was so nearly specular that energy reflected from the outer portions of the illuminated patch was directed outside of the receiving-antenna aperture, so that masking the illumination of a part of this outer region by the pad had little effect on the received signal.

The reason for the marked degradation of the height record when the reflection was less specular is not so obvious, but the result suggests that in this case the return from the blocked portion of the patch somehow had a range-noise content that was significantly lower than the average, so that its removal increased the net noise level generated. The reason for this circumstance must be connected with some difference in the kind of multiple paths that can exist for different illuminated areas. Upon considering the results of all the absorbing-pad experiments together, it seems very probable that the only significant received signals are those originating from the water surface in the region viewed by the main lobe of the receiving antenna. If this hypothesis is accepted as proven, there are three multipath mechanisms that can be visualized. The first involves the depth of the target area along the range axis and occurs because of the slopes of larger waves across the illuminated patch and the smaller waves and ripples that are viewed in their entirety at a given instant. This form of multipath will always be present and might be considered to be the most likely. Two-path theory sets definite upper bounds on the absolute value of the range errors that can be produced in this way.

A second multipath mechanism which involves a secondary reflection from the gondola is diagrammed in Fig. 52, where the angles of incidence have been somewhat exaggerated for clarity. None of the absorbing-pad tests rule out a stray path of this nature, and, as can be seen in the close-up photograph, Fig. 47, the underside of the gondola is an excellent reflector. However, for energy striking the gondola to reilluminate the main lobe patch at near vertical incidence, it must be initially scattered or otherwise deflected through approximately half the offset angle of the antennas, or about 8.5 degrees. Since large area reconstructed wave slopes rarely reached this figure, a scattering mechanism seems the most probable. This scattering process would have to operate twice, once to deliver energy to the critical area of the gondola and once to redirect the reflected signal into the main lobe of the receiving antenna. The double scattering involved and the geometric loss in reillumination of the water would seem to make this path inherently much weaker than the desired signal, but this assumption is not inconsistent with the experimental results in view of the wide range of fading which

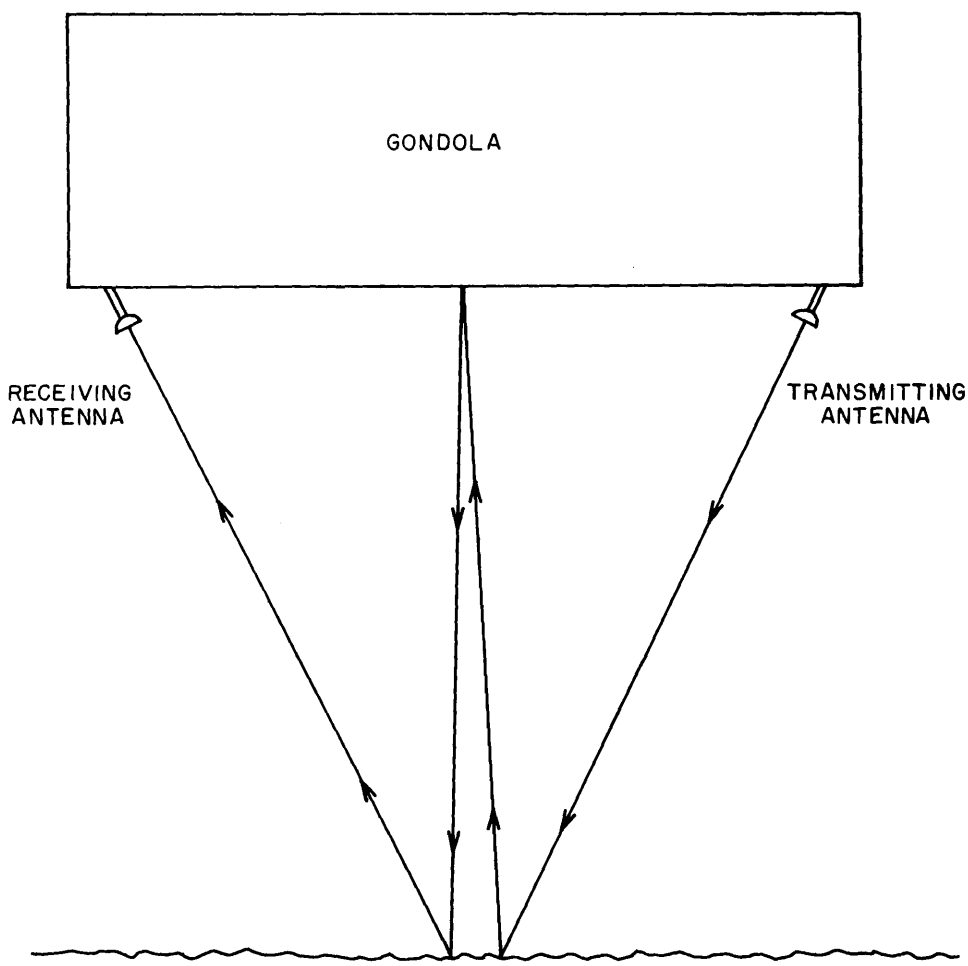

Fig. 52 - A possible stray signal path

typically occurred. Two-path theory indicates that at the wider frequency deviations in use increasing-range errors would predominate, while at the narrower deviations fairly large decreasing-range errors can occur with similar probability. This also is not inconsistent with the experimental observations.

A third way in which a differential path length could be created involves a horizontal reflection or skip across the illuminated patch. This method would permit path differences of the same order of magnitude as the patch diameter, which is much larger than any difference which could be created by the depth of the target in range. The creation of such a skip path would involve scattering at 90 degrees and rescattering after the horizontal translation into the effective aperture of the receiving antenna, and the level of such a signal would be expected to be relatively low. However, this again is not inconsistent with observation, since sharp range-noise spikes of high amplitude are virtually always associated with a fairly deep fade in signal level.

Returning to the question of why range noise markedly increased when the illumination of the northern part of the patch was blocked, it can be said that a possible explanation lies in the fact that energy illuminating this region would have the least chance of being scattered back into the main lobe of the receiving antenna after a horizontal skip and so would be more likely to arrive with the minimum possible delay, which is generally also the delay representing the desired range. It also seems likely that energy reflected or scattered to the bottom of the gondola from the northern part of the patch would be less effective in reilluminating the patch area with a delayed signal, although relative probabilities are not as easy to evaluate in this case. It is difficult to see why errors generated by the depth of the patch area in range would vary substantially from one part of the patch to another.

A final test for stray signal paths was made next, and this too had a negative result. The vertical panel at the transmitting antenna was moved to the south, or far side, of the dish to block any signals entering back lobes via a reflection from structure. No visible change in the height or signal amplitude records could be observed.

At this point in the exercise the wind increased briefly, and a striking correlation between wind speed and the frequency of large negative spikes was observed. Within a period of 15 minutes the average wind speed built up from less than 2 mph to 7.5 mph and then decreased again to less than 5 mph. Within less than a minute after the speed touched 7 mph frequent large (representing over 7 nsec range delay) negative spikes were observed. Within two minutes of the time the speed fell back to 5 mph a decrease in amplitude and frequency of the spikes was noted, and during a five-minute period, when the speed fluctuated between 3 and 5 mph the height noise fell further to almost the initial level. The wind eventually decreased to a average speed of 2 mph, at which time the noise level was at least as low as during the earlier 2-mph interval. It should be remembered that the anemometer was mounted on the bridge structure about 165 ft above the water, so that the velocities at the surface may have been somewhat different, but with a large expanse of unobstructed water lying upwind (to the north) the trends in velocity should be similar at the surface. Figure 53 and Fig. 54 illustrate these low-wind phenomena.

During the next 21 minutes the wind speed fluctuated between 3.5 and 5 mph, and during this calm period some correlation between the height and amplitude records could be seen, with deep fades more likely on the side slopes of waves than at the crests or troughs. However, there were many exceptions to this pattern, and it would not have been possible to predict the wave record with any certainty by inspecting the amplitude record. Fades deeper than 45 db were quite rare during this period, and the path loss remained below 35 db for periods of 10 to 12 seconds, whereas frequent fades to losses of 55 or 60 db normally occur. At signal maximums the level was less than 20 db below the transmitter output, approaching the calculated loss for a perfectly specular reflection.

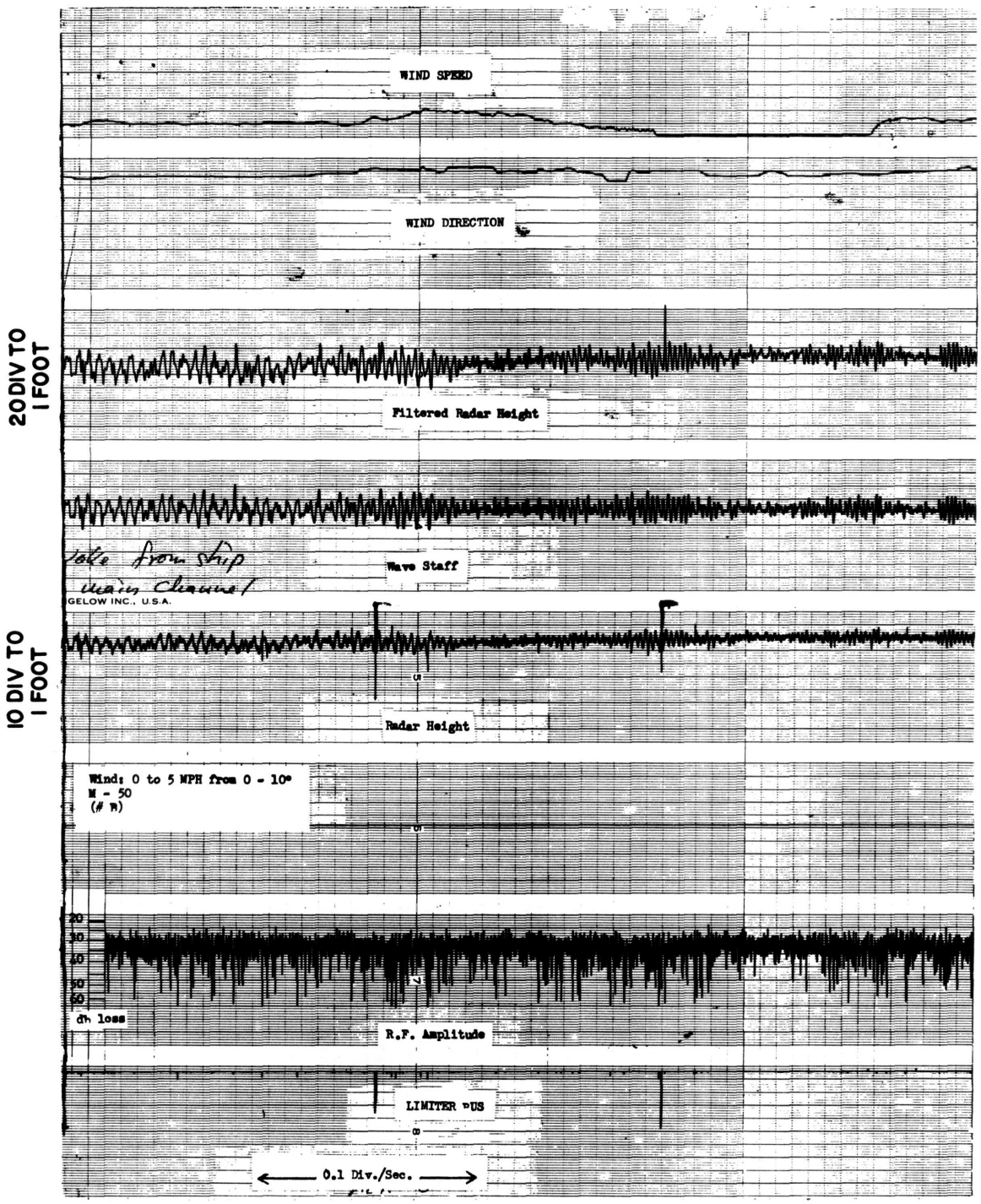

(a) Accurate radar recording of long, low swells under very light wind conditions

Fig. 53 - Illustration of the effect of increasing wind speed

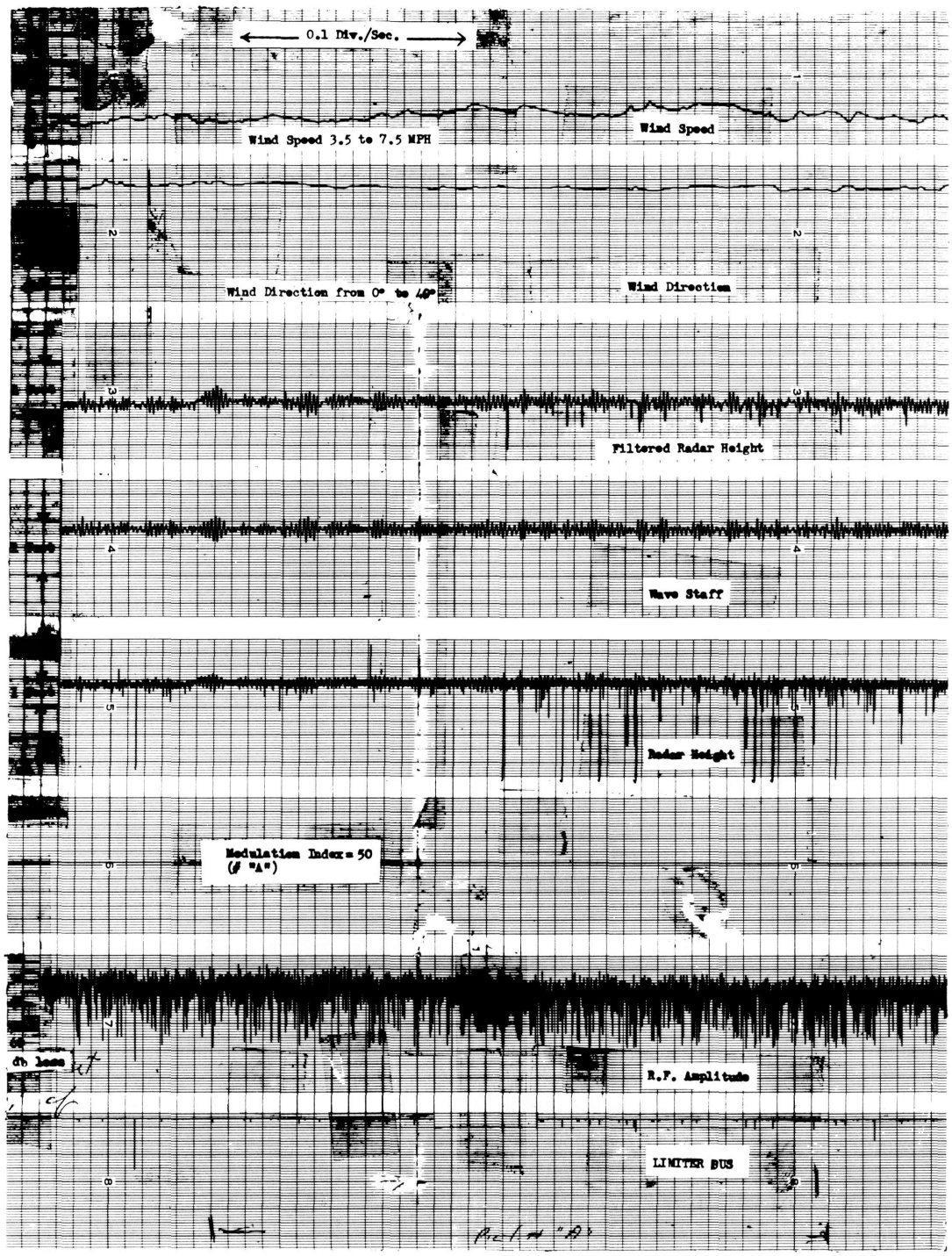

(b) An example of the abrupt onset of radar noise spiking when the wind rises

Fig. 53 (Cont'd) - Illustration of the effect of increasing wind speed

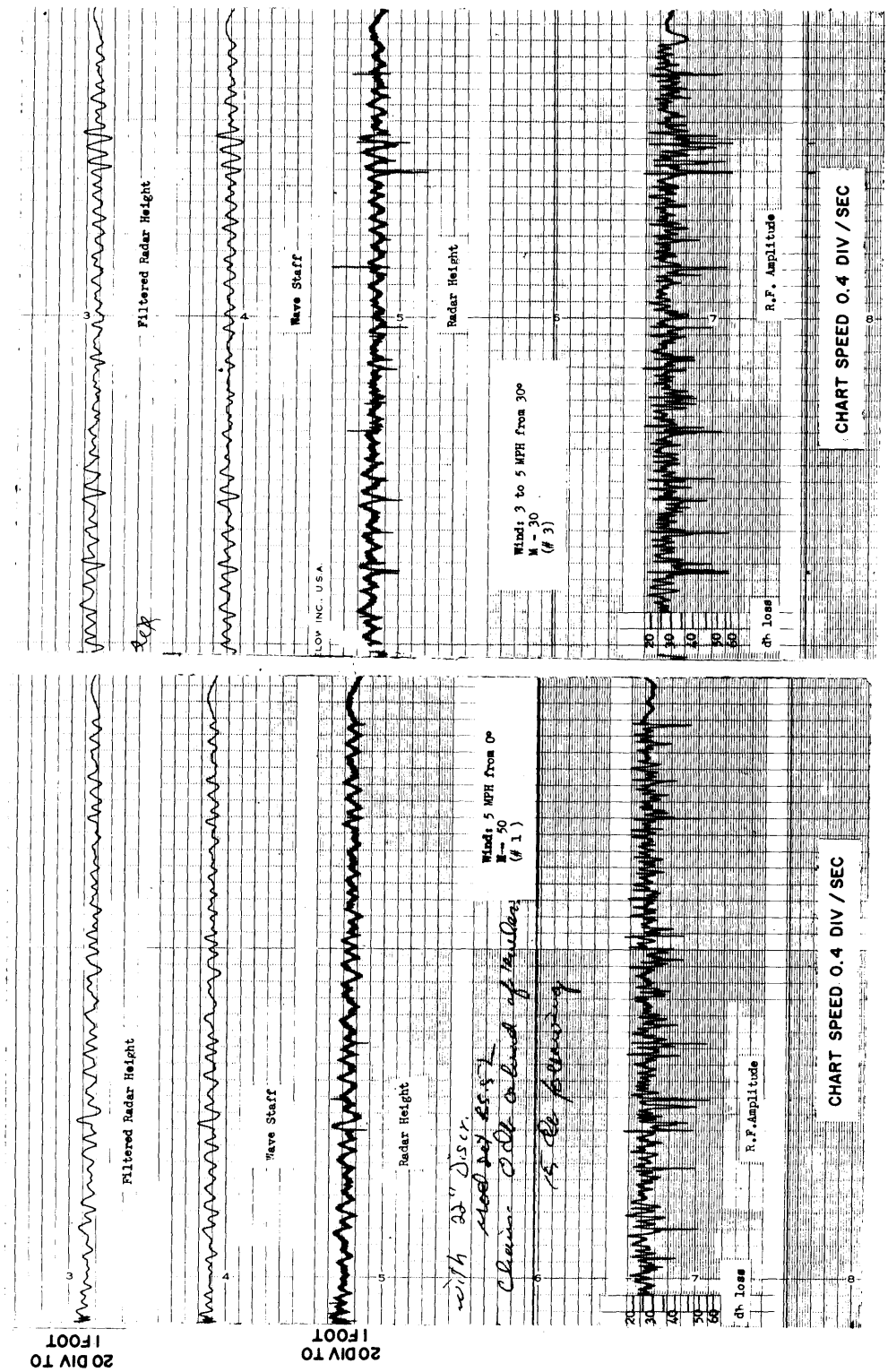

Fig. 54 - Examples of very light wind recordings using different modulation indexes, showing that when wind is under 5 mph radar noise levels can be very low and deep fading rare

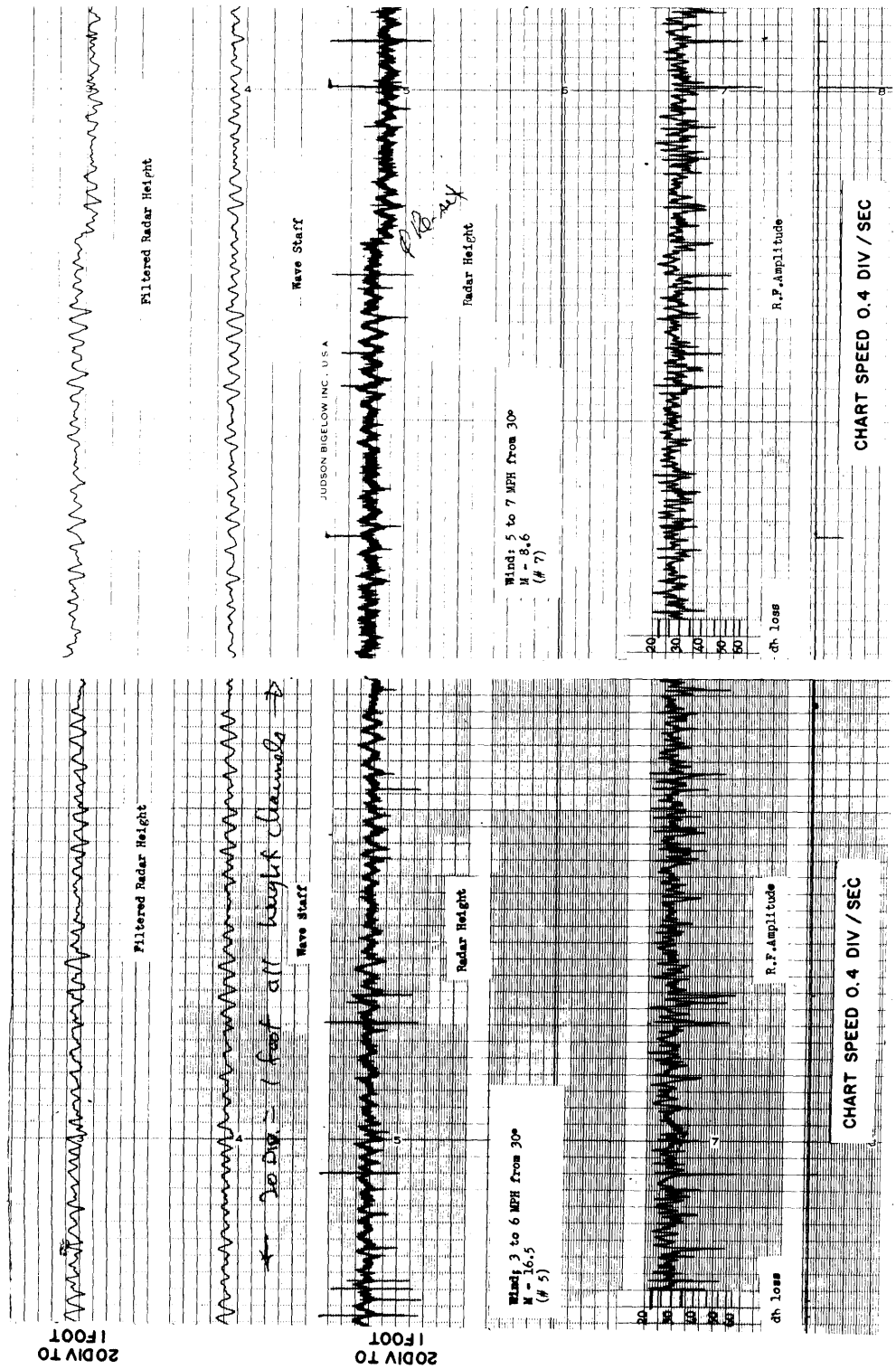

Fig. 54 (Cont'd) - Examples of very light wind recordings using different modulation indexes, showing that when wind is under 5 mph radar noise levels can be very low and deep fading rare

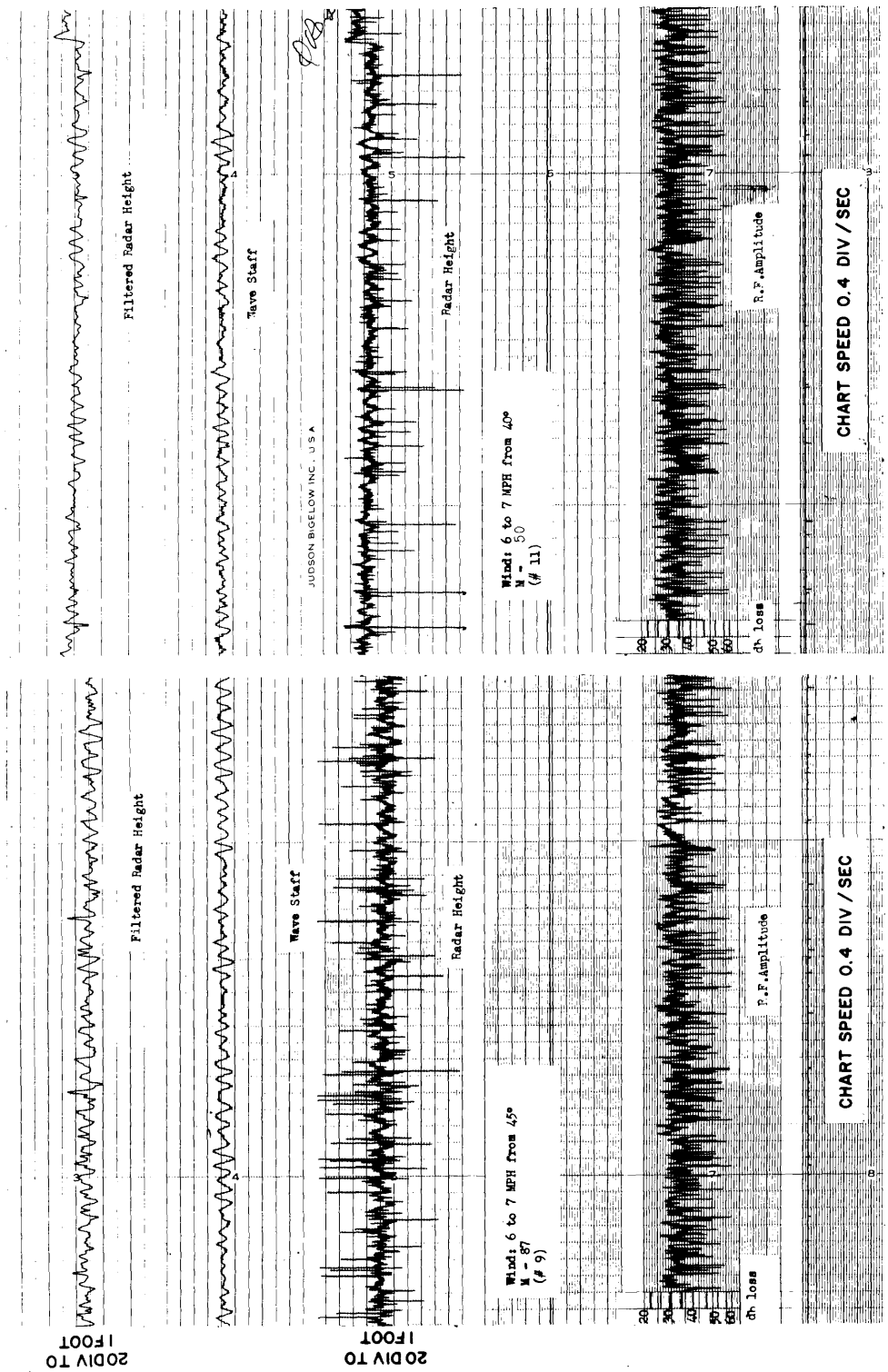

Fig. 55 - Examples of light wind recordings, showing the transition to deep fading and sharp range noise spiking that always occurs at velocities between 5 and 7 mph, compared with Fig. 54, which illustrates very light wind recordings

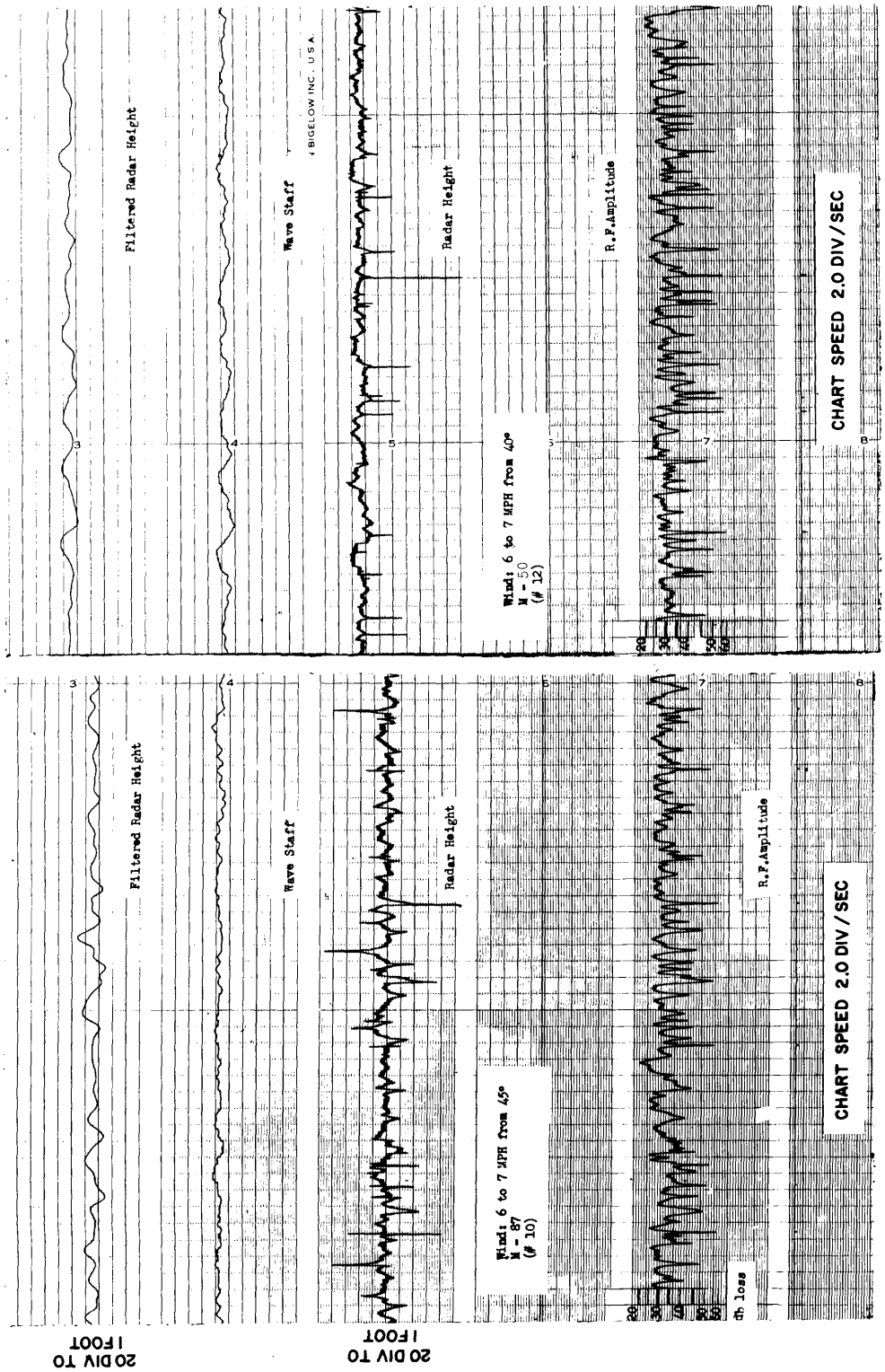

Fig. 56 - Light wind recordings at higher chart speed, showing nature of correlation between deep fading and range-noise spikes

Figure 54a shows a sample of the record made using a modulation index of 50. During a three-minute run only five noise spikes occurred in the height record, and the largest of these represented only a 1.2 nsec delay, or 0.6 ft of wave height.

Wave slopes were estimated by calculating the lengths from the deep-water gravity-wave relationship described earlier, $L = 5.12T^2$ ft, and the average reconstructed slopes between crests and adjacent troughs ranged from 1 to 3 degrees. The maximum slopes would of course be higher, but not by as much as 2 to 1, and more probably closer to a 1.5 to 1 ratio. (The factor is $\pi/2$ for a sinusoidal shape.) The wind remained below 5 mph while data were taken using four different modulation indices: 50, 30, 16.5, and 8.6. Both deep fades and height spikes were extremely rare under all conditions, with no significant change in rate of occurrence under the various operating conditions (Fig. 54). During operation at the 8.6 index the wind rose above 5 mph once more and at times reached 7.0 mph during the last 3.5 minutes of the run. There was, however, no observable change in the character of the records. The recording was interrupted for about five minutes while a change was made to the maximum modulation index, and when recording was resumed the wind speed was still less than 7 mph, but deep amplitude fades were starting to appear, and within one minute the pattern of height spikes characteristic of operation at this index was fully developed. During this transition there was no significant change in the pattern of the predominating 0.2 to 0.4 ft waves which had about two-second periods, but small superimposed ripples about 0.05 ft high became more prominent in the wave-staff record. These had periods of 0.3 to 0.5 seconds and were now evident throughout the record, except when masked by the steeper slopes of the larger waves. The wind was relatively steady between 6.5 and 7.5 mph during the remaining eight minutes of the run, when an index of 87 was used, and the character of the records did not change appreciably. After changing back to an index of 50 the wind died down to 5 mph once again and remained within 0.5 mph of this speed for the remaining minutes of the April 14th exercise. During this interval the modulation index was changed to 16.5 again and finally back to 50 for the last data run of the day. Examples from this series of records are shown in Figs. 55 and 56. The frequency of occurrence of deep fades and height spikes was somewhat variable but was abnormally low most of the time at all modulation indexes, and occasionally approached the very low rates observed during the interval of low winds earlier in the day. Small short-period ripples could still be seen in the wave-staff record at this time, but they were not as prominent as they had been when the wind was stronger.

The correlated changes in wind and radar records that were observed during this exercise are strong evidence that capillary waves or very small waves in the transition region between surface tension and gravity-controlled waves must have a crucial influence on the radar-reflection phenomena even at near-vertical incidence. Transitions between frequent deep fading and a near absence of deep fades took place too rapidly to allow even small gravity waves to build up or decay, and at times the radar records changed drastically without any observable alteration in the wave-staff record. A wind speed of about 5 mph appeared to represent the point of transition, with speeds appreciably higher leading to a fading and height-noise pattern typical of high winds in general, while speeds below 5 mph led to a marked reduction in the frequency of deep fades and of height-noise spikes. At speeds under 2 mph height-noise spikes of significant amplitude were virtually absent, as were fades to more than 25 db below signal maxima. During these marked changes in the radar record, virtually the same pattern of low gravity waves persisted, and the wave staff apparently did not record the complete spectrum of small ripples which modified the radar return. This failure to record very small features may have been partly due to the masking effects of other waves, which were producing faster rates of change at the wave staff, and partly to the size of the wave-staff sensing element, which was a spiral wire wound on a 5/16-in.-diameter core and thus had limited resolution for small surface features. It is also possible that the staff was large enough to disturb the pattern of the small capillary waves and prevent their being recorded at their actual amplitude.

Any comments on the way in which the presence of small ripples modifies the radar return must be at least partly speculative, because of the complexity of the reflector phenomenon, but scattering is almost certainly involved. The radar wavelength in this case was 3.16 cm, or 0.104 ft. Two points of reflection spaced only a quarter-wave length apart in range, 0.79 cm or 0.026 ft, will thus lead to signals in phase opposition at the radar, and deep nulls would be expected to occur at least occasionally whenever the depth of a complex target in range exceeded a quarter-wave length. In every case when radar data were taken at the Bay Bridge Facility, the gravity-wave system created depths of many quarter-wave lengths within the illuminated patch on the water, and the additional depth added by the capillary-wave structure would not in itself be expected to have an appreciable effect on the character of the amplitude scintillation. It was, however, observed that deep fades were virtually prohibited when the wind was very low, under about 2 mph, and that between 2 mph and around 7 mph a marked change in the nature of the scintillation occurred, with deep fades becoming more and more frequent as the wind rose. A steady wind of close to 5 mph seemed to produce an intermediate condition, where deep fades were entirely absent at times for several consecutive seconds and at other times were fairly frequent. The difference in maximum fading depth under low wind and high wind conditions was as much as 25 db.

A logical explanation of this variation in scintillation behavior seems to lie in the differing contributions of different parts of the illuminated patch in the two cases. Were the reflection to be purely specular, as from a perfect radio mirror, only the center portion of the patch would contribute to the received signal, since energy reflected from the outer areas would be directed outside the aperture of the receiving antenna. In the case of the Bay Bridge geometry the "active" area would have a diameter about 1/4 that of the total area illuminated. However, since the reflected energy was never consistently deflected outside of the receiving-antenna aperture by the gravity-wave slopes, a certain amount of scattering or beam broadening must always have occurred which would cause the active area of the patch to be expanded but with tapered intensity of reflection as viewed from the receiving antenna. As scattering at higher angles becomes pronounced, the whole area on the surface which was effectively illuminated by the transmitting antenna might contribute essentially equally intense reflections in the direction of the receiving antenna. The radar target would then become equivalent to a uniformly illuminated aperture which was continually being tilted or otherwise distorted in the range direction. Under this condition deep nulls in the received signal would be certain to occur, whereas the combination of nonuniform effective illumination and small-angle scattering in the nearly specular case could give an effect analogous to a simple broadening of the transmitted beam, so that over the angles of deflection produced by the larger waves no deep nulls were ever produced. Whether or not this particular hypothesis is entirely correct, it appears from all of the Bay Bridge observations that continual deep fading represents the typical condition for reflection from a relatively small area of the water surface at near vertical incidence. The absence of frequent deep fades is evidently an exceptional condition and has never been observed except when the wind was so low that the normal capillary-wave structure was not fully developed.

General Comments on the Bay Bridge Data

Upon considering all of the data recorded at the Bay Bridge Facility, there are some further generalizations that can be made. Aside from the changing wind and wave conditions, which had to be taken as they came, the principal experimental variable was the frequency deviation of the FM-CW radar. As noted previously, the transmitted bandwidth of this system could be continuously varied up to a maximum of nearly 400 Mc/sec. During the Bay Bridge exercises the modulation index was ordinarily set to one of five discrete values: 8.6, 16.5, 30, 50, or 87. At the modulation frequency of 2.215 Mc/sec these indexes corresponded to values ΔF of 19, 36.5, 66.5, 111, and 193 Mc/sec respectively. The energy of the transmitted signal is largely confined to a bandwidth of $2\Delta F$

for these deviations so that the range of bandwidths involved is from about 40 to 385 Mc/sec. Normally the bandwidth of the interferometer discriminator was adjusted for maximum output at the chosen deviation, although at times tests were made by quickly reducing the deviation while a broader band discriminator was still in use. Not all the available bandwidths were used during all exercises, but enough comparisons were made to establish the trend of the range noise under most of the wave conditions encountered. The following observations may be made on the basis of these comparisons:

1. When the wind was very low, and when deep fading did not occur, the range noise level was very low and substantially the same over the full range of frequency deviations in use. The radar was then able to reproduce an accurate profile for any waves that the illuminated patch could resolve, limited only by the system noise level of less than 0.1 ft of height.

2. For all conditions where winds were moderate (over 5 mph) or high, frequent deep fading was found to occur, and the range noise of highest amplitude took the form of short spikes. Over the region covered by the four lower frequency deviations (19 to 111 Mc/sec) there was always an increase in the number or size of the noise spikes as the deviation was reduced. At times the change was quite marked for each step in deviation, and at other times a shift of one step, say from an index of 50 to 30, did not cause an obvious degradation of the radar record. However, the trend was consistent and was never seen to reverse.

3. The trends of increasing-range and decreasing-range spikes versus the frequency deviation were somewhat different. The size and rate of occurrence of the large increasing-range or downward spikes consistently decreased as the deviation was increased over the whole range of values used, including the maximum of 193 Mc/sec. Under wave conditions that led to large spikes (range delay over 5 nsec) every second or so at the narrow deviations, large spikes became extremely rare at the maximum deviation. However, large increasing-range spikes representing over 8 nsec of range delay (or 4 ft of wave height) were possible occasionally at any frequency deviation used.

Decreasing-range or upward spikes were limited in size in a manner which appeared to be a function of the frequency. The largest upward spikes recorded occurred at the lowest frequency deviation and represented about 4 nsec of delay. There was a progressive decrease in the maximum size as the deviation was increased until at 111 Mc/sec no spike of over 1.5 nsec was ever recorded under any wave or wind condition. However, between 111 Mc/sec and the maximum deviation of 193 Mc/sec the trend reversed, and at the wider deviation spikes of up to 3.5 nsec were seen again. The size appeared to be absolutely limited to a value between 3.5 and 4.0 nsec, or at least the probability of larger values was so low as to give this impression.

4. The opposing trends of upward and downward noise spikes in the region of frequency deviations between 111 and 193 Mc/sec made the choice of an optimum deviation dependent on wave conditions. There were times when a better radar record could be obtained using the wider deviation and other times when the reverse was true.

5. The trends of decreasing-range and increasing-range noise spikes versus wind and wave conditions is also found to be different. As the wind builds up after a protracted calm period, upward spikes appear first when using the maximum deviation of 193 Mc/sec (Modulation index of 87). At this point in the wave development downward spikes may still be rare at all frequency deviations. As small, short gravity waves become evident in the wave-staff record some upward spiking is seen using a deviation of 111 Mc/sec (Modulation index of 50), and a further increase takes place at 193 Mc/sec. Frequency and amplitude of these upward or decreasing-range spikes appears to be a maximum for intermediate wind and wave conditions during a buildup of the sea state.

Under higher wind conditions, when the sea state is more fully developed, upward spiking may be nearly nonexistent when using a deviation of 111 Mc/sec, and the trend also reverses at a deviation of 193 Mc/sec, although the decrease is not as marked.

Large increasing-range spikes become possible whenever the wind exceeds about 5 mph, but the noise level may remain fairly low when the wind is as high as 11 mph depending on wave conditions. As in the case of decreasing-range noise, the least favorable condition seems to be that of rising wind and sea state. When the wind remains above about 12 mph, downward spiking always contributes a significant noise level but varies considerably from one wave condition to another and does not necessarily follow the trend of the wind speed over the range above 12 mph.

6. When the wind dies down rapidly, leaving the heights of the larger gravity waves substantially unchanged, radar noise of all types decreases almost to the level seen under flat calm wind and wave situations. It then becomes possible to follow the wave profile accurately even without filtering of any of the noise energy.

7. As a further generalization, it may be said that the correlation between range-noise spikes and deep amplitude fading is such that almost all of the radar records could have been significantly improved by some form of amplitude gating. Such a gating system would interrupt the height record whenever the received signal amplitude fell below a threshold. The height signal would be clamped at its current level or placed in a "coast" mode that would extend the trace along an extrapolated slope. At the Bay Bridge the larger increasing-range spikes occurred only during the deepest fades to a path loss of over 55 db and could have been gated out by interrupting only a small percentage of the record. Decreasing-range spikes occurred when the signal was at least 10 db higher in level and could only have been eliminated by throwing away a larger portion. In many cases this loss would still have been advantageous, since the probability of a spike was quite high in the region of path loss between 45 and 50 db. In one section of record made at a deviation of 193 Mc/sec an upward spike of over 2 nsec delay accompanied one out of every three fades to over 50 db and one out of every six fades to over 45 db of path loss. As the threshold was decreased to below 45 db a region would have been reached where prolonged interruptions of the height record could have occurred, and the record would have been gated off needlessly on more and more occasions. In a field-wave profiling system a variable threshold might be advisable to allow the operator to achieve the best compromise. The way in which use of amplitude gating would have altered the choice of an optimum frequency deviation is not entirely clear from the data available, but under at least some conditions it seems likely that it would have tipped the balance in favor of a deviation near 100 Mc/sec where the predominant increasing-range errors could have been controlled by a relatively low-amplitude threshold.

Discussion of Excerpts from the Bay Bridge Chart Records

Composite figures in the sequence numbered 51 through 79 present samples of the actual chart records made under a number of wind and wave conditions. The complete records form the basis for the generalizations which have been made concerning the character of the scintillation noise and its relationship to the transmission bandwidth in use. The figures can show only a small percentage of the total footage recorded, but an effort has been made to select representative portions of each record. The individual samples are labeled with the wind speed and direction recorded at the time, as well as with the modulation index in use and the date of the exercise. Where the discriminator was optimized for a bandwidth greater than that in use this is also noted.

Three different chart speeds are represented by these samples: 0.1 div./sec, 0.4 div./sec, and 2.0 div./sec. The highest speed is of interest mainly in showing how the fine structure of the amplitude-scintillation pattern is related to the radar range noise spiking. The filtered radar record and the wave-staff record always have matched calibrations of 20 lines to one foot of wave height, and the crests of the waves are in the positive direction. The calibration of the "fast" or only slightly filtered radar record was frequently set to half-amplitude, ten lines to one foot of height, in order to more nearly accommodate the noise spikes, and five lines to one foot was occasionally used.

Water-wave statistics derived from samples of the wave-staff records for the exercises of April 26th, 27th, and 28th are shown in Figs. 70, 72, 74, 76, 78 and 80, and excerpts of the complete chart record taken at corresponding times during the various exercises are presented in Figs. 69, 71, 73, 75, 77, and 79. The wave length and radar depth histograms in Figs. 70 through 80 are based on the "calculated" or "reconstructed" values obtained by scaling the wave records as was shown in Fig. 48, and all of the reservations discussed in connection with this process should be kept in mind when these diagrams are compared with the corresponding wave-staff records. In particular, it should be pointed out that the mean values obtained are not directly related to the oceanographers' significant wave height or average wavelength, in which the smaller waves are dropped from the summation of heights and are not included in scaling lengths (27). Recalling that the half-power diameter of the illuminated patch was about four feet, it is evident that the calculated lengths in the first three blocks of the histogram represent waves that could not be resolved by the radar, that the fourth block represents a transition region, and that only waves having the lengths tabulated in the final four blocks would be resolved with high accuracy.

The "radar depth" was obtained for each pair of height and calculated length values and is the variation of range delay within the half-power circle of the illuminated patch. The values tabulated are based on the assumption of a sinusoidal wave shape. When the calculated horizontal crest-to-trough spacing was equal to or less than the patch diameter, the radar depth was based on the full observed height. The radar-depth histograms show that even under the calmest conditions calculated depths represent over one wavelength of the microwave carrier. Under higher wind and wave conditions the depth distribution is broad, and depths of many wavelengths can occur.

The sample sizes for individual blocks in the histograms are sometimes relatively small, since the total number of half-waves per sample was 50 to 100. Thus sample-to-sample fluctuations in a given block should not be regarded as very meaningful. However, it is believed that the overall envelopes of the distributions offer a useful means of comparing the wave characteristics that are significant from the radar point of view.

The "maximum slopes," ψ_{max}, were taken to be the maximum slopes of sinusoids having the observed heights and calculated lengths, and the mean value listed is simply the average for all "half-waves" scaled for a given sample. These slope values are seen to vary by a factor of more than 10 to 1 over the range of conditions observed.

The height-length plots of Figs. 70 through 78 were made by plotting the calculated half-length of each half-wave that was scaled against its associated crest-to-trough height. The data samples used were the same as for the corresponding histograms. The continuous curves shown are contours of constant wave slope, and it is seen that the slope is quite variable within every sample and that waves of widely varying height may have the same slope. The quantization of the wavelengths which is evident is due to scaling the original wave periods to the nearest 0.1 second. The slope contours are labeled with the maximum value based on a sinusoidal shape, and the 25-degree value corresponds to an aspect ratio (crest-to-crest length)/(height) of 5.7. An actual aspect ratio of 7 has been stated to be the theoretical minimum for stable gravity waves, and

ratios for most "reconstructed" waves are seen to exceed this limiting value, although a few do not in the higher wave samples.

The plots for three different samples on April 26 show the shift in distribution as the waves build up under the action of a moderate wind. In the first sample, Fig. 70, although the waves are all very low, a substantial proportion have lengths that the radar can resolve, and these long waves are at least as high as the shorter waves that cannot be followed accurately. The result is that a visual comparison of radar and wave-staff records gives the impression that the radar profile is reasonably accurate. In the second and third samples, Figs. 72 and 74, on the other hand the proportion of waves that can be resolved is much smaller, and these waves are lower than many shorter, steeper waves. Under this condition the correspondence between radar and wave-staff records is relatively poor. On April 27 and April 28 the correspondence between radar and wave-staff records is much better than for the last samples, on April 26, and this would be expected from the nature of the wave distributions shown in Figs. 76, 78, and 80. The distribution of Fig. 76 displays a more nearly uniform range of slope values at all values of height than that for any other sample, so that length and height values trend upward together, and waves large enough to be prominent in the record are in most cases also long enough to be accurately resolved. It may be noted that the method of scaling used biases the distribution somewhat against the longer and higher waves, since one of these may be broken up into two or more shorter or shallower waves in the tabulation. Thus, the length-height plots give a somewhat pessimistic picture of the extent to which a given wave pattern can be followed by the radar.

The general nature of the water surface is shown in some cases by the photographs presented in Fig. 81. The scale of these vertical views was established from the angle of view of the camera lens and also with reference to objects of known size in some pictures (such as the wave-staff electronics case). The circle which is inked on these photographs represents the half-power diameter of the radar patch, and the actual observed wavelengths can be compared to the patch size in these pictures.

Most of the data samples in the figures have been presented in chronological order, and the figures are largely self-explanatory. A brief log of the various exercises is given below.

April 14, 1965, Figs. 51 and 53 through 56. Winds were light and variable in the region of transition between very low radar scintillation and a typical moderate-wind level of noise. Waves were never much over 0.5 ft in height and were generally lower. Modulation indexes of 87, 50, 30, 16.5, and 8.6 were used.

April 18, Figs. 57 through 61. Winds were moderate at the start, then died down to a dead calm and remained below 4 mph for the remainder of the exercise. The longer waves remained relatively constant in height and exceeded one foot at times. Modulation indexes of 87, 50, 30, 16.5, and 8.6 were used.

April 20, Figs. 62 through 65. Winds were moderate throughout the exercise varying between 10 and 17 mph. Wave conditions were relatively constant, with heights exceeding one foot. Modulation indexes of 87, 50, 30, 16.5, and 8.6 were used.

April 25, Figs. 66 through 68. Winds were light at the start of the exercise and increased gradually to 13 mph while the records were made. Waves of longer periods first decreased in height, and then built back up to about the same maximum height of around 0.5 ft. Modulation indexes of 87, 50, 30, and 16.5 were used.

April 26, Figs. 69 through 74. Wind speed registered zero at the start of the exercise, then increased gradually to a maximum of 13 mph. Fairly long, low swells were present at first with short-period, wind-driven waves building up to over 0.5 ft at the

end of the exercise. A modulation index of 50 was used in all the examples shown. Histograms of calculated wave lengths and radar depths as well as height-length plots are included in the series of figures for this date.

April 27, Figs. 75 and 76. Winds were relatively high on this date, exceeding 33 mph at the end of the exercise, the highest speed reached during any data-recording period. Waves at times reached heights of 2.5 ft and were among the highest recorded during any Bay Bridge exercise. A modulation index of 50 was in use when the example shown in Fig. 75 was recorded. A histogram of calculated wave lengths and radar depths and a height-length plot are given in Fig. 76. In the radar depth histogram, the depth intervals for each bar of the graph are twice as large as in the other histograms shown.

April 28, Figs. 77 through 80. Winds were fairly steady and moderate throughout the exercise, remaining within the range from 10 to 16 mph. Wave conditions were also relatively stable, and some waves exceeded 1.5 ft in height. Modulation indexes of 50, 30, 16.5, and 8.6 were all used. A histogram of calculated wavelengths and radar depths and a height-length plot are given in Fig. 78. Four histograms are shown in Fig. 80.

Two of the data samples for the April 14th exercise deserve special comment. Figure 53a shows recordings of long, low swells during an interval of very light winds. These swells were intermittent in nature and were apparently generated by ocean-going ships passing in the main channel under the Bay Bridge 2250 yards to the west of the radar installation. The chart speed was reduced to 0.1 div./sec during this time, and the waves shown have periods ranging from 3.6 to 6.5 sec and calculated lengths from 66 to 216 ft.

Figure 53b shows a data sample taken a few minutes after the sample of Fig. 52a when the wind had increased slightly, and shows the sudden transition in the radar noise pattern which can occur under these circumstances.

Applicability of the Interferometer Discriminator Multipath Theory to the Bay Bridge FM-CW Radar

Derivation of the basic theoretical results for the FM-CW balanced interferometer radar is based on the following assumptions:

1. The system transmits a wave having pure frequency modulation impressed on the carrier, and the modulating function is a single-frequency sinusoid.

2. The frequency discriminator is a perfectly balanced interferometer driving detectors which are perfectly matched and have exactly square-law action.

3. There are no significant internal multiple paths or phase-versus-frequency anomalies in any part of the microwave assembly.

4. Any amplification which takes place ahead of the discriminator is linear, so that no compression or amplitude limiting occurs for the modulation frequency.

5. The discriminator is followed by a limiter and phase-bridge combination sensitive only to the phase of the fundamental modulation frequency component of the signal.

Design specifications and bench tests indicate that the system did not depart significantly from the ideal with respect to assumptions 4 and 5. The modulation was, however, known to be slightly imperfect, and the discriminator and crystals may have been slightly unbalanced. Modulation imperfections arise because of a slight variation of BWO power

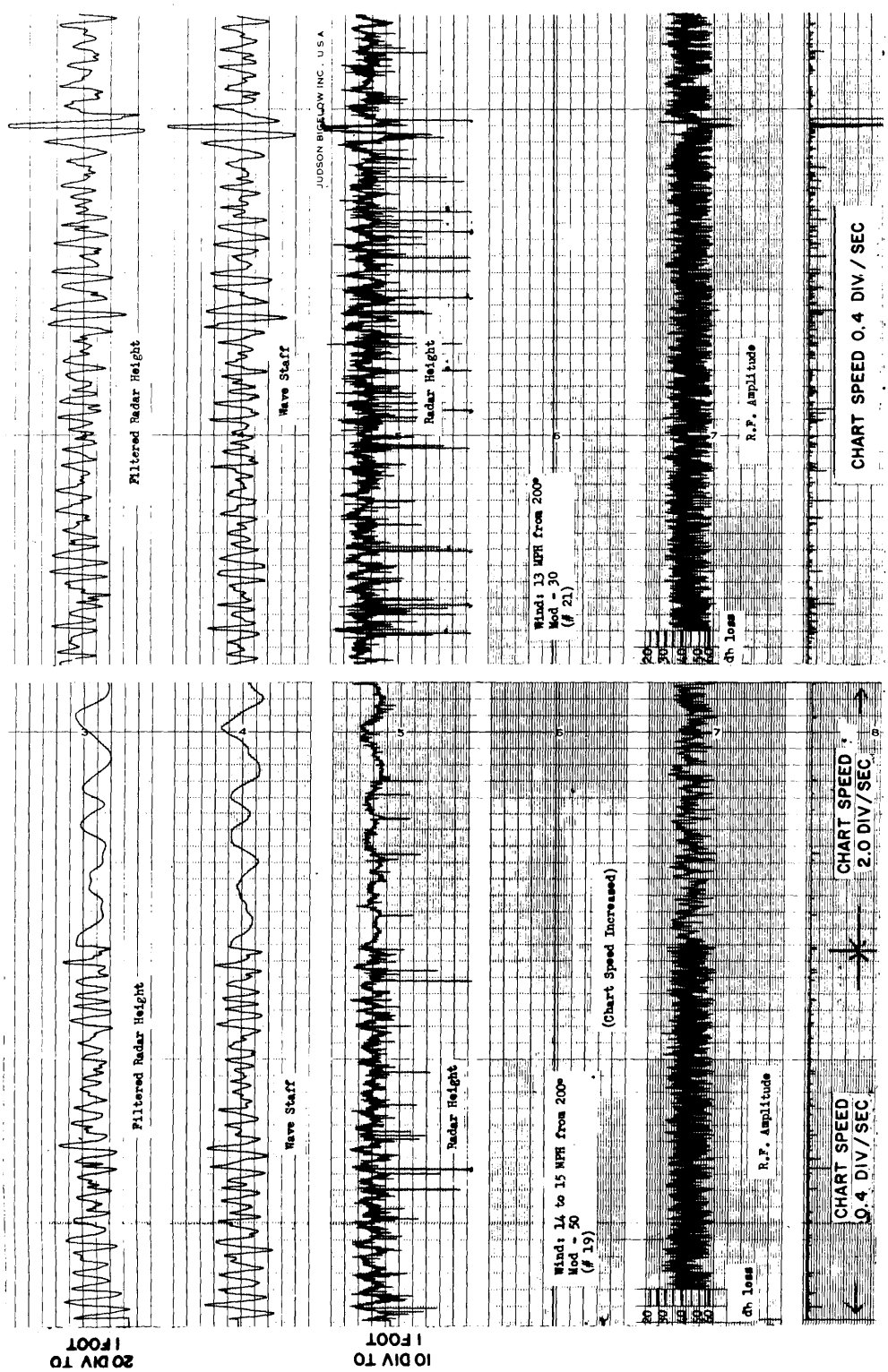

Fig. 57 - Examples of moderate wind recordings using different modulation indexes, showing the accurate radar profiling possible when waves are long enough to resolve and an adequately high modulation index is in use

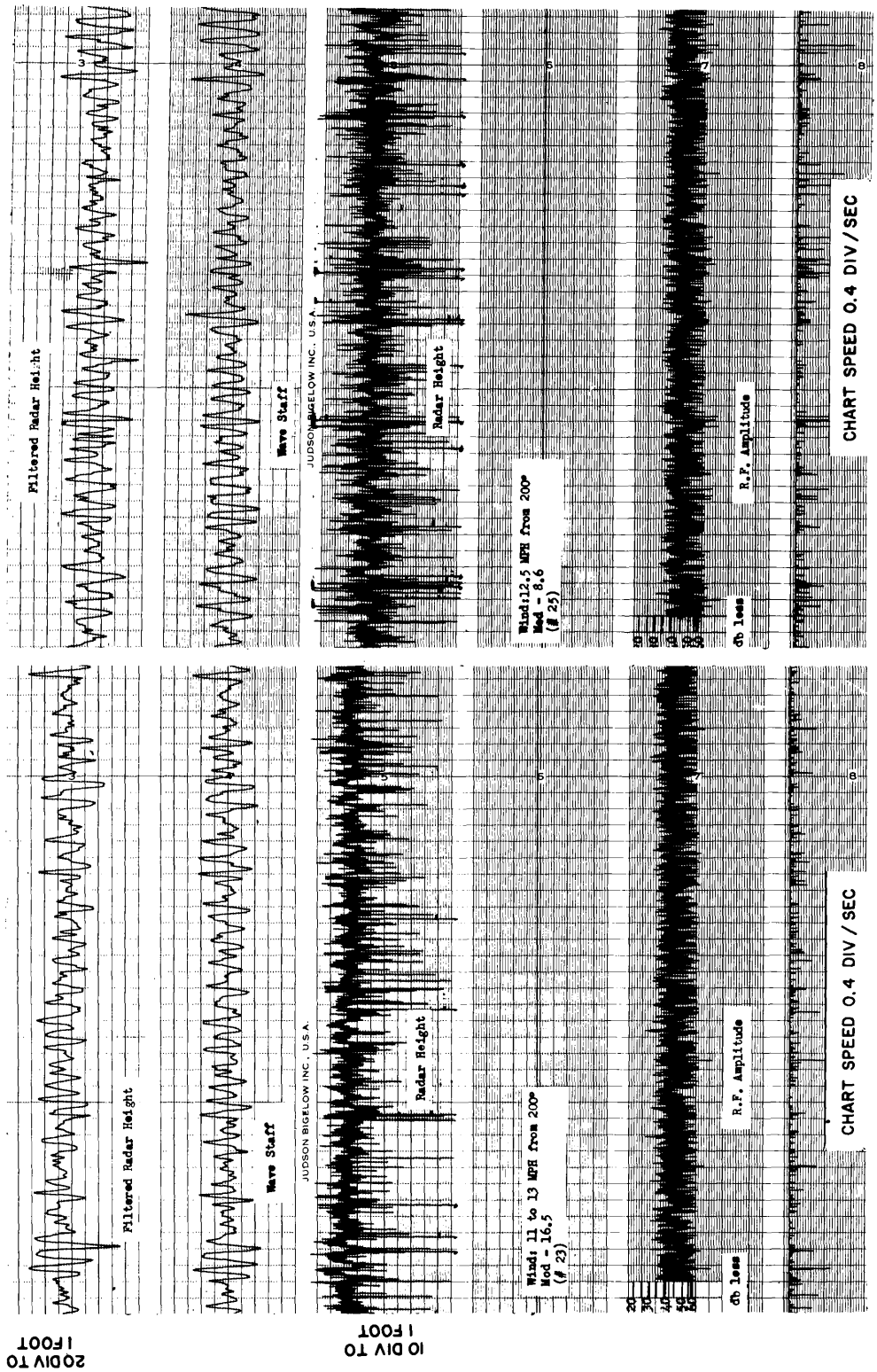

Fig. 57 (Cont'd) - Examples of moderate wind recordings using different modulation indexes, showing the accurate radar profiling possible when waves are long enough to resolve and an adequately high modulation index is in use

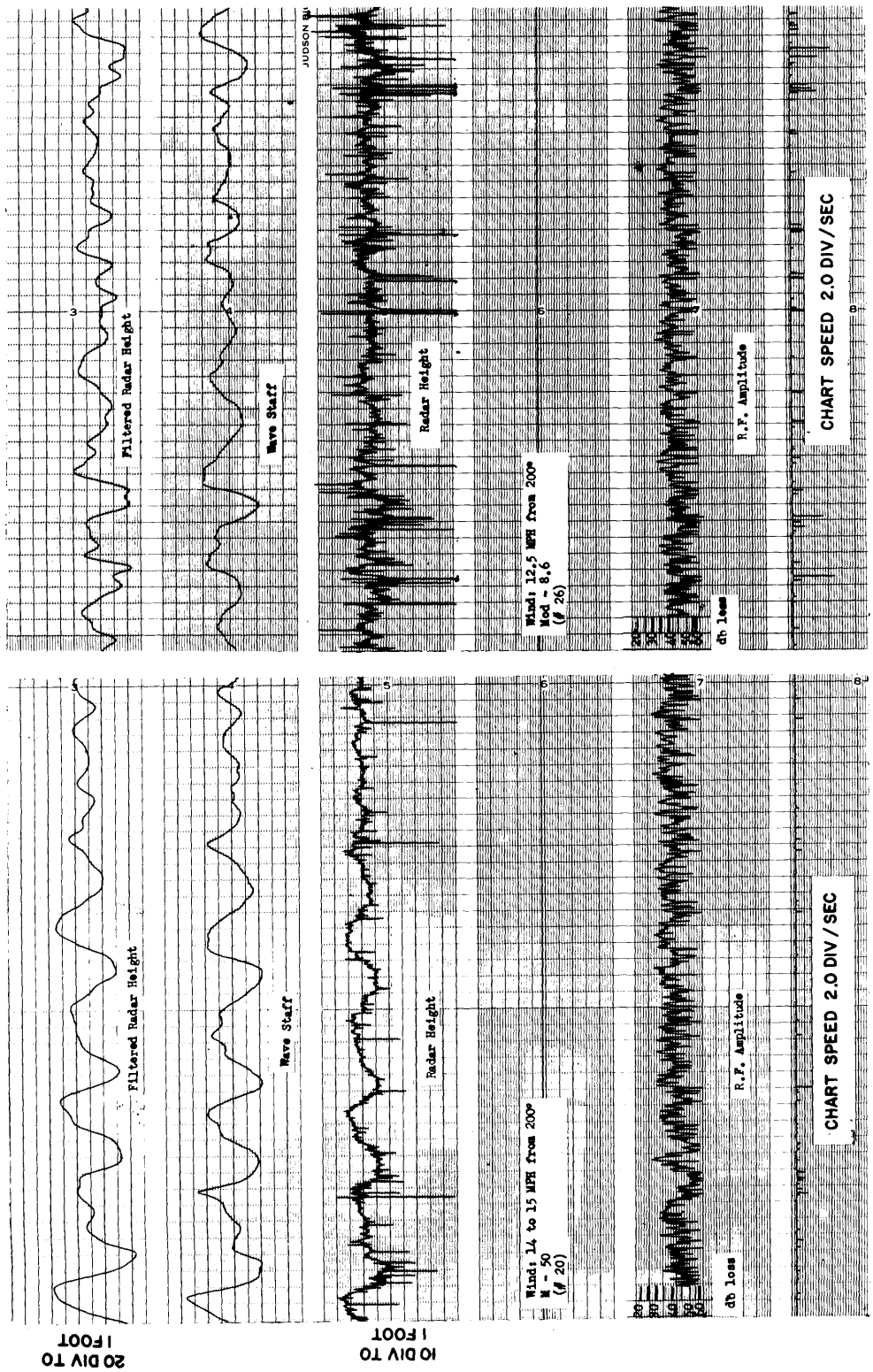

Fig. 58 - Examples of higher speed moderate wind recordings at two modulation indexes, showing the marked increase in radar range noise which can occur when the index is too low

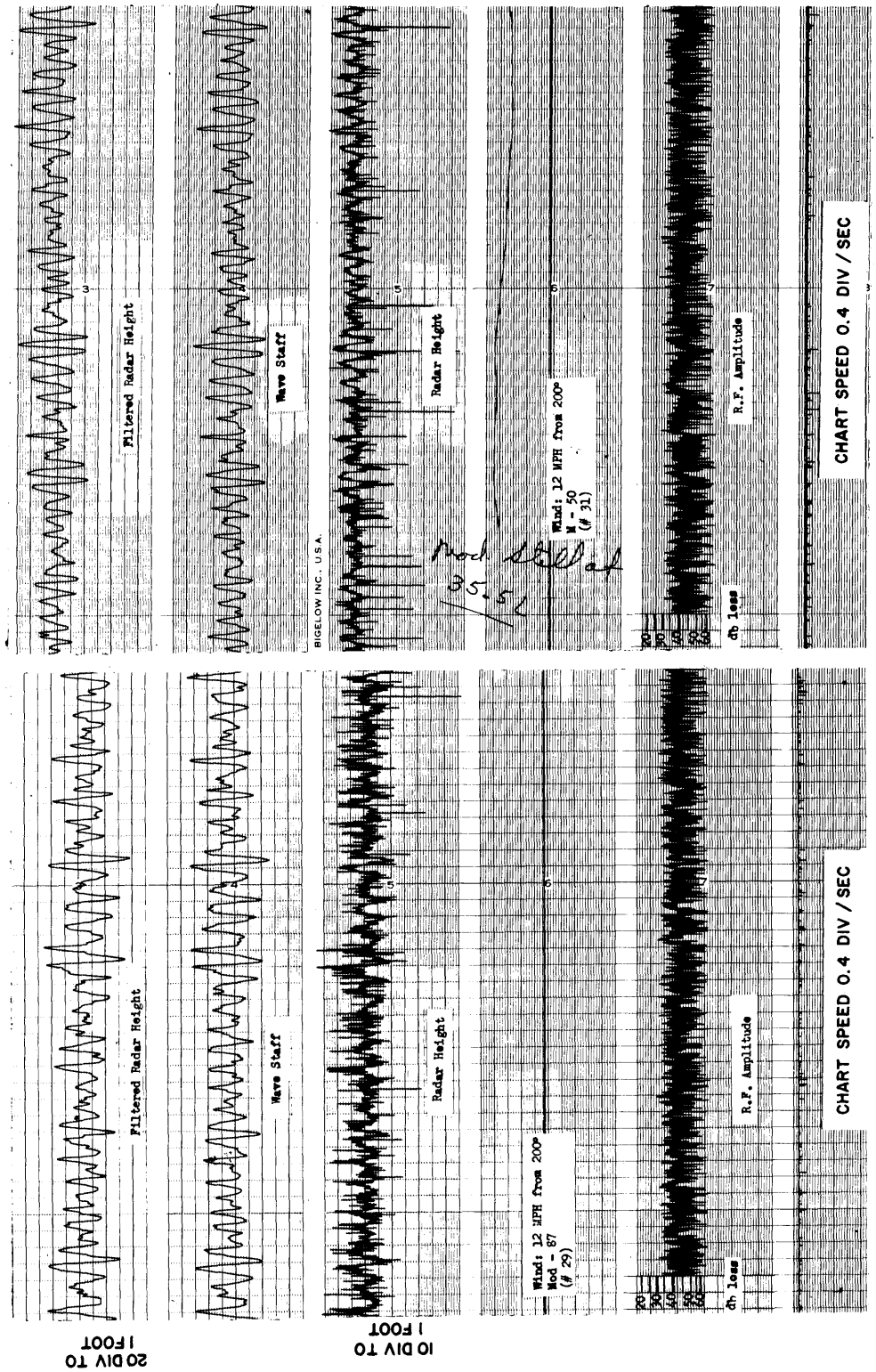

Fig. 59 - Examples of moderate wind recordings which illustrate a rapid comparison of performance at different modulation indexes by using a single discriminator matched to the widest frequency deviation and which show an index of 50 to produce the lowest radar noise level

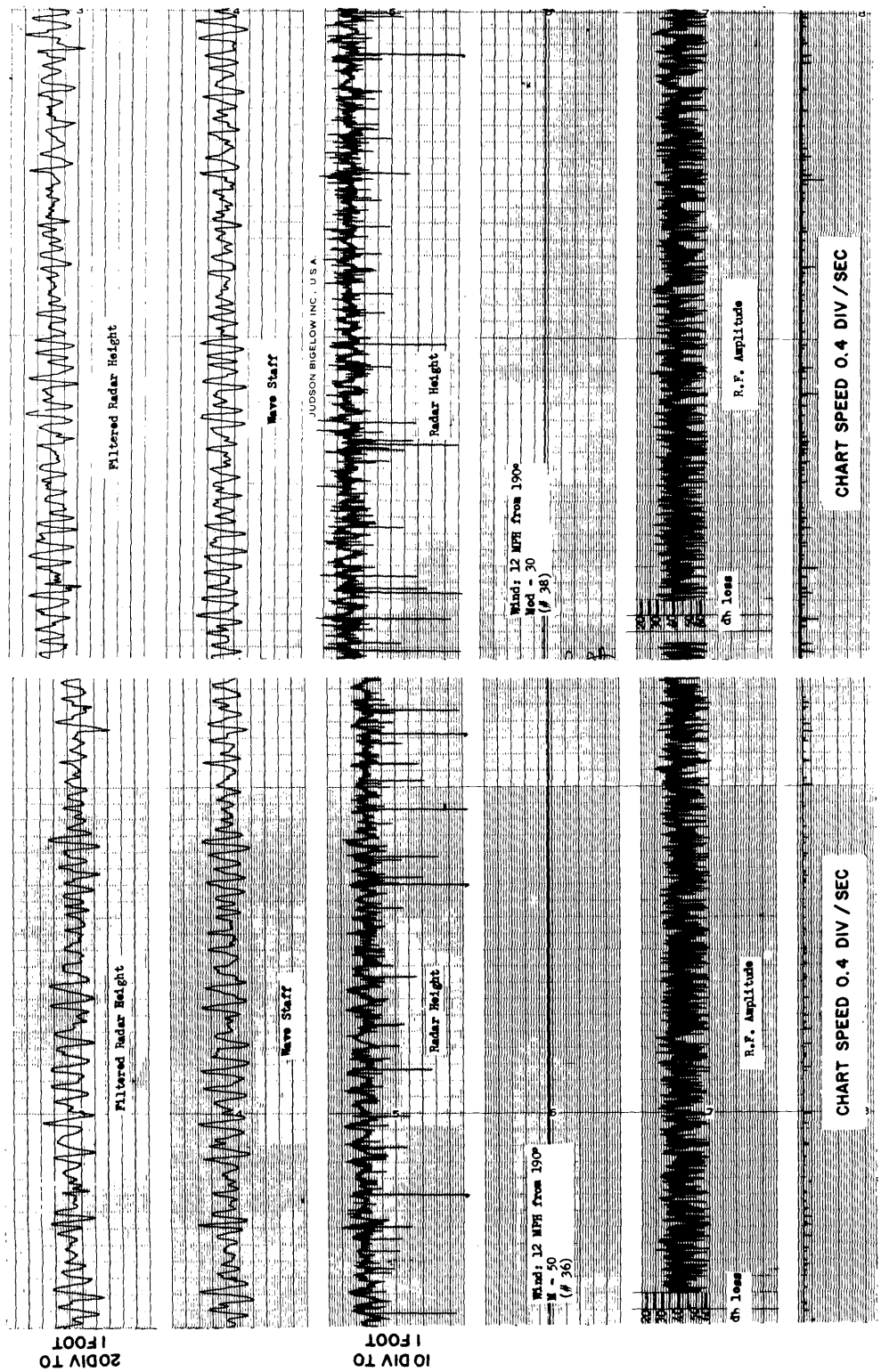

Fig. 59 (Cont'd) - Examples of moderate wind recordings which illustrate a rapid comparison of performance at different modulation indexes by using a single discriminator matched to the widest frequency deviation and which show an index of 50 to produce the lowest radar noise level

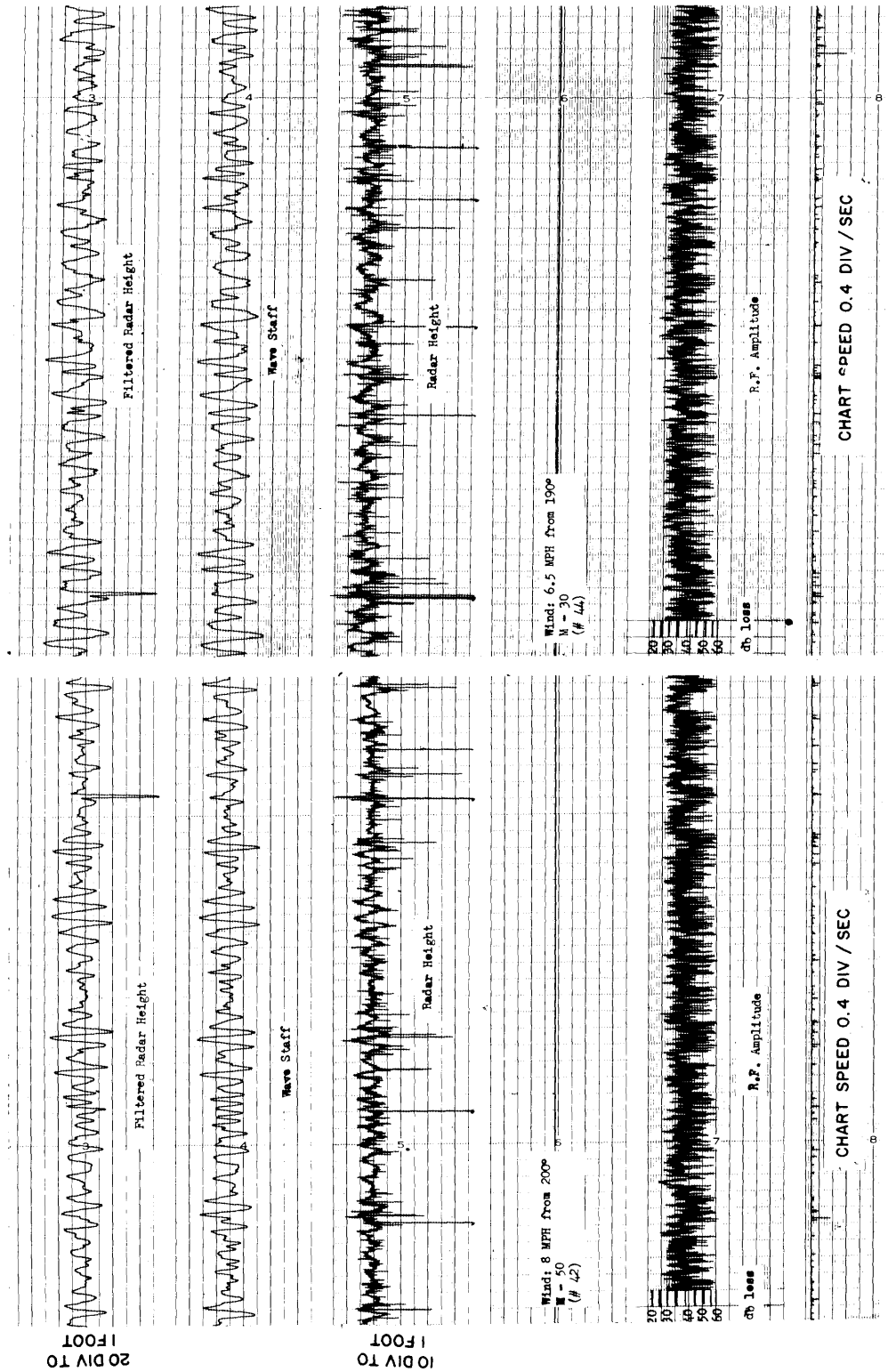

Fig. 60 - Examples of recordings made during a period of decreasing light winds which compare performance at different modulation indexes using discriminators optimized for each frequency deviation and which show a progressive increase in radar noise as the index is reduced

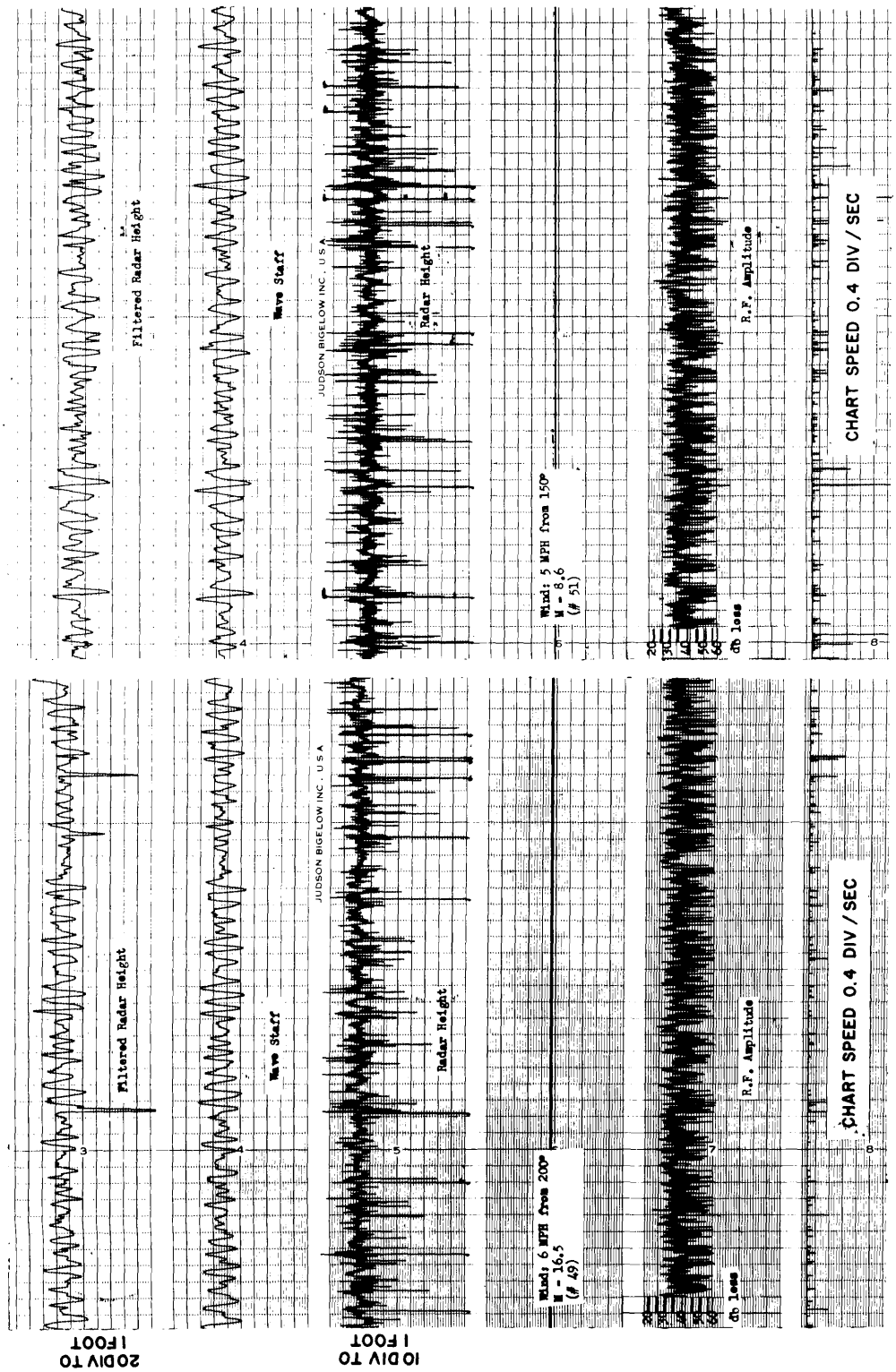

Fig. 60 (Cont'd) - Examples of recordings made during a period of decreasing light winds which compare performance at different modulation indexes using discriminators optimized for each frequency deviation and which show a progressive increase in radar noise as the index is reduced

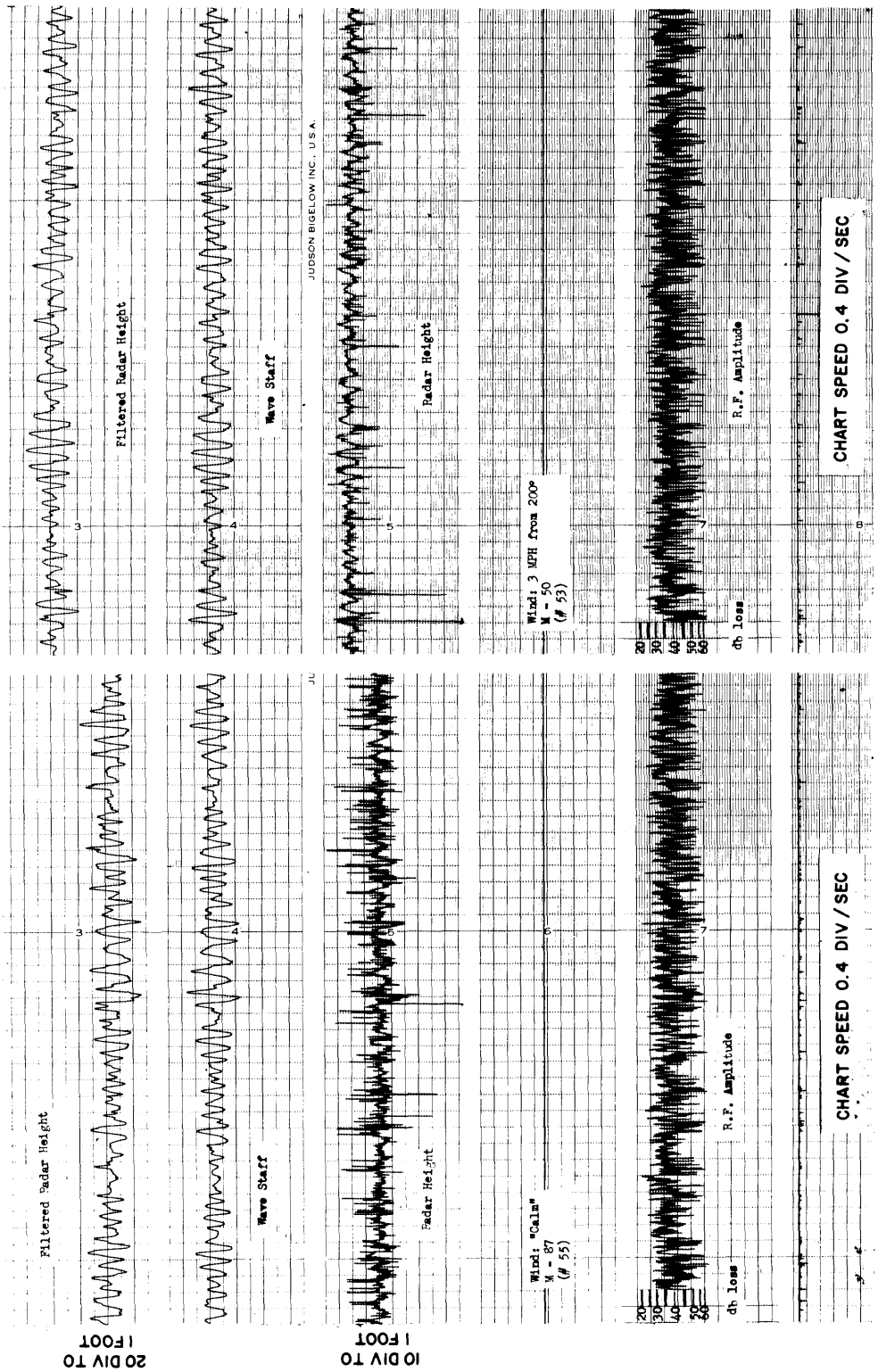

Fig. 61 - Examples of recordings made just after the wind had rapidly decreased to nearly a dead calm which compare performance at two modulation indexes and which show noise spikes to remain numerous at an index of 87 while radar noise immediately becomes very low at an index of 50

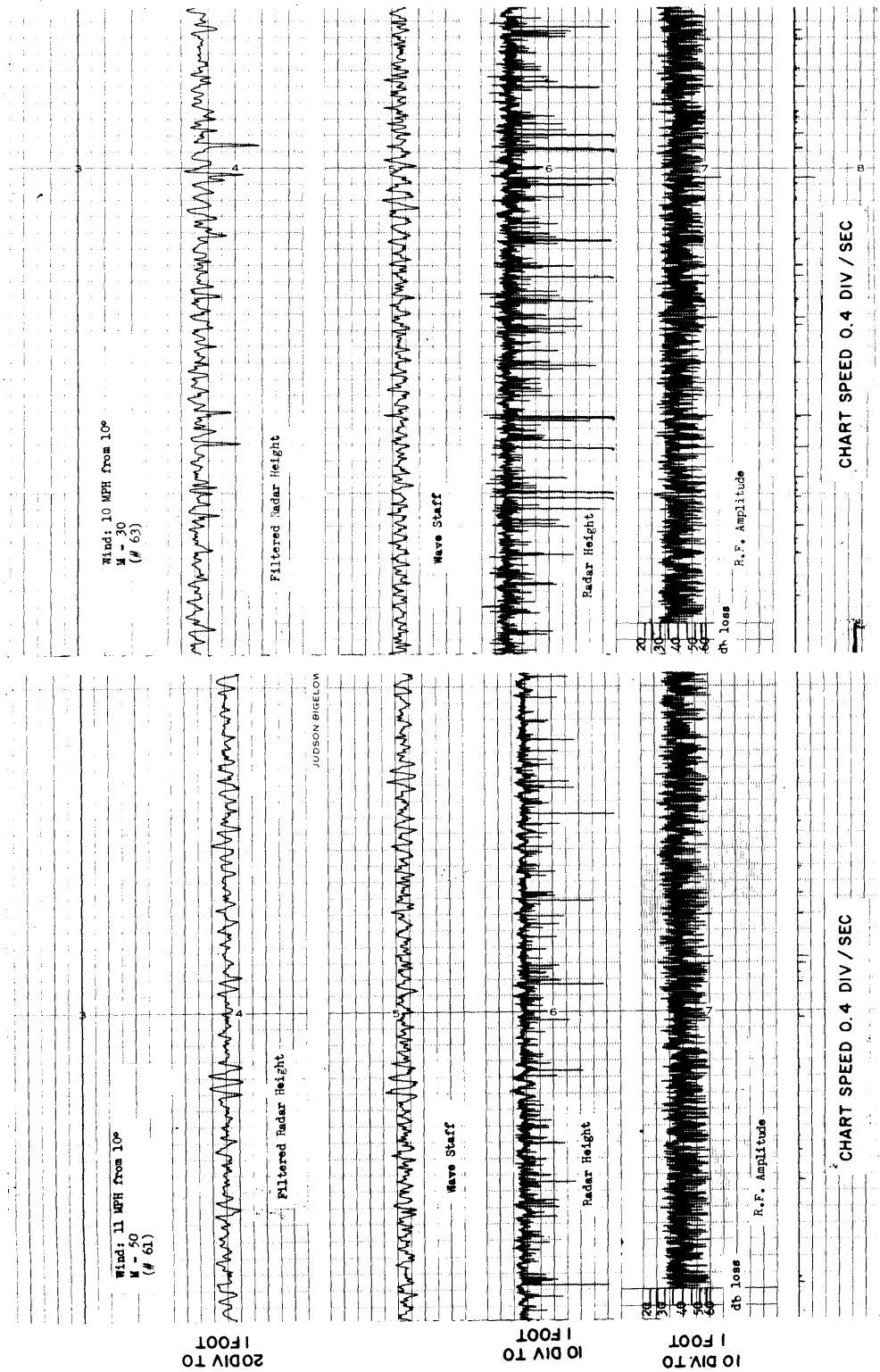

Fig. 62 - Examples of recordings made under conditions of fairly light and variable winds and low waves which illustrate a situation where many waves are too short to be resolved by the radar but where the progressive increase in radar noise as the modulation index is reduced below 50 is similar to that observed when waves are longer and the profile more accurately reproduced. Note the changes in the unfiltered radar height scale when using the modulation indexes of 16.5 and 8.6.

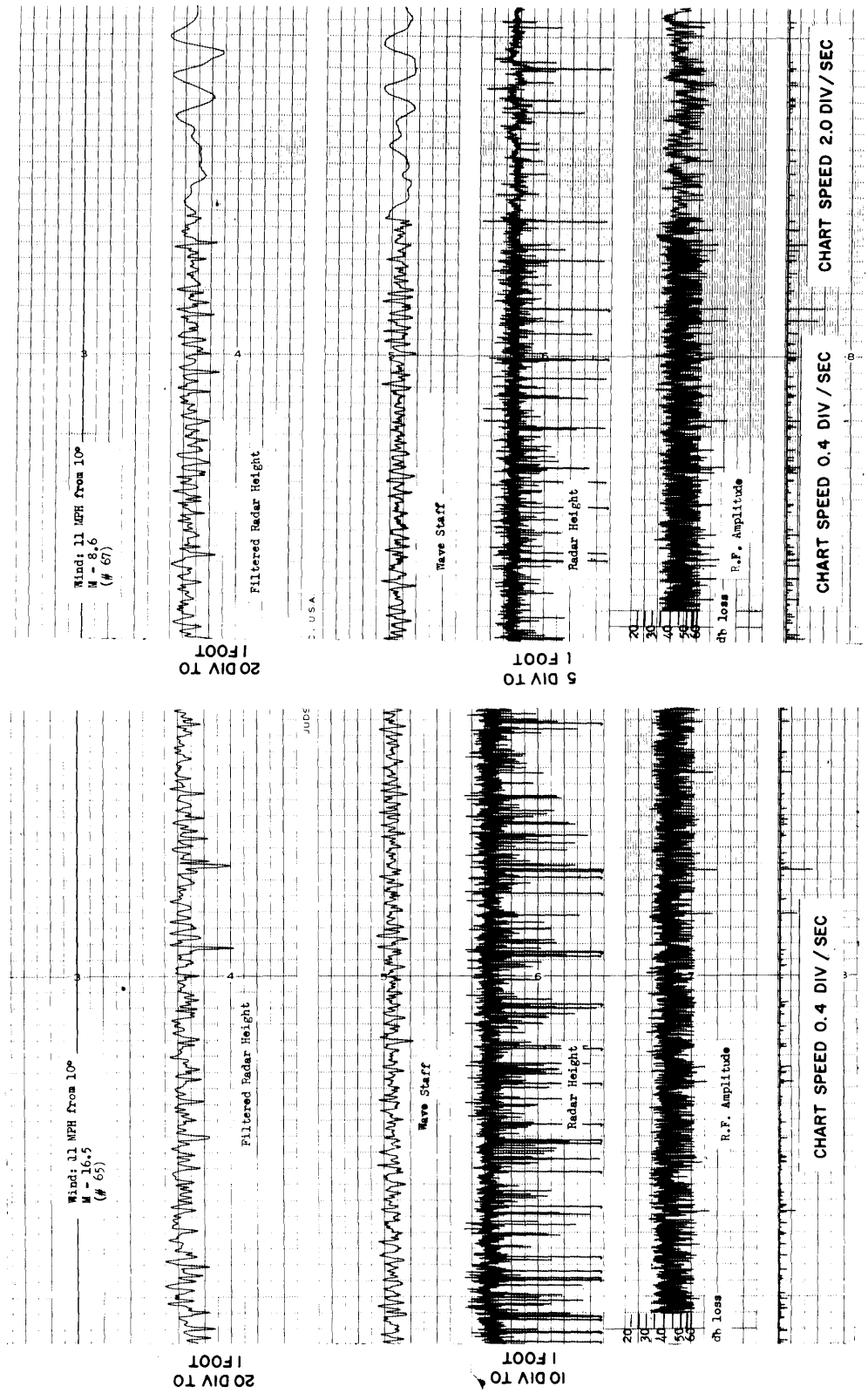

Fig. 62 (Cont'd) - Examples of recordings made under conditions of fairly light and variable winds and low waves which illustrate a situation where many waves are too short to be resolved by the radar but where the progressive increase in radar noise as the modulation index is reduced below 50 is similar to that observed when waves are longer and the profile more accurately reproduced. Note the changes in the unfiltered radar height scale when using the modulation indexes of 16.5 and 8.6.

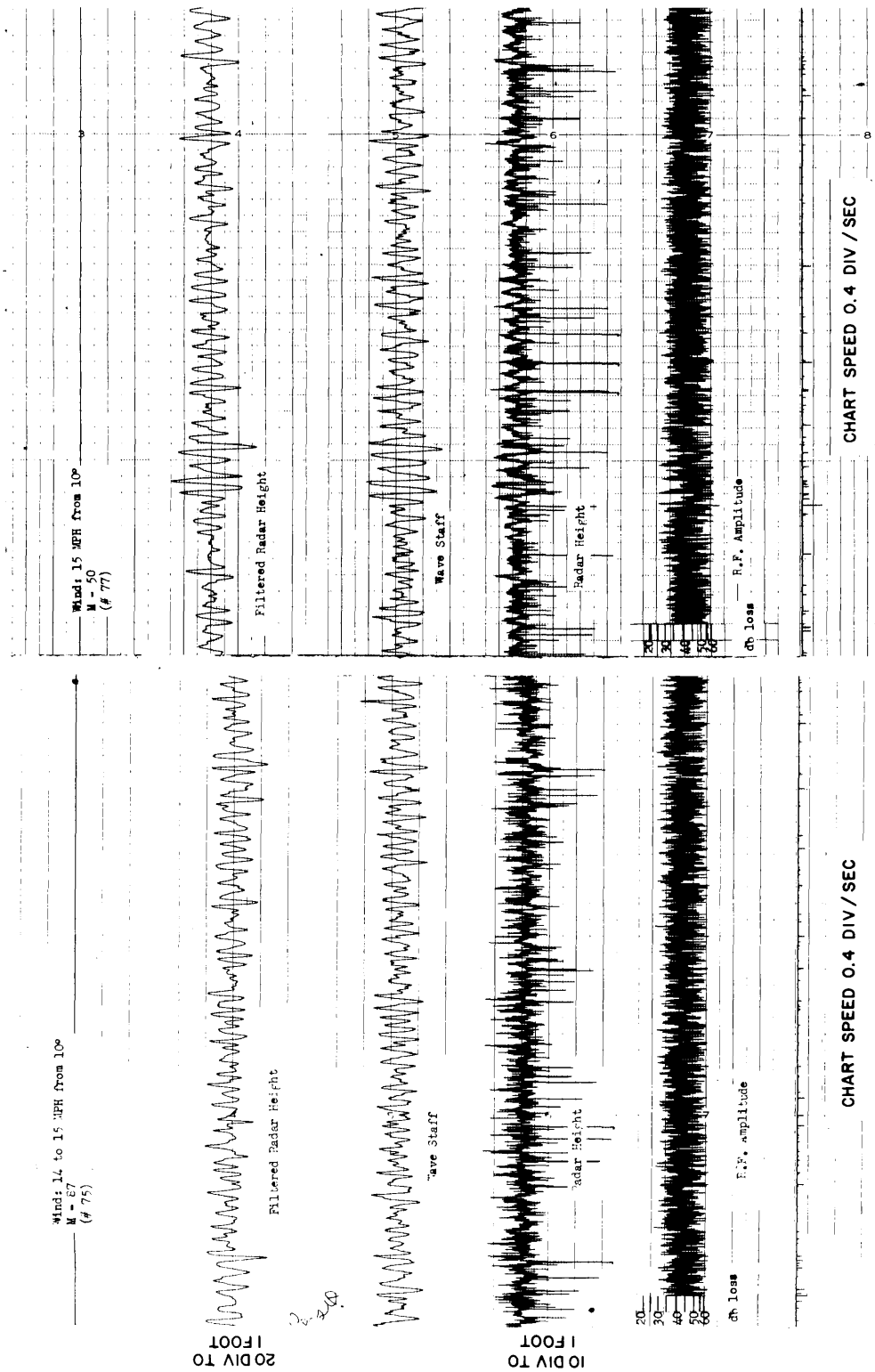

Fig. 63 - Examples of recordings made under moderate wind conditions when some waves were too short to be resolved and which show typical differences in the radar noise patterns when changing the modulation index from 87 to 50

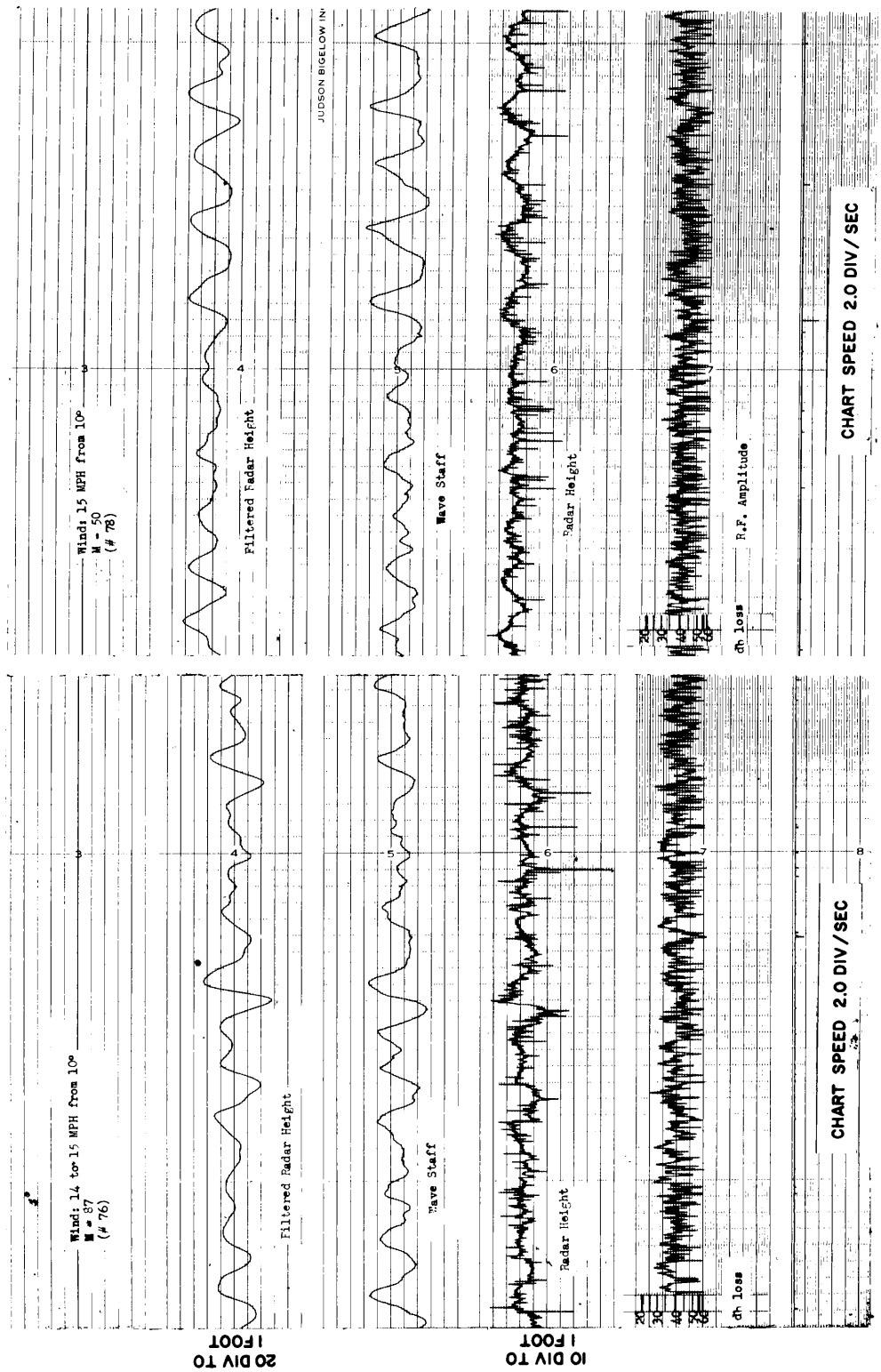

Fig. 63 (Cont'd) - Examples of recordings made under moderate wind conditions when some waves were too short to be resolved and which show typical differences in the radar noise patterns when changing the modulation index from 87 to 50

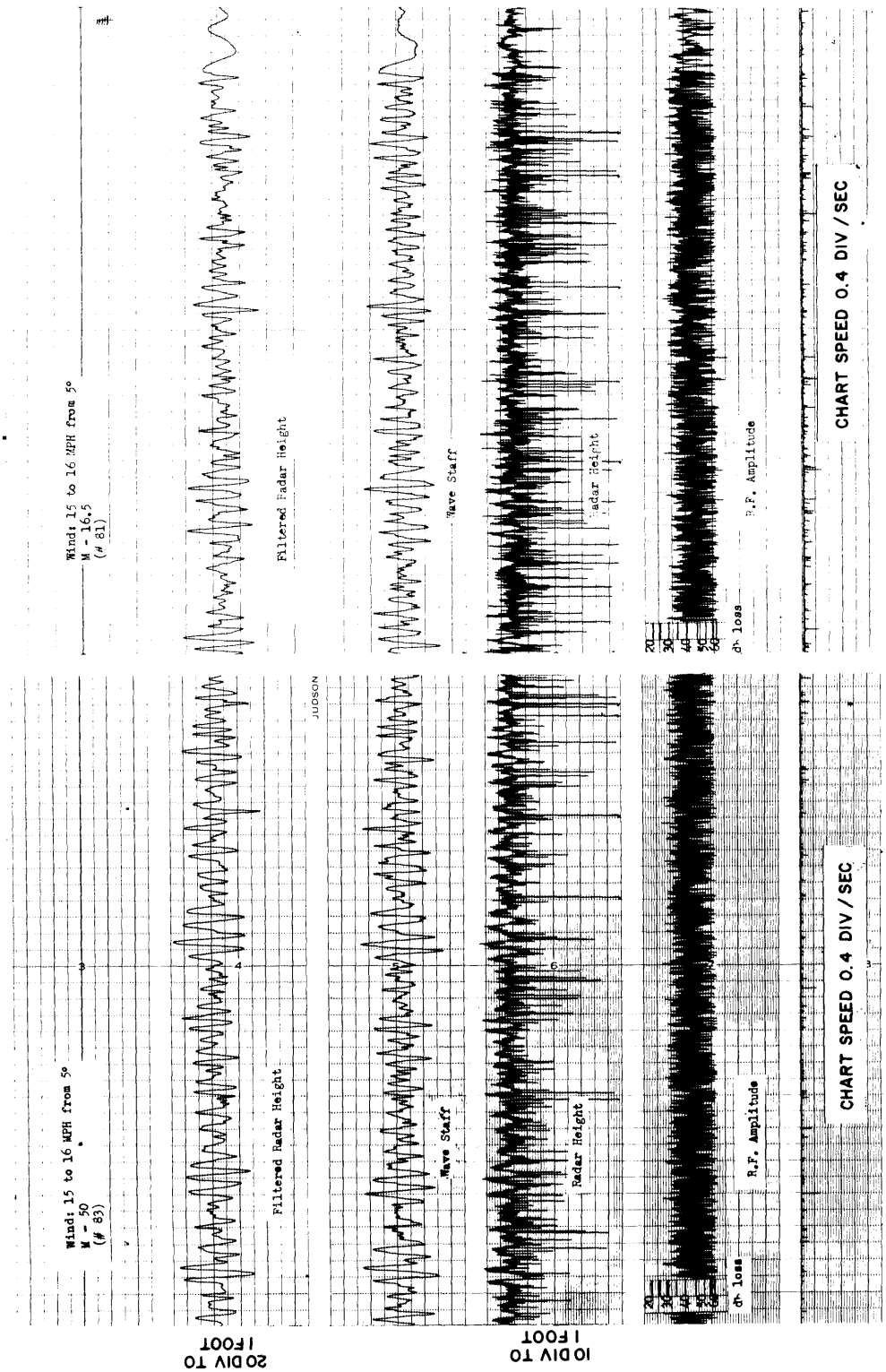

Fig. 64 - Examples of recordings under conditions of steady moderate winds when most waves were long enough to be resolved and which show fairly accurate radar profiling at the lower modulation index of 16.5, although the radar range noise is typically lower, using an index of 50

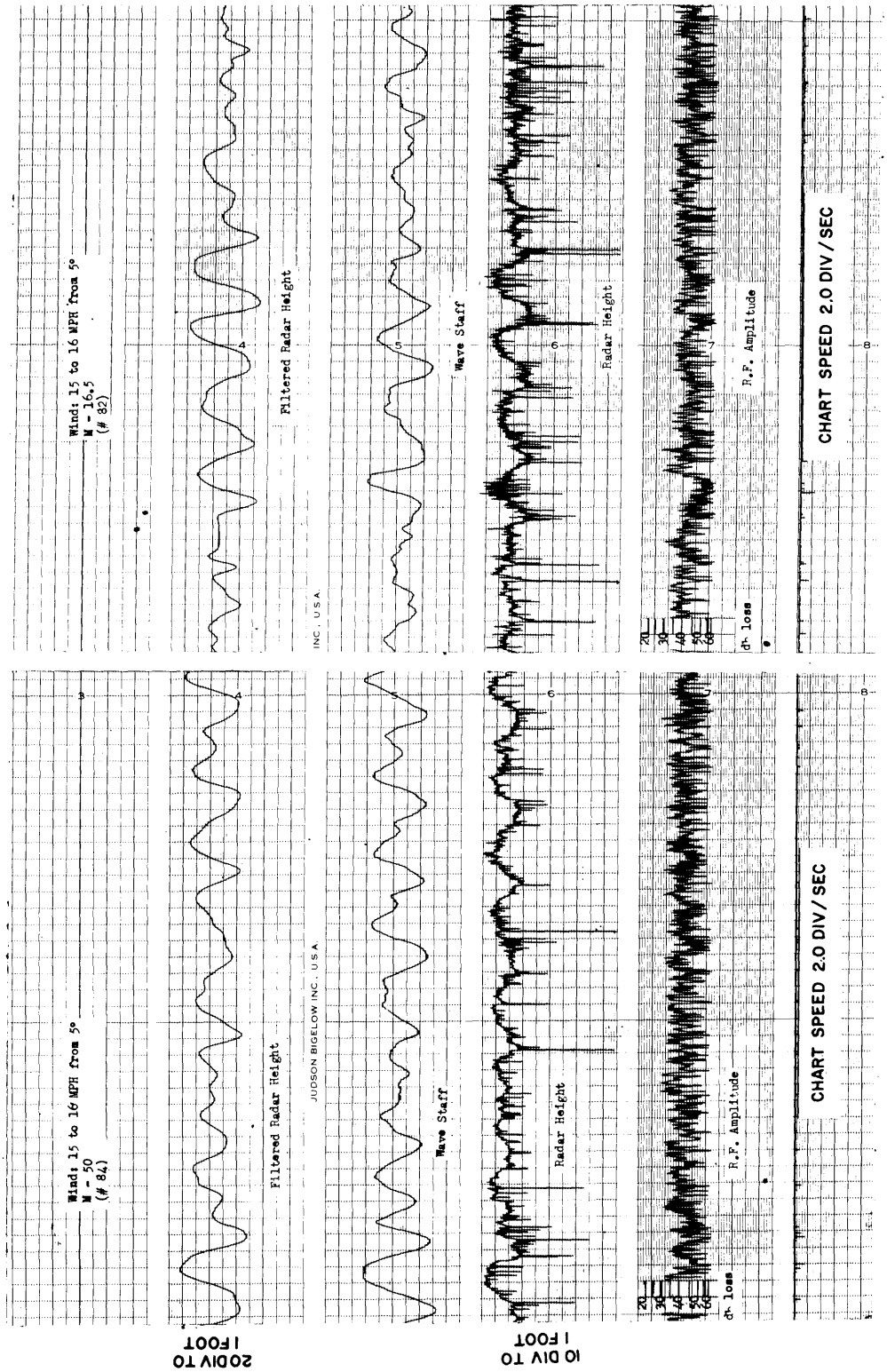

Fig. 64 (Cont'd) - Examples of recordings under conditions of steady moderate winds when most waves were long enough to be resolved and which show fairly accurate radar profiling at the lower modulation index of 16.5, although the radar range noise is typically lower, using an index of 50

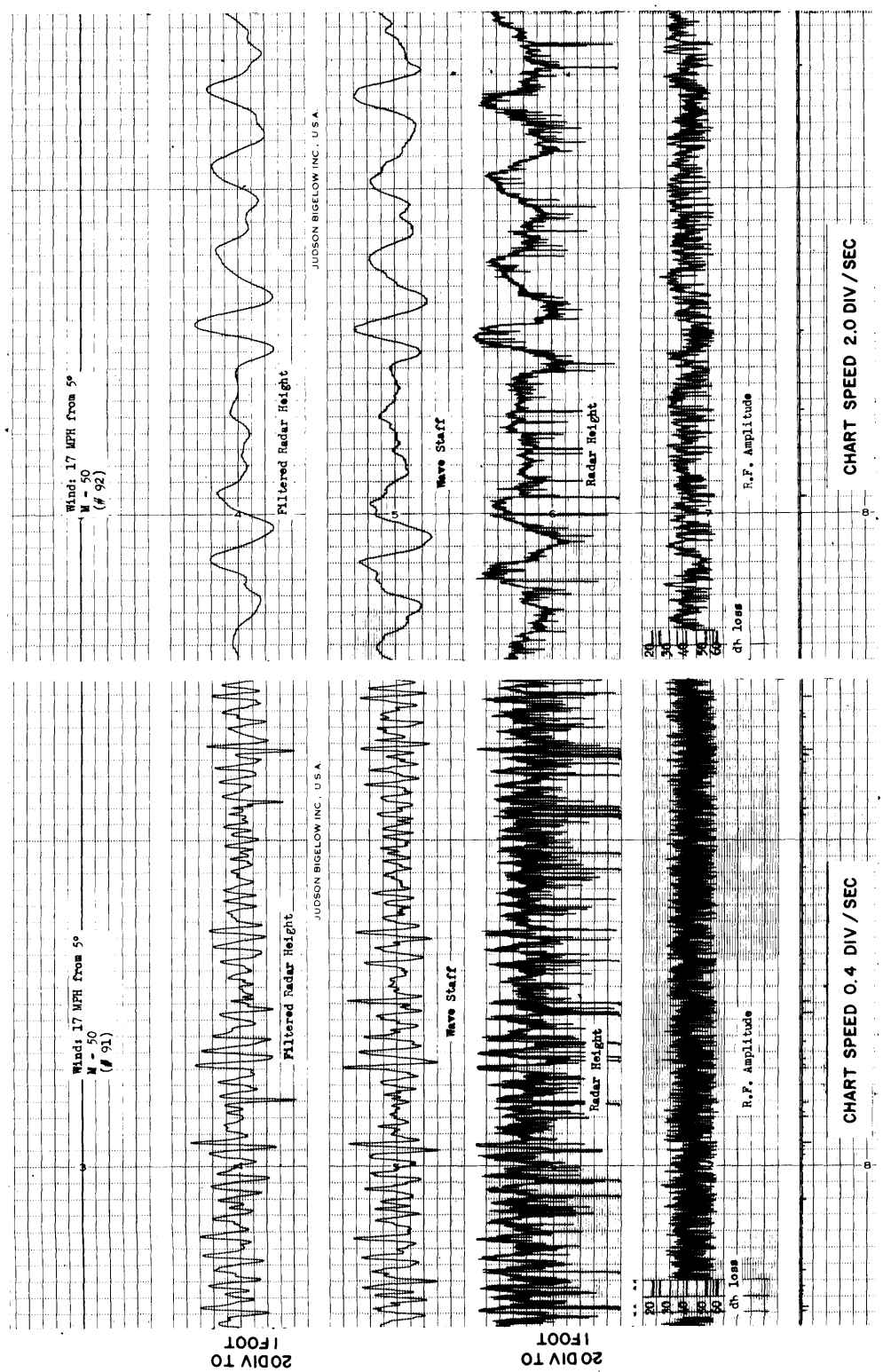

Fig. 65 - Examples of recordings made under conditions of moderate steady winds the same as those of Fig. 64, but with the amplitude of the unfiltered radar trace doubled to match the wave staff and filtered radar records

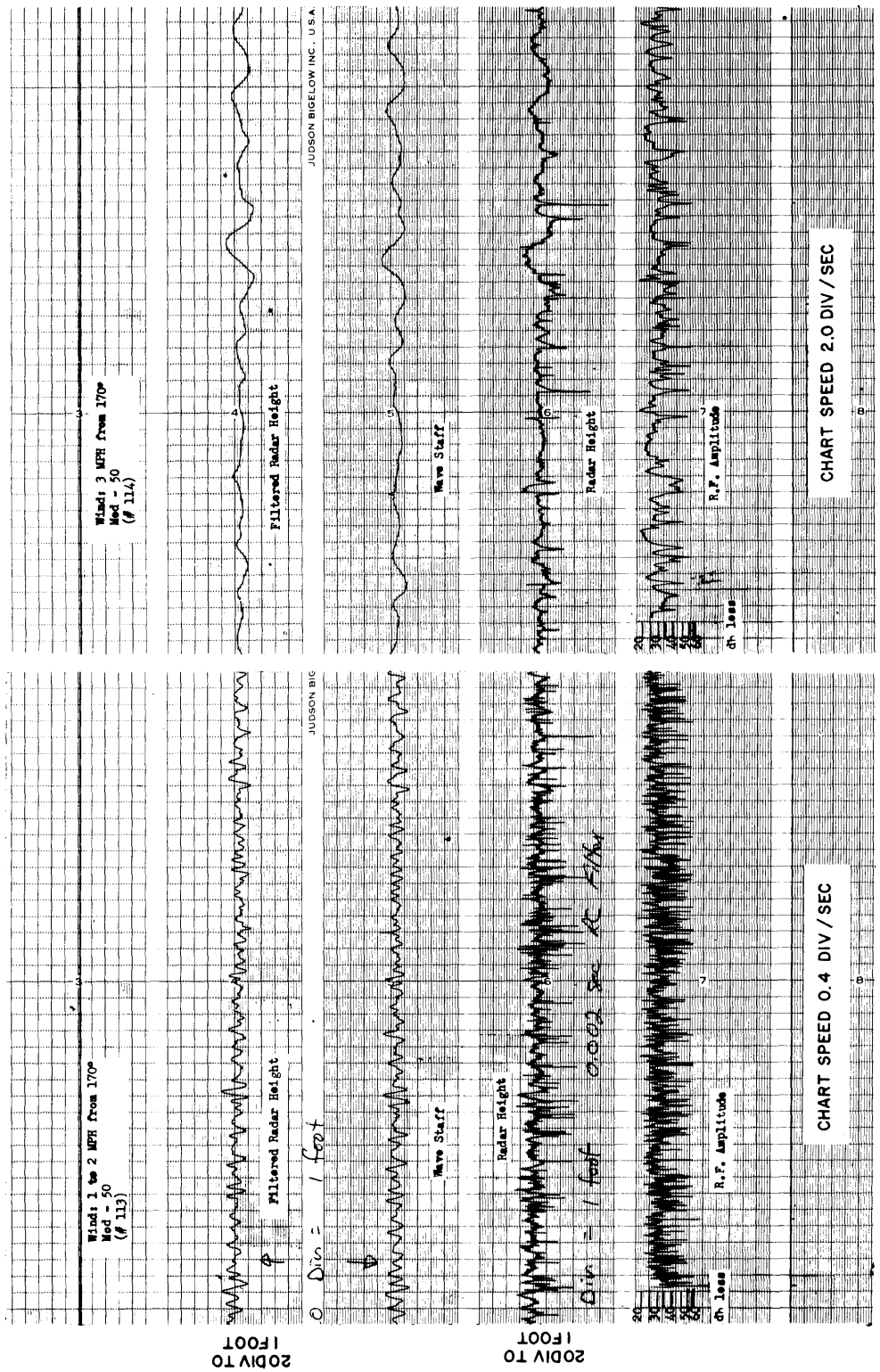

Fig. 66 - Examples of recordings made with all wave-trace amplitudes matched and under conditions of very light winds and low waves, many too short to be resolved, and which in contrast with Fig. 54 show fairly frequent deep fading and higher radar noise levels which trend upward as the modulation index is reduced in the manner characteristic of moderate and high wind conditions

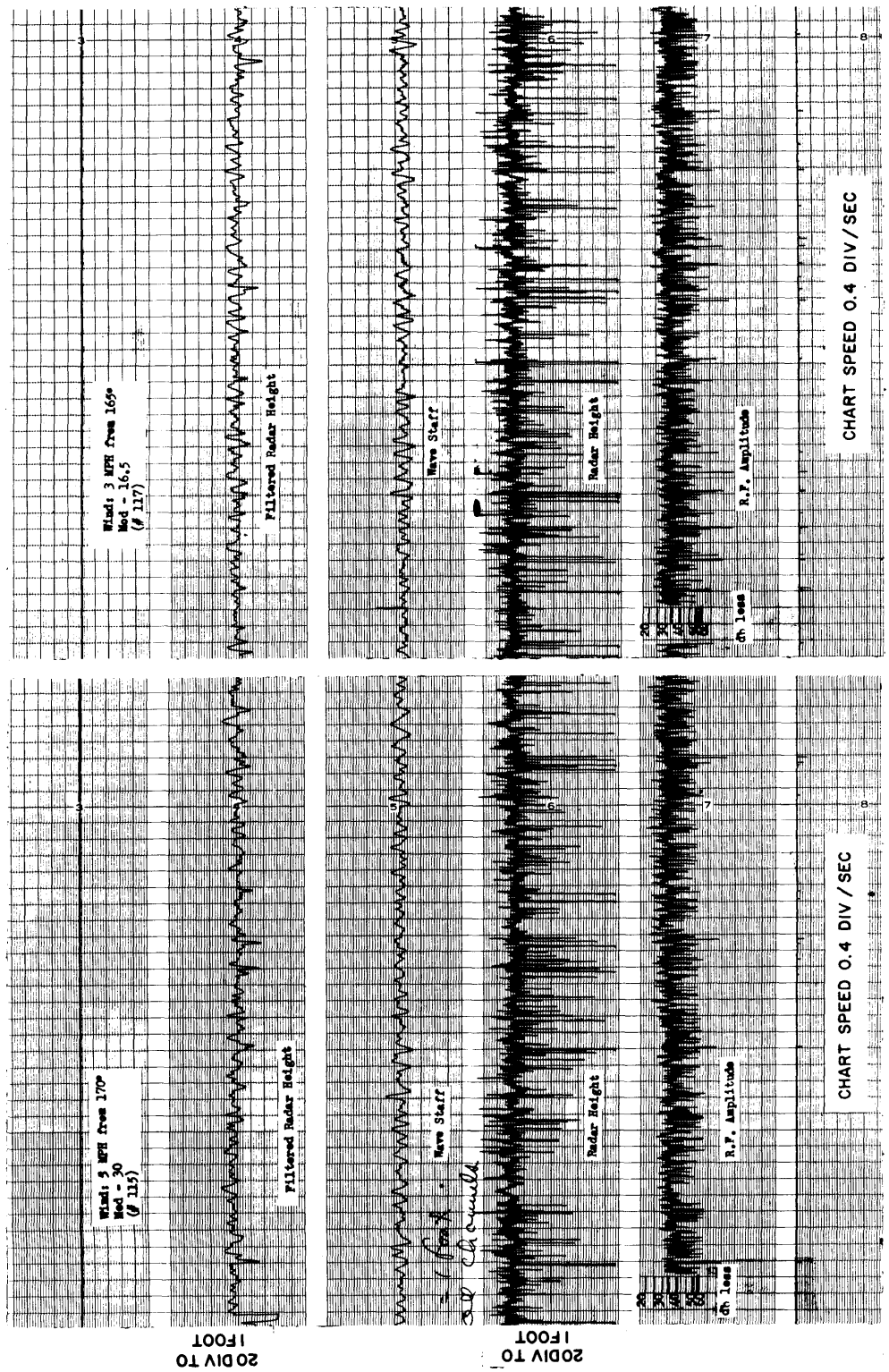

Fig. 66 (Cont'd) - Examples of recordings made with all wave-trace amplitudes matched and under conditions of very light winds and low waves, many too short to be resolved, and which in contrast with Fig. 54 show fairly frequent deep fading and higher radar noise levels which trend upward as the modulation index is reduced in the manner characteristic of moderate and high wind conditions

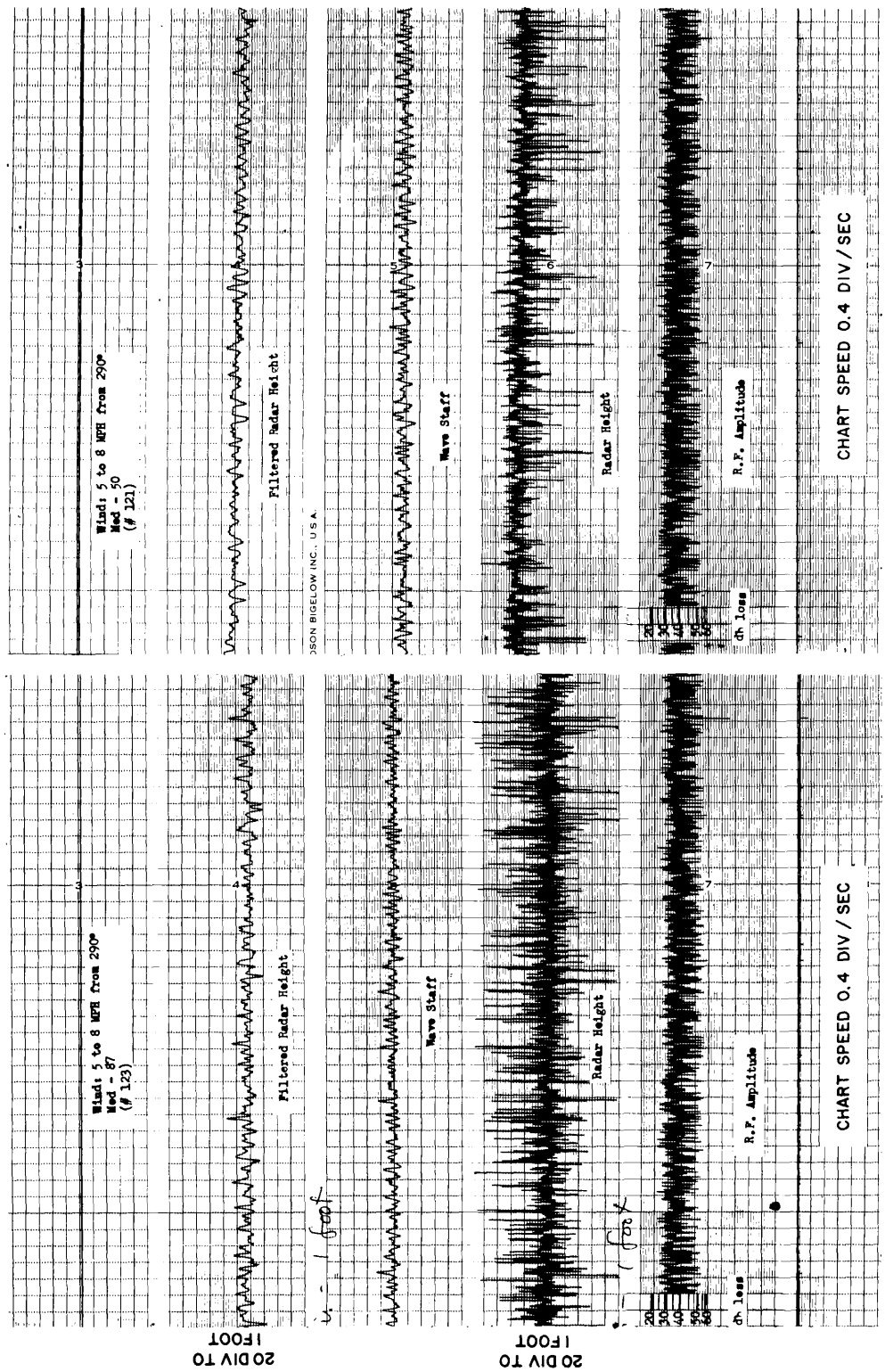

Fig. 67 - Examples of recordings made with all wave-trace amplitudes matched and under conditions of rising but still light winds and low waves, most too short to resolve, and which illustrate an especially marked contrast between the radar noise patterns when using the two modulation indexes of 87 and 50

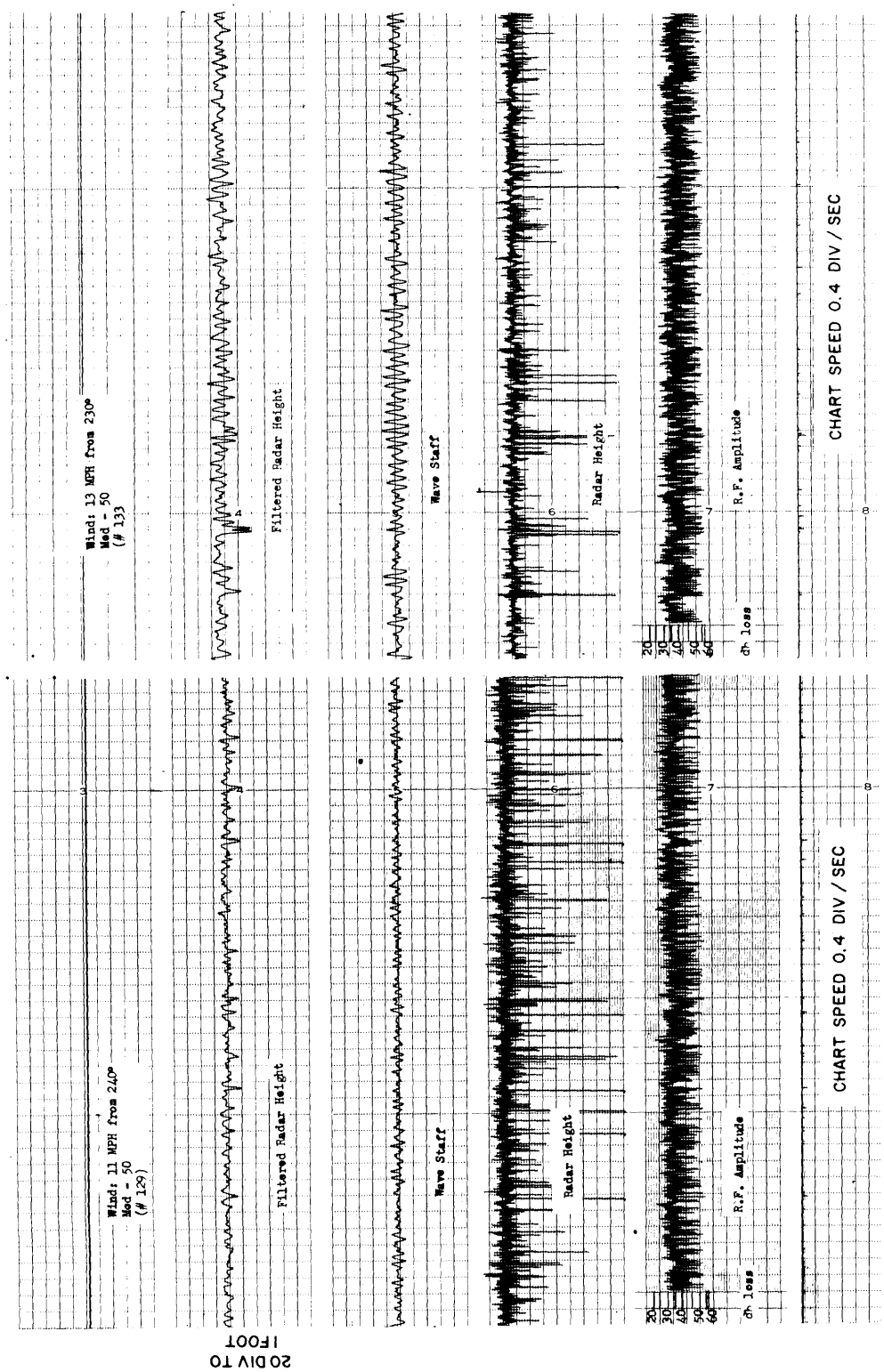

Fig. 68 - Examples of recordings made with all wave-trace amplitudes matched and which span a period of time when gravity waves were building up under the influence of a steady moderate wind, illustrating a case where wave conditions were markedly altered while radar noise remained relatively unchanged

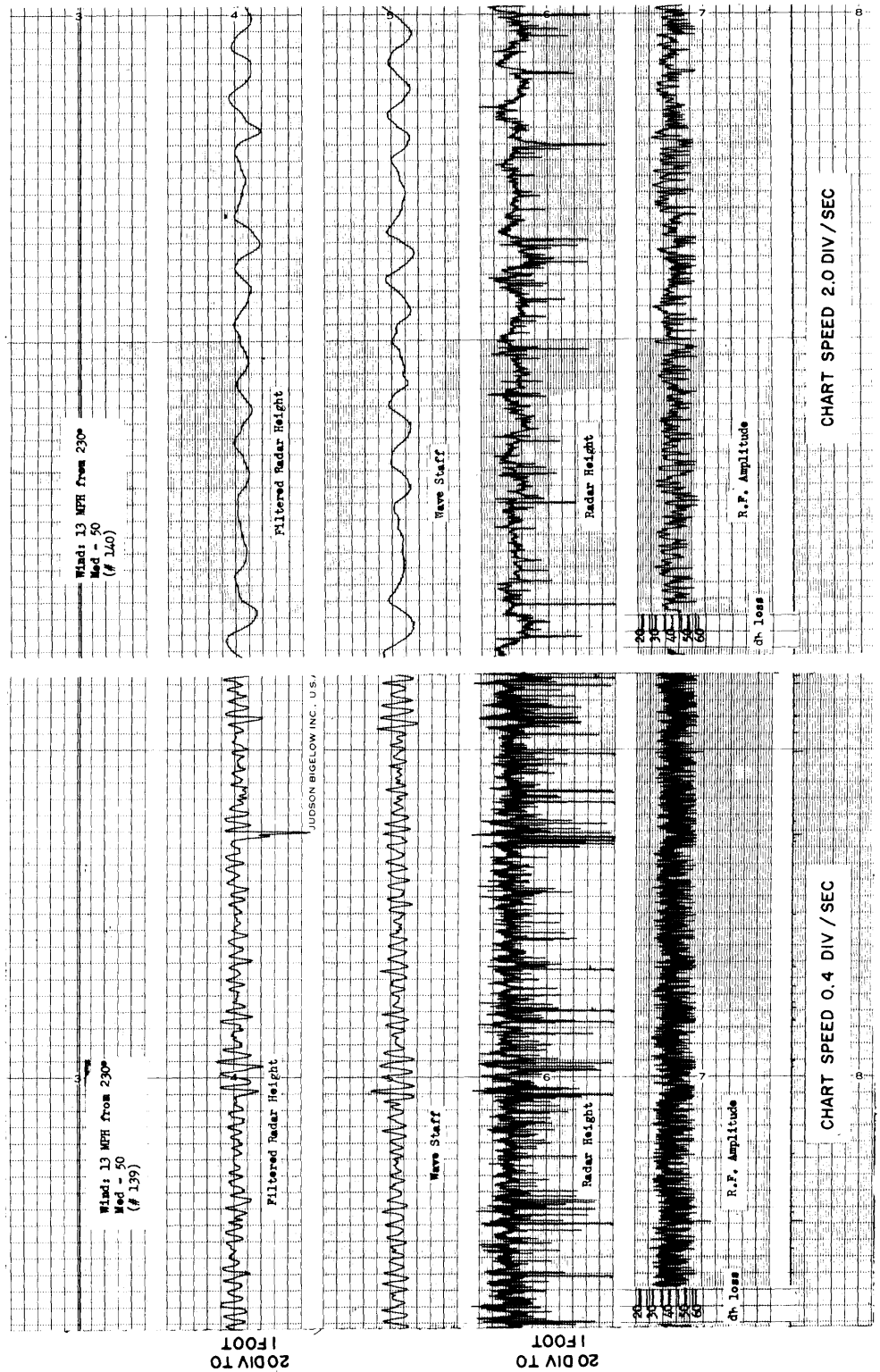

Fig. 68 (Cont'd) - Examples of recordings made with all wave-trace amplitudes matched and which span a period of time when gravity waves were building up under the influence of a steady moderate wind, illustrating a case where wave conditions were markedly altered while radar noise remained relatively unchanged

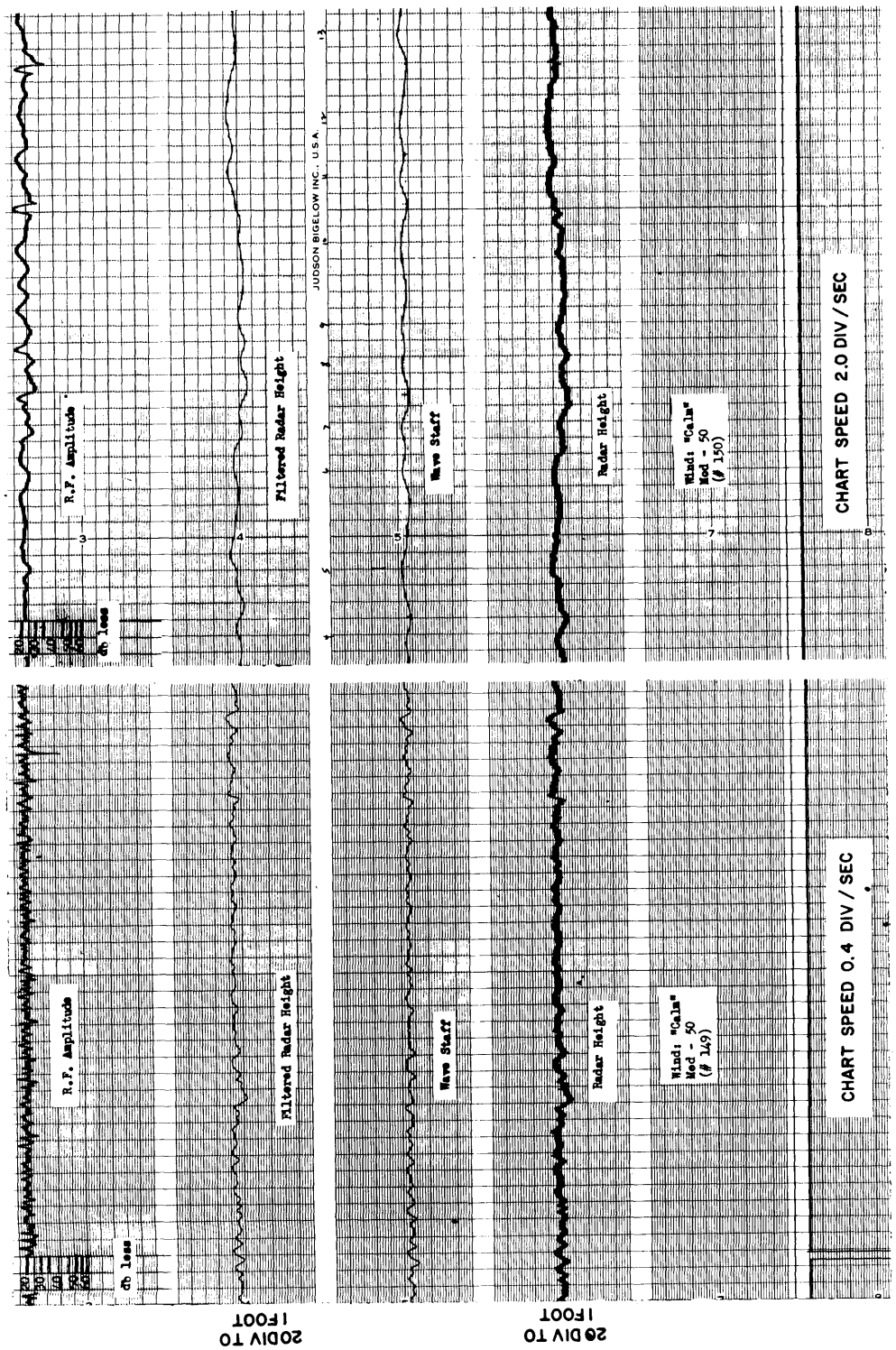

Fig. 69 - Examples of recordings made with all wave-trace amplitudes matched, under dead calm conditions with winds too light to spin the anemometer, with low relatively long waves present, and illustrating the very low radar noise level and near absence of deep fading typical of such situations

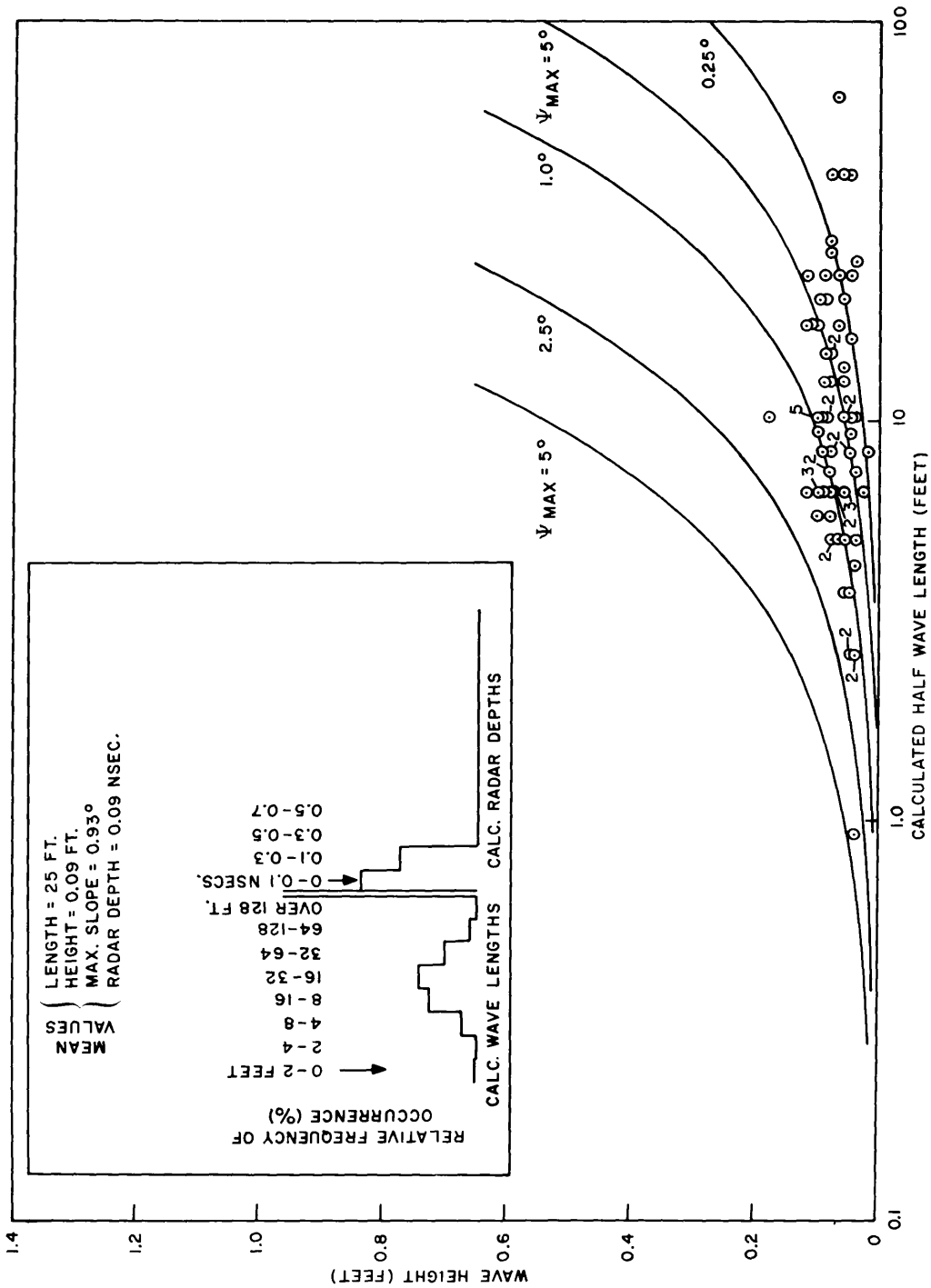

Fig. 70 - Histograms of calculated wavelength and calculated radar depth, and a plot of height-length relationships for a section of the wave staff record sampled in Fig. 69, with contours of maximum slope of a sinusoidal wave superimposed on the height-length plot

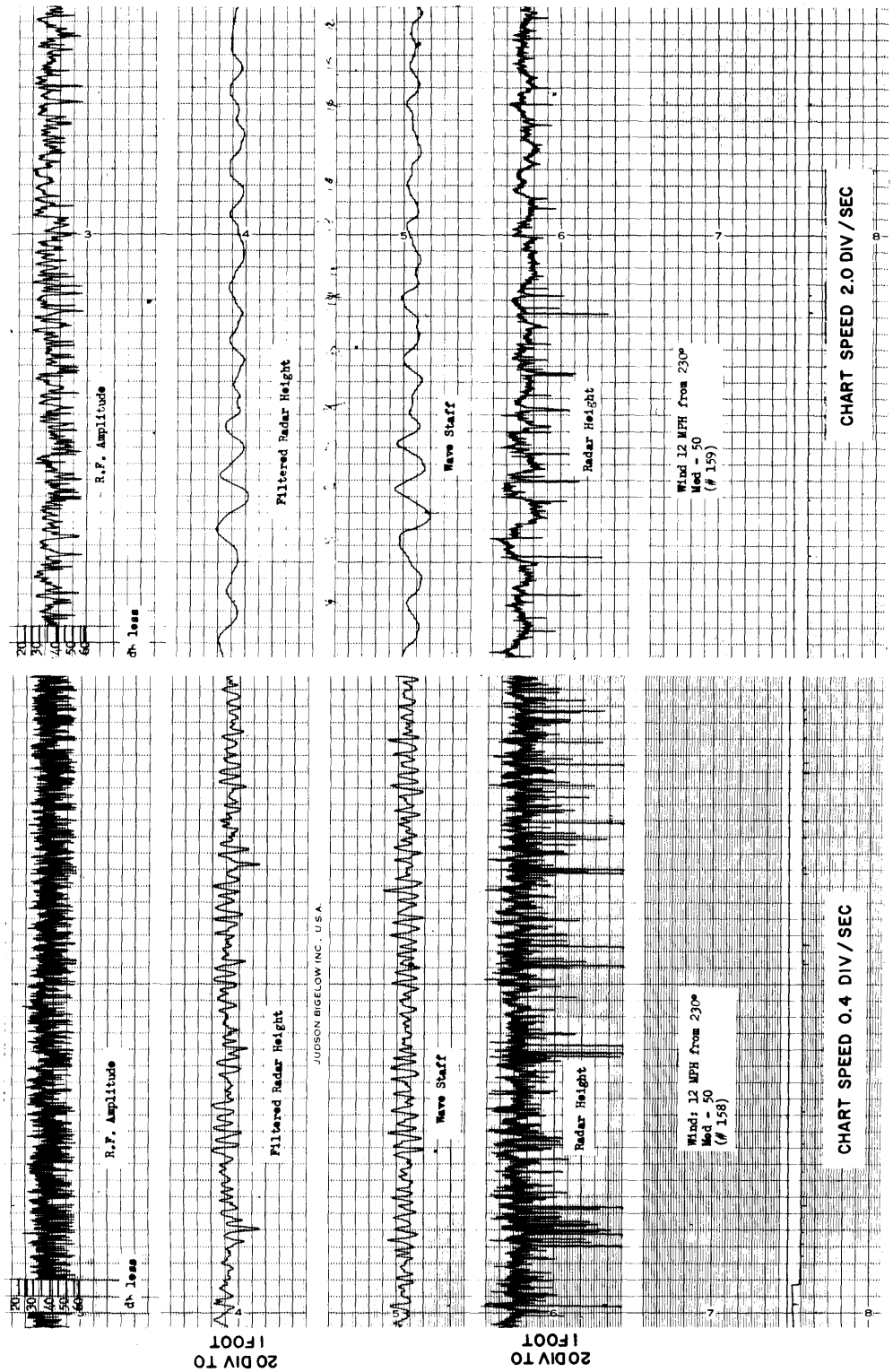

Fig. 71 - Examples of recordings made with all wave-trace amplitudes matched, under conditions of moderate winds with many waves too short to be resolved, and illustrating a typical radar noise pattern

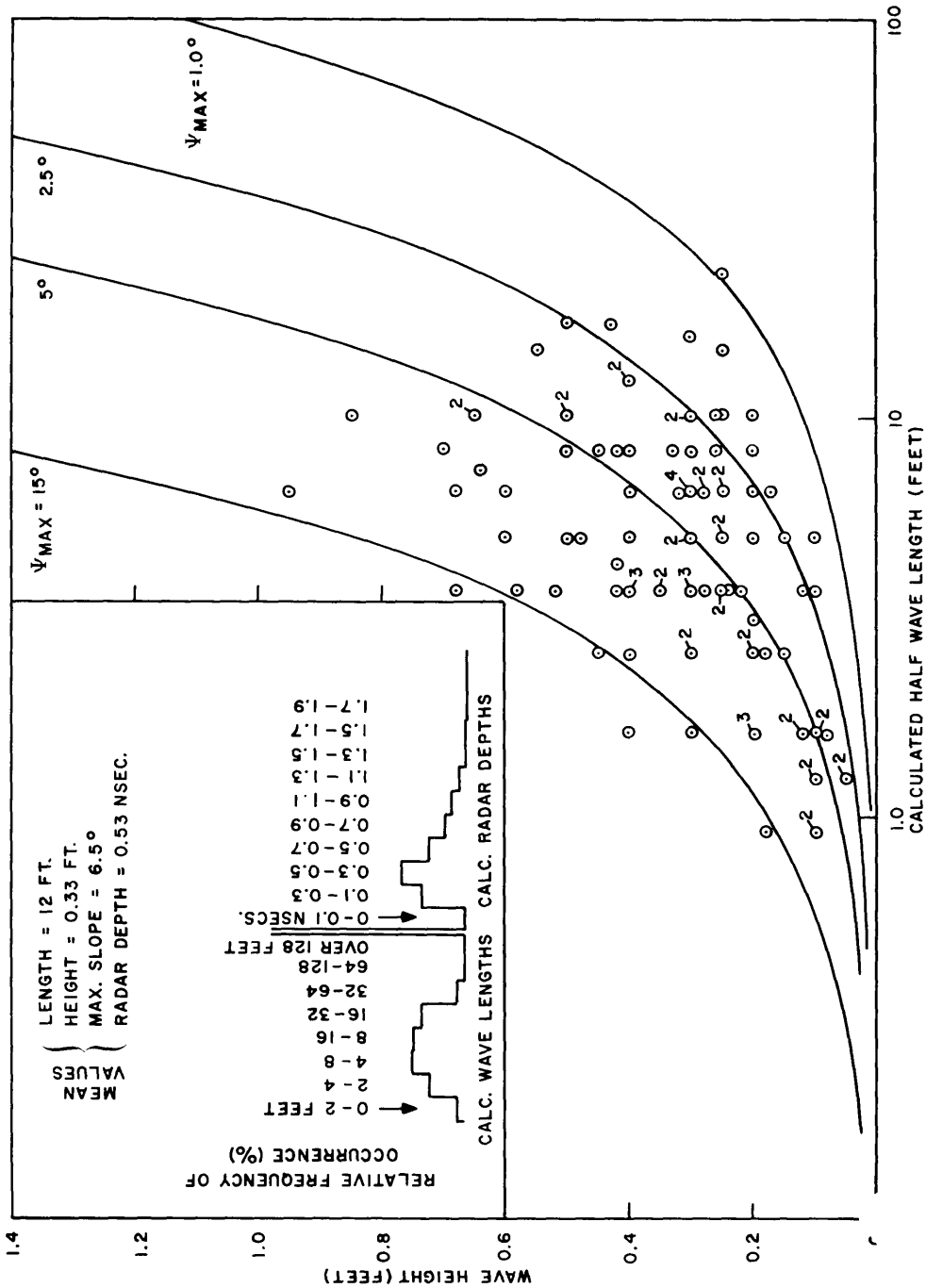

Fig. 72 - Histograms of calculated wavelength and calculated radar depths, and a plot of height-length relationships for a section of the wave staff record sampled in Fig. 71, with contours of maximum slope for a sinusoidal wave superimposed on the height-length plot

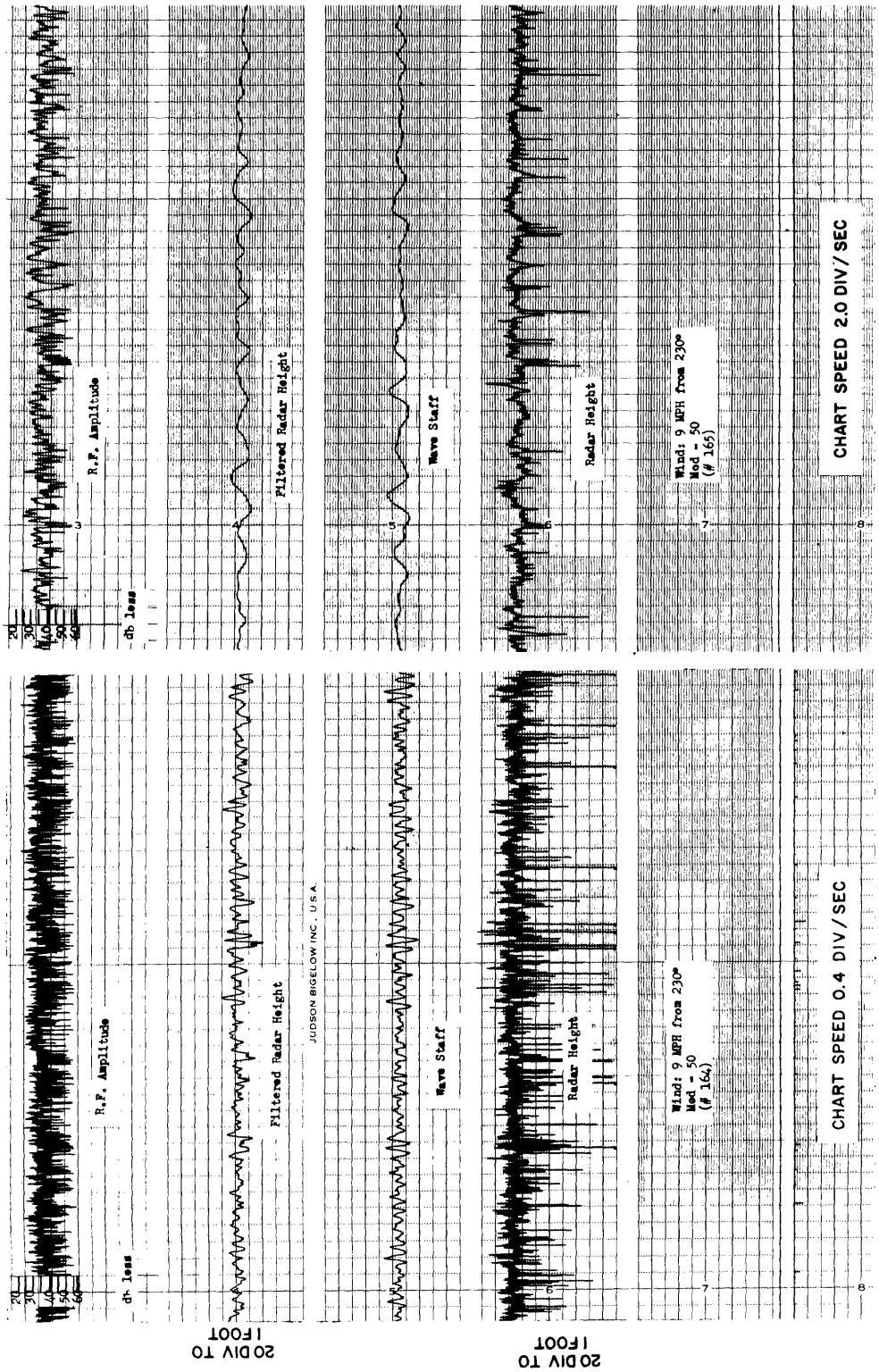

Fig. 73 - Examples of recordings made with all wave-trace amplitudes matched under conditions of light to moderate winds, with many waves too short to be resolved, and showing a radar noise pattern typical of this condition

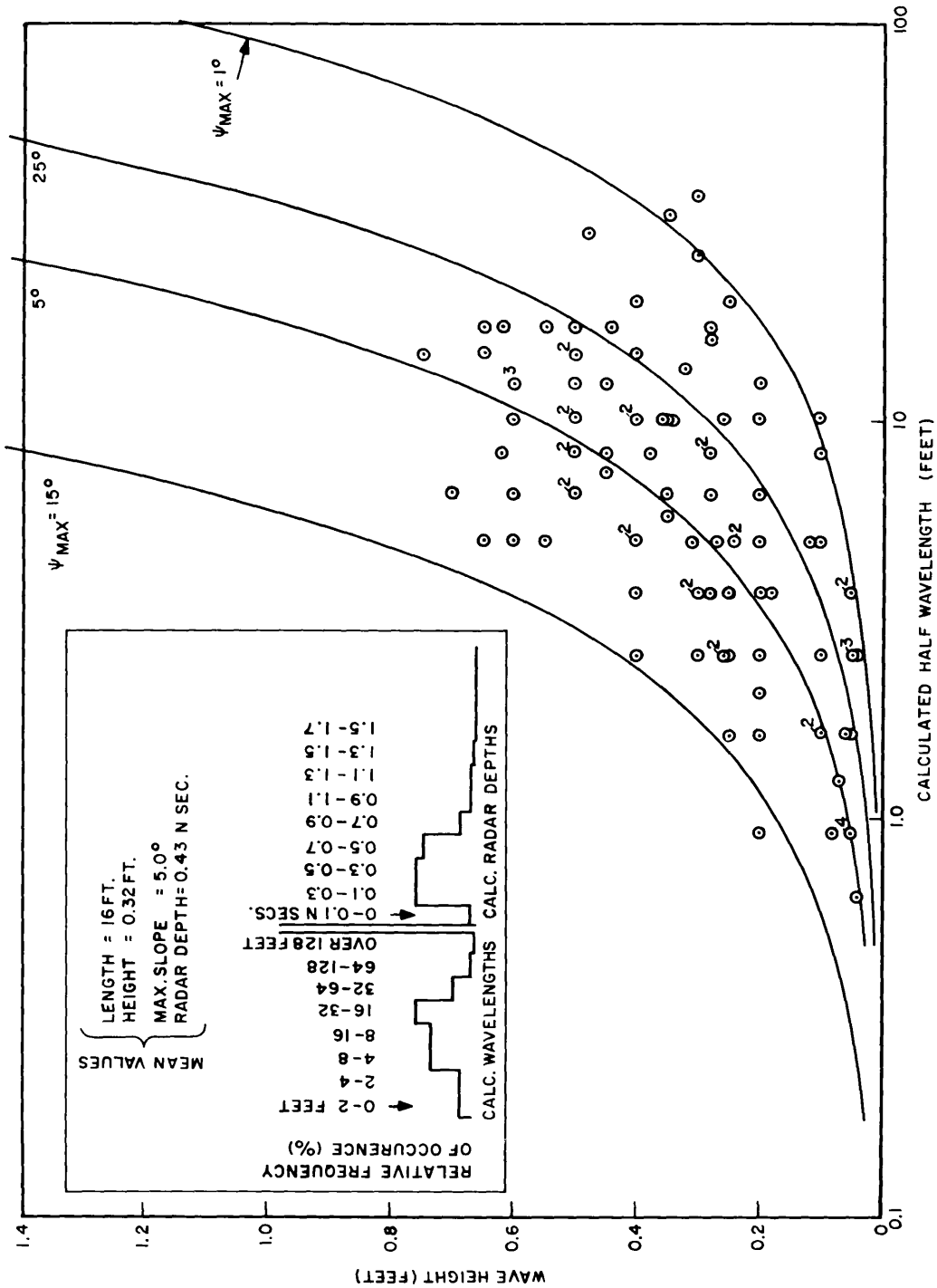

Fig. 74 - Histograms of calculated wavelengths and calculated radar depths and a plot of height-length relationships for a section of the wave-staff record sampled in Fig. 73, with contours of maximum slope for a sinusoidal wave superimposed on the height-length plot

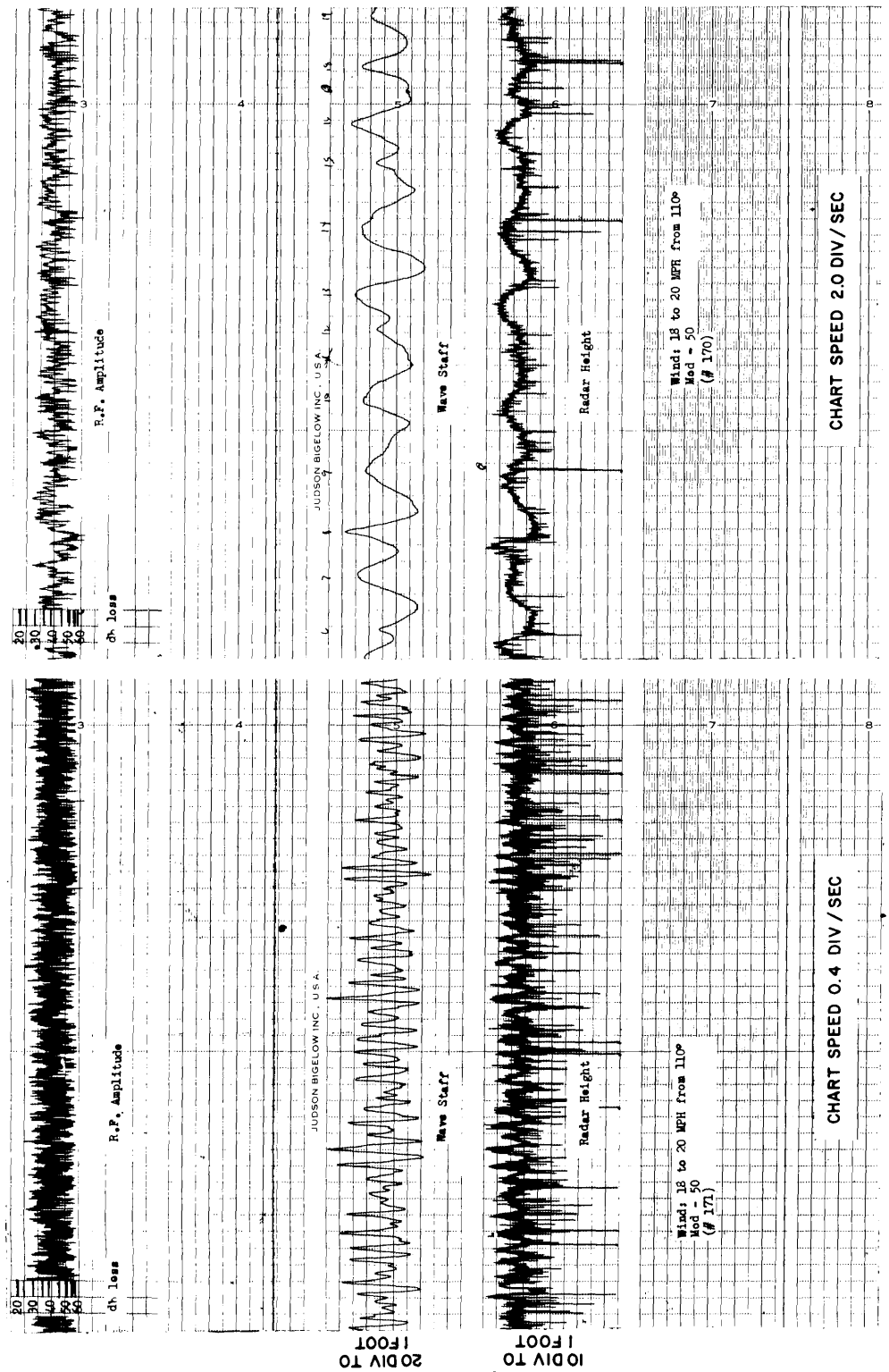

Fig. 75 - Example of recordings made with unfiltered radar trace half amplitude, under conditions of relatively high winds and relatively high waves, and showing an absolute level of radar-range noise somewhat higher than usually seen under moderate conditions. (Operating conditions were abnormal on this date in that the "Filtered Radar" channel was inoperative, and the wave staff was frequently blown out of position, so that the radar and wave-staff traces cannot be expected to correlate exactly.)

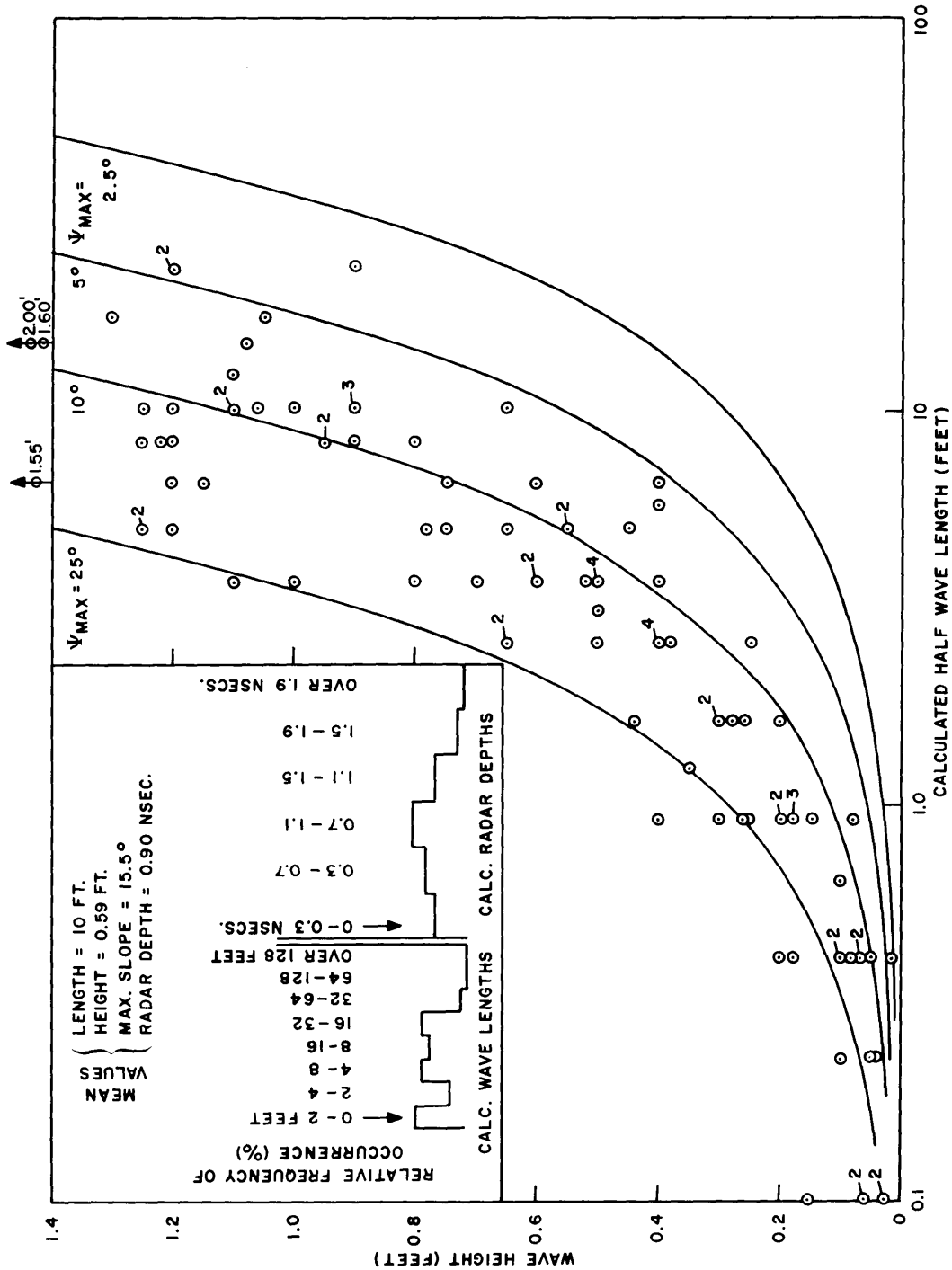

Fig. 76 - Histograms of calculated wavelengths and calculated radar depths, and a plot of height-length relationships for a section of the wave staff record sampled in Fig. 75, with contours of maximum slope for a sinusoidal wave superimposed on the height-length plot

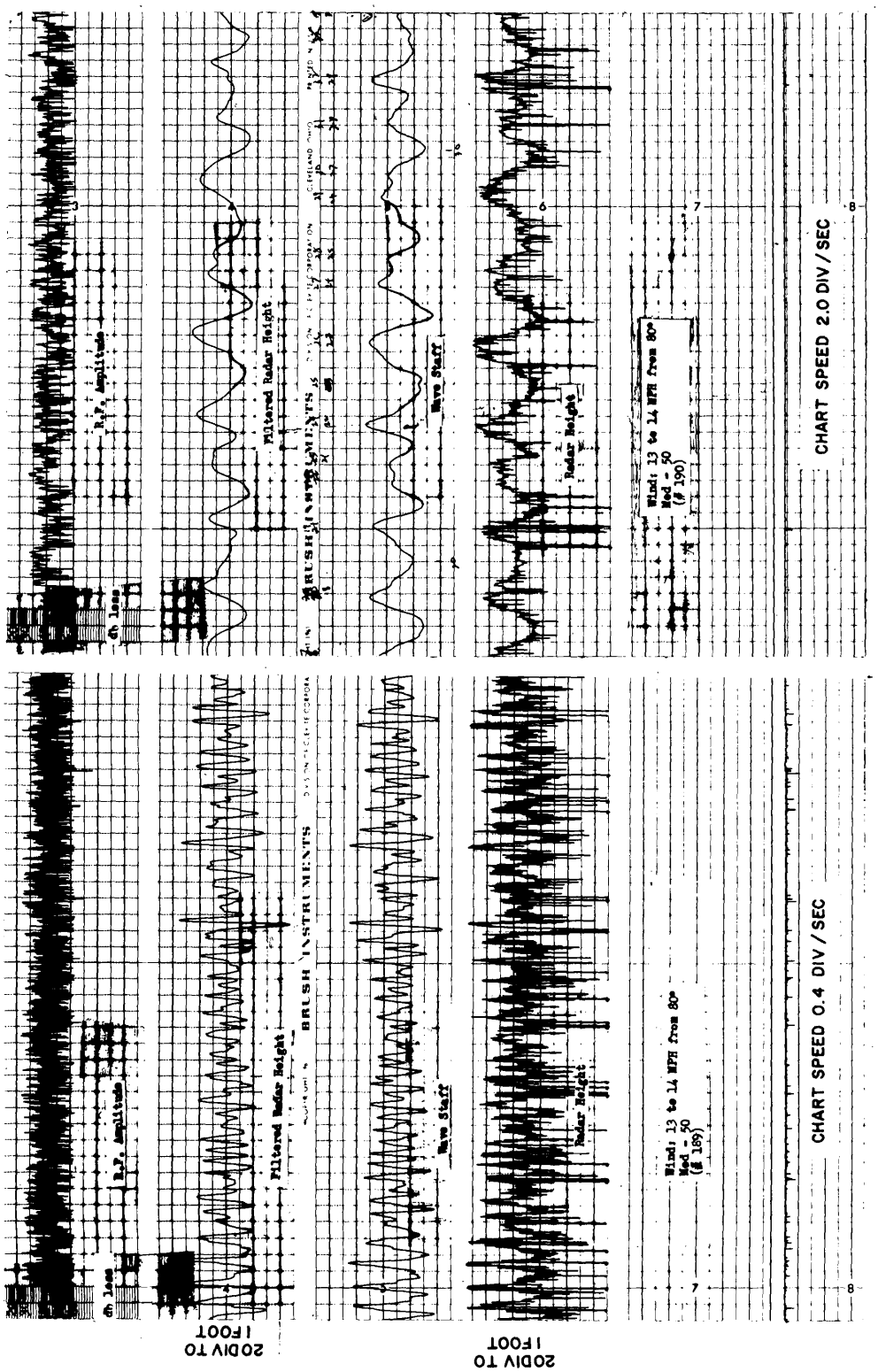

Fig. 77 - Example of recordings made with all wave-trace amplitudes matched under conditions of moderate winds and relatively high waves and showing good correlation between radar and wave-staff traces and a typical pattern of radar-range noise

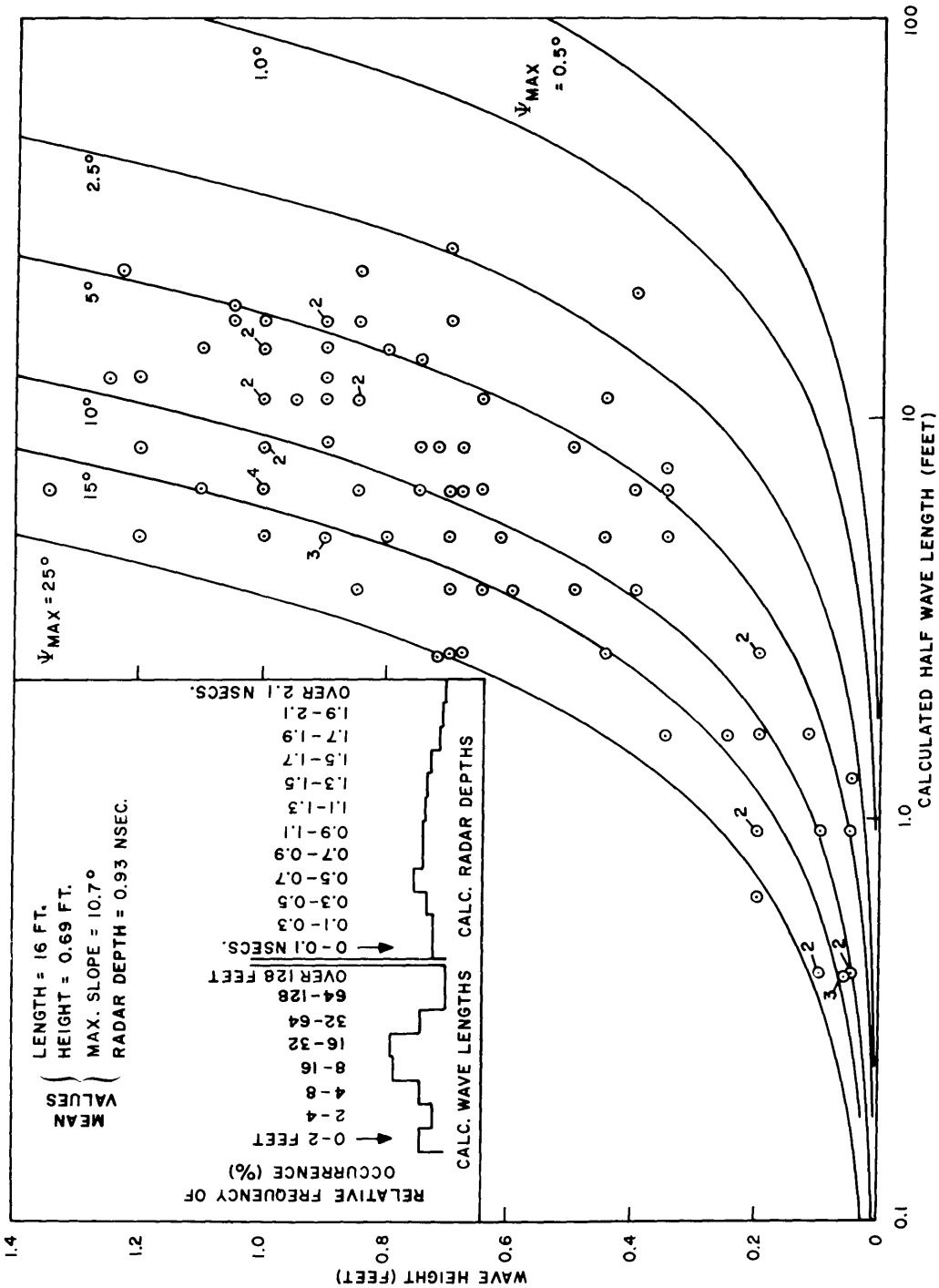

Fig. 78 - Histograms of calculated wavelengths and calculated radar depths, and a plot of height-length relationships for a section of the wave staff record sampled in Fig. 77, with contours of maximum slope for a sinusoidal wave superimposed on the height-length plot

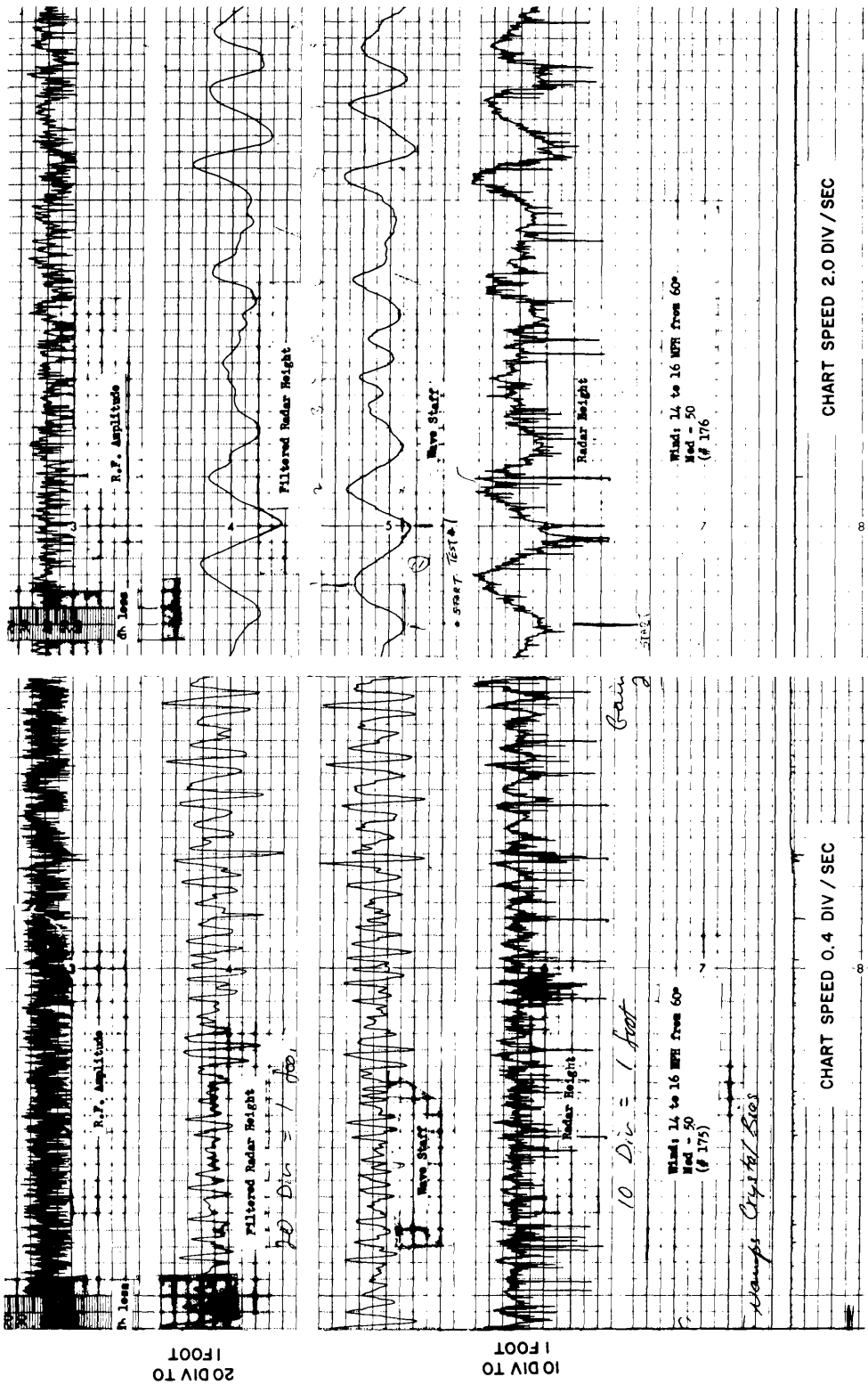

Fig. 79 - Examples of recordings made under conditions of moderate wind and relatively high waves using different indexes, and showing good correlation between radar and wave-staff traces at an index as low as 16.5, with the lowest radar noise typically observed at an index of 50

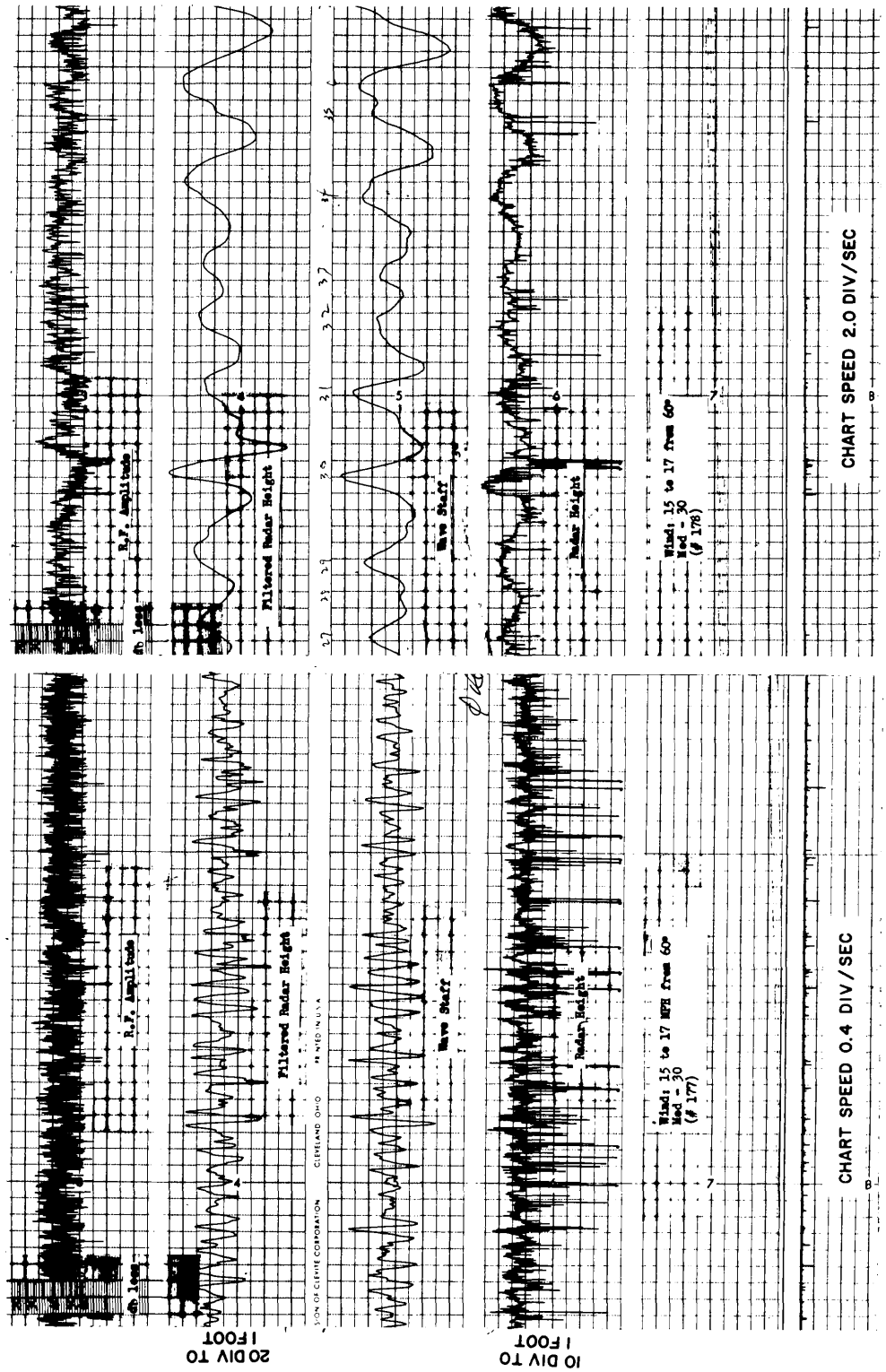

Fig. 79 (Cont'd) - Examples of recordings made under conditions of moderate wind and relatively high waves using different indexes, and showing good correlation between radar and wave-staff traces at an index as low as 16.5, with the lowest radar noise typically observed at an index of 50

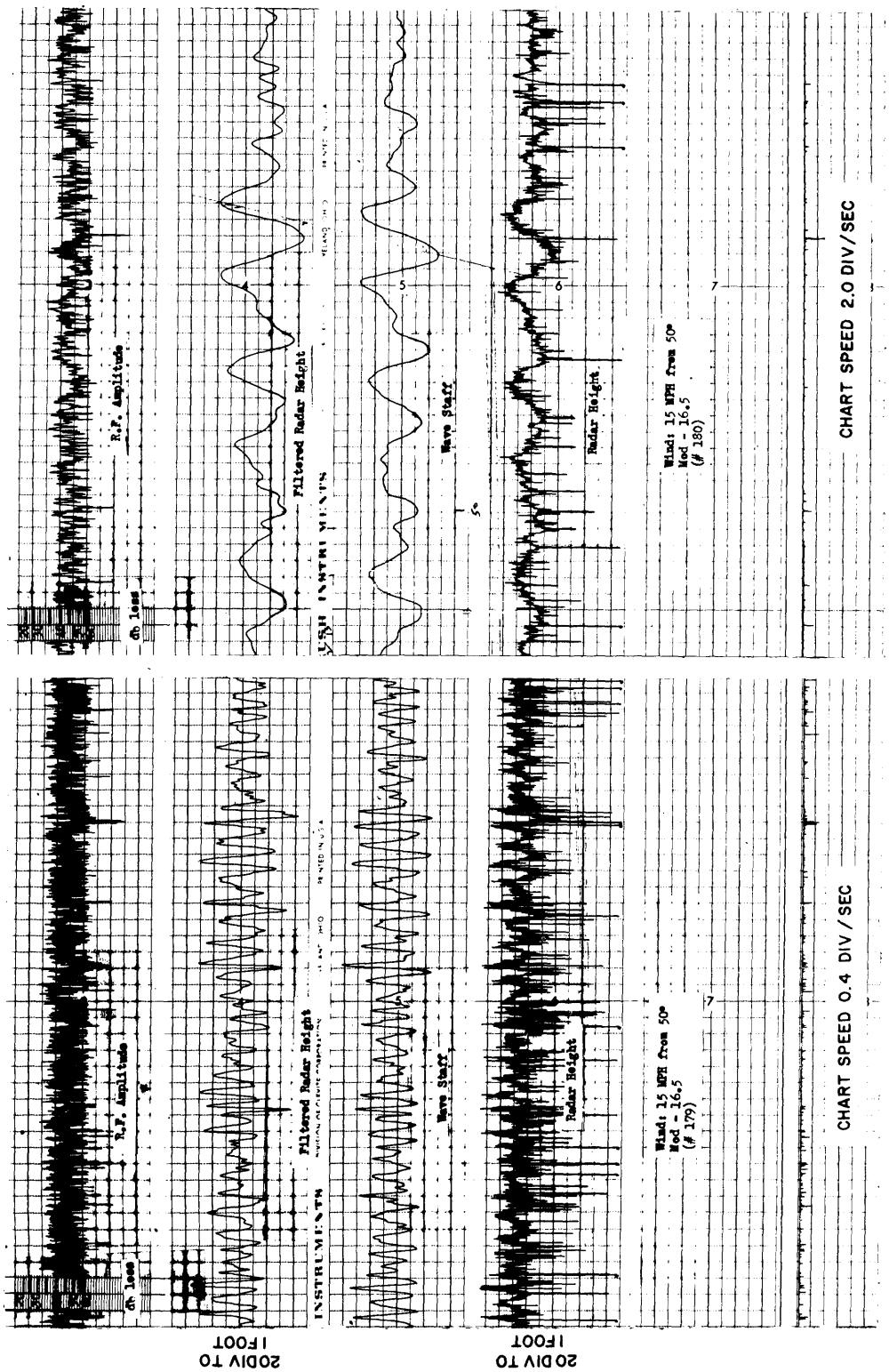

Fig. 79 (Cont'd) - Examples of recordings made under conditions of moderate wind and relatively high waves using different indexes, and showing good correlation between radar and wave-staff traces at an index as low as 16.5, with the lowest radar noise typically observed at an index of 50

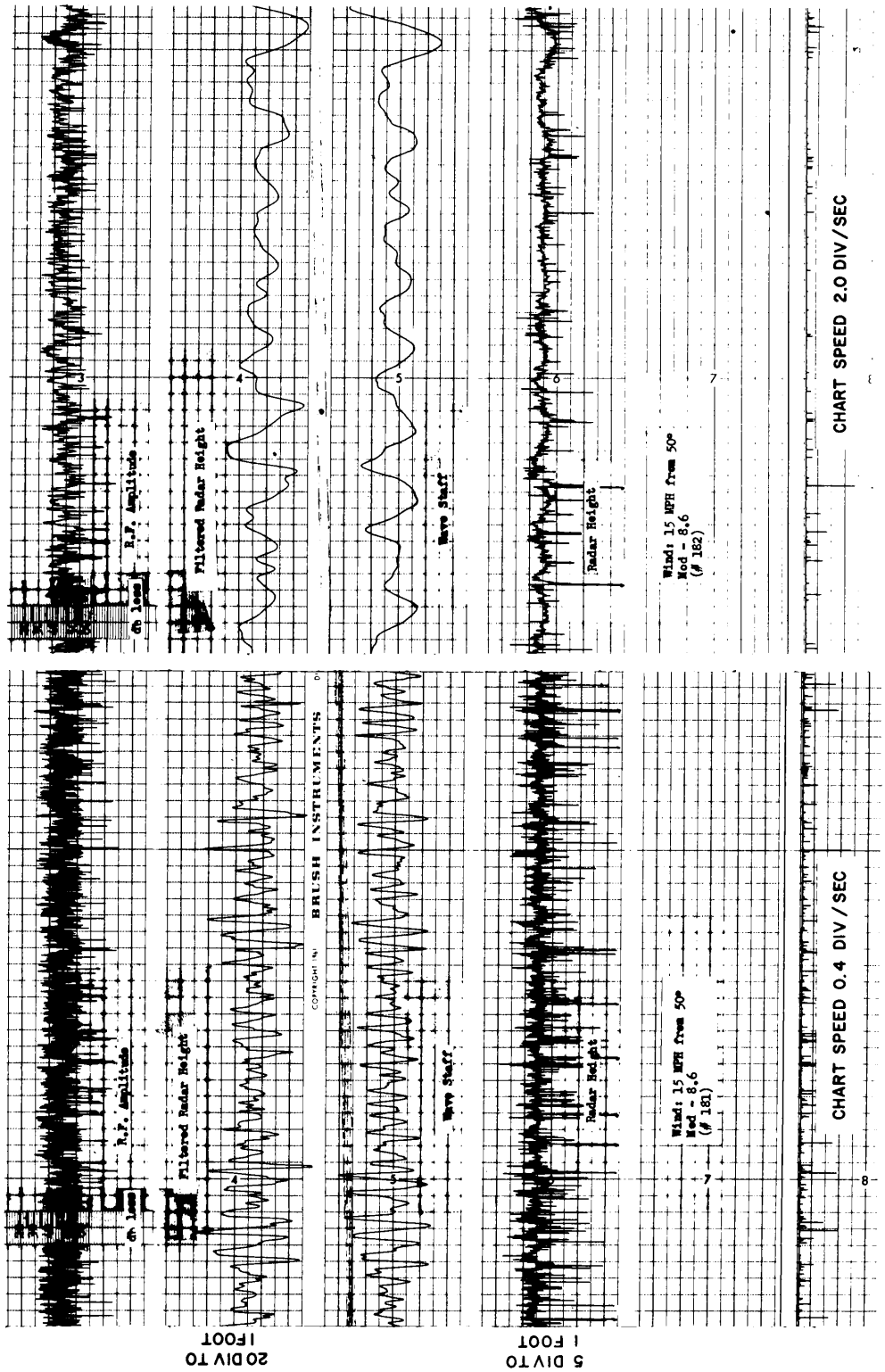

Fig. 79 (Cont'd) - Examples of recordings made under conditions of moderate wind and relatively high waves using different indexes, and showing good correlation between radar and wave-staff traces at an index as low as 16.5, with the lowest radar noise typically observed at an index of 50

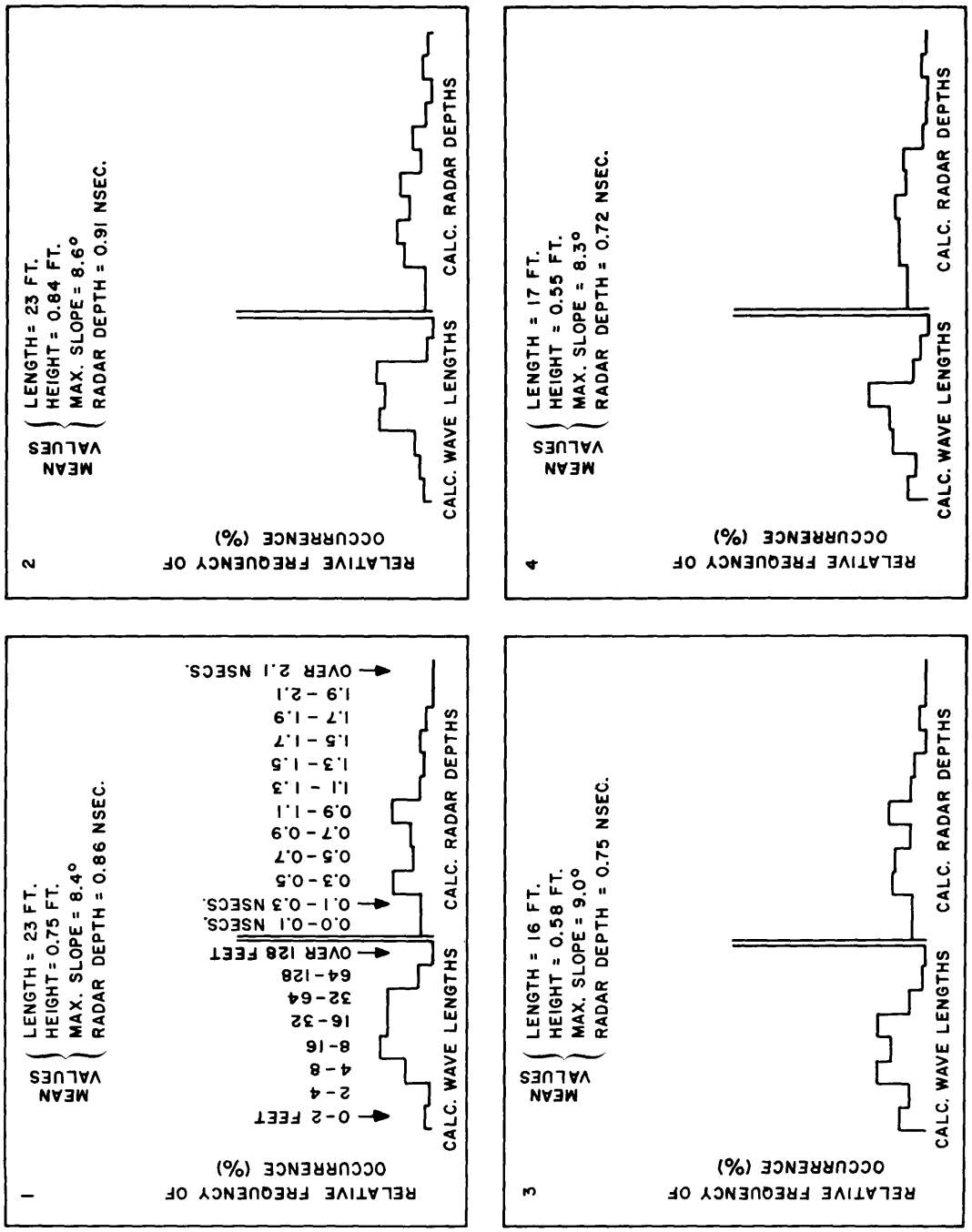

Fig. 80 - Histograms of calculated wavelengths and calculated radar depths taken from four sections of the wave-staff record sampled in Fig. 79

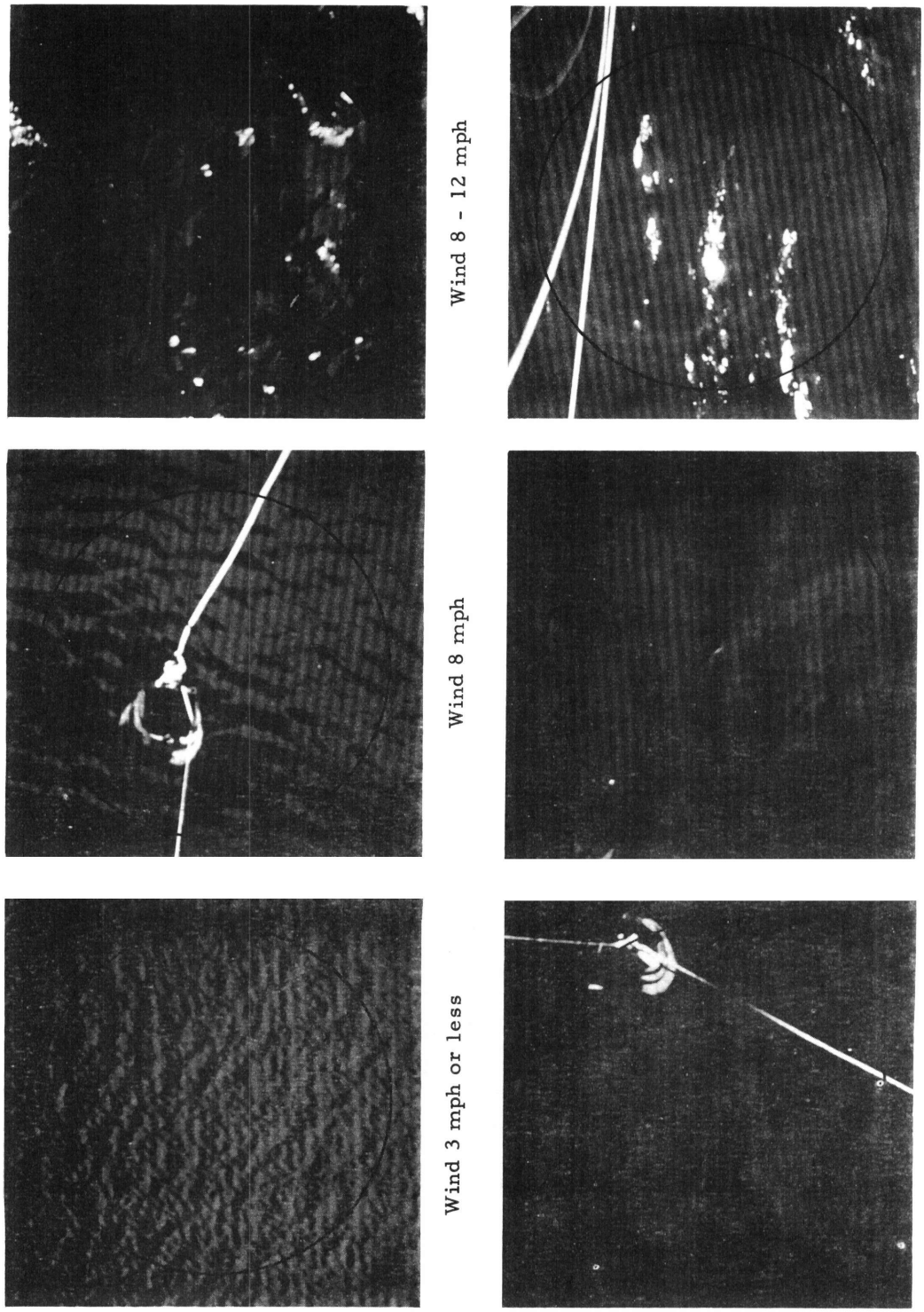

Fig. 81 - Photographs of the water surface looking vertically downward with overlays showing the size of the circles of half-power radar illumination

with frequency and a slight nonlinearity of the frequency versus electrode-voltage characteristic. In addition, there was some nonlinearity in the modulator at the highest deviations used. The amplitude modulation generated by the BWO was estimated to be less than 10 percent at maximum deviation. The harmonic distortion in the modulator was mostly second harmonic and was about 5 percent at the maximum deviation and much smaller at all lower deviations. Discriminator unbalance was not measured precisely for the Bay Bridge components, but later measurements have led to the estimate that detector outputs probably differed by no more than 10 percent.

In view of the selection of the fundamental frequency component of the modulation by bandpass postdetection amplifiers, it is difficult to see why small percentages of harmonic modulation would alter the result. Bench tests with the multipath simulator showed no significant changes when modulator harmonics were suppressed by a filter, and it therefore seems safe to conclude that this effect was not significant in the field.

It is not so obvious that residual AM is unimportant, and it was difficult to check this point experimentally by eliminating all significant amplitude effects. However, deliberately adding additional in-phase AM did not cause any marked increase in simulator range errors. It should be noted that while the AM introduced by the amplitude-frequency characteristic of the BWO may include harmonic terms, the fundamental term can have no quadrature component, and the total AM envelope must possess mirror symmetry about the zero-crossings of the FM envelope. This follows from the fact that the BWO characteristic has no appreciable "hysteresis." That is, essentially identical power outputs occur at a given electrode voltage, whether the frequency is being swept up or swept down at a given moment.

In order to explore AM effects further, the theoretical analysis was expanded to include the cases of both fundamental and second-harmonic AM of the mirror-symmetrical kinds. The results of these calculations showed that the amounts of AM which could have conceivably existed in the field system would have had no significant effect on the multipath range noise.

The question of discriminator unbalance was also checked theoretically. In this case it was found that unbalance caused the range errors for particular rf phase relationships to be slightly different, but that the overall limits of the error excursion did not change significantly for any amount of unbalance that could have existed.

The question of internal multipath effects and phase characteristics is perhaps the most difficult to resolve fully. At the time of the Bay Brdige experiments the role that internal characteristics could play was not fully appreciated, and not all of the microwave components used were completely evaluated experimentally. During work with the multipath simulator it was found that range errors generated by varying rf phase in a two-path simulation could be increased if the recombined signal was split again and subjected to a second two-path transmission, where the differential delay was appreciable but the rf phase relationship was fixed. Thus a sufficiently severe internal reflection or sufficiently high phase-versus-frequency slope could modify the range noise level generated by target scintillation, even though no time-varying changes occurred in the internal phase relationships. The generally good agreement obtained between theory and waveguide simulator results show that these effects must be small when standard components of good quality are assembled with ordinary care. The items used at the Bay Bridge were of similar quality but were not individually identifed in the case of all waveguide bends and straight sections, and in the case of all of the coaxial cables used to interconnect the traveling-wave tubes. The coaxial cables were later found to be the poorest and most variable components from the standpoint of VSWR, and the Bay Bridge radar may have been somewhat poorer than the waveguide simulator from the standpoint of the level of internal reflections. However, even the poorest of the components

measured could not ordinarily have accounted for an appreciable modification of the results by this mechanism. Thus it would have required some unusual combination of circumstances to make internal multipath phenomena significant at the Bay Bridge.

The best conclusion that can be reached at the present time is that the Bay Bridge FM-CWradar did not depart from the theoretical assumptions in any experimentally significant way.

Explanation of the Observed Range Noise in Terms of the Two-path FM-CW Theory

The various ways in which target scintillation-range noise may arise have been touched on elsewhere in this report. They may be summarized briefly as follows.

In the first place, the desired signal may fade due to scintillation to the point where the receiver output is affected by signal arriving over a weak stray path. The stray path may not involve the target at all, or it may involve the target and some other reflecting or scattering structure. Stray paths are evidently a practical limitation rather than an unavoidable theoretical one, but in view of the wide ranges of fading which have been observed the limitation may be a very real one. Secondly, the depth of the target in range may be exaggerated during multipath cancellations to produce range offsets larger than the physical extent of target. This effect is unavoidable, since the illuminated patch in the wave-profiling application always has appreciable depth, and the system must therefore be designed to keep range errors generated in this way within acceptable limits. In the third place, multiple scattering or reflection within the illuminated patch may create signal paths having greater delays than those represented by the target depth in range. In the most likely case involving a sequence of only two reflections or scatterings, an upper limit would be placed on these delays by the effective diameter of the patch.

The application of the idealized two-path theory to the real target case must obviously be made with the realization that the physical situation is in general vastly more complex. However, the theory appears to offer a useful insight into real target behavior in spite of the simplification that it represents. The following reasoning has been used. The sort of amplitude scintillation observed indicates that the illuminated patch on the water behaves as though it were composed either of a relatively small number of randomly phased scatterers or of a more or less uniformly illuminated sheet distorted in depth by the wave motion. The target never behaves as though it were composed of a very large number of randomly phased scatterers, even though the capillary-wave structure creates such a large number of potential points of reflection within the illuminated patch. Given this observed behavior of the target, it would not appear extremely improbable for the reflected signal to reduce to a two-path situation occasionally. Thus, any type of range error which was permitted by the two-path theory would be expected to occur at times, and the fact that it never occurred could be taken as evidence that the assumed path delays or amplitude ratios were not physically possible.

In the case of multiple paths, each involving a single reflection at the target, it seems likely that the two-path theory applied for the various possible physical depths would yield the worst possible range errors. Here, the addition of other paths having intermediate delays to a basic two-path configuration would be expected to reduce rather than exaggerate the error. In the case of the multiple reflection or scattering mechanism which has been suggested, another degree of complexity exists, and application of the two-path constraints is probably not as well justified. On the other hand, where definite stray paths involving measurable physical distances are involved, application of the two-path theory seems quite straightforward.

Proceeding to consideration of specific features of the Bay Bridge data, reference will be made to a number of the figures in the section on two-path theory. As discussed in this section, the parameters involved are the differential range delay, the amplitude ration and the modulation index of the FM-CW radar. Since the modulation frequency was always the same (2.215 Mc/sec), specification of the index amounts to specification of the frequency deviation, which is actually the more fundamental parameter. The specific values of modulation index used in the selected figures are identical to those used in the field, within the limits of experimental accuracy.

The most serious range noise observed at the Bay Bridge took the form of increasing-range spikes which could have high amplitudes, and this phenomenon will be analyzed first. According to two-path theory, large increasing-range excursions may be produced in three basic ways. First, the physical depth of the target during a near cancellation of approximately equal signals may become exaggerated. Second, the desired signal may fade to a level close to that of an appreciably longer path having a differential delay at least comparable to the observed range delay error. Third, the desired signal may fade to the point where a still weaker but very much longer path having a delay many times the observed error can affect the receiver.

Referring to Fig. 9 and Figs. 82 through 86, it is seen that the range errors predicted for the first mechanism of near cancellation of strong signals do not fit the observed facts. In the first place, errors as large as those observed (over 8 nsec range delay) cannot be produced by any two-path combination involving a physically possible target depth and any amplitude ratio whatsoever. This is true at all of the modulation indexes used. In the second place, such errors as are predicted would have a comparable if not exactly equal probability of occurring in the decreasing-range direction, whereas the records show no upward spikes comparable to the large downward spikes under discussion. The largest value of the amplitude ratio, b, that is shown in this series of figures is 0.98, but the peak range delay reached by the out-of-phase, or $\theta = \pi$, envelope in this case is essentially the largest that can be produced. The range offset passes through zero and changes sign at b equal to 1.0. If this value is substituted into the equations, an offset of zero at zero target depth is calculated, and for finite target depths the out-of-phase envelope coincides with the in-phase envelope. The change of sign at b equal to 1.0 is apparently a discontinuity, however, so that when b differs from unity by any finite amount a maximum delay very nearly that seen in the figures at b equal to 0.98 becomes possible.

The reasoning concerning the second possible mechanism is somewhat more complex and goes as follows. We must first consider how a path delay of 8 nsec or more, representing a travel distance of about the same number of feet, could arise, keeping in mind that the signal level must be comparable to that of the total received signal during a fade. The propagation experiments with absorbing pads would seem to virtually rule out the existence of such a path involving the laboratory structure at a level this high, so that the only likely mechanism appears to be a multiple reflection at the water surface. In order to create a differential of eight or more feet, the signal would either have to be redirected at more than two points, or the path would have to involve points well outside the four-foot half-power circle of the illuminated patch. Both of these mechanisms would appear only to offer the possibility of a very weak signal, but they cannot be entirely ruled out on the basis of present knowledge. If we assume that the necessary long delay can exist, we must then examine the behavior of the two-path error versus the modulation index. Figure 12 and Figures 82 through 86 provide this information, and it can be seen that the theory predicts nearly equal errors at all of the modulation indexes in use. At first sight this appears to be in conflict with the observation that range errors of this sort become less probable as the index is increased. This conflict may be explained by recalling that these errors always occur during a deep fade and noting the observed fact that deep fades in themselves are less frequent when the higher indexes are in use.

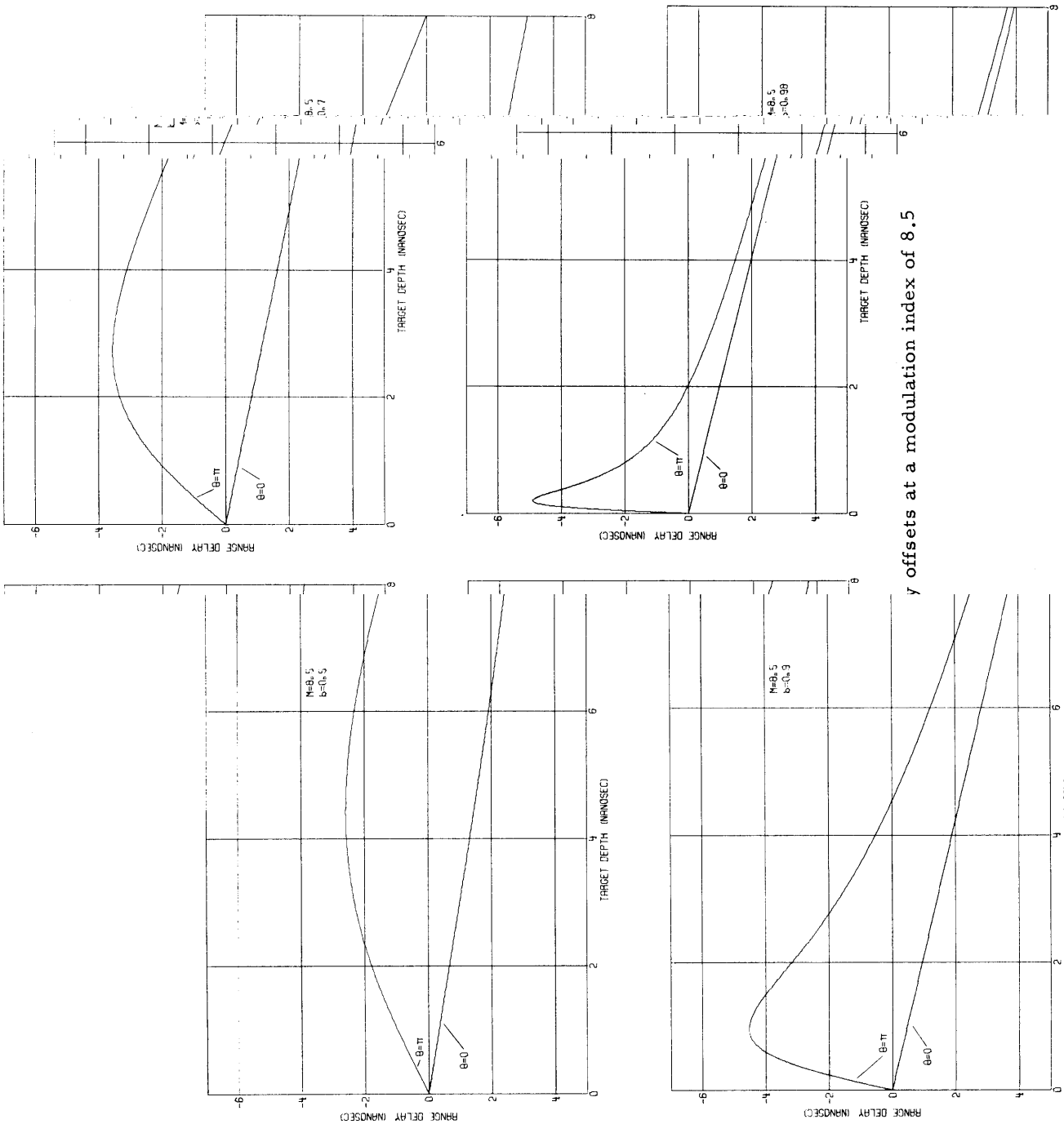

y offsets at a modulation index of 8.5

Fig. 82 - Two-path range-delay

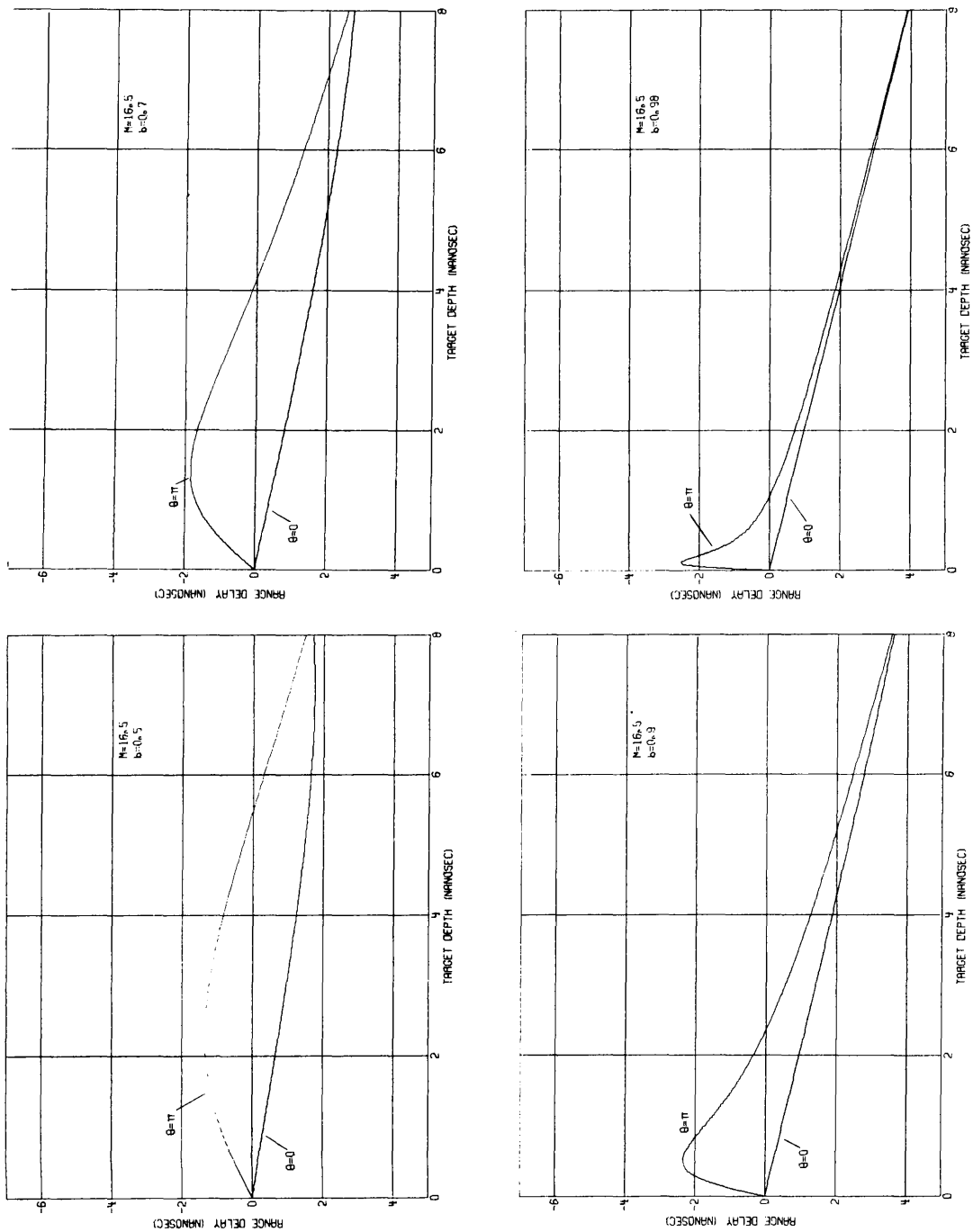

Fig. 83 - Two-path range-delay offsets at a modulation index of 16.5

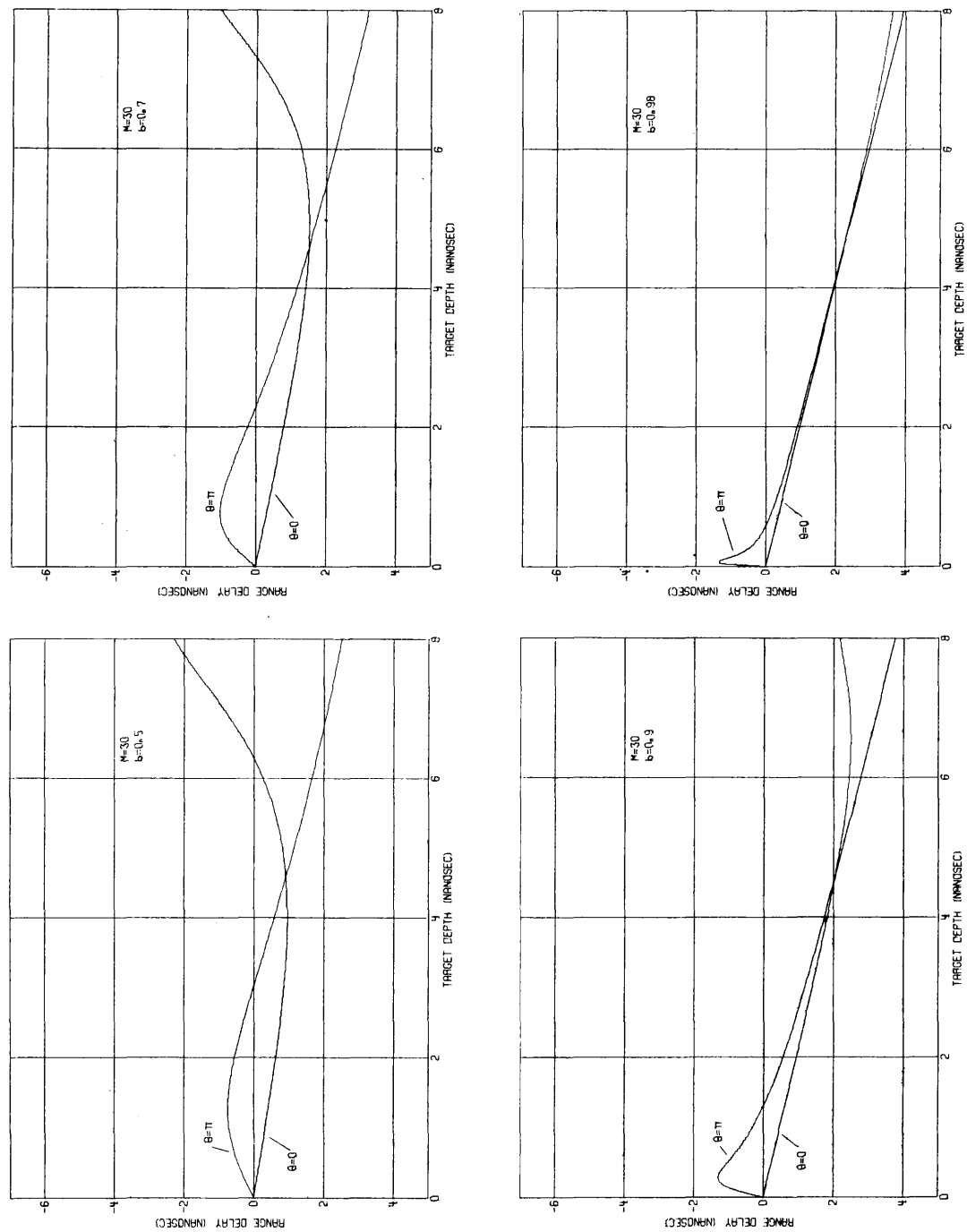

Fig. 84 - Two-path range-delay offsets at a modulation index of 30.0

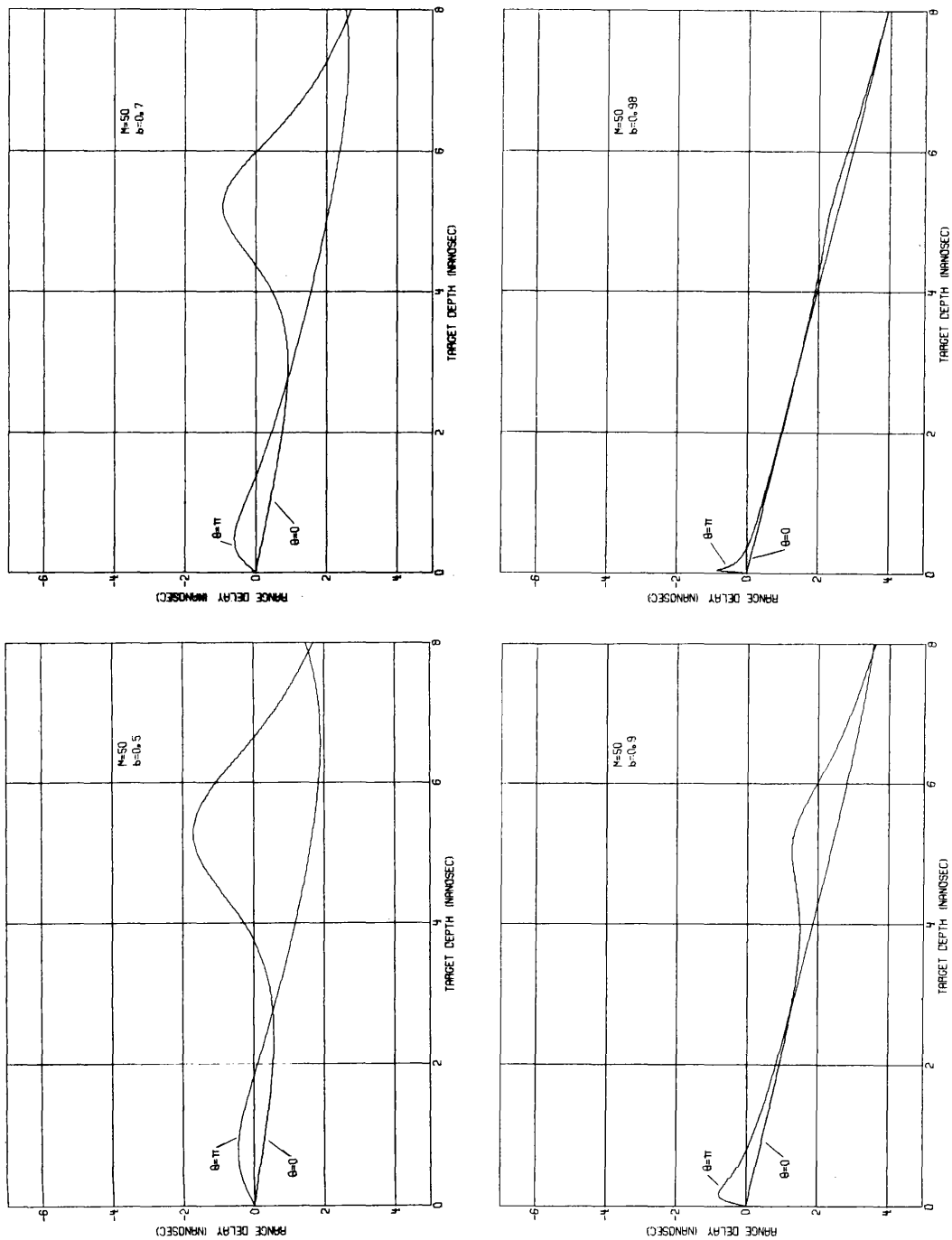

Fig. 85 - Two-path range-delay offsets at a modulation index of 50.0

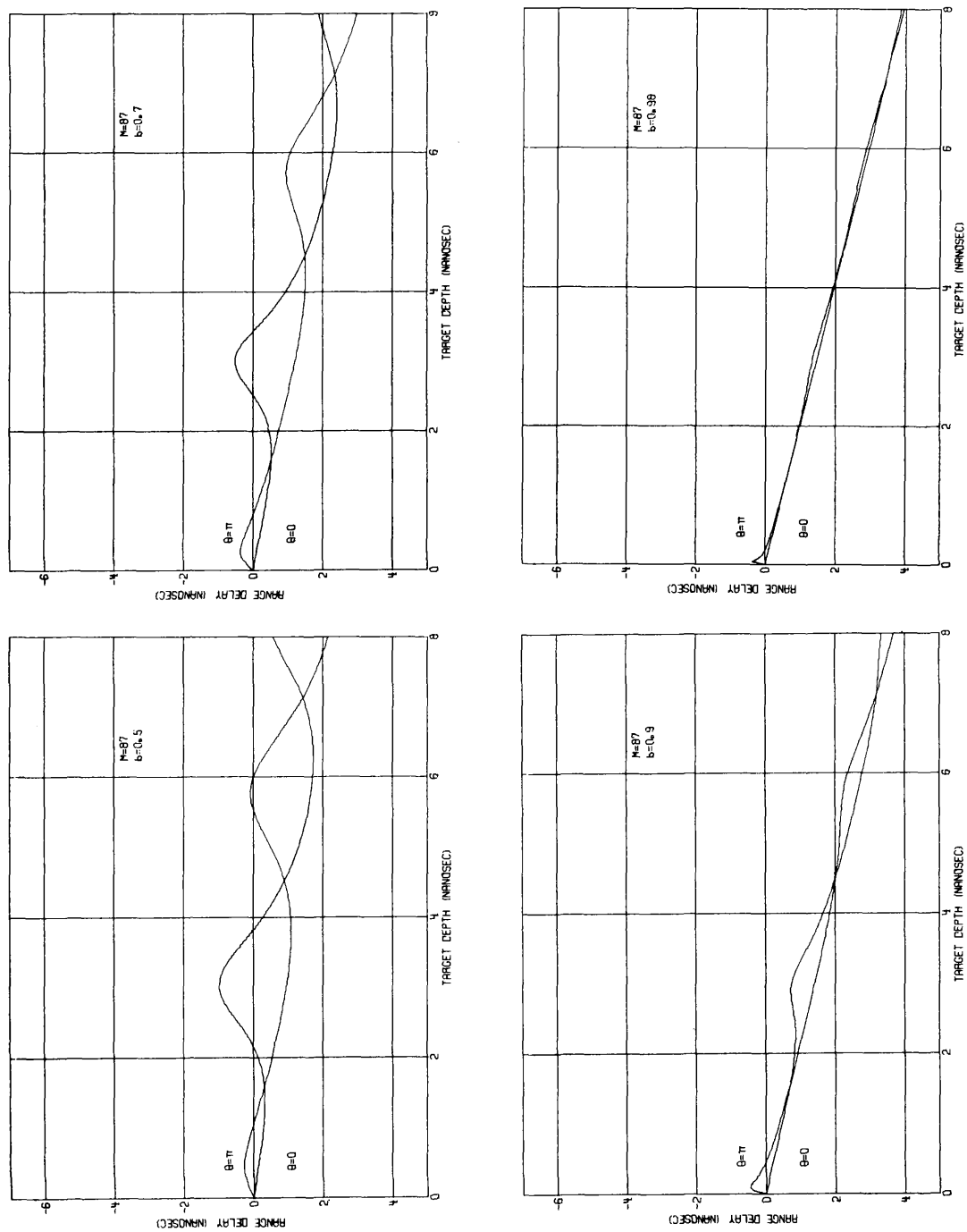

Fig. 86 - Two-path range-delay offsets at a modulation index of 87.0

However, there is another discrepancy which is difficult to account for and seems to be strong evidence that the large increasing-range errors do not arise from comparable path delays. As mentioned in the preceding discussion, it has been consistently observed that decreasing-range spikes have a very low rate of occurrence and are restricted to a low amplitude (a range of no more than 1.5 nsec) when operating with a modulation index near 50. This has been true under all wind and wave conditions. Referring to Fig. 85, we see that with an intermediate path differential of about 5.3 nsec a decreasing-range displacement of 1.8 nsec can occur. This maximum value is produced only at an amplitude ratio close to 0.5, but comparable errors occur over a range of ratios. We may note further that this maximum decreasing-range error is produced when the rf carriers are in phase, $\theta = 0$, so the signals involved are reinforcing each other. Additive signals may also produce increasing-range errors, but for an 8-nsec delay to produce an 8-nsec spike the desired signal must fade to a level somewhat below the level of the delayed path, or at least 6 db farther down than for a maximum decreasing-range error. Assuming that 8 nsec or greater delays can be produced, it seems virtually certain that smaller delays would be much more probable. We thus have a case of the sort postulated at the beginning of this discussion, where the errors permitted by two-path theory are in fact never observed. While one might not attach great significance to the difference between the predicted maximum of 1.8 nsec and the observed 1.5 nsec, the discrepancy between the expected rate of occurrence (greater than that for increasing-range spikes) and the observed rate (very much lower) seems to defy explanation. The most likely inference appears to be that significant signals with path differences of the order of 5.3 nsec virtually never occur, and, because the mechanism is assumed to be the same, significant signals having longer delays are also virtually prohibited. The conclusion to be drawn from these arguments is that the large increasing-range spikes that occur so consistently cannot be convincingly explained on the basis of our second hypothesis of secondary paths having delays comparable to the errors.

The remaining two-path hypothesis is that of a relatively weak signal arriving over a path having a relatively long delay. The possibility of one such path has already been discussed and the geometry illustrated in Fig. 48b. In this case the delay would be close to 125 nsec, representing nearly 90 degrees of phase shift at the modulating frequency. The range errors that are predicted by the two-path theory are shown in Fig. 87.

Note that although the range error falls to a relatively low value at some point on each of the envelopes, it is not generally possible to take advantage of this fact by choosing a critical modulation index. This is true because the location of the critical points is actually a function of a product involving both the path delay and the frequency deviation, which is in turn proportional to the modulation index at a given modulation frequency. This point was discussed in the section on theoretical analysis, and is illustrated by Fig. 9 of that section for the cases of shorter range delays. At the Bay Bridge, where the most likely long stray path evidently involved a reflection from the target area on the water surface, the path delay could have changed by more than enough to shift the long-path error from a minimum to a maximum. Only in the case of a very stable path involving structure alone could the range-error plots for a long delay be traced out experimentally by varying the modulation index. This was never possible at the Bay Bridge site.

Assuming that the maximum errors indicated in the figures can occur at any nearby index, it will be seen that the observed increasing-range offsets can be accounted for if it is postulated that the desired signal fades to a level about 10 db above that of the stray path (an amplitude ratio of about 0.3). There is also a downward trend in the error for a given ratio as the modulation index is increased, although it is not as pronounced as the trend in the experimental data. The tendency for the rate of occurrence of deep fades to decrease at the higher indexes could account for the greater observed

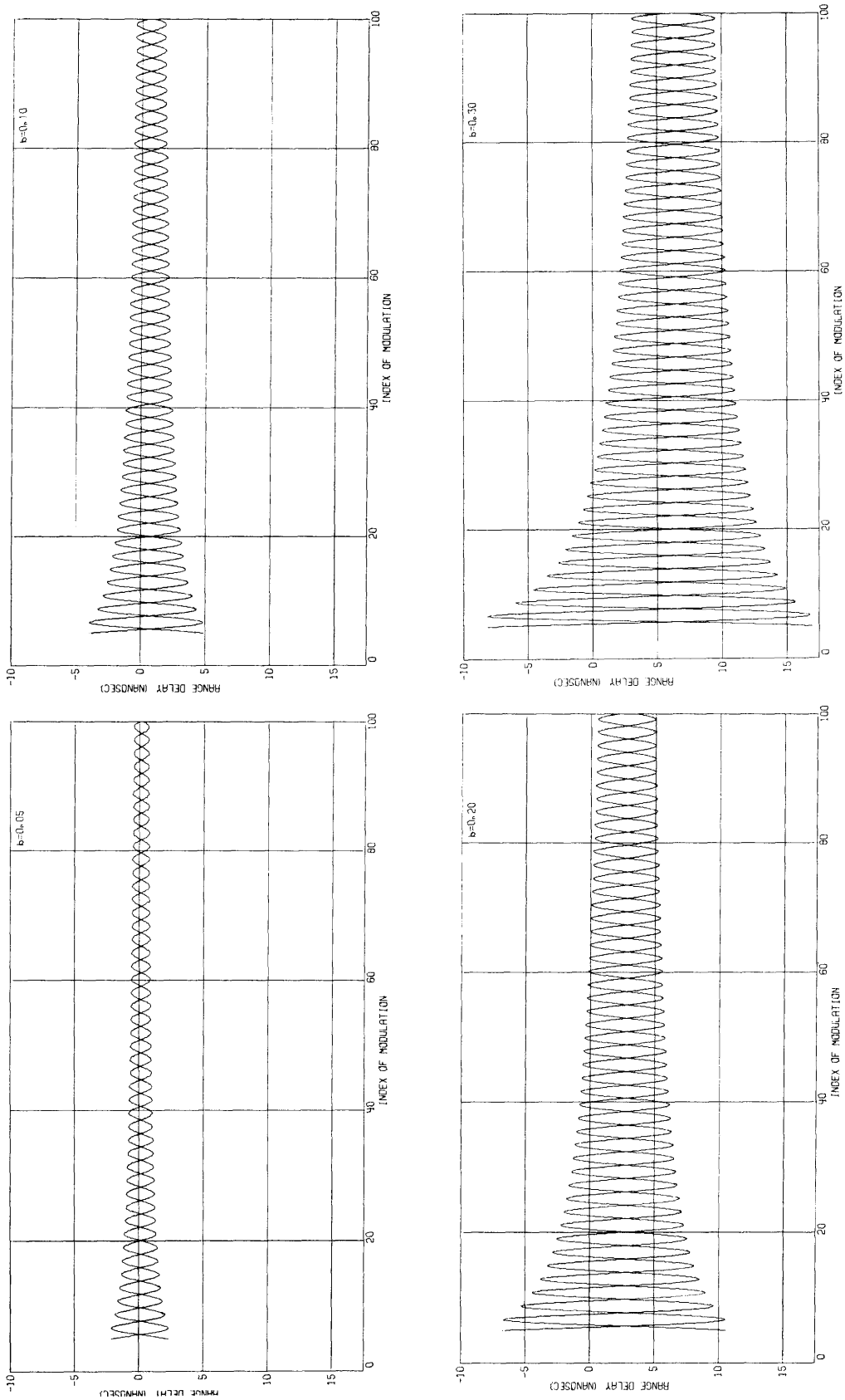

Fig. 87 - Range-delay offsets for a long stray propagation path, introducing a delay of 125 nsec

noise reduction. This hypothesis is not in conflict with the observation of small and infrequent decreasing-range errors at an index near 50, since no long path amplitude ratio can produce such errors in excess of about 0.8 nsec, and these occur over a more restricted range of amplitude and rf phase relationships than do larger increasing-range errors. We are thus led to the conclusion that the large increasing-range errors which often represented a substantial part of the total range noise were very probably caused by a long stray propagation path.

The possibility of a stray-path signal such as that assumed here was considered at the time that data were being taken at the Bay Bridge, but short of covering a substantial part of the underside of the laboratory with absorbing material no effective remedy could be conceived. The feasibility of doing this was considered, but in view of the difficulty involved and the limited time available it was eventually decided not to attempt the treatment. As mentioned earlier, an airborne wave-profiling system would be expected to suffer to a much smaller and perhaps a negligible extent from the contributions of stray paths of this sort.

Another very consistent experimental observation was the appearance of frequent, fairly large (2 to 3 nsec) decreasing-range spikes when the modulation index was increased from 50 to the vicinity of 87. The effect was observed under all radar operating conditions and all wind and wave conditions throughout the entire exercise. Upon reviewing the two-path range-delay curves, in Figs. 12 and 13 we find that only for a shorter secondary stray path, which would change the sign of the amplitude ratio b and give range delays of sign opposite to those plotted, does the theory predict decreasing-range errors of the magnitude observed. However, it seems impossible for a path shorter than the desired range by only 2 or 3 nsec to have existed during all of the wave conditions under which the effect occurred. When much shorter paths, having correspondingly greater delay differences relative to the desired signal path, are considered, the predicted trend of the range errors versus the modulation index does not fit the experimental facts. For such paths as might be conceivably be introduced by direct leakage between antennas or reflections from gondola structure, the differential delays are so large that the range-error curves would have numerous maxima and minima, similar to those seen in Fig. 87 for a delay of 125 nsec. In these cases the maximum possible range error would vary only slightly as the index changed from 50 to higher values, and this would be true even for the 10 to 12 nsec shorter differential that would exist for a reflection from wave-staff hardware.

After examining the range-delay curves for 2 to 4 nsec longer path differentials, such as could be produced by a horizontal skip, we find that the trend of the range delay versus modulation index does follow that observed. At an index of 50 for delays between 1.8 and 3.7 nsec, no decreasing-range errors are possible, and only an error of about 0.5 nsec can be generated by smaller delays. At an index of 87, on the other hand, decreasing-range errors are possible over this same range of delays. The maximum error occurs for an in-phase or additive condition and an amplitude ratio of about 0.5, with the longer path the weaker. Since it is observed that the signal commonly fades to a path loss of 45 to 50 db when maximum decreasing-range errors are produced, the mechanism discussed does not seem highly improbable. The fact that signal addition rather than cancellation is involved would increase the likelihood that the resultant would be strong enough to override the desired signal.

The reasoning just given shows that the trend of decreasing-range errors versus modulation index can be predicted on the basis of two-path theory and a not unlikely physical mechanism. The magnitude of the predicted error, however, falls short of the observed value by a factor of about 3 to 1. The maximum predicted error is just about 1 nsec, while errors of over 3 nsec are observed, although values of 2 to 2.5 nsec are more likely. Errors of over 3.5 nsec appear to be either impossible or highly

improbable, so that there is an effective upper bound on the magnitude of the larger observed error just as there is on the smaller computed error.

Since the index of 87 represented the maximum that was used, it is reasonable to ask whether or not errors were being generated or exaggerated in the microwave components of the radar. In an attempt to answer this question the microwave multipath simulator was set up using the same modulator and essentially the same TWT and rf discriminator lineup that was used during one series of exercises at the Bay Bridge. However, no decreasing-range errors of the magnitude observed could be produced at a modulation index of 87 by any two-path simulation. No peculiar behavior was observed as the index was increased from 50 to 87, and the results agreed closely with the two-path theory. Thus, all the evidence available indicates that the effect is a valid experimental finding.

In an attempt to explain more fully the experimental results, equations were set up for a limited number of three-path cases. Since the primary fading mechanism seems to be one of interference, it is not unlikely that the residual signal from a cancellation of two strong paths would be combined with a third delayed weaker path. Errors were calculated following this assumption, using both small delays of the order of magnitude of the target depth and intermediate delays of the order of magnitude of the patch diameter. The range-delay errors that result in the cases of some specific three-path configurations have been shown in Figs. 19, 20, and 21 of the theoretical discussion. These figures are plotted according to the same format as Fig. 9, which illustrates the two-path case. The trends of the errors are similar in many instances for the three-path and two-path cases, and the maximum decreasing-range error is virtually the same except in the plots of Fig. 20. In this case, one of the three paths was assumed to be slightly shorter than the desired range and another slightly longer. In the Bay Bridge situation it seems impossible to account for the existence of a shorter path having the required differential of about 3 nsec, and the experimental data have thus not been fully explained up to the present time.

At the lower modulation indexes used, all of the observed range errors fall within the range of magnitudes allowed by two-path theory when the various multipath mechanisms are considered together. In many cases more than one physical mechanism could theoretically have accounted for a given range-noise effect. For example, either a long, weak, stray path or a cancellation involving only the target depth could account for decreasing-range errors of several nanoseconds at the two lowest indexes used. Under these circumstances it does not seem possible to draw any firm conclusions as to the minimum frequency deviation needed for acceptable results under conditions where all stray paths had been made negligible. However, on the basis of the two-path theory it would seem reasonable to use a frequency deviation of at least 50 Mc/sec. For substantially lower values exaggeration of the target depth can become appreciable. At the deviation of 36.5 Mc/sec (modulation index of 16.5) used in plotting Fig. 83, fractional nanosecond depths can be exaggerated to give range offsets of ±2.5 nsec or ±1.25 ft of height outside the physical extent of the target. Where wave heights of the order of 1 ft are to be recorded, it would seem wise to avoid errors of this magnitude, even though much of the noise energy can be removed by judicious filtering. At a deviation of about 66 Mc/sec (modulation index of 30) the maximum possible offset is ±1.4 nsec, or ±0.7 ft of height, which seems more acceptable.

Possible Improvements in the Wave-Profiling Techniques Used at the Bay Bridge Facility

Although the Bay Bridge FM-CW radar was not in any sense the prototype of an optimum system for field use, no significant deficiencies in the performance of the radar itself could be found. Thus, it is believed that improved wave-profiling performance can

be brought about only by an improved installation with respect to stray-path control or by changes in system specifications or techniques. Aside from the elimination of all significant stray-path signals, the following additions or changes might be considered.

1. As mentioned in discussing the Bay Bridge data, the use of amplitude gating appears to offer a means of substantially reducing range errors, especially those due to weak, long stray paths. Amplitude gating at the Bay Bridge would have given improved results on most if not all occasions without any other change being made in the system or in installation geometry.

2. Taking the trend of the observed data together with the predictions of the two-path theory, it seems likely that some further reduction in range noise could have been obtained by using still greater transmitted bandwidths. There is reason to hope that increasing-range noise would have been further reduced as the bandwidth was raised and that eventually decreasing-range spikes would have been reduced as well. However, this method may not represent the most economical way of attacking the problem.

3. It is possible that the use of predetection hard limiting, such as is accomplished in normal reception of FM broadcast transmissions, would improve results, but this assumption cannot be taken for granted. The two-path range errors for the balanced-interferometer system and the ideal limiting receiver can be compared by examining Figs. 88 through 91 and referring back to the section on theoretical analysis, Fig. 22. The well-known strong-signal capture effect is evident at the higher modulation indexes for the target depth of 3.0 nsec in all of the figures illustrating the ideal limiter case, and the ideal receiver would thus have an advantage in minimizing errors caused by weak signals having relatively long delays. Note, however, that should the desired signal ever fade below the level of the delayed path, the apparent range would instantly jump by the full amount of the delay, which would represent less desirable behavior than that of the interferometer receiver. As the differential delay is reduced, larger and larger bandwidths are required to effect capture, and for the delays represented by typical target depths in range the bandwidth is probably impractically large. To effect capture where the differential delay is 0.5 nsec would require six times the maximum experimental bandwidth, or about 3,000 Mc/sec. Note also that the required bandwidth is virtually unchanged over the full range of amplitude ratios from 0.5 to 0.98 that is displayed in the figures. With less than perfect limiting, the bandwidth required for capture would be expected to increase for ratios near unity.

For the range of modulation indexes below the capture region, the errors produced by the ideal receiver exceed those that occur with the interferometer. The significance of the difference may be judged by recalling that all negative range offsets, here plotted in the decreasing-range direction, are actually outside of the physical extent of the target and may be projected in either direction when the amplitude ratio can be inverted. Thus an offset of minus unity, or one target depth, actually means a possible exaggeration of the physical extent by a factor of 3 to 1. Referring again to Figs. 88 through 91, it can be seen that the bandwidths needed to avoid significant exaggeration of shallow targets are very much larger in the ideal receiver case. The conclusion that is reached on the basis of two-path theory is that the ideal receiver responding only to the instantaneous frequency as defined by the rate of change of the rf phase, offers improved results under some conditions but far poorer results under other conditions when practical transmitted bandwidths are used.

In the case of the more complicated real target, it is possible that the degradation in the shallow-target case will be less marked, and it is also possible that the capture effect will not bring about the predicted improvement in the case of longer delayed paths. Here the circumstances may be analogous to those encountered by Arguimbau and his associates (12) when using a nearly ideal FM receiver for communication over an

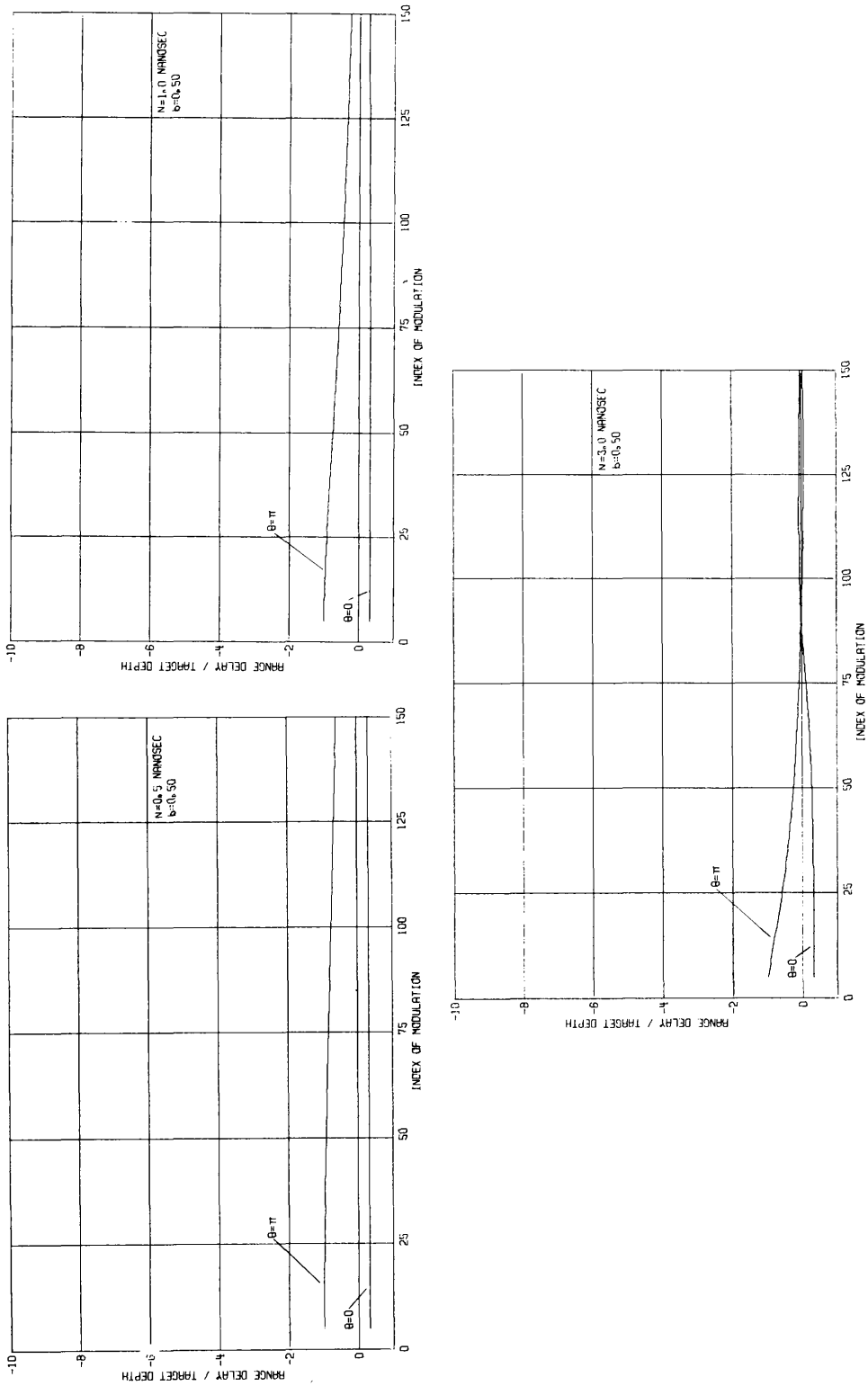

Fig. 88 - Target depth exaggeration for the ideal limiter and linear discriminator, amplitude ratio equal to 0.5

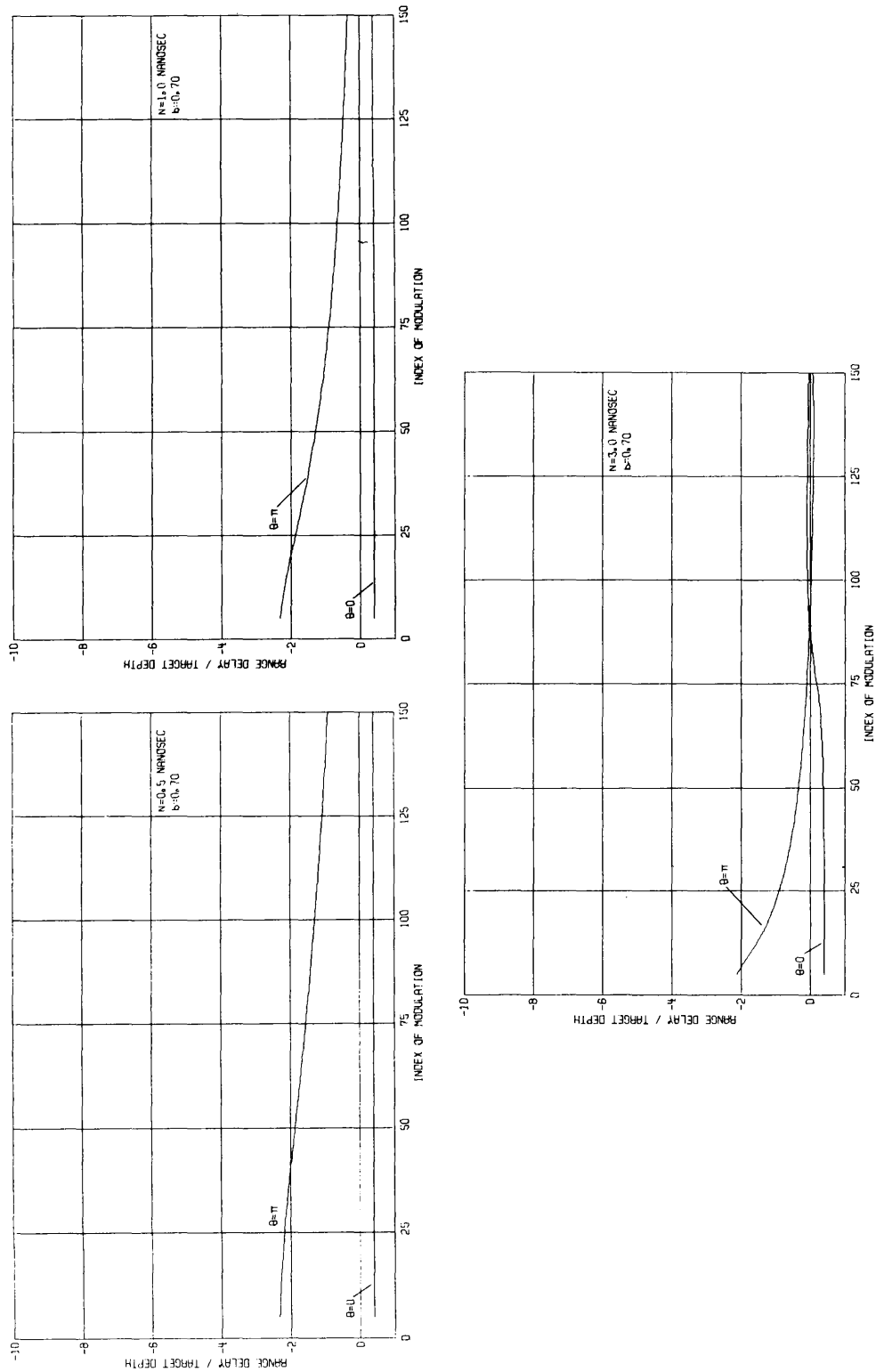

Fig. 89 - Target depth exaggeration for the ideal limiter and linear discriminator, amplitude ratio equal to 0.7

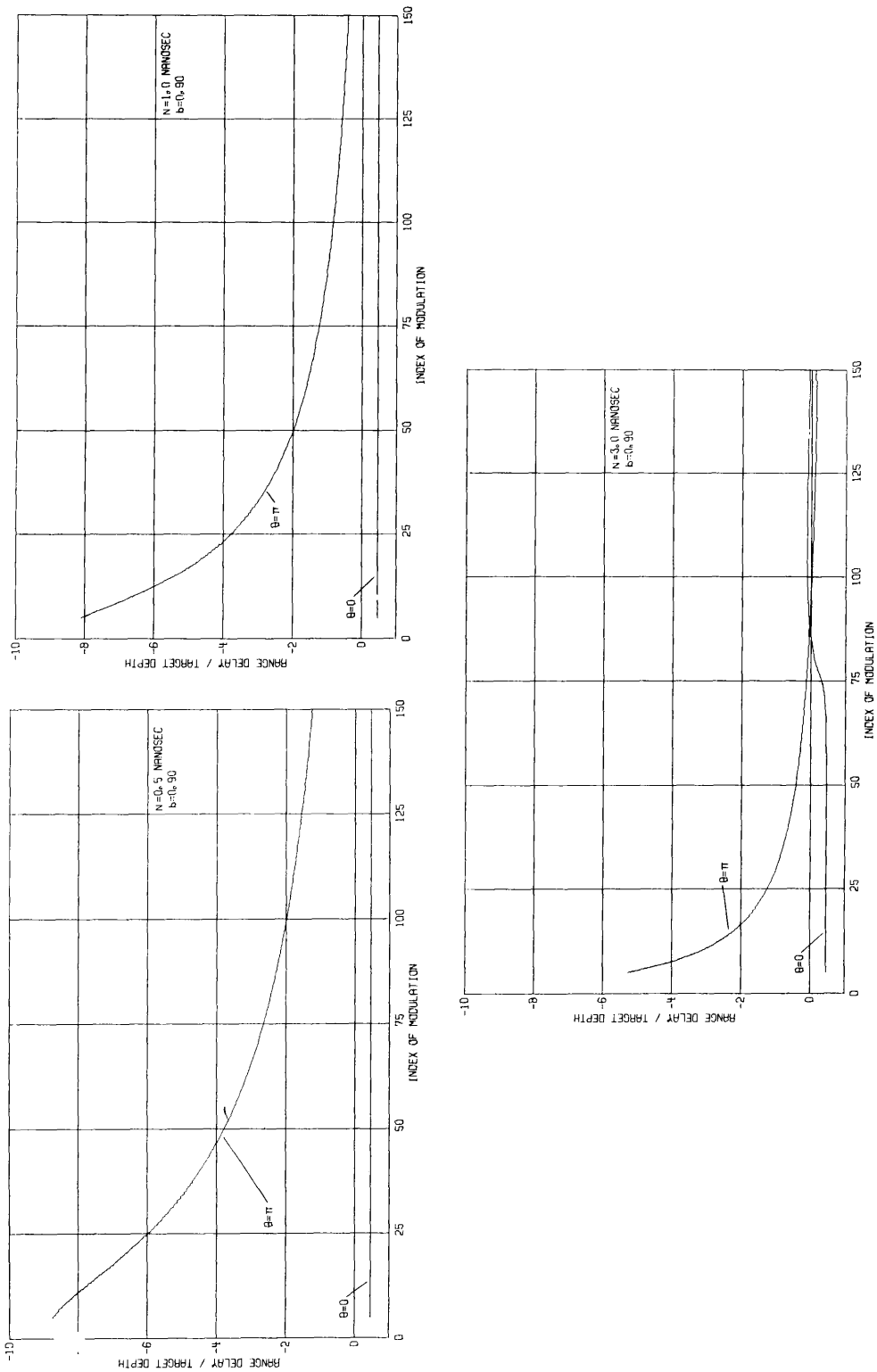

Fig. 90 - Target depth exaggeration for the ideal limiter and linear discriminator, amplitude ratio equal to 0.9

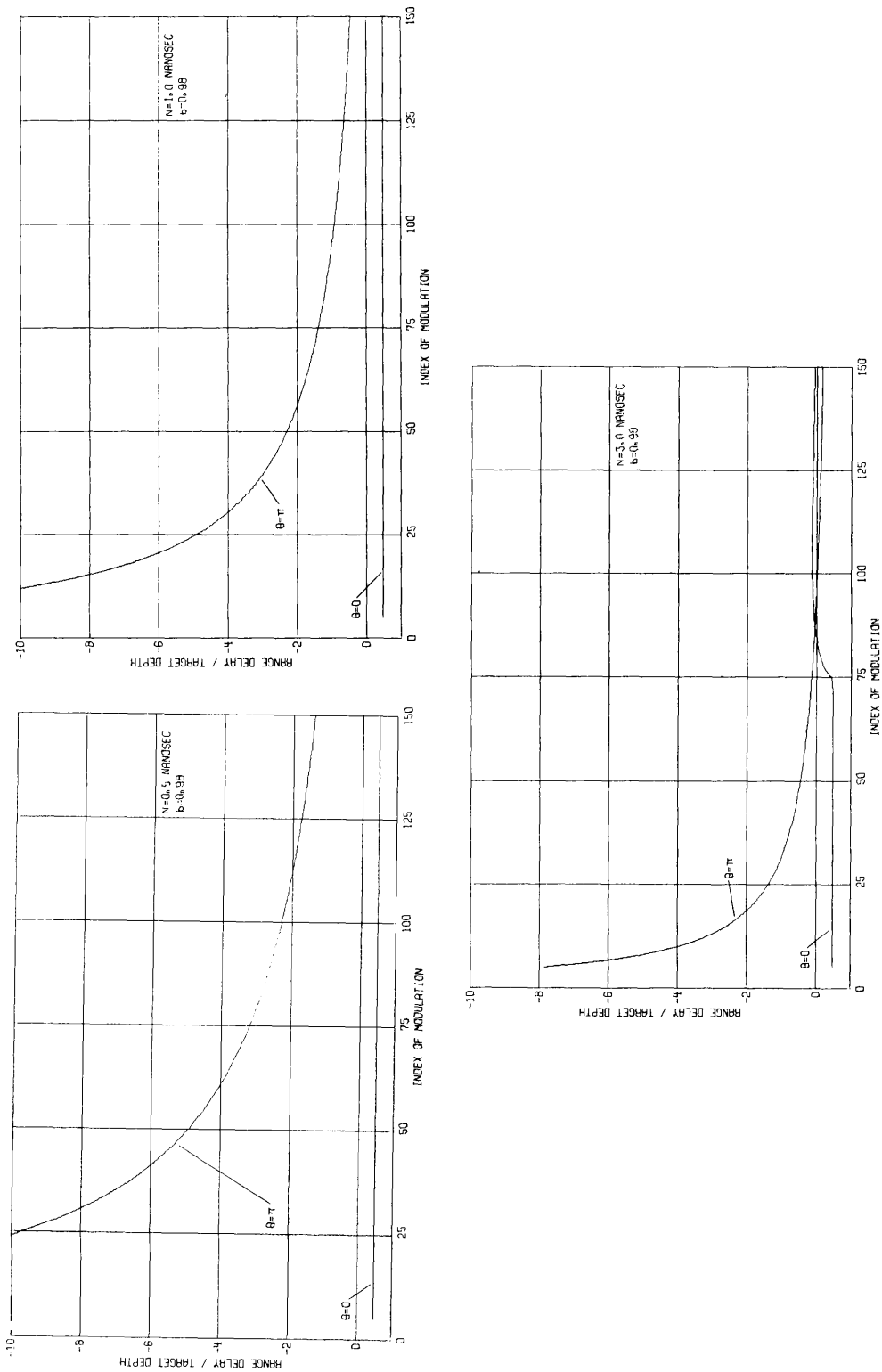

Fig. 91 - Target depth exaggeration for the ideal limiter and linear discriminator, amplitude ratio equal to 0.98

ionospheric path. In this case it was found that in general there was no single path over which a sufficiently predominating signal arrived, and the capture mechanism could not operate to recover an undistorted modulation. The ocean-wave-profiling situation may well be similar.

4. Where large differential delays are involved, a range-discrimination capability would help to control errors. Such delays might occur due to a direct leakage of energy between antennas or through a duplexer or because of a twice-range double reflection. In either case the differential would be equal to the range delay for the operating height. An FM-CW system of the sort used at the Bay Bridge has no inherent range resolution, but this could be provided by a frequency-tracking filter, as suggested by Morrow (25). In other types of FM-CW ranging systems, range discrimination can be provided in various ways by signal processing.

5. There is a definite possibility that circularly polarized radiation would help to control some types of scintillation noise by reducing the depth of fading of desired signals or by weakening delayed paths involving multiple scattering or reflection. A further extension of this line of investigation would be the use of some form of the polarization diversity discussed by Allen (28).

6. Various methods for compensating or correcting multipath distortion have been described in the literature in connection with communications systems (29-32). These techniques are based on the examination of the received signal and the recognition that distortion has occurred in view of the a priori knowledge available about the transmitted signal. Such distortion would be evident, for example, if amplitude modulation were to appear on the received wave when pure FM had been transmitted, if the received modulation spectrum were broader than had been transmitted, or if pulse shapes were distorted in a pulse-code-modulation link. Having recognized the nature of the distortion, the system then attempts to repair the damage by some form of corrective linear signal processing, possibly using a model of the transmitted signal as a reference. In the case of single-tone pure FM, one might attempt to correct for AM on the received wave and at the same time eliminate any harmonics of the modulation frequency that appeared. If the multipath configuration constantly varied as it does in wave profiling, the corrective processing would also have to be constantly varied. It cannot be said that these techniques would not be of some value in the wave-profiling case, but the problem appears to be inherently more difficult to solve than the usual communications problem. In the first place, the distortion of the received wave may be so slight as to be difficult to observe. In the case of exaggeration of the depth of a shallow target, the range offset may be significant while the amplitude modulation is very small and the amplitude of harmonics of the modulation frequency is very low. In the second place, it is by no means certain that correcting the observable defects in the signal would simultaneously correct the small fundamental-frequency phase shifts that are the significant errors in the wave-profiling case. In analyzing the effects of bandpass networks on a frequency-modulated wave, it has been found that approximate theories which successfully predict harmonic content fail to predict accurately the phase shift of the fundamental (33). This outcome suggests that a filtering or processing technique which corrected harmonic distortion to a certain degree could not be depended upon to correct phase or range errors to the same extent. Only further analysis or experiment could settle this point definitely.

* * *

To summarize the improvements that might be made while adhering to the same basic type of FM-CW radar, we can say that the use of amplitude gating appears to offer improved performance in virtually all situations, including the existence of unavoidable long stray paths. This technique should be made available in any future experimental system.

Greater transmitted bandwidths than have yet been used may be advantageous and should be tried if possible. Only field experience can determine the benefits that can be obtained.

The overall advantage, if any, of using predetection limiting is not clear-cut. Theory indicates that in the two-path case performance would be improved under some circumstances but markedly degraded in others. The complexity of the real target may prevent both the predicted improvement and the predicted degradation from occurring. Again only field work can provide the final answer.

Some range-resolution capability would be an advantage and should be provided, if feasible. It will not be needed if all stray signal paths can be made insignificant.

Use of circular polarization or polarization diversity offers a possibility of a further reduction of scintillation noise at its source, and the final word on the wave-profiling problem cannot be said until these techniques are tried.

The use of corrective processing or signal repair does not appear to be an attractive technique in ocean-wave profiling at the present time. In view of the complexity of the instrumentation needed, the lack of any body of information on which to base the straightforward design of the corrective signal processor, and the lack of evidence that the best possible corrective processing would actually reduce ranging errors, it is felt that the other system changes mentioned should be given first attention.

Significance of the Bay Bridge Results in Ocean-Wave Profiling

Although the operating conditions of an airborne ocean-wave profiling system will differ in some respects from the Bay Bridge installation, many of the experimental and theoretical findings should be applicable. In general, the results obtained are grounds for considerable optimism about the use of microwave FM-CW radar for ocean-wave measurement. At the Bay Bridge facility, in spite of stray propagation paths that apparently contributed to the range noise observed, it was generally possible to obtain useful wave profiles when waves were only 0.5 to 1.0 ft high. If comparable results can be obtained over the ocean, even considering the resolution limit of a larger illuminated patch, then ocean-wave data satisfying all ordinary oceanographic requirements can be recorded. An estimate of how nearly comparable results might be in the two situations might be made by considering those parameters which will necessarily differ.

The airborne system will operate at a greater range from the water, probably about 500 ft instead of 62 ft, and the illuminated patch will very probably be larger, perhaps three or four times the Bay Bridge half-power diameter of 4 ft. Thus a more sensitive receiver will evidently be needed, but this improvement should not be beyond the state of the art. The larger patch may change the scintillation pattern somewhat, and if the carrier frequency is raised to permit the use of smaller antennas, a further change may take place. However, these changes would not be likely to alter the fundamental nature of the scintillation phenomena and may actually be for the better, as they may tend to result in higher scintillation rates relative to the wave-profile frequencies, permitting more effective filtering of range-noise spikes. The greater operating range will almost certainly make a stray path involving a double reflection between the aircraft and the water very much weaker and probably negligible in comparison to the desired signal. This was apparently not always the case at the Bay Bridge.

A further change in the character of the target scintillation may result from the fact that the wave pattern is being scanned at a velocity that is high in most cases compared with the wave-propagation velocities. This in effect gives waves of all lengths nearly

the same effective velocity relative to the radar patch, whereas the true velocities as seen by a fixed wave staff are much higher for the longer waves. As a consequence, more ripples and small wavelets will be seen by the airborne system during the time that a large, long wave is being scanned. As in the case of an increased patch size, this difference would not be expected to change seriously the nature of the scintillation that could occur, and if there were any change in the relative rate of fading it appears in this case also that it would increase, causing a further reduction in the extent to which the scintillation noise spectrum overlapped the wave-profile frequency range.

In the airborne profiler, direct local leakage and stray paths involving local structure, which were evidently not a factor at the Bay Bridge, will become more significant as they compete with a weaker desired surface reflection. These effects may be minimized by the choice of a modulating frequency that will place the envelopes of the principal leakage paths out of phase with the desired signal envelope. Errors may, however, be nulled exactly only for one path length and for one operating altitude, so that every effort needs to be made to keep stray signals at a low level. Experience at the Bay Bridge indicates that a solution of these problems should be possible.

The increased size of the illuminated patch will increase the possible differential delays which the target can generate. The depth of the target area in range should not be a serious matter, since these delays will still bear much the same relationship to the range delays represented by the profile of the larger waves which the larger patch can resolve. Since the delays are longer on an absolute basis, it will take a smaller frequency deviation to avoid exaggeration of the physical depth, according to the two-path theory. The possibility of much longer stray paths involving a horizontal skip is a more serious consequence of a large illuminated patch, since the length of these paths is not related directly to the wave height, and it will sometimes be desirable to measure waves only a foot or two in height even in the ocean. In this case the size of the patch would be much larger relative to the profile heights than it was at the Bay Bridge, and errors comparable to the patch size would be correspondingly more significant. The Bay Bridge data strongly suggest, although they do not rigorously prove, that differential delays of this sort can occur. If this is indeed the case, then these delays rather than the depth of the target in range may limit the performance of the ocean-wave system. Two-path theory indicates that use of a sufficiently large frequency deviation will insure that range errors will not be significantly greater than a fraction of the path length governed by the amplitude ratio, according to the factor $k = b^2/(1 + b^2)$, where b is the amplitude ratio. At smaller frequency deviations the errors may exceed k, and in this region there will be a most favorable and a least favorable frequency deviation, depending upon the predominant path delay. The Bay Bridge results show larger errors than the theory predicted under some conditions. These errors represented range delay only slightly smaller than the delay for the half-power diameter of the patch, whereas theory predicted about one-third this value. Thus one cannot place too much confidence in quantitative prediction where this target mechanism is in operation. In any case, if horizontal skip does occur, large range offsets are possible during even a moderately deep fade, and some form of amplitude gating may be necessary to cope with this problem.

CONCLUSIONS

General Findings

The overall conclusion, reached on the basis of the theoretical and experimental studies reported here, is that microwave radar offers a means of obtaining ocean-wave profiles that are accurate enough to fill all ordinary oceanographic needs. The radar system must, however, be carefully designed, with all of the effects of the inevitable target scintillation given the proper consideration. In order to reduce the magnitude of the scintillation range noise to an acceptable level, it appears necessary to employ a

broad transmitted spectrum, probably extending over a bandwidth in excess of 100 Mc/sec. It does not appear possible to alter substantially the spectrum required in a given wave-profiling situation by any manipulation of the other radar system parameters, although the exact bandwidth needed for optimum results may depend somewhat on the waveform transmitted and on the type of signal processing used in the receiver.

The experimental work has in particular demonstrated the feasibility of using a sufficiently broadband FM-CW system for precise range measurements over water, and it has been concluded that a successful airborne all-weather wave-profiling system could be based on this concept. No attempt has been made to prove that the FM-CW approach is the optimum one under all circumstances, since other techniques are clearly applicable. The use of a pulse system having a sufficiently short pulse available is one of these, and the final choice would obviously involve both economic and technical considerations. However, when radar systems representing roughly comparable engineering investments are considered, there appears to be no technique which is clearly superior to the FM-CW system which has been analyzed.

Of the wave-profiling techniques not involving radar, the only promising one appears to be an optical system based on modulated laser ranging. The ultimate accuracy that such a system could achieve would depend in part on the extent of optical penetration of the surface interface and also on the amount of beam broadening needed to avoid excessive loss of the received signal owing to reflection from tilted wave facets. No data have yet been released that would permit radar and laser accuracies to be strictly compared under open ocean conditions. Assuming that profiling accuracy was comparable and adequate for both systems, which may well be the case, choice would be dictated by aircraft installation problems, economic considerations, and the importance of the all-weather capability of the radar.

Suggested Specifications for an FM-CW Wave-Profiling Radar System

In view of the observations made at the Bay Bridge, it is recommended that an FM radar intended for general ocean-wave profiling tasks have the following characteristics.

1. The receiver sensitivity and dynamic range should be calculated to be adequate under these assumptions:

a. The maximum signal may be less than 3 db below the signal for a specular reflection at the water surface, but will more commonly be 10 or 15 db below this level.

b. The minimum signal during a brief fade may be as much as 35 db below the maximum, and fading over a range of 25 db will always occur.

c. Residual effects of signal-amplitude variation, such as the direct translation of an amplitude change into a wave-height offset, are to be negligibly small over at least the first 20 db of range below maximum signal and controlled to the extent that they can be effectively filtered from the profile record over the remainder of the specified dynamic range.

2. In a prototype system, a variable frequency deviation should be provided with a maximum deviation of at least ±100 Mc/sec available. (Field experience is needed to determine the transmitted bandwidth actually necessary.)

3. A provision should be made for amplitude gating which would involve interrupting the profile record whenever the received signal faded below a set threshold. This threshold should preferably be derived from the maximum signal level currently

experienced, so that gating would occur a certain number of decibels below the maximum. At least until field experience has determined what the optimum settings are, the threshold should be adjustable by the operator.

4. A filter, or preferably a set of filters, should be provided for processing the wave-height signal when desired. Something more sophisticated than a simple RC integrator is indicated where real-time viewing of the record is to be done. The phase characteristics should be linear across the pass band to prevent distortion of the profile shape.

5. In a system that is to be used in any sense as a radar research tool as well as a data-collection device, two additional features are strongly recommended. First, provision should be made for a broadband recording of the height signal with all significant range-noise components reproduced. Second, provision should be made for recording an output proportional to the instantaneous amplitude of the received signal. The bandwidth of this channel should be adequate to reproduce all the significant features of the scintillation pattern, including the very fast, deep fades which are always seen.

To summarize the wave-profiling design problem, we may say that the conditions under which an airborne wave-profile radar must operate are less favorable in some respects and more favorable in others than were the conditions at the Bay Bridge facility. The less favorable circumstances include the need to cope with a greater loss over the propagation path (perhaps 15 to 20 db greater), increased vulnerability to signals arriving over local stray paths, and an illuminated patch that is larger relative to the heights of the waves that are to be recorded. The more favorable circumstances include decreased vulnerability to signals produced through reillumination of the water by energy reflected from the antennas or structure, and the prospect of somewhat higher scintillation rates relative to the wave-profile frequencies. It appears that the increased path loss may be overcome in a straightforward manner by reasonable increases in transmitter power and/or receiver sensitivity, and that local stray paths can be adequately controlled by antenna placement and the use of microwave absorbing material. The larger patch size makes possible peak range errors that are larger relative to the profile signal, but maximum errors are always associated with deep fading, and it appears likely that amplitude gating will permit range noise to be adequately controlled. Decreased vulnerability to reillumination of the water is an important advantage, since this kind of stray path is the most difficult to control, and higher relative scintillation rates will mean that more range-noise energy can be removed by filtering.

It seems reasonable to conclude that a radar system such as that specified could provide ocean-wave profiles of value for almost all oceanographic purposes. Further field experience will be needed to determine the ultimate accuracy which can be achieved with microwave radar.

Techniques for the Evaluation of an Airborne Wave-Profiling System

During test of an airborne system, it will obviously never be possible to make the kind of point-by-point profile comparisons that were made at the Bay Bridge. However, it should be noted that many of the conclusions that were drawn from the Bay Bridge results could have been reached almost as well without the use of the wave-staff record. An observer viewing records such as the broadband radar traces shown, for example, in Figs. 51, 64, and 74 could have little doubt that the radar was following the contour of the larger waves, even without the staff record as a reference. Thus, if a record of this character can be obtained in the air, the observer will be justified in placing a great deal of confidence in the result, and the use of a filter to produce a cleaner trace for real-time viewing or graphical analysis will be entirely legitimate. If, on the other hand,

the low-frequency profile components are so masked by the noise that they cannot be visually followed in a broadband recording, the accuracy of the system is in doubt, and while filtering may extract a record having the appearance of a profile signal, its resemblance to the true surface contour will be very questionable. It is believed that a broadband height record accompanied by a broadband amplitude-scintillation record will permit satisfactory operation of a wave-profile system to be judged to a large extent without reference to any oceanographic instrumentation. If this evidence is taken together with a statistical comparison of the wave-profile spectra with spectra obtained by a wave staff or other direct measurement, then conclusive evaluation should be possible.

Provision of broadband signal outputs is thus considered vitally important in any prototype wave-profiling radar. Lacking such records, the observer must depend entirely on statistical comparisons or relatively crude visual observations of the sea surface, and the evaluation of the system will be far more laborious as well as more questionable in its accuracy. Experience at the Bay Bridge shows that a system of potentially high accuracy will produce a broadband height record characterized by relatively short, sharp noise spikes superimposed on a recognizable wave-profile signal that can be followed visually. Furthermore, there should be a high degree of correlation between large noise spikes and deep amplitude fading. If these characteristics are not observed, this circumstance should be taken as an indication that the radar installation is inadequate in one or more respects. Observation of the way in which the character of the height noise depends upon the transmitted bandwidth may give a clue as to the nature of the signal paths involved in error generation. In a case where special instrumentation is to be added to an existing design, precautions must be taken to assure an adequate dynamic range in all of the circuits handling the profile signal, keeping in mind the fact that noise spikes of the same order of magnitude as the radar patch diameter may exist even when wave heights are low. Thus, even when using the most sensitive height range of the system, where the filtered record might accommodate one or two feet of height, the broadband record might have short noise spikes representing perhaps an additional five to eight feet of height superimposed on the wave-profile trace. If the internal circuitry does not meet the necessary requirements, it should be relatively simple to provide special amplifiers which would do so, and this provision should be made whenever any serious evaluation of the system is to be accomplished.

ACKNOWLEDGMENTS

The authors wish to acknowledge the assistance of the personnel of the Optics Division responsible for the operation of the Chesapeake Bay Bridge Facility. Their continuing cooperation during the entire period of the exercise greatly facilitated the experimental program.

REFERENCES

1. Morrow, C.M., "Ocean Wave Profiling Radar System," NRL Rept. 6052, Apr. 21, 1964

2. Kelly, E.J., "The Radar Measurement of Range, Velocity and Acceleration," IRE Trans. on Military Electronics, Vol. MIL-5, No. 2, pp 51-57, Apr. 1961

3. Skolnik, M.I., "Theoretical Accuracy of Radar Measurements," IRE Trans. on Aeronautical and Navigational Electronics, Vol. ANE-7, No. 4, pp 123-129, Dec. 1960

4. Dunn, J.H., Howard, D.D., and King, A.M., "Phenomena of Scintillation Noise in Radar-Tracking Systems," IRE Proc. Vol. 47, No. 5, pp 855-863, May 1959

5. Crosby, M.G., "Frequency Modulation Propagation Characteristics," IRE Proc. Vol. 24, No. 6, pp 898-913, June 1936

6. Crosby, M.G., "Observations of Frequency-Modulation Propagation on 26 Megacycles," IRE Proc. Vol. 29, No. 7, pp 398-403, July 1941

7. Corrington, M.S., "Frequency-Modulation Distortion Caused by Multipath Transmission," IRE Proc. Vol. 33, No. 12, pp 878-891, Dec. 1945

8. Meyers, S.T., "Nonlinearity in Frequency-Modulation Radio Systems Due to Multipath Propagation," IRE Proc.,Vol. 34, No. 5, pp 256-265, May 1946

9. Stumpers, F.L.H.M., "Interference Problems in Frequency Modulation," Philips Research Reports, Vol. 2, pp 136-160, 1947

10. Gerks, I.H., "An Analysis of Distortion Resulting from Two-Path Propagation," IRE Proc. Vol. 37, No. 11, pp 1272-1277, Nov. 1949

11. Wheeler, H.A., "Common-Channel Interference Between Two Frequency-Modulated Signals," IRE Proc., Vol. 30, No. 1, pp 34-50, Jan. 1942

12. Arguimbau, L.B., and Granlund, J., "The Possibility of Transatlantic Communication by Means of Frequency Modulation," Proc. of the National Electronics Conference, Vol. 3, pp 644-653, 1947

13. Arguimbau, L.B., Granlund, J., Manna, E.E., and Stutt, C.A., "Transatlantic Frequency-Modulation Experiments," MIT Research Lab. of Electronics Technical Report No. 278, Sept. 20, 1954

14. Sollenberger, T.E., "Multipath Phase Errors in CW-FM Tracking Systems," IRE Trans. on Antennas and Propagation, Vol. AP-3, No. 4, pp 185-192, Oct. 1955

15. Vinti, J.P., "Theory of the Multipath Propagation of Frequency-Modulated Waves," Aberdeen Proving Ground, Ballistic Research Laboratories Report No. 1025, Sept. 1957

16. Becker, H.D., "Amplitude and Phase Distortion in FM Communication and Tracking Systems due to Multipath Interference," Conference Proceedings, 2nd National Convention on Military Electronics, Washington, D.C., June 1958, Professional Group on Military Electronics, Institute of Radio Engineers, New York pp. 270-277, 1958

17. Howard, D.D., "Errors Caused by Complex Sea Surface in a Continuous Height Recording System," NRL Radar Division Technical Memorandum, May 23, 1956

18. Saunders, W.K., "Post-War Developments in Continuous-Wave and Frequency-Modulated Radar," IRE Trans. on Aerospace and Navigational Electronics, Vol. ANE-8, No. 1, pp 7-19, March 1961

19. Wimberly, F.T., and Lane, J.F., Jr., "The AN/APN-22 Radio Altimeter," IRE Transactions on Aeronautical and Navigational Electronics, Vol. ANE-1, No. 2, pp 8-14, June 1954

20. Boesch, P.W., and Hardinger, K.E., "Low-Altitude FM Altimeter," Harry Diamond Laboratories, Report No. TR-740, Aug. 10, 1959, ASTIA No. AD 225570

21. Kalmus, H.P., Cacheris, J.C., and Dropkin, H.A., "Nonquantized Frequency-Modulated Altimeter," IRE Trans. on Aeronautical and Navigational Electronics, Vol. ANE-1, No. 2, pp 15-21, June 1954

22. Horton, B.M., "Noise-Modulated Distance Measuring Systems," IRE Proc. Vol. 47, No. 5, pp 821-828, May 1959

23. Silver, S., et al., "Microwave Antenna Theory and Design," pp 569-572 Vol. 12, M.I.T. Radiation Laboratory Series, McGraw Hill Book Co. Inc., New York, N.Y.

24. Morrow, C.M., "Radar Altimeter-Ocean Wave Profiler," Radar Return Transactions, Part 1, ASTIA Document AD-244937, pp 169-197, May 1959

25. Morrow, C.M., "Radar System," U.S. Patent No. 3,307,182, Feb. 28, 1967

26. Kinsman, B., "Wind Waves: Their Generation and Propagation on the Ocean Surface," Prentice-Hall, Inc., Englewood Cliffs, N.J., pp 126-133, 1965

27. Pierson, W.J., Jr., Neumann, G., and James, R.W., "Practical Methods for Observing and Forecasting Ocean Waves by means of Wave Spectra and Statistics," H.O. Pub. No. 603, U.S. Navy Hydrographic Office, pp 154-156, 1955

28. Allen, P.J., "Control and Measurement of Antenna Polarization," NRL Memo. Rept. 1734, July 1966

29. Wilmotte, R.M., "Reduction of Interference in FM Receiver by Feedback Across the Limiter," IRE Proc. Vol. 40, No. 1, pp 34-36, Jan. 1952

30. Wilmotte, R.M., "Reception of an FM Signal in the Presence of a Stronger Signal in the Same Frequency Band, and Other Associated Results," IEE Proc. Vol. 101, Part III, pp 69-75, Mar. 1954

31. Bello, P.A., "Some Techniques for the Instantaneous Real-Time Measurement of Multipath and Doppler Spread," IRE Trans. on Communications Technology, Vol. COM-13, No. 3, pp 285-292, Sept. 1965

32. Rudin, H., Jr., "Automatic Equalization Using Transversal Filters," Bell Tel. Labs., IEEE Spectrum, Vol. 4, No. 1, pp 53-59, Jan. 1967

33. Izatt, J.B., "The Distortion Produced When Frequency-Modulated Signals Pass Through Certain Networks," IEE Proc. Vol. 110, Electronics Quarterly, pp 149-156 (1963)

GLOSSARY OF TERMS

A return from T_1

B return from T_2

C discriminator delayed return from T_1

D discriminator delayed return from T_2

E return from T_3

F discriminator delayed return from T_3

G $2m \sin pN/2$

H height of water wave from crest to trough

K the fractional frequency change

L length of a water wave in feet

M range delay in seconds

N propagation time delay due to target spacing $T_1 - T_2$

P $2m \sin p\,[(N - \mu + \sigma)/2]$

Q $2m \sin p\,[(N - \mu - \sigma)/2]$

R radar range

T period of the water wave in seconds

U $2m \sin p\,[(\mu + \sigma)/2]$

V $2m \sin p\,[(\mu - \sigma)/2]$
phase velocity

X $2m \sin p\,[(\sigma/2)]$

Y $2m \sin p\,[(N + \sigma)/2]$

Z $2m \sin p\,[(N - \sigma)/2]$

ω carrier frequency

θ rf phase between T_1 and T_2

b relative target strength

c velocity of light

d $2r$

f frequency: f_1 or f_2 rf frequencies in a waveguide simulator
f_c cut off frequency in a waveguide
f_m modulation frequency
f_0 design center frequency of a waveguide simulator

i index number in a summation series

k limiting range error factor for very large frequency deviations

m index of modulation

n index number in a summation series

p modulation frequency

r target spacing

t time

x $[1 - (f_c/f_1)^2]$

Z relative strength of a third target

Δt time interval

σ discriminator delay

Δx $[2K + K^2]$

H_n height of water wave "n"

L_n length of water wave "n", waveguide path "n", or free space path "n"

T_n target "n"

$T_n/2$ half-period of water wave "n"

E_1 return from T_1

E_2 return from T_2

E_0 discriminator output

$J_n(\ )$ Bessel function, first kind, n_{th} order

ΔF frequency deviation (either side of carrier)

AA $(2 + \delta^2 \cos p\sigma) J_1(X) - (\delta^2/2) J_3(X)$

BB $(2 + \delta^2 \cos p(N + \sigma)) J_1(Y) - (2 + \delta^2 \cos p(N - \sigma)) J_1(Z) - (\delta^2/2)(J_3(Y) - J_3(Z)$

CC $(J_0(Y) - J_2(Y)) \cos p\frac{N+\sigma}{2} - (J_0(Z) - J_2(Z)) \cos p\frac{N-\sigma}{2}$

DD $(2 + \delta \cos p\sigma + \delta^2 \cos 2p\sigma) J_1(X) - (\delta \cos p\sigma + (\delta^2/2)) J_3(X) + (\delta^2/2) J_5(X)$

$$EE \begin{cases} [2 + \delta \cos p(N+\sigma) + \delta^2 \cos 2p(N+\sigma)] J_1(Y) - [\delta \cos p(N+\sigma) + (\delta^2/2)] J_3(Y) \\ [2 + \delta \cos p(N-\sigma) + \delta^2 \cos 2p(N-\sigma)] J_1(Z) - [\delta \cos p(N-\sigma) + (\delta^2/2)] J_3(Z) \\ + (\delta^2/2)[J_5(Y) - J_5(Z)] \end{cases}$$

$H(b,\theta,G)$ $(-b)^n n^{-1} J_1(nG) \cos(n\theta)$

λ_0 free-space wavelength at design frequency f_0

λ_c cutoff wavelength in waveguide

λ_g waveguide wavelength

λ free-space wavelength

ΔD or ΔD_g waveguide path difference

ΔD_{fs} free-space path difference

ϕ_{fs} free-space rf phase angle

ϕ_g waveguide rf phase angle

ψ_{max} maximum slope of a water wave based on a sinusoidal shape

δ percentage AM

ω_d error term in the output of an ideal limiter discriminator

ω radian frequency

ω_p radian frequency of modulation in the general case of any modulated carrier

ω_{in} radian frequency of the in-phase zero-crossing of a phase-frequency function

ω_{out} radian frequency of the out-of-phase zero-crossing of a phase-frequency function

β efficiency of diode 1

γ efficiency of diode 2

μ target spacing $(T_1 - T_3)$

Mc/sec 10^6 cycles per second, or megacycles per second

Gc/sec 10^9 cycles per second, or gigacycles per second

nsec 10^{-9} second, or nanosecond

BS boresight or position in space of the primary path

SB_1 sideband vector from point 1 in the primary path

SB_2 sideband vector from point 2 in the secondary path

SB_{12} two path vector sum of $SB_1 + SB_2$

SB'_{12} two path vector difference of $SB_1 - SB_2$

rf radio frequency

FM-CW frequency modulated - continuous wave

AM amplitude modulation

FM frequency modulation

ϕ an rf phase angle in radians
an rf phase angle between T_1 and T_3

$\phi(\omega)$ an rf phase angle in radians which is a function of ω

ϕ_2 phase angle between phasor E_2 and phasor E_1

ϕ_s phase angle between the resultant phasor E_S and phasor E_1

D_p propagation distance to a target and back $(D = 2R)$

$\Delta\phi$ target induced phase displacement of each line of a signal spectrum relative to its neighbor

$\Delta\phi_1$ phase displacement for a single element target

$\Delta\phi_{in}$ phase displacement for a two element target with the signals adding in phase

$\Delta\phi_{out}$ phase displacement for a two element target with the signals adding out of phase

$\Delta\omega$ a frequency interval in radians

$\Delta\omega_{(peak)}$ frequency separation of the peaks of a phase-frequency function

$\Delta\omega_{(out)}$ width of the high slope interval of the phase-frequency function around the out-of-phase zero crossing

E-plane containing the electric vector of a linearly polarized electromagnetic wave

H-plane containing the magnetic vector of a linearly polarized electromagnetic wave

E_1 phasor representing the return from target T_1

E_2 phasor representing the return from target T_2

E_s phasor representing the return from the sum of E_1 and E_2

T_1, T_2, T_3 target elements 1, 2, and 3, respectively

This page intentionally left blank.

Security Classification

DOCUMENT CONTROL DATA - R & D

(Security classification of title, body of abstract and indexing annotation must be entered when the overall report is classified)

1. ORIGINATING ACTIVITY *(Corporate author)*
Naval Research Laboratory
Washington, D.C. 20390

2a. REPORT SECURITY CLASSIFICATION
Unclassified

2b. GROUP

3. REPORT TITLE
SCINTILLATION RANGE NOISE AND RELATED PHENOMENA IN WATER WAVE PROFILING WITH MICROWAVE RADAR

4. DESCRIPTIVE NOTES *(Type of report and inclusive dates)*
An interim report on the problem.

5. AUTHOR(S) *(First name, middle initial, last name)*
Arno M. King, Christopher M. Morrow, Chauncey G. Myers, and Calvin L. Moody

6. REPORT DATE
September 3, 1968

7a. TOTAL NO. OF PAGES
183

7b. NO. OF REFS
33

8a. CONTRACT OR GRANT NO.
NRL Problem R02-13

b. PROJECT NO.
RF 001-02-41-4004

c.

d.

9a. ORIGINATOR'S REPORT NUMBER(S)
NRL Report 6641

9b. OTHER REPORT NO(S) *(Any other numbers that may be assigned this report)*

10. DISTRIBUTION STATEMENT
This document has been approved for public release and sale; its distribution is unlimited.

11. SUPPLEMENTARY NOTES

12. SPONSORING MILITARY ACTIVITY
Department of the Navy
(Office of Naval Research)
Washington, D.C.

13. ABSTRACT

Wave-profile recording by radar from a low-flying conventional aircraft offers a means of rapidly collecting large amounts of oceanographic data over wide areas of the ocean in a relatively short time. A series of radar experiments has been conducted from a laboratory suspended beneath the Chesapeake Bay Bridge. The purpose of the series of experiments was to study the problems of wave-profile recording and to make comparisons with standard radar altimetry.

Theoretical and experimental analyses based on the work conducted at the bridge laboratory indicate that target-scintillation noise limits the accuracy of a microwave radar used for wave profiling. However, it has been concluded that a properly designed airborne FM-CW radar can produce ocean-wave recordings of sufficient accuracy for all ordinary oceanographic purposes. The specifications for such a system have been developed. One of the basic requirements has been found to be a broad transmitted spectrum, probably in excess of 100 Mc/sec; this requirement appears to be independent of the exact form which the radar system takes.

DD FORM 1 NOV 65 1473 (PAGE 1)

S/N 0101-807-6801

Security Classification

14. KEY WORDS	LINK A ROLE	LINK A WT	LINK B ROLE	LINK B WT	LINK C ROLE	LINK C WT
Radar						
Microwave radar						
Water waves						
Scintillation						
Noise						
Wave profiling						
FM-CW radar						
Reflective effects						
Radar reflections						